SEMMELWEIS EGYETEM

DOKTORI ISKOLA

Ph.D. értekezések

3237.

GARÁDI ZSÓFIA

A gyógyszerészeti tudományok korszerű kutatási irányai

című program

Programvezető: Dr. Antal István, egyetemi tanár

Témavezető: Dr. Béni Szabolcs, egyetemi docens

ADVANCING STRUCTURAL AND ISOMERIC CHARACTERIZATION OF HUMAN MILK OLIGOSACCHARIDES USING ^{1}H-^{15}N NMR SPECTROSCOPY

PhD thesis

Zsófia Garádi

Doctoral School of Pharmaceutical Sciences

Semmelweis University

Supervisor:	Szabolcs Béni, Ph.D.
Official reviewers:	Márta Mazákné Kraszni, Ph.D. István Timári, Ph.D.
Head of the Complex Examination Committee:	István Antal, Ph.D.
Members of the Complex Examination Committee:	Zoltán Szakács, Ph.D. Gergely Völgyi, Ph.D.

Budapest
2025

TABLE OF CONTENTS

LIST OF ABBREVIATIONS

1D	One-dimensional
2'-FL	2'-Fucosyllactose
2D	Two-dimensional
3'-SL	3'-Sialyllactose
6'-SL	6'-Sialyllactose
COSY	Correlation Spectroscopy
d	Doublet
D_2O	Deuterium Oxide
dd	Doublet of doublets
ddd	Doublet of doublet of doublets
DFLNnH	Difucosyllacto-*N*-neohexaose
dp	Degrees of polymerization
DSS	3-(Trimethylsilyl)-1-propanesulfonic acid sodium salt
EFSA	European Food Safety Authority
ESI	Electrospray Ionization
FDA	Food and Drug Administration
Fuc	Fucose
FUT2	Fucosyltransferase 2
FUT3	Fucosyltransferase 3
Gal	Galactose
GC	Gas Chromatography
Glc	Glucose
GlcNAc	*N*-Acetylglucosamine
HCl	Hydrochloric Acid
HMBC	Heteronuclear Multiple Bond Correlation
HMO	Human Milk Oligosaccharide
HPLC	High-Performance Liquid Chromatography
HSQC	Heteronuclear Single Quantum Coherence
LacNAc	*N*-acetyllactosamine
LC	Liquid Chromatography
Le^x	Lewis X antigen

LNB	Lacto-*N*-biose
LNFP II	Lacto-*N*-fucopentaose II
LNFP III	Lacto-*N*-fucopentaose III
LNH	Lacto-*N*-hexaose
LNnH	Lacto-*N*-neohexaose
LNnT	Lacto-*N*-neotetraose
LNT	Lacto-*N*-tetraose
LSTa	Sialyllacto-*N*-tetraose a
LSTb	Sialyllacto-*N*-tetraose b
m	Multiplet
MFLNH III	Monofucosyllacto-*N*-hexaose III
MFLNnH I	Monofucosyllacto-*N*-neohexaose I
MFLNnH II	Monofucosyllacto-*N*-neohexaose II
MS	Mass Spectrometry
ms	Milliseconds
Neu5Ac	*N*-Acetylneuraminic Acid
NMR	Nuclear Magnetic Resonance
NOE	Nuclear Overhauser Effect
NOESY	Nuclear Overhauser Effect Spectroscopy
o.l.	Overlapped
ROESY	Rotating-frame Overhauser Effect Spectroscopy
Sia	Sialic Acid
t	Triplet
TOCSY	Total Correlation Spectroscopy

1. INTRODUCTION

1.1. Human milk oligosaccharides

Human milk oligosaccharides (HMOs) are the third most abundant solid component in breast milk, after lactose and lipids. These complex carbohydrates play a crucial role in infant nutrition, far beyond their initial perception as mere nutrients. HMOs possess a range of biological activities, including prebiotic effects, antiadhesive properties against pathogens, modulation of the immune system, regulation of intestinal epithelial cells, and contribution to brain development. [1]. While most glycans are typically conjugated to proteins or lipids, HMOs occur unconjugated in human milk [2]. Despite their indigestibility by human enzymes, HMOs exert their effects by shaping the gut microbiota, enhancing the gut barrier function, and modulating immune responses [3]. These diverse roles emphasize the potential for promoting health from infancy to adulthood [4,5]. The recognition of HMOs' functions has led to their consideration as a gold standard in infant nutrition [6,7]. Regulatory agencies, such as the FDA in the United States and EFSA in the European Union, have acknowledged the safety and beneficial properties of certain HMOs, leading to their approval as ingredients in infant formulas and dietary supplements [7,8]. Research has identified nearly 200 distinct HMO structures, ranging from simple to highly complex glycans composed of three to more than 30 monosaccharide units [9–12].

1.1.1. Chemical structure and diversity of HMOs

HMOs exhibit a remarkable diversity in their chemical structures, which are composed of five major monosaccharides: glucose (Glc), galactose (Gal), *N*-acetylglucosamine (GlcNAc), fucose (Fuc), and the sialic acid (Sia) primarily in the form of *N*-acetylneuraminic acid (Neu5Ac). Each HMO molecule contains lactose (Galβ1-4Glc) at the reducing end, which can be extended through β1-3 or β1-6 linkages by lacto-*N*-biose (Galβ1-3GlcNAc, type 1 chain) or *N*-acetyllactosamine (Galβ1-4GlcNAc, type 2 chain). The elongated HMO chain or the lactose can undergo fucosylation in α1-2, α1-3, or α1-4 linkages, and/or sialylation in α2-3 or α2-6 linkages, resulting in a wide range of structural variations [1]. The general structure of HMOs can be seen in Figure 1, while the HMO structures investigated herein are represented in Figure 2.

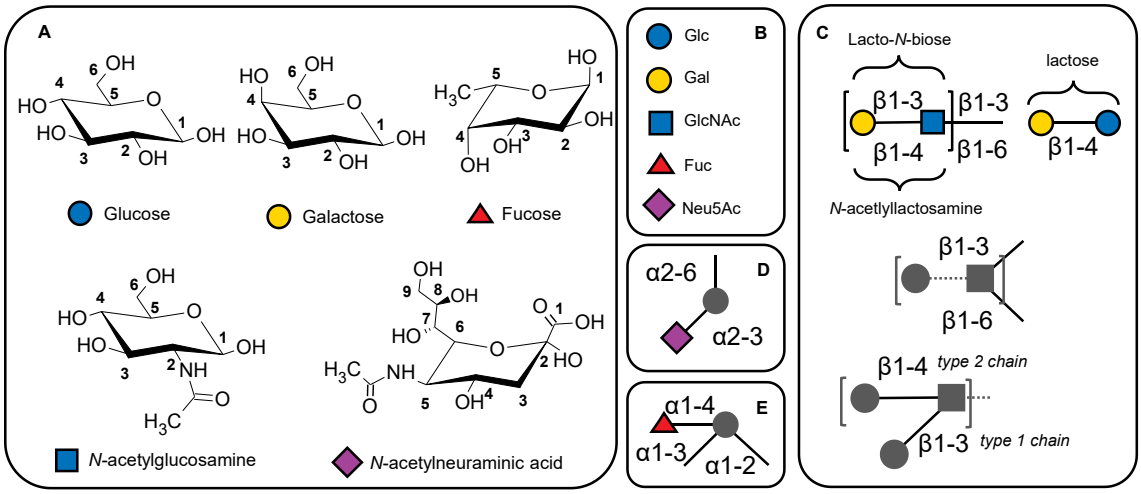

Figure 1. Representation of HMO structures. (**A**) Structure and atomic numbering of the monosaccharide building blocks of HMOs. (**B**) Monosaccharide building blocks of HMOs using Symbol Nomenclature For Glycans (SNFG) [11]. (**C**) General HMO structure, including chain elongation possibilities and modification sites of the HMO backbone. (**D**) Sialylation sites. (**E**) Fucosylation sites [13].

HMOs can be categorized based on their core structures into two main groups: neutral HMOs and acidic HMOs. Neutral HMOs are further divided into fucosylated and non-fucosylated types, while acidic HMOs contain sialic acid residues. Key representatives of HMOs in breast milk include 2'-fucosyllactose (2'-FL), lacto-*N*-tetraose (LNT), and lacto-*N*-neotetraose (LNnT). Among these, 2'-FL is the most abundant, comprising about 30% of total HMOs [14,15]. The overall concentration of HMOs in breast milk is highly dynamic, ranging from approximately 20-25 g/L in colostrum to 5-15 g/L in mature milk, with substantial interindividual variation influenced by maternal genetics and lactation stage [1]. While 2′-FL is most prevalent, it lacks an *N*-acetyl group. In contrast, several HMOs containing *N*-acetyl residues–such as LNT, LNnT, LNFP II, LNFP III, 3′-SL, 6′-SL, LSTa, LSTb, and even more complex structures like DFLNnH and MFLNH III–are present in concentrations ranging from 0.2 to 1.0 g/L depending on maternal Secretor status and other factors [16,17]. These *N*-acetylated structures represent a substantial portion of the total HMO pool and are biologically relevant due to their general functional roles.

Recent advancements in HMO production technologies have explored alternative biosynthetic platforms to improve both structural diversity and scalability. While microbial fermentation remains the dominant method for industrial HMO production,

plant-based expression systems have been developed to synthesize a wide range of HMOs, including complex structures such as lacto-*N*-fucopentaose I, which are typically difficult to produce via microbial fermentation [18].

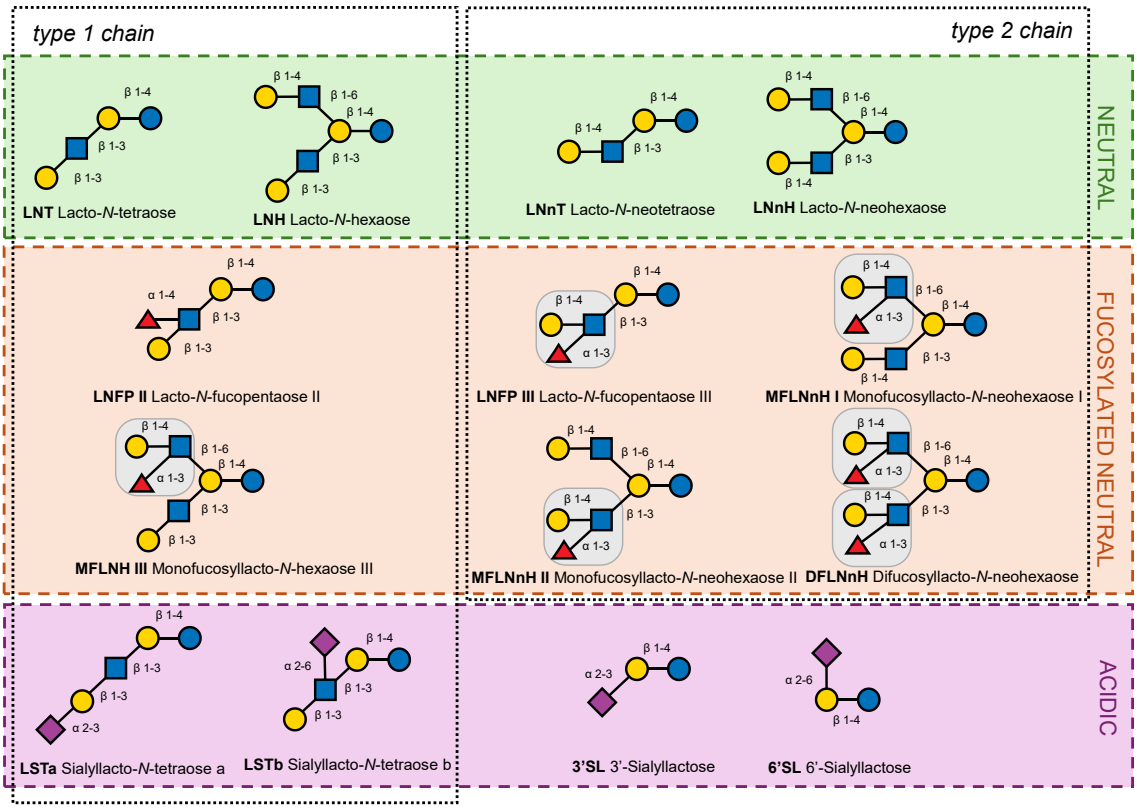

Figure 2. Schematic representation of investigated HMOs from this work, detailing monosaccharide linkages and structural categories. Grey circles indicate Lewis X (Le^x) motifs. (The chemical structures of all investigated HMOs are shown in Figures A1 and A2 in the Appendix.)

1.1.1.1. Genetic factors influencing HMO composition

The composition and abundance of HMOs vary significantly among lactating women, largely due to genetic factors, particularly those involving glycosyltransferase genes. These genetic variations play a crucial role in determining the specific HMO profile in human milk [1,19].

One primary genetic determinant of HMO composition is the Secretor gene (FUT2), which encodes α-1,2-fucosyltransferase. This enzyme adds fucose to the HMO backbone, resulting in fucosylated HMOs. Women who are Secretor-positive, produce milk rich in fucosylated HMOs such as 2'-fucosyllactose, whereas those who are Secretor-negative have significantly lower levels of these HMOs [20,21].

Another key gene influencing HMO composition is the Lewis gene (FUT3), which encodes α-1,3/4-fucosyltransferase. Secretors with functional FUT2 and FUT3 genes produce a broader range of HMOs, including both α-1,2 and α-1,3/α-1,4 fucosylated oligosaccharides. In contrast, non-Secretors or individuals with inactive FUT3 genes have a more restricted HMO profile [1,22]. The interaction between FUT2 and FUT3 activities creates a complex pattern of HMOs and determines the expression of various Lewis determinants, including Lewis a (Le^a), Lewis b (Le^b), Lewis X (Le^x), and Lewis y (Le^y). These structural variations depend on the linkage pattern of the outermost Gal (β1-3 or β1-4), and the linkage of Fuc to the internal GlcNAc (α1-4 or α1-3) [2].

Beyond individual glycosyltransferase genes, epigenetic factors and gene-environment interactions also influence HMO composition. Maternal diet, health status, and hormonal changes during lactation can affect the expression of glycosyltransferase genes, thereby contributing to HMO variability [19].

1.1.2. Functional roles of HMOs

1.1.2.1. Antimicrobial and antiviral effects

One of the primary roles of HMOs is their antimicrobial and antiviral properties. HMOs act as soluble decoy receptors that prevent pathogens from attaching to the intestinal epithelial glycocalyx, thereby reducing the risk of infection. For instance, HMOs such as 2'-FL and LNT have been shown to inhibit the adhesion of pathogens like *Campylobacter jejuni* and *Entamoeba histolytica* to intestinal cells [23,24]. Additionally, HMOs exhibit antimicrobial and antibiofilm effects against bacteria such as Group B Streptococcus (GBS) and *Staphylococcus aureus*, significantly inhibiting their growth and biofilm formation [25–27].

1.1.2.2. Modulation of intestinal epithelial cells

HMOs also directly influence intestinal epithelial cells, enhancing barrier function and modulating cell proliferation and differentiation. They have been shown to increase the proliferation of crypt cells under inflammatory conditions, which may protect against necrotizing enterocolitis [28]. Furthermore, HMOs can alter the structure of the intestinal epithelial cell glycocalyx layer, enhancing its thickness and reducing pathogen adherence [29].

1.1.2.3. Immune modulation

In addition to their direct antimicrobial effects, HMOs modulate the immune system. They can influence cytokine production and promote a balanced Th1/Th2 response, potentially reducing excessive mucosal leukocyte infiltration and activation [1,30]. For example, HMOs such as disialyllacto-*N*-tetraose (DSLNT) have been shown to suppress inflammation and support the maturation of the intestinal mucosal immune system [23].

1.1.2.4. Support of beneficial microbiota

Another critical function of HMOs is their role in shaping the gut microbiota. HMOs selectively promote the growth of beneficial bacteria, particularly *Bifidobacterium* species, which are prevalent in the guts of breastfed infants [26]. These bacteria can ferment HMOs, producing short-chain fatty acids that enhance gut barrier function and protect against pathogens [31]. The fermentation products of HMOs, such as acetate, also contribute to the preservation of intestinal barrier integrity by upregulating proteins responsible for maintaining tight junctions [32,33].

1.1.2.5. Contribution to brain development

HMOs also contribute significantly to brain development and cognitive function as they are a source of sialic acid, which is crucial for brain development [34]. Sialic acid is a component of gangliosides and glycoproteins in the brain that play key roles in neurodevelopment. Studies have shown that breastfed infants, receiving high levels of sialylated HMOs through human milk, have higher concentrations of sialic acid in their brains compared to formula-fed infants [35]. This increased availability of sialic acid from HMOs supports the formation of neural cell membranes and synaptic connections, which are vital for cognitive functions and learning abilities [36]. Animal studies have demonstrated that dietary sialic acid enhances learning and memory, suggesting a direct link between HMOs and improved cognitive outcomes in breastfed infants [37].

1.1.3. Analytical techniques for HMO characterization

1.1.3.1. Structural Elucidation of HMOs

The structural characterization of HMOs is a complex but critical task in understanding their biological functionality. HMOs exhibit remarkable structural complexity, arising from their variations in monosaccharide composition, glycosidic linkages, and branching

patterns. This diversity necessitates advanced analytical methods that can unravel their intricate structures with precision.

Among these, mass spectrometry (MS) has emerged as the cornerstone for HMO analysis due to its high sensitivity and ability to analyse complex biological mixtures. Over the years, MS-based approaches have evolved to address the unique challenges posed by HMOs. Electron transfer dissociation (ETD) has been particularly effective in identifying branching and linkage patterns by producing abundant cross-ring cleavage products, critical for differentiating structural isomers [38]. Complementing this, ultraviolet photodissociation (UVPD) offers superior fragmentation capabilities compared to traditional collision-induced dissociation (CID), enabling detailed analysis of sialylation and fucosylation patterns, which are essential for understanding functional differences among isomeric HMOs [39]. Label-free LC-ESI-MS/MS has further enhanced structural selectivity by employing glycan-specific fragmentation strategies, allowing for high-throughput analysis of both neutral and acidic HMOs while overcoming challenges associated with co-elution phenomena [40,41]. Recent studies employing negative-ion ESI-MS^n have enabled the sequencing of difucosylated nona- and decasaccharides, revealing novel backbone structures and branching patterns that were previously uncharacterized [42]. This multi-stage MS approach, combined with CID and tandem MS techniques, has provided deeper insights into the fine structural details of high-degree polymerization HMOs.

Ion mobility mass spectrometry (IM-MS) enhances MS by separating ions based on their shape-to-charge ratios. Techniques such as trapped ion mobility spectrometry (TIMS) provide high-resolution separation, making it possible to distinguish isomeric HMOs that are otherwise indistinguishable by MS alone [43,44]. The measurement of collision cross-section (CCS) values in IM-MS has provided an additional layer of identification for HMOs, serving as a structural fingerprint to identify and differentiate isomers with precision. Studies have shown that CCS values are sensitive to both structural and electronic variations, providing a robust means of resolving complex HMO mixtures. This approach is particularly effective when combined with tandem MS, as it allows for the simultaneous acquisition of structural and compositional data [45,46].

Hybrid methods, such as those combining IM-MS with MS/MS or electronic excitation dissociation (EED) with fixed-charge derivatization, have further expanded the analytical

toolkit. EED, for example, enables de novo sequencing of native glycans at the MS^2 level, eliminating the need for time-consuming derivatization steps like permethylation [47]. This not only simplifies sample preparation but also enhances the accuracy and efficiency of glycan analysis.

Advancements in computational tools and machine learning algorithms are now being leveraged to process and interpret the vast datasets generated by these advanced techniques. Automated methods integrating IM-MS and MS data are increasingly being adopted for large-scale HMO analysis [48].

While MS techniques are at the forefront of HMO structure analysis, NMR spectroscopy remains a critical tool for confirming stereochemical configurations and glycosidic linkages. Despite its inherently low sensitivity, NMR spectroscopy provides valuable insights into the structural complexity of HMOs, helping elucidate isomeric linkages and fine structural features that are challenging to capture by other methods.

The foundational role of NMR in HMO analysis began with simpler 1D NMR techniques, particularly ^{1}H and ^{13}C spectra, which enabled the identification of basic structural motifs [49]. Early applications also utilized chemical shift analysis and scalar coupling to understand glycosidic linkages and configurations. For example, in the study of simple oligosaccharides such as 2'-FL, ^{1}H coupling constants and heteronuclear ^{1}H-^{13}C coupling constants were analysed to confirm linkage configurations, with molecular simulations complementing experimental data to refine the dynamic conformations [50].

With advancements in NMR spectroscopy, investigation of more complex HMOs became possible, revealing their intricate branching and linkage patterns. Multidimensional techniques such as COSY, TOCSY, and HSQC enabled the resolution of overlapping signals, characterization of branching patterns, and identification of spin systems within sugar residues. For highly complex HMOs, such as lacto-*N*-decaose from human milk, 2D NMR measurements have been employed to investigate branching and fucosylation patterns [51,52]. Notably, NOESY and ROESY experiments introduced spatial interaction mapping, revealing intra- and inter-residue proximity. NOE cross-peaks proved the stereochemistry of glycosidic linkages in oligosaccharides with densely packed branching [51].

The study by van Leeuwen *et al*. introduced a rapid ^{1}H NMR-based method for classifying milk groups based on Lewis and Secretor blood group epitopes in HMOs. This approach

significantly simplified the identification of (α1-2)-, (α1-3)-, and (α1-4)-linked fucose residues, enabling the categorization of HMOs into specific milk groups [53]. Since its publication, this method has been widely adopted and further refined in subsequent research, highlighting its lasting impact of the NMR method on HMO studies [54,55].

Several studies emphasize the routine use of NMR methods for structural characterization of synthesized HMOs. A study by Xiao and co-workers demonstrated the practicality of NMR in structure verification, especially in the context of chemoenzymatic strategies, pointing out the critical role of NMR in synthetic glycan research [56].

NMR spectroscopy has also become an indispensable tool for analysing both HMO and non-HMO metabolites in human milk. Praticò *et al*. applied ^{1}H NMR to rapidly characterize the metabolomic profiles of human milk, including fucosylated HMOs and other bioactive components [57]. Smilowitz and co-workers quantified a wide array of metabolites, illustrating distinct variations tied to secretor phenotypes [58]. Spevacek *et al*. highlighted dynamic changes in metabolite concentrations during early lactation for term and preterm milk [59]. Expanding this scope, Wang and co-workers identified unique non-HMO metabolite profiles associated with Lewis-negative and non-Secretor mothers [60]. Collectively, these studies underscore the utility of NMR for unveiling the compositional and functional diversity of HMOs.

1.1.3.2. Chromatographic techniques for HMO analysis

Chromatographic techniques, often coupled with advanced detection systems, provide key tools for resolving the structural complexity of HMOs and understanding their biological functions.

HPLC is one of the most employed techniques for HMO analysis. Different stationary phases enable HPLC's adaptability to various analytical challenges. Reversed-phase chromatography (RPC) and hydrophilic interaction liquid chromatography (HILIC) are frequently used to profile neutral and acidic HMOs. These techniques have also been applied in industrial settings to ensure rigorous quality control of HMOs, particularly for impurity profiling and structural characterization. For instance, validated HPLC methods, combined with NMR spectroscopy, have been employed to achieve full mass balance closure and detect byproducts in industrially produced 2'-FL, enhancing the precision of HMO characterization [61].

HILIC provides robust separation for sialylated HMOs due to its interaction with the hydrophilic moieties of the oligosaccharides [62,63]. Pre-column derivatization is a widespread practice in HPLC to enhance sensitivity and detection. For instance, tagging HMOs with fluorescent labels such as 2-aminobenzamide (2-AB) significantly improves their chromatographic and mass spectrometric profiles. This approach facilitates the resolution of isomeric structures that are otherwise challenging to distinguish [64]. Porous graphitic carbon (PGC) chromatography provides excellent resolution for isomers, including α/β anomeric forms. To prevent anomeric splitting, the separation of reducing sugars typically involves reductive derivatization to their alditol form. Despite its efficacy, PGC's high susceptibility to contamination and retention variability over time pose operational challenges [65].

Capillary electrophoresis (CE) is a powerful electromigration technique that combines high-resolution separation with minimal sample requirements. CE has been applied in capillary zone electrophoresis (CZE) and capillary gel electrophoresis (CGE) modes for HMO analysis [62]. When coupled with laser-induced fluorescence (LIF), CE offers a complementary technique for HMO analysis. CE excels in resolving acidic oligosaccharides like 3'- and 6'-sialyllactose, which often exhibit overlapping chromatographic behaviour in HPLC systems. The high resolving power of CE is particularly advantageous for analysing isomers, owing to its sensitivity to charge-to-size ratios [62,63,66,67]. Recent advancements in multicapillary gel electrophoresis (MCGE) have further enhanced throughput and resolution. Using borate-crosslinked gels, this method achieves exceptional separation efficiency for both neutral and acidic HMOs, demonstrating its potential for high-throughput applications [66].

High-pH Anion Exchange Chromatography (HPAEC) coupled with pulsed amperometric detection (PAD) is well-established for its ability to resolve neutral and acidic HMOs without prior derivatization. However, pre-fractionation to separate neutral and acidic HMOs is often necessary, increasing analysis time. Although PAD provides a low detection limit, its structural information is limited, necessitating MS coupling for comprehensive analysis [62,64,68].

GC (coupled with MS), although less commonly used for oligosaccharides, remains a valuable technique for specific applications, such as the quantification of fucosylated HMO isomers. Methods employing trimethylsilyl derivatization enhance volatility and

stability, enabling accurate quantification of key HMOs like 2'-fucosyllactose and 3-fucosyllactose [68].

1.1.3.3. Analytical methods for HMO quantification

The field of HMO analysis has advanced significantly, with diverse methods now available to quantitatively assess these compounds in a variety of matrices, including breast milk, infant formula, dietary supplements, infant urine and feces, and even foods containing added HMOs. These techniques address the complexity and diversity of HMO structures, providing robust and accurate quantification that supports both scientific research and industrial applications.

HPLC has been widely employed, often coupled with refractive index (RI) detection for specific HMOs such as 2'-FL and 3-FL in various food matrices like milk and yogurt. These methods achieve high linearity, precision, and reproducibility, making them suitable for stability and shelf-life studies in food products [69]. Similarly, derivatization techniques enhance fluorescence detection, enabling the simultaneous analysis of multiple HMOs in infant formula and adult nutritionals with high specificity and sensitivity [70].

MS techniques, often combined with LC, have significantly advanced HMO quantification by offering unparalleled sensitivity and structural specificity. Methods like PGC-LC-MS allow simultaneous quantification of neutral and acidic HMOs with accurate calibration and validation across complex biological matrices [65,71]. Another example is HPAEC-PAD, which has proven to be accurate for resolving structurally similar HMOs such as 2'-FL and lactose in lactose-rich environments like infant formula [72].

A combined approach utilized ^{1}H NMR spectroscopy alongside HPAEC-PAD and PGC-LC-MS to analyse HMOs in maternal milk and infant feces. Absolute concentrations of 3-FL in human milk were determined using HPAEC-PAD, while its concentration in infant fecal samples, along with 16 other major HMO structures, was quantified by PGC-LC-MS. To complement the quantitative analysis, ^{1}H NMR was utilized to determine the relative levels of fucosylated epitopes, enriching the structural information obtained from these measurements and providing deeper insights into HMO profiles and their metabolic transformations [73].

Recently, a novel quantitative NMR method was developed to overcome challenges in HMO analysis caused by spectral overlap with sample impurities. This method offers high precision and accuracy in measuring 2'-FL and 3-FL in complex food matrices, outperforming conventional chromatography-based approaches in simplicity and speed of sample preparation [74].

Additionally, advances in automated data processing tools, such as LC/MS search libraries, further streamline high-throughput analysis, integrating quantification with structural elucidation [75].

Rapid methods are increasingly recognized in industrial contexts, such as the reductive amination techniques used for labelling HMOs with UV-active compounds. These methods, characterized by reduced runtime and reliance on widely available instrumentation, are pivotal for large-scale quality control and regulatory compliance [76].

1.2. ^{15}N NMR spectroscopy for glycan characterization

The application of ^{15}N NMR spectroscopy has significantly advanced the structural characterization of glycans, particularly glycosaminoglycans (GAGs) such as heparin, heparan sulfate (HS), and hyaluronan (HA). These linear polysaccharides, composed of alternating uronic acid and hexosamine residues, exhibit complex patterns of sulfation and acetylation, making their molecular-level characterization challenging. Integrating ^{15}N NMR, particularly through ^{1}H-detected techniques, enables the elucidation of specific structural motifs critical for their biological activity.

GAGs like heparin and HS contain *N*-acetylglucosamine (GlcNAc) and *N*-sulfo-glucosamine (GlcNS) residues, which are amenable to analysis via ^{15}N NMR. These residues are central to understanding glycan microstructure due to the sensitivity of their nitrogen chemical shifts to sulfation and neighbouring chemical environments [77]. One of the initial ^{15}N NMR-based method developments by Limtiaco et al. focused on detecting ^{15}N in amino sugars through long-range couplings to carbon-bound protons, making it suitable for glycan analysis. TheIMPACT-HNMBC (improved and accelerated constant-time proton nitrogen multiple-bond correlation) pulse sequence is particularly effective for molecules with fast N-H exchange, such as amino sugars containing *N*-sulfo substitutions or unmodified amino groups [78].

Langeslay and colleagues expanded the application of ^{1}H-^{15}N NMR spectroscopy for GAG characterization. Their work focused on optimizing experimental conditions to detect nitrogen-linked protons in sulfamate groups, overcoming challenges posed by fast proton exchange in aqueous environments [79,80]. They developed sensitive techniques, including ^{1}H-^{15}N HSQC and HSQC-TOCSY to assign NMR resonances to structural motifs such as GlcNS residues and sulfation patterns. These have been applied to the characterization of heparin, heparan sulfate, and pharmaceutical derivatives [79,81]. Similarly, Beecher and Larive extended this approach to unmodified glucosamine (GlcN) and 3-*O*-sulfoglucosamine ($GlcN_3S$) in aqueous solutions, achieving the first direct detection of their amine protons through ^{1}H-^{15}N HSQC. Their work characterized solvent exchange properties and temperature dependencies, paving the way for deeper insights into GAG microstructures [82,83].

^{15}N NMR spectroscopy was also influential in the structural analysis of hyaluronan oligosaccharides. By employing ^{15}N- and ^{13}C-isotopic labelling Blundell *et al*. achieved complete sequence-specific assignments of nuclei in hyaluronan oligomers up to decasaccharides. Their studies provided critical insights into end-effects, the dynamic perturbations from terminal residues on internal structures, and their significance in understanding hyaluronan's polymeric conformation in solution [84,85].

The reduced signal overlap inherent in ^{15}N spectra provides a clear advantage in simplifying the interpretation of complex data sets, particularly compared to the dense signal environments typical in ^{1}H- and ^{13}C-based analyses. For example, Pomin's studies demonstrated that ^{1}H-^{15}N chemical shifts could reliably distinguish sulfation patterns within GAG components, even in mixtures, and introduced isotopic ^{15}N-labelling to enhance sensitivity and trace metabolic pathways in cell cultures [86]. In a later study, Pomin investigated the fast exchange properties of the sulfamate proton in GlcNS and employed techniques such as dynamic nuclear polarization (DNP) to improve ^{15}N signal detection, allowing detailed analysis of both monosaccharides and GAG chains in solution [87].

2. OBJECTIVES

The primary objective of this work is to explore and characterize the structural complexity and isomeric diversity of HMOs using advanced NMR techniques, particularly ^{1}H-^{15}N HSQC and related methodologies. This research aims to develop ^{15}N NMR-based methods to distinguish isomeric tri-, tetra-, and pentasaccharide HMO structures, as well as to perform comprehensive ^{1}H-^{15}N NMR analyses of hexa-, hepta-, and octasaccharide HMOs containing Lewis X motifs, isolated from human milk. These include performing complete resonance assignments (^{1}H, ^{13}C, and ^{15}N) of all investigated HMOs to identify unique structural motifs and distinguish isomers, as well as investigating the structural connectivity within HMOs to elucidate their spatial configurations.

This work introduces, for the first time, the observation of the ^{15}N nucleus into the NMR characterization of HMOs. By a systematic investigation of ^{15}N and ^{1}H chemical shifts of *N*-acetylglucosamine (GlcNAc) and *N*-acetylneuraminic acid (Neu5Ac) moieties, the study aims to enhance the identification of isomeric structures. Furthermore, the research investigates several complex HMOs, including LNH, LNnH, and their derivatives containing Lewis X antigen (Galβ1–4(Fucα1–3)GlcNAc–) building blocks. Notably, many of these HMOs, are being extensively analysed via NMR for the first time, with their exact structures determined and reported.

By achieving these objectives, the research aims to advance the understanding of HMO structural diversity and establish a framework for their detailed characterization using non-destructive, high-resolution NMR methods.

3. METHODS

3.1. Chemicals

Tri-, tetra- and pentasaccharide HMOs; lacto-*N*-tetraose (LNT), lacto-*N*-neotetraose (LNnT), sialyllacto-*N*-tetraose a (LSTa), sialyllacto-*N*-tetraose b (LSTb), lacto-*N*-fucopentaose II (LNFP II), lacto-*N*-fucopentaose III (LNFP III), 3'-sialyllactose (3'-SL), and 6'-sialyllactose (6'-SL) were obtained from DSM (Hørsholm, Denmark). Hexa-, hepta- and octasaccharide HMOs; lacto-*N*-hexaose (LNH), lacto-*N*-neohexaose (LNnH), monofucosyllacto-*N*-neohexaose I (MFLNnH I), monofucosyllacto-*N*-neohexaose II (MFLNnH II), monofucosyllacto-*N*-hexaose III (MFLNH III), and difucosyllacto-*N*-neohexaose (DFLNnH) were isolated from human milk.

While the details of HMO preparation are beyond the scope of this dissertation, the isolation procedure is thoroughly described in the publication on which this work is based (see chapter 9: Bibliography of the candidate's publications). Briefly: human milk samples were collected from healthy volunteers at various postpartum stages, all screened for major infectious diseases. The samples were classified based on donor status using ^{1}H NMR analysis and processed accordingly [53]. Defatting, protein and lactose removal, desalting, and fractionation steps were carried out to isolate the oligosaccharide fraction. Neutral and sialylated HMOs were obtained via ion-exchange chromatography. Further purification steps included gel permeation chromatography and HPLC to yield defined oligosaccharide fractions.

Additional chemicals and reagents included deuterium oxide D_2O (99.9 atom% D), 3-(trimethylsilyl)-1-propanesulfonic acid sodium salt (DSS) and *N*-acetyl-D-glucosamine from Merck (Darmstadt, Germany), *N*,*N*′,*N*″,*N*‴-tetraacetylchitotetraose from Carbosynth (Compton, United Kingdom) and sodium phosphate and HCl from Reanal (Budapest, Hungary). Freshly prepared ultrapure water was obtained using the Select Fusion water purification system (SUEZ Water Technologies & Solutions, Feasterville-Trevose, PA, USA).

3.2. Instrumentation

Instrumentation included the SevenCompact S210 pH-meter and standard reference buffers (pH 2.00, 4.01, and 7.00) from Mettler-Toledo (Greifensee, Switzerland). NMR spectra were recorded using two Bruker Avance III systems (Bruker Biospin GmbH,

Rheinstetten, Germany): a HDX instrument (^{1}H: 799.68 MHz, ^{13}C: 201.10 MHz, ^{15}N: 81.04 MHz) equipped with an 800 SA ^{1}H&^{19}F/^{13}C/^{15}N TCI cryoprobe, and a HD instrument (^{1}H: 600.05 MHz, ^{13}C: 150.89 MHz, ^{15}N: 60.81 MHz) equipped with a Prodigy cryo-probehead. Both systems were operated at room temperature (295 or 298 K) and controlled using TopSpin 3.5 software (patch level 7) with pulse programs from the Bruker software library.

3.3. Sample preparation

For the purchased HMOs (tri- to pentasaccharides), solutions were prepared at a target concentration of 10 mM whenever sufficient substance quantities were available. For isolated HMOs (hexa- to octasaccharides), the available amounts were limited, thus, the entire available sample (approximately 1–2 mg) was used. The HMOs were dissolved in a minimal volume of a 9:1 H_2O:D_2O solvent mixture containing 5 mM sodium phosphate (NaH_2PO_4), and the pH was adjusted to 3.0 with 0.1 M HCl. DSS (0.5 mM) was used as the NMR chemical shift reference for both ^{1}H and ^{13}C nuclei.

Most HMOs were prepared in 500 µl of buffer using standard 5 mm Wilmad 541 (CortecNet, Voisins-Le-Bretonneux, France) or Norell Standard Series (Merck, Darmstadt, Germany) NMR tubes, while mass-limited samples were dissolved in 300 µl buffer and measured in D_2O-matched Shigemi BMS-005TB tubes (Merck, Darmstadt, Germany) to maximize sensitivity.

3.4. NMR methods

3.4.1. NMR spectroscopic parameters and data analysis

The chemical shifts (δ) for ^{1}H and ^{13}C nuclei were referenced to the internal standard (DSS), while the coupling constants (J) are given in Hz. Heteronuclear ^{15}N NMR experiments were performed at natural abundance. The ^{15}N resonances were deduced from the heteronuclear 2D spectra with chemical shifts relative to liquid ammonia. Assignments for ^{1}H and ^{13}C shifts were validated through cross-experiments. Signal overlap was managed by selective pulse excitation and fine-tuning of experimental parameters. Spectral processing and analysis were performed using TopSpin 3.5. software.

3.4.2. NMR experiments

The resonance assignments of tri- to pentasaccharide HMOs were achieved using the following pulse sequences from the Bruker software library without modification: ^{13}C (zgpg30), DEPTQ (deptqgpsp), ^{1}H-^{1}H COSY (cosygpmfqf), ^{1}H-^{13}C HSQC (hsqcedetgpsisp2.2), ^{1}H-^{13}C selective HSQC (shsqcetgpsisp2.2), ^{1}H-^{13}C HMBC (hmbcgplpndqf), ^{1}H-^{1}H ROESY (roesyphpr.2), ^{1}H-^{1}H TOCSY (mlevphpr.2), selective gradient TOCSY (seldigpzs), and selective gradient ^{1}H-^{1}H ROESY (selrogp) experiments.

For hexa- to octasaccharide HMOs, the same pulse sequences were applied. Although, DEPTQ, ROESY, and TOCSY experiments required no modifications, the remaining pulse sequences were adapted to include solvent suppression.

3.4.2.1. NMR experiments with solvent suppression

The low pH and high H_2O content of the NMR buffer was critical for observing amide proton resonances, which provide valuable structural insights. However, the overlap between the H_2O resonance and certain anomeric proton signals necessitated the use of high-quality solvent suppression to achieve accurate resonance assignments. To address this, pulse programs from the Bruker library were modified by separating the D1 relaxation delay from the presaturation delay, now encoded as the D2 delay parameter. These modifications ensured optimal solvent suppression while preserving amide signal integrity. The power level for presaturation was individually tested for each experiment to prevent signal reduction via saturation transfer. The modified D2 parameter was also integrated into the 1D ^{1}H (zgpr) pulse sequence with solvent suppression, ensuring consistency across all experiments.

NMR experiments for tri- to pentasaccharide HMOs were conducted using a 600 MHz NMR instrument. The experimental parameters were as follows:

The ^{1}H spectra were recorded in a 7211.539 Hz (12.0 ppm) spectral width (SWH), with 32 scans (NS) and 16 dummy scans (DS). The size of the fid was 32768 (TD), and receiver gain was set automatically. Transmitter frequency offset (O1) was set based on the water ^{1}H resonance. The 90° pulse (P1) was set by calibration for each sample individually. The delay parameters (D1, D2) were set to 2 s.

The ^{1}H-^{15}N HSQC (hsqcetgpsi2) spectra were acquired with a spectral width (SWH) 6009.615 Hz (10.0 ppm) in F2 and 608.147 Hz (10.0 ppm) in F1. A total of 64 scans (NS) and 16 dummy scans (DS) were recorded, along with 2048 complex points (TD) in F2 and 64 in F1. Transmitter frequency offset (O1) parameters in F2 and F1 were set based on preliminary trial experiments. In addition, 2 s relaxation delays were used (D1, D2).
The ^{1}H-^{15}N HSQC-TOCSY (hsqcdietgpsi) spectra were acquired with a spectral width (SWH) 6009.615 Hz (10.0 ppm) in F2 and 608.025 Hz (10.0 ppm) in F1. From 650 to 715 scans (NS) and 16 dummy scans (DS) were recorded, along with 2048 complex points (TD) in F2 and 64 in F1. Transmitter frequency offset (O1) parameters in F2 and F1 were set based on preliminary trial experiments. In addition, 2 s relaxation delays were used as D1 and D2, while D9 was set to 120 ms.

NMR experiments for hexa- to octasaccharide HMOs were conducted using an 800 MHz NMR instrument. The experimental parameters were as follows:
The ^{1}H spectra were recorded in a 9578.544 Hz (12.0 ppm) spectral window (SWH), with 8 scans (NS) and 8 dummy scans (DS). The size of the fid was 65536 (TD), and receiver gain was set based on preliminary trial experiments. Transmitter frequency offset (O1) was set to the water ^{1}H resonance and optimized to yield FID with minimum area. The 90° pulse (P1) was set by calibration for each sample individually. Following the relaxation delay D1 of 18 s, presaturation was achieved by the delay D2 of 2 s and a typical power level of 50-70 μW. Selective 1D TOCSY spectra were started from NH and isolated anomeric CH resonances to observe the high-resolution multiplets in each individual monosaccharide units representing a distinct spin system, applying R-SNOB pulse shapes for selective excitation and mixing times of 20, 40, 60 and 120 ms. Selective 1D ROESY spectra from the same signals were also acquired with 300 ms mixing time to explore spatial relationships.
The ^{1}H-^{15}N HSQC spectra were acquired with a spectral width (SWH) between 6880.734 and 6402.049 Hz (8.6 - 8.0 ppm) in F2 and between 162.082 and 324.163 Hz (2.0 - 4.0 ppm) in F1. A total of 32-64 scans (NS) and 16-32 dummy scans (DS) were recorded, along with 1600-1800 complex points (TD) in F2 and 16-64 in F1. In addition, 0.1-1 and 2 s relaxation delays were used for D1, D2, respectively.

4. RESULTS

4.1. Optimization of experimental conditions

The optimization of experimental conditions was critical to ensuring reliable and reproducible NMR data. To achieve this, *N*-acetylglucosamine (GlcNAc) was selected as a model compound. GlcNAc is not only commercially available but also one of the five fundamental building blocks of HMOs. Its biological relevance and structural simplicity make it an excellent representative for studying exchangeable amide (NH) protons in HMOs. These protons, known for their solvent exchange properties, are highly sensitive to experimental conditions, making them an ideal focus for our study.

An H_2O:D_2O mixture in a 9:1 ratio was chosen for the solvent to maintain a suitable environment for the NH proton. This composition allowed the observation of the NH resonance in the ^1H spectra while providing a sufficient deuterium lock for NMR. As the amide NH proton resonance is influenced by solvent exchange rates, and these rates are pH-dependent, an initial investigation focused on identifying the optimal pH range for maximizing signal intensity.

Unbuffered GlcNAc samples were analysed over a pH range of 3.0–9.0. This approach minimized the potential interference of buffer components in accelerating exchange rates. The NH resonance was monitored via integration in ^1H NMR spectra. The results (Figure 3) indicated that sharper peaks with greater integral values were consistently observed within the pH range of 3.0–5.0. This observation aligns with prior findings by Green *et al*., who demonstrated the influence of lower pH values on line widths and exchange rates, particularly for amide protons in glycosaminoglycan derivatives [88].

Following measurements were performed using buffered solutions to refine conditions. While increasing buffer concentrations from 5 mM to 50 mM enhanced buffer capacity, it was accompanied by a noticeable decrease in NH resonance intensity, particularly at higher pH values (Figure 4). This reduction likely stemmed from enhanced exchange rates catalysed by buffer anions. A pH of 3.0 and 5 mM phosphate-buffer concentration were chosen as a compromise, balancing optimal NH signal intensity and sufficient buffer capacity.

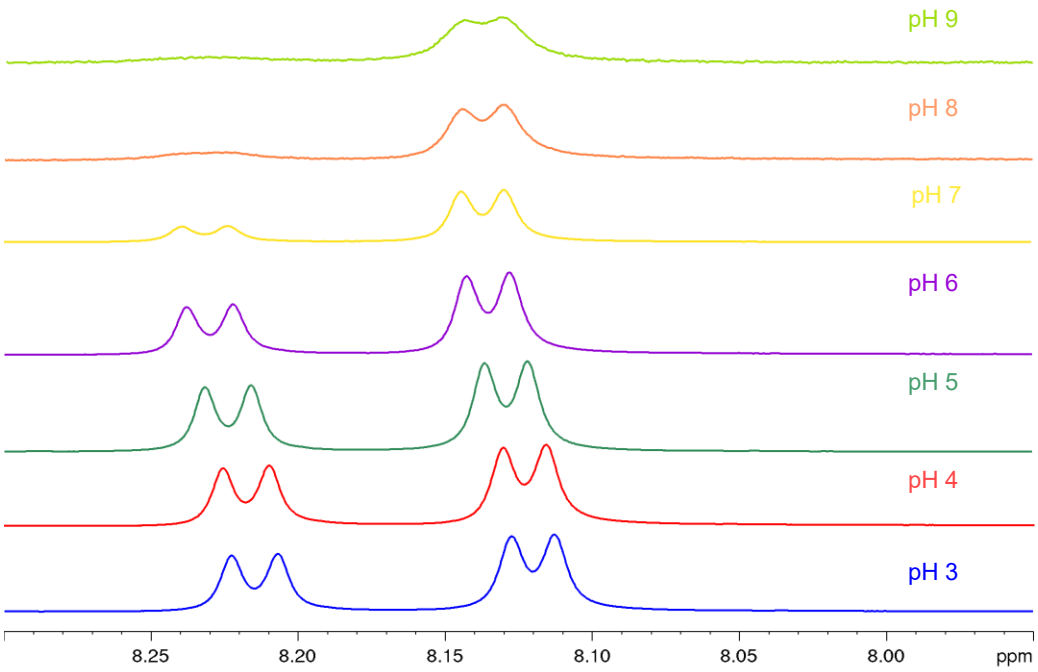

Figure 3. Selected region of the ^{1}H NMR spectra of GlcNAc in H_2O:D_2O 9:1 *v/v* unbuffered solution indicating the ^{1}H NMR resonances of the amide NH protons of GlcNAc anomers in the range of pH 3.0-9.0. The amide resonances of GlcNAc β- and α-anomers at pH 3 were detected at δ 8.22 and δ 8.12 ppm, respectively [13].

Efficient solvent suppression was crucial to the successful observation of GlcNAc NH resonances, as water typically generates a dominant signal in aqueous NMR. The amide NH signal is particularly sensitive to saturation transfer and exchange effects with water, which can dominate the spectra if not carefully managed. Among the various available solvent suppression techniques, the presaturation method (zgpr pulse sequence) was selected for its simplicity and effectiveness in our further experimental setup.

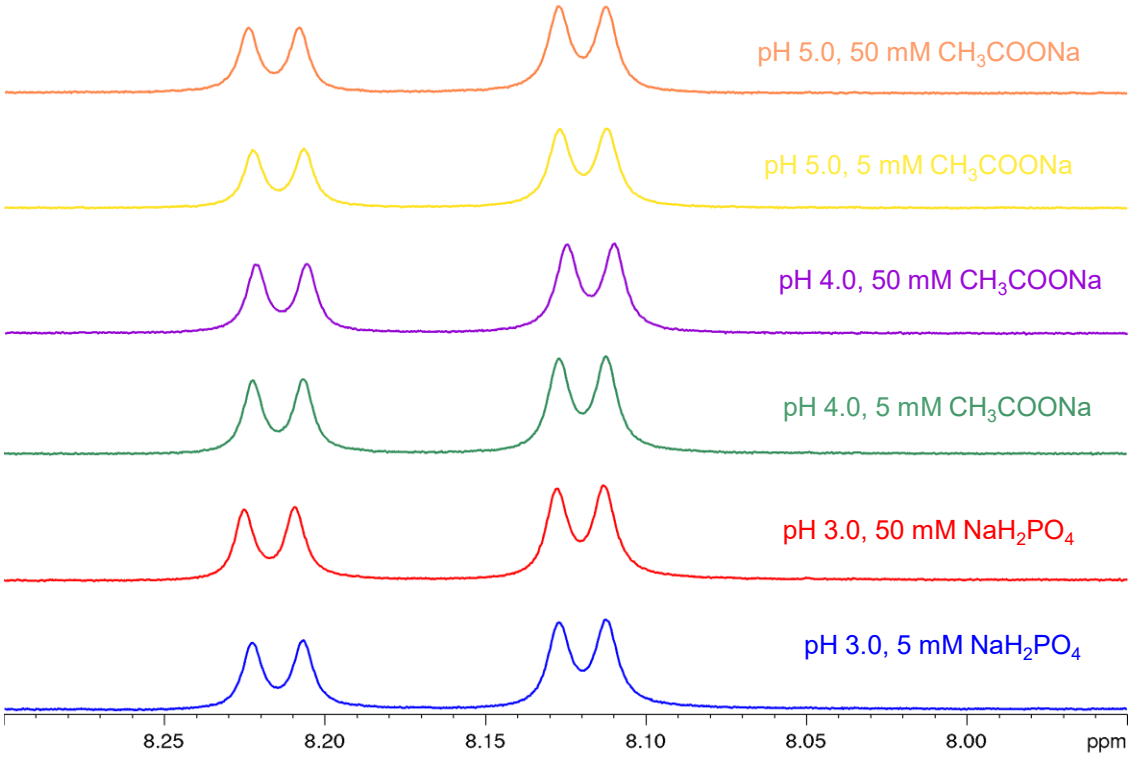

Figure 4. Selected regions of the ^{1}H NMR spectra of GlcNAc in a H_2O:D_2O 9:1 *v/v* solution, recorded within the pH range of 3.0–5.0. Phosphate- and acetate-based buffers were used at concentrations of 5 mM and 50 mM. The anomeric NH proton resonances of GlcNAc are observed at δ 8.22 ppm (β anomer) and δ 8.12 ppm (α anomer).

This method, which involves selectively saturating the water signal prior to acquisition, provided a robust solution for our needs. However, the implementation required precise adjustment of pulse sequence parameters to decouple presaturation from the main sequence relaxation delays. This adjustment ensured that solvent suppression did not inadvertently saturate the exchangeable NH resonances. The utility of such modifications for sensitive proton detection is well supported in the foundational work on solvent suppression methods, which outlined the theoretical and practical framework enabling such targeted optimization [89].

The optimized parameters were applied to ^{1}H-^{15}N HSQC (hsqcetgpsi2) and ^{1}H-^{15}N HSQC-TOCSY (hsqcdietgpsi) sequences, integrating presaturation into the experimental design. Power levels and relaxation delays were carefully calibrated to maximize NH signal detection while avoiding sample degradation or overheating. The results, as shown

in Figure 5, highlight the improvements in spectral clarity and resolution achieved through these modifications.

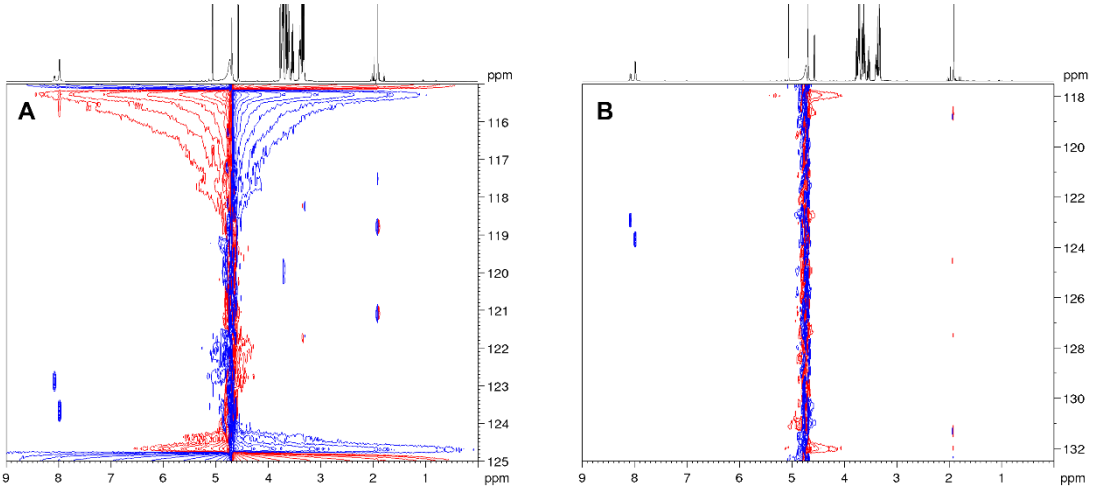

Figure 5. ^{1}H-^{15}N HSQC spectra of GlcNAc in H_2O:D_2O 9:1 *v/v* at pH 3.0 with the pulse sequence hsqcetgpsi2 unmodified (**A**) and with presaturation (**B**).

4.2. Complete ^{1}H, ^{13}C, and ^{15}N resonance assignments of the HMO samples

4.2.1. Introduction to HMO resonance assignments

The structural elucidation and comprehensive NMR analysis of HMOs represent a critical step toward understanding their complex structural diversity and biological significance. While the tri-, tetra-, and pentasaccharides investigated herein, are more widespread, complete NMR assignments for these molecules remain notably absent from the literature. Although previous studies have employed NMR techniques to investigate some of these HMOs for certain structural or functional purposes [50,52,53,55,57,73,90–95], these works focused on limited aspects rather than providing comprehensive resonance assignments.

The isolated hexa-, hepta-, and octasaccharides represent more complex HMOs, posing additional challenges. The incomplete or altogether absent resonance assignments for these HMOs in existing studies underscore the need for advanced structural analysis. For instance, while Dua *et al*. in 1985 identified some distinctive non-overlapping ^{1}H resonances in LNH and its mono- and difucosylated derivatives [90], and Bandara *et al*. presented synthesized hexasaccharides LNH and LNnH with corresponding NMR spectra, no in-depth characterization of these or related HMOs had been conducted

[91,92]. Moreover, the exact structural details of certain HMOs, such as MFLNnH I and II, particularly regarding the fucose binding site, remained unresolved until now [90,96–98].

This study represents the first in the literature to observe NH proton resonances in HMOs, leveraging heteronuclear ^{1}H-^{15}N correlation to expand the scope of structural insights. The novel observation of NH proton resonances provides additional dimensions of information, facilitating the unambiguous assignment of amide groups and connectivity between monosaccharide units.

The ^{1}H, ^{13}C, and ^{15}N NMR resonance assignment of the HMOs were deduced from 1D and 2D NMR spectra using 3-10 mM HMO solutions in an H_2O:D_2O 9:1 (*v*/*v*) mixture, prepared in a 5 mM phosphate-buffered pH 3.0 solution with 0.5 mM DSS as chemical shift reference.

The workflow employed for resonance assignment integrates various NMR experiments and is applicable to the range of HMOs with the degrees of polymerization (dp) studied here. Despite the variations in structure and complexity, the fundamental approach remains consistent.

4.2.2. NMR experimental approach and workflow

The ^{1}H NMR spectrum served as the primary entry point for resonance assignment in all cases (Figure 6A and 7A). Depending on the composition of the analysed HMO –whether it contained one or two GlcNAc units or one GlcNAc and one Neu5Ac unit– one or two strongly downfield-shifted NH resonances were observed in the ^{1}H spectra (Figure 6A, 6B and 7A). While the anomeric region was relatively well-resolved for HMOs with smaller dp values (Figure 7A), more complex HMOs exhibited significant crowding and, in some cases, overlap with the water resonance (Figure 6C). These characteristics highlighted the need of complementary experiments to eliminate uncertainties. To map the spin systems of individual monosaccharides, 1D TOCSY series were recorded (Figure 6D). These experiments provided essential insights into the multiplicity patterns of overlapping resonances and facilitated the identification of specific building blocks.

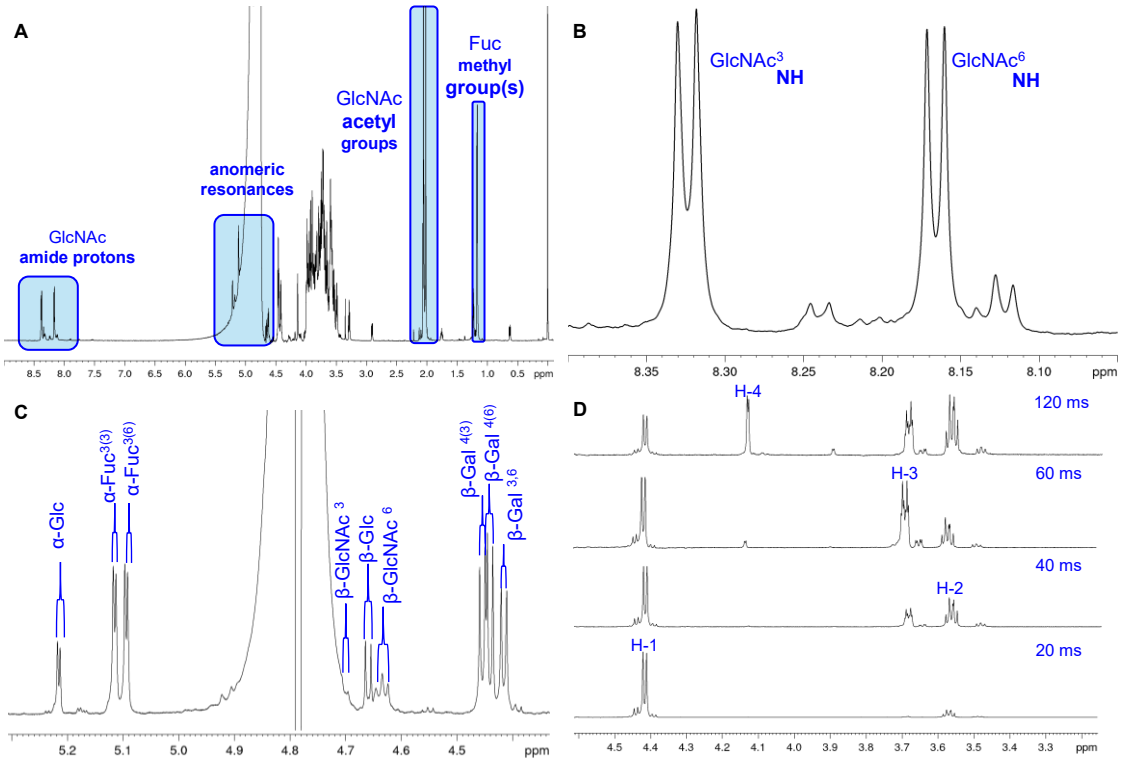

Figure 6. Representative ^{1}H NMR spectrum sections of HMOs with dp 6-8 containing two GlcNAc moieties. (**A**) Characteristic ^{1}H spectral regions of MFLNnH II. (**B**) Two distinct amide resonances in the ^{1}H spectrum of LNH. (**C**) Assignment of each anomeric ^{1}H resonance of DFLNnH. (**D**) Selective gradient ^{1}H TOCSY series of the resonance δ 4.42 (β-Gal^{3,6} H-1) [99].

Additionally, 2D TOCSY spectra were recorded across the entire chemical shift range to confirm assignments and resolve ambiguities (Figure 7D). Singlet resonances of acetyl-groups and doublet resonances of fucose's methyl-groups were distinctly observed in the ^{1}H spectrum at lower chemical shift values, aiding in the identification of these structural motifs (Figure 6A and 7A). In cases of severe overlap, particularly in the densely populated region between 3.5–4.0 ppm, band-selective ^{1}H-^{13}C HSQC spectra were contributory (Figure 7C). These experiments in conjunction with DEPTQ spectra allowed the assignment of individual carbon resonances and resolution of ambiguities due to spectral overlap. To establish ^{1}H-^{1}H connectivities between well-resolved resonances, COSY spectra were recorded. For long-range correlations, the HMBC spectrum proved invaluable, confirming ^{1}H-^{13}C resonance assignments and elucidating connectivity between monosaccharide units. This was particularly useful for resolving structures of HMOs containing multiple acetyl groups. To confirm stereochemistry and spatial relationships among the building blocks, 2D ROESY and selective 1D ROESY

experiments were conducted (Figure 7E). These experiments verified inter-residue connectivities and provided critical information about the spatial arrangement of the HMOs. The complete resonance assignment of the investigated HMOs can be found in Tables 1-4.

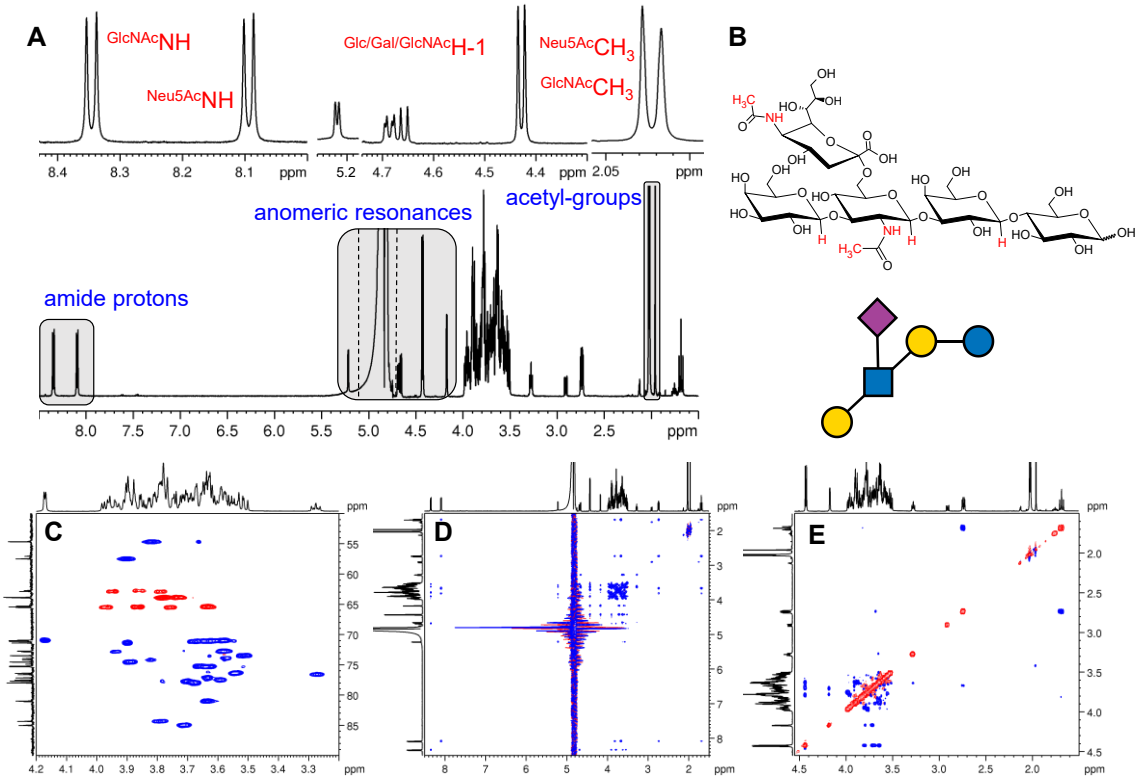

Figure 7. Representative spectra of the NMR workflow shown using the example of the pentasaccharide LSTb. (**A**) The 600 MHz ^{1}H NMR spectrum of LSTb using solvent suppression highlighted the characteristic ^{1}H spectral regions. (**B**) The molecular structure of LSTb. (**C**) The "carbohydrate" region of ^{1}H-^{13}C HSQC spectrum of LSTb. (**D**) 2D ^{1}H-^{1}H TOCSY spectrum of LSTb. (**E**) Selected ^{1}H-^{1}H 2D ROESY spectral region of LSTb [13].

4.2.3. Resonance assignment of tri-, tetra-, and pentasaccharide HMOs

Table 1. The complete ^{1}H, ^{13}C, and ^{15}N resonance assignment of LNT, LNnT, LNFP III, and LNFP III in H_2O: D_2O 9:1 *v/v* solvent at pH 3.0 [13].

	LNT			LNnT			LNFP II			LNFP III		
	^{1}H	**m, *J* [Hz]**	**$^{13}C/^{15}N$**	**^{1}H**	**m, *J* [Hz]**	**$^{13}C/^{15}N$**	**^{1}H**	**m, *J* [Hz]**	**$^{13}C/^{15}N$**	**^{1}H**	**m, *J* [Hz]**	**$^{13}C/^{15}N$**
						α-Glc						
1	5.22	d, 3.7	94.6	5.22	d, 3.7	94.6	5.22	d, 3.7	94.6	5.22	d, 3.7	94.6
2	3.57	dd, 9.9, 3.8	74.0	3.57	dd, 9.9, 3.8	74.0	3.57	dd, 9.9, 3.8	74.0	3.57	dd, 9.9, 3.8	74.0
3	3.82	t, 9.5	74.2	3.82	t, 9.3	74.2	3.82	t, 9.4	74.2	3.82	t, 9.4	74.2
4	3.63	t, 9.5	81.0	3.63	t, 9.3	81.0	3.63	t, 9.4	80.9	3.63	t, 9.4	81.0
5	3.94	m	72.8	3.94	m	72.8	3.94	m	72.8	3.94	m	72.8
6	3.86	m	62.7	3.86	m	62.7	3.85	m	62.7	3.85	m	62.7
						β-Glc						
1	4.66	d, 7.9	98.5	4.66	d, 7.9	98.5	4.66	d, 7.9	98.5	4.66	d, 7.9	98.5
2	3.27	m	76.6	3.27	m	76.6	3.27	m	76.6	3.27	m	76.6
3	3.63	m	77.1	3.63	m	77.1	3.63	m	77.1	3.63	m	77.1
4	3.64	m	80.9	3.64	m	80.9	3.63	m	81.0	3.64	m	80.9
5	n.a.		n.a.	n.a.		n.a.	n.a.		n.a.	n.a.		n.a.
6a	3.95	dd, 12.0, 2.0	62.9	3.95	dd, 12.0, 2.0	62.9	3.95	dd, 12.1, 2.0	62.8	3.95	dd, 12.0, 2.0	62.8
6b	3.79	dd, 12.2, 5.0		3.79	dd, 12.2, 5.0		3.79	dd, 12.1, 5.0		3.79	dd, 12.0, 5.0	
						β-Gal						
1	4.43/4.43	d, 7.7	105.60/57	4.43/4.43	d, 7.9	105.61/58	4.42/4.42	d, 7.9	105.62/58	4.42/4.42	d, 7.9	105.61/58
2	3.60/3.58	dd, 9.8, 7.8	72.80/77	3.60/3.58	dd, 9.8, 7.9	72.76/73	3.59/3.57	dd, 9.8, 7.9	72.75/73	3.59/3.57	dd, 9.8, 7.9	72.76/73
3	3.74/3.72	t, 3.0	84.72/69	3.72/3.71	t, 3.0	84.78/76	3.72/3.70	t, 3.0	84.81/78	3.71/3.69	t, 3.0	84.81/78
4	4.15	d, 3.2	71.13/10	4.15	d, 3.2	71.14/12	4.15	d, 3.4	71.12/10	4.15	d, 3.4	71.19/09
5	n.a.		n.a.	n.a.		n.a.	n.a.		n.a.	n.a.		n.a.
6	3.76	m	63.78/77	3.76	m	63.78/77	3.76	m	63.79/78	3.76	m	63.79/77
						β-GlcNAc						
1	4.72/4.72	d, 8.4	105.3	4.69/4.69	d, 8.3	105.46	4.69/4.69	d, 8.5	105.4	4.70/4.70	d, 8.5	105.3

2	3.90	m	57.5	3.80	m	58.0	3.95	m	58.6	3.96	m	58.7
NH	8.36	d, 9.6	122.48	8.27	d, 9.5	122.98	8.44	d, 9.8	122.39	8.41	d, 9.8	122.27
CO			177.7			177.7			177.5			177.5
CH_3	2.02	s	25.0	2.03	s	25.0	2.03	s	25.1	2.02	s	25.0
3	3.80	t, 9.6	84.8	3.73	m	75.0	4.07	t, 9.6	78.6	3.87	m	77.5
4	3.57	t, 9.6	71.2	3.73	m	80.8	3.75	t, 9.6	74.8	3.94	m	75.7
5	3.47	ddd, 10.0, 5.0, 2.3	77.9	3.58	m	77.3	3.53	dt, 9.5, 3.0	77.9	3.57	m	77.8
6a	3.90	m	63.3	3.95	dd, 12.2, 2.0	62.6	3.94	m	62.4	3.97	m	62.4
6b	3.78	dd, 12.5, 5.3		3.85	dd, 12.2, 4.7		3.86	dd, 12.5, 3.2		3.87	m	
						β-Gal						
1	4.43	d, 8.4	106.2	4.47	d, 7.8	105.53	4.50	d, 7.7	105.55	4.45	d, 7.8	104.46
2	3.52	dd, 9.8, 7.8	73.5	3.54	dd, 9.8, 7.8	73.8	3.48	dd, 9.8, 7.7	73.3	3.49	dd, 9.8, 7.9	73.8
3	3.64	dd, 10.0, 3.0	75.3	3.67	dd, 10.0, 3.3	75.3	3.62	dd, 9.8, 3.4	75.1	3.65	dd, 9.8, 3.3	75.3
4	3.90	d, 3.4	71.3	3.92	d, 3.5	71.3	3.88	d, 3.5	71.2	3.90	d, 3.4	71.2
5	n.a.		n.a.	n.a.		n.a.	n.a.		n.a.	n.a.		n.a.
6	3.76	m	63.8	3.75	m	63.84	3.72	m	64.5	3.72	m	64.3
									α-Fuc			
1							5.02	d, 4.0	100.7	5.12	d, 4.0	101.3
2							3.80	dd, 10.5, 4.0	70.6	3.69	dd, 10.4, 4.0	70.5
3							3.88	dd, 10.3, 3.3	72.0	3.90	dd, 10.4, 3.3	72.0
4							3.79	d, 3.3	74.8	3.79	d, 3.3	74.2
5							4.87	o.l.	69.6	4.83	o.l.	69.4
CH_3							1.17	d, 6.7	18.1	1.17	d, 6.6	18.0

Table 2. The complete ^{1}H, ^{13}C, and ^{15}N resonance assignment of LSTa, LSTb, 3'SL, and 6'SL in H_2O: D_2O 9:1 *v/v* solvent at pH 3.0 [13].

	LSTa			LSTb			3'SL			6'SL		
	^{1}H	**m, *J* [Hz]**	**$^{13}C/^{15}N$**	**^{1}H**	**m, *J* [Hz]**	**$^{13}C/^{15}N$**	**^{1}H**	**m, *J* [Hz]**	**$^{13}C/^{15}N$**	**^{1}H**	**m, *J* [Hz]**	**$^{13}C/^{15}N$**
						α-Glc						
1	5.22	d, 3.7	94.6	5.22	d, 3.8	94.6	5.22	d, 3.8	94.6	5.22	d, 3.7	94.6
2	3.57	dd, 9.9, 3.8	74.0	3.57	dd, 9.9, 3.8	74.0	3.57	dd, 9.9, 3.8	74.0	3.60	dd, 9.8, 3.8	73.9
3	3.82	t, 9.4	74.2	3.82	t, 9.4	74.2	3.83	t, 9.4	74.2	3.84	t, 9.3	74.4
4	3.63	t, 9.4	81.1	3.63	t, 9.4	81.1	3.66	t, 9.4	80.9/80.8	3.61	t, 9.3	82.4/82.3
5	3.94	m	72.8	3.94	m	72.8	3.94	m	72.8	3.95	m	72.7
6	3.86	m	62.7	3.86	m	62.7	3.88	m	62.7	3.88	m	62.9
						β-Glc						
1	4.66	d, 8.0	98.5	4.66	d, 7.9	98.5	4.66	d, 8.0	98.6	4.66	d, 8.0	98.4
2	3.27	m	76.6	3.28	m	76.6	3.28	dd, 9.0, 8.0	76.7	3.30	t, 8.6	76.6
3	3.63	m	77.2	3.63	m	77.2	3.63	t, 9.2	77.1	3.63	m	77.4
4	3.64	m	81.0	3.64	m	81.0	3.67	dd, 9.5, 8.3	80.9/80.8	3.61	m	82.4/82.3
5	n.a.		n.a.	n.a.		n.a.	3.59	ddd, 9.5, 5.0, 2.0	77.5	3.63	m	77.4
6a	3.95	dd, 12.0, 2.0	62.8	3.95	dd, 12.0, 2.0	62.9	3.96	dd, 12.3, 2.0	62.8	3.95	dd, 12.3, 2.0	63.0
6b	3.79	dd, 12.2, 5.0		3.79	dd, 12.2, 5.0		3.82	dd, 12.3, 5.0		3.79	dd, 12.3, 4.4	
						β-Gal						
1	4.43/4.43	d, 7.9	105.60/58	4.43/4.43	d, 7.7	105.60/57	4.52	d, 7.7	105.3	4.42	d, 7.9	105.93/90
2	3.60/3.58	dd, 9.8, 7.9	72.80/78	3.59/3.57	dd, 9.8, 7.9	72.78/74	3.57	dd, 9.9, 7.9	72.2	3.53	dd, 9.8, 7.9	73.6
3	3.74/3.72	t, 2.9	84.65/63	3.72/3.70	t, 3.3	85.04/84.99	4.11/4.10	t, 3.0	78.21/20	3.67/3.65	t, 3.0	75.2
4	4.15	d, 3.2	71.12/10	4.17	d, 3.3	70.97/94	3.95	d, 3.0	70.2	3.93	d, 3.3	71.33/31
5	n.a.		n.a.	n.a.		n.a.	n.a.		n.a.	n.a.		n.a.
6	3.78	m	63.79/78	3.78	m	63.92/91	3.74	m	63.85/84	3.96 3.59	m	66.3
						β-GlcNAc						
1	4.73/4.72	d, 8.4	105.2	4.69/4.68	d, 8.54	105.4						
2	3.90	m	57.4	3.98	m	57.5						
NH	8.34	d, 9.6	122.30	8.35	d, 9.6	122.50						
CO			177.68			177.67						
CH_3	2.02	s	25.1/24.8	2.02	s	25.0						
3	3.80	t, 9.5	84.9	3.79	t, 9.5	84.4						
4	3.57	t, 9.5	71.2	3.63	t, 9.5	71.1						

5	3.47	ddd, 10.0, 5.3, 2.2	77.9	3.54	ddd, 9.8, 5.2, 2.2	76.4						
6a	3.90	m	63.3	3.97	dd, 10.8, 5.7	65.5						
6b	3.78	dd, 12.0, 5.3		3.76	d, 10.8							
				β-Gal								
1	4.50	d, 7.8	106.1	4.43	d, 7.7	106.1						
2	3.54	dd, 9.7, 8.0	71.9	3.52	dd 10.0, 7.8	73.5						
3	4.08	dd, 9.7, 3.0	78.3	3.63	dd, 10.0, 3.3	75.3						
4	3.93	d, 3.0	70.0	3.90	d, 3.4	71.4						
5	n.a.		n.a.	n.a.		n.a.						
6	3.72	m	63.8	3.78/3.74	m	63.9						
						α-Neu5Ac						
1			176.5			176.1			176.5			176.10/09
2			102.3			102.9			102.4			102.9
3α	1.78	t, 12.1	42.5	1.68	t, 12.1	42.8	1.80	t, 12.2	42.3	1.74	t, 12.2	42.8
3β	2.75	dd, 12.4, 4.7		2.74	dd, 12.3, 4.7		2.75	dd, 12.4, 4.7		2.70	dd, 12.4, 4.6	
4	3.68	ddd, 12.4, 4.7, 2.2	71.2	3.68	m	71.1	3.68	ddd, 11.7, 9.7, 4.7	71.2	3.65	ddd, 11.7, 9.7, 4.6	71.2
5	3.84	m	54.4	3.82	m	54.7	3.85	m	54.5	3.85	m	54.6
CH_3	2.02	s	25.1/24.8	2.03	s	24.8	2.03	s	24.8	2.02	s	24.8
NH	8.07	d, 9.3	122.91	8.09	d, 9.3	123.14	8.08	d, 9.3	122.98	8.06	d, 9.4	123.01
CO			177.72			177.79			177.8			177.7
6	3.62	dd, 10.4, 1.8	75.5	3.66	dd, 10.4, 1.8	75.2	3.62	dd, 10.4, 1.8	75.6	3.72	dd, 10.4, 1.7	75.2
7	3.59	d, 9.0	70.8	3.58	d, 9.0	71.0	3.59		70.9	3.56	d, 9.0	71.2
8	3.87	m	74.7	3.88	m	74.5	3.88	m	74.6	3.89	m	74.6
9a	3.85	m	65.3	3.87	m	65.4	3.87	m	65.4	3.88	m	65.5
9b	3.64	m		3.63	m		3.64	m		3.64	m	

4.2.4. Resonance assignment of hexa-, hepta-, and octasaccharide HMOs

Table 3. The complete ^{1}H, ^{13}C, and ^{15}N resonance assignment of LNH, LNnH, and MFLNH III in H_2O: D_2O 9:1 *v/v* solvent at pH 3.0 [99].

LNH	**^{1}H**	**m, *J***	**^{13}C / ^{15}N**	**LNnH**	**^{1}H**	**m, *J***	**^{13}C / ^{15}N**	**MFLNH III**	**^{1}H**	**m, *J***	**^{13}C / ^{15}N**
α-Glc				**α-Glc**				**α-Glc**			
1	5.21	d, 3.8	94.6	**1**	5.22	d, 3.4	94.6	**1**	5.22	d, 3.8	94.6
2	3.58	dd, 9.9, 3.8	74.0	**2**	3.58	dd, 10.0, 3.8	74.0	**2**	3.58	m	74.0
3	3.82	t, 9.5	74.2	**3**	3.82	t, 9.6	74.2	**3**	3.83	m	74.2
4	3.60	m	81.7/81.6	**4**	3.60	m	81.5/81.6	**4**	3.60	m	81.7
5	3.93	m	72.7	**5**	3.93	m	72.7	**5**	3.93	m	72.7
6	3.86	m	62.7	**6**	3.86	m	62.7	**6**	3.86	m	62.7
β-Glc				**β-Glc**				**β-Glc**			
1	4.66	d, 7.9	98.5	**1**	4.66	d, 8.2	98.5	**1**	4.66	d, 7.8	98.5
2	3.29	dd, 10.0, 8.1	76.7	**2**	3.28	dd, 9.9, 8.0	76.7	**2**	3.28	dd, 10.0, 8.0	76.7
3	3.64	m	77.2	**3**	3.64	m	77.2	**3**	3.64	m	77.2
4	3.60	m	81.7/81.6	**4**	3.60	m	81.5/81.6	**4**	3.60	m	81.7
5	3.62	m	n.a.	**5**	n.a.		n.a.	**5**	3.62	m	n.a.
6a	3.94	d, 12.0	62.8	**6a**	3.94	d, 12.0	62.8	**6a**	3.95	m	62.9
6b	3.79	d, 12.0	62.8	**6b**	3.79	d, 12.0	62.8	**6b**	3.80	m	62.9
β-Gal ^{3,6}				**β-Gal ^{3,6}**				**β-Gal ^{3,6}**			
1	4.42	d, 7.8	105.66/65	**1**	4.42	d, 7.9	105.7	**1**	4.42	d, 7.8	105.7
2	3.58	m	72.7	**2**	3.58	m	72.6	**2**	3.58	m	72.7
3	3.72	t, 3.3	84.43/40	**3**	3.70	t, 3.0	84.5	**3**	3.72	t, 3.2	84.4
4	4.14	d, 3.0	71.2	**4**	4.14	d, 3.0	71.2	**4**	4.13	d, 3.0	71.1
5	3.82	m	76.2	**5**	3.82	m	76.2	**5**	3.82	m	76.1
6a	3.98	m	71.4	**6a**	3.98	m	71.3	**6a**	3.97	m	71.4
6b	3.83	m	71.4	**6b**	3.83	m	71.3	**6b**	3.83	m	71.4
β-GlcNAc ^{3}				**β-GlcNAc ^{3}**				**β-GlcNAc ^{3}**			
1	4.72	d, 8.0	105.2	**1**	4.69	d, 8.3	105.4	**1**	4.72	d, 8.3	105.2

2	3.89	m	57.5	**2**	3.79	m	58	**2**	3.89	m	57.5
NH	**8.32**	**d, 9.6**	**122.37**	**NH**	**8.24**	**d, 9.5**	**122.88**	**NH**	**8.32**	**d, 9.6**	**122.37**
CO			177.7	**CO**			177.7	**CO**			177.7
CH_3	2.02	s	25.0	**CH_3**	2.03	s	25.0	**CH_3**	2.02	s	25.0
3	3.80	m	84.8	**3**	3.73	m	75.0	**3**	3.80	m	84.8
4	3.57	t, 9.5	71.2	**4**	3.73	m	80.8	**4**	3.57	t, 9.3	71.2
5	3.47	m	77.9	**5**	3.58	m	77.25	**5**	3.47	m	77.9
6a	3.90	m	63.3	**6a**	3.96	d, 12.0	62.7	**6a**	3.90	m	63.3
6b	3.78	m	63.3	**6b**	3.85	d, 12.0	62.7	**6b**	3.78	m	63.3
β-GlcNAc [6]				**β-GlcNAc [6]**				**β-GlcNAc [6]**			
1	4.63	d, 8.0	103.7	**1**	4.63	d, 8.0	103.7	**1**	4.63	d	103.5
2	3.75	m	57.8	**2**	3.75	m		**2**	3.90	m	58.4
NH	**8.17**	**d, 9.0**	**121.81**	**NH**	**8.17**	**d, 9.1**	**121.81**	**NH**	**8.31**	**d, 9.6**	**121.18**
CO			177.3	**CO**			177.3	**CO**			177.1
CH_3	2.05	s	25.2	**CH_3**	2.06	s	25.2	**CH_3**	2.05	s	25.3
3	3.72	m	75.2	**3**	3.72	m	75.2	**3**	3.89	m	77.5
4	3.72	m	81.1	**4**	3.72	m	81.1	**4**	3.92	m	76.0
5	3.60	m	77.4	**5**	3.61	m	77.4	**5**	3.60	m	78.1
6a	3.99	d, 12.0	62.8	**6a**	3.99	d, 12.0	62.8	**6a**	4.00	d, 12.0	62.6
6b	3.84	d, 12.0	62.8	**6b**	3.84	d, 12.0	62.8	**6b**	3.86	d, 12.0	62.6
β-Gal [3(3)]				**β-Gal [4(3)]**				**β-Gal [3(3)]**			
1	4.43	d, 7.6	106.2	**1**	4.47	d, 7.8	105.56/54	**1**	4.43	d, 7.6	106.2
2	3.52	dd, 10.5, 9.6	73.5	**2**	3.54	dd, 10.0, 8.0	73.8	**2**	3.52	dd, 10.5, 8.0	73.2
3	3.64	dd, 10.0, 3.6	75.29	**3**	3.66	dd, 10.0, 3.8	75.3	**3**	3.65	dd, 9.8, 3.3	75.3
4	3.91	d, 3.2	71.3	**4**	3.92	m	71.4	**4**	3.92/3.90	d, 2.8	71.3/71.2
5	3.70	m	78.0	**5**	3.72	m	78.1	**5**	3.70	m	78.0
6	3.76	m	63.8	**6**	3.76	m	63.8	**6**	3.76	m	63.8
β-Gal [4(6)]				**β-Gal [4(6)]**				**β-Gal [4(6)]**			
1	4.46	d, 7.8	105.55	**1**	4.46	d, 7.8	105.56/54	**1**	4.44	d, 7.6	104.5

2	3.54	dd, 10.3, 8.0	73.8	**2**	3.54	dd, 10.0, 8.0	73.8	**2**	3.49	m	73.8
3	3.66	dd, 10.0, 3.3	75.33	**3**	3.66	dd, 10.0, 3.8	75.3	**3**	3.65	dd, 9.8, 3.3	75.3
4	3.92	d, 3.0	71.4	**4**	3.92	m	71.4	**4**	3.92/3.90	d, 2.8	71.3/71.2
5	3.72	m	78.1	**5**	3.72	m	78.1	**5**	3.59	m	77.6
6	3.76	m	63.8	**6**	3.76	m	63.8	**6**	3.72	m	64.3
								α-Fuc $^{3(6)}$			
								1	5.09	d, 3.8	101.3
								2	3.69	dd, 10.4, 3.9	70.5
								3	3.90	dd, 10.4, 3.2	72.0
								4	3.79	d, 2.0	74.7
								5	4.82	o.l.	69.4
								CH_3	1.17	d, 6.5	18.0

Table 4. The complete ^{1}H, ^{13}C, and ^{15}N resonance assignment of MFLNnH I, MFLNnH II, and DFLNnH in H_2O: D_2O 9:1 *v/v* solvent at pH 3.0 [99].

MFLNnH I	**^{1}H**	**m, *J***	**^{13}C / ^{15}N**	**MFLNnH II**	**^{1}H**	**m, *J***	**^{13}C / ^{15}N**	**DFLNnH**	**^{1}H**	**m, *J***	**^{13}C / ^{15}N**
α-Glc				**α-Glc**				**α-Glc**			
1	5.22	d, 3.7	94.6	**1**	5.22	d, 3.7	94.6	**1**	5.22	d, 3.7	94.6
2	3.58	dd, 9.8, 3.8	74.00	**2**	3.58	dd, 9.8, 3.8	74.0	**2**	3.58	dd, 9.8, 3.8	74.0
3	3.82	t, 9.3	74.2	**3**	3.82	t, 9.3	74.2	**3**	3.82	t, 9.3	74.2
4	3.60	m	81.7/81.8	**4**	3.60	m	81.6	**4**	3.60	m	81.7/81.6
5	3.93	m	72.7	**5**	3.93	m	72.7	**5**	3.93	m	72.7
6	3.86	m	62.7	**6**	3.86	m	62.7	**6**	3.86	m	62.7
β-Glc				**β-Glc**				**β-Glc**			
1	4.66	d, 7.9	98.5	**1**	4.66	d, 8.0	98.5	**1**	4.66	d, 7.9	98.5
2	3.28	dd, 10.1, 8.1	76.7	**2**	3.29	dd, 10.1, 8.1	76.7	**2**	3.28	dd, 10.1, 8.1	76.7
3	3.63	m	77.2	**3**	3.63	m	77.2	**3**	3.63	m	77.2
4	3.60	m	81.7/81.8	**4**	3.60	m	81.5	**4**	3.60	m	81.7/81.6
5	n.a.		n.a.	**5**	n.a.		n.a.	**5**	n.a.		n.a.
6a	3.94	d, 12.0	62.8	**6a**	3.94	d, 12.0	62.8	**6a**	3.94	d, 12.0	62.8
6b	3.79	d, 12.0	62.8	**6b**	3.79	d, 12.0	62.8	**6b**	3.79	d, 12.0	62.8
β-Gal ^{3,6}				**β-Gal ^{3,6}**				**β-Gal ^{3,6}**			
1	4.42	d, 7.9	105.7	**1**	4.41	d, 7.8	105.7	**1**	4.42	d, 7.8	105.7
2	3.58	m	72.69/62	**2**	3.57	m	72.62/60	**2**	3.57	m	72.6
3	3.70	t, 3.0	84.51/49	**3**	3.69	t, 3.0	84.54/52	**3**	3.69	t, 3.0	84.54/52
4	4.13	d, 3.1	71.1	**4**	4.14	d, 3.0	71.15/13	**4**	4.13	d, 3.3	71.1
5	3.82	m	76.1	**5**	3.82	m	76.1	**5**	3.82	m	76
6a	3.97	m	71.3	**6a**	3.97	m	71.3	**6a**	3.97	m	71.3
6b	3.83	m	71.3	**6b**	3.83	m	71.3	**6b**	3.83	m	71.3
β-GlcNAc ^{3}				**β-GlcNAc ^{3}**				**β-GlcNAc ^{3}**			
1	4.69	d, 8.3	105.4	**1**	4.70	d, 8.2	105.2	**1**	4.70	d, 8.3	105.2
2	3.80	m	58.0	**2**	3.95	ddd, 9.7, 9.5, 8.2	58.7	**2**	3.96	ddd, 9.7, 9.5, 8.3	58.7
NH	**8.24**	**d, 9.5**	**122.88**	**NH**	**8.38**	**d, 9.7**	**122.19**	**NH**	**8.38**	**d, 9.7**	**122.19**

CO			177.6	**CO**			177.4	**CO**			177.4
CH_3	2.03	s	25.0	**CH_3**	2.02	s	25.0	**CH_3**	2.02	s	25.0
3	3.73	m	75.0	**3**	3.87	t, 9.5	77.45/42	**3**	3.87	t, 9.5	77.44/42
4	3.73	m	80.8	**4**	3.94	m	75.7	**4**	3.94	m	75.7
5	3.58	m	77.25	**5**	3.57	m	77.8	**5**	3.57	m	77.8
6a	3.96	d, 12.2	62.7	**6a**	3.97	m	62.4	**6a**	3.97	m	62.4
6b	3.85	dd, 12.1, 4.6	62.7	**6b**	3.87	m	62.4	**6b**	3.87	m	62.4
β-GlcNAc [6]				**β-GlcNAc [6]**				**β-GlcNAc [6]**			
1	4.63	d	103.5	**1**	4.63	d, 8.1	103.7	**1**	4.63	d, 8.2	103.5
2	3.90	m	58.4	**2**	3.75	m	57.8	**2**	3.90	m	58.4
NH	**8.31**	**d, 9.6**	**121.18**	**NH**	**8.17**	**d, 9.0**	**121.82**	**NH**	**8.32**	**d, 9.3**	**121.19**
CO			177.1	**CO**			177.3	**CO**			177.1
CH_3	2.05	s	25.3	**CH_3**	2.05	s	25.2	**CH_3**	2.05	s	25.3
3	3.89	m	77.56/53	**3**	3.72	m	75.3	**3**	3.89	m	77.55
4	3.92	m	76.0	**4**	3.72	m	81.1	**4**	3.92	m	76.0
5	3.60	m	78.1	**5**	3.61	m	77.4	**5**	3.60	m	78.1
6a	4.00	d, 11.4	62.6	**6a**	3.99	dd, 12.2, 1.8	62.8	**6a**	4.00	d, 12.0	62.6
6b	3.86	dd, 12.4, 3.8	62.6	**6b**	3.84	dd, 12.2, 5.7	62.8	**6b**	3.86	d, 12.0	62.6
β-Gal [4(3)]				**β-Gal [4(3)]**				**β-Gal [4(3)]**			
1	4.47	d, 7.7	105.5	**1**	4.45	d, 7.7	104.5	**1**	4.45	d, 7.8	104.45
2	3.54	dd, 9.7, 8.0	73.77	**2**	3.49	dd, 10.8, 7.9	73.9	**2**	3.49	dd, 10.1, 8.0	73.85/82
3	3.67	dd, 10.0, 3.3	75.33	**3**	3.65	dd, 10.1, 3.3	75.3	**3**	3.65	dd, 9.8, 3.3	75.30/29
4	3.92	d, 3.2	71.4	**4**	3.90	d, 3.2	71.2	**4**	3.90	d, 3.1	71.15/14
5	3.60	m	78.1	**5**	3.59	m	77.6	**5**	3.59	m	77.6
6	3.76	m	63.8	**6**	3.72	m	64.3	**6**	3.73	m	64.29/28
β-Gal [4(6)]				**β-Gal [4(6)]**				**β-Gal [4(6)]**			
1	4.44	d, 7.8	104.5	**1**	4.46	d, 7.7	105.6	**1**	4.44	d, 7.8	104.53
2	3.49	dd, 9.5, 8.0	73.82	**2**	3.54	dd, 10.3, 8.0	73.8	**2**	3.49	dd, 10.1, 8.0	73.85/82
3	3.65	dd, 9.8, 3.3	75.29	**3**	3.66	dd, 10.1, 3.3	75.3	**3**	3.65	dd, 9.8, 3.3	75.30/29

4	3.90	d, 3.2	71.1	**4**	3.92	d, 3.1	71.4	**4**	3.90	d, 3.1	71.15/14
5	3.59	m	77.6	**5**	3.72	m	78.1	**5**	3.59	m	77.6
6	3.72	m	64.3	**6**	3.76	m	63.8	**6**	3.73	m	64.29/28
α-Fuc $^{3(6)}$				**α-Fuc $^{3(3)}$**				**α-Fuc $^{3(3)}$**			
1	5.09	d, 3.9	101.3	**1**	5.12	d, 3.9	101.3	**1**	5.12	d, 3.9	101.28
2	3.69	dd, 10.4, 3.8	70.5	**2**	3.69	dd, 10.4, 4.0	70.5	**2**	3.69	dd, 10.3, 3.9	70.5
3	3.89	dd, 10.4, 3.2	72.0	**3**	3.90	dd, 10.4, 3.2	72.0	**3**	3.90	dd, 10.4, 3.5	72.04/02
4	3.79	d, 2.6	74.7	**4**	3.79	d, 2.7	74.7	**4**	3.79	d, 2.7	74.7
5	4.82	o.l.	69.4	**5**	4.82	o.l.	69.4	**5**	4.82	o.l.	69.42/38
CH_3	1.17	d, 6.6	18.0	**CH_3**	1.17	d, 6.6	18.0	**CH_3**	1.17	d, 6.6	18.0
								α-Fuc $^{3(6)}$			
								1	5.09	d, 3.9	101.32/31
								2	3.69	dd, 10.3, 3.9	70.5
								3	3.89	dd, 10.4, 3.5	72.04/02
								4	3.79	d, 2.7	74.7
								5	4.82	o.l.	69.42/38
								CH_3	1.17	d, 6.6	18.0

5. DISCUSSION

5.1. General phenomena in NMR spectra across HMOs of varying complexity and instrumentation

The HMOs were analysed using two different NMR spectrometers depending on their dp. For HMOs with dp 3–5 (tri- to pentasaccharides), spectra were recorded at 600 MHz, while for the more complex HMOs with dp 6–8 (hexa- to octasaccharides), limited sample amounts and spectral resolution challenges necessitated the use of an 800 MHz spectrometer.

A common feature observed across all HMOs was the presence of the reducing-end Glc residue, which consistently exhibited both α- and β-anomeric forms. As a result, two sets of resonances were assigned to this residue, clearly marked as separate building blocks in the assignment tables (Tables 1-4). In certain cases, particularly for the β-Glc residue, the H-5 resonance could not be unambiguously assigned due to strong overlap, an issue noted in both the dp 3–5 and dp 6–8 HMOs.

The resonance doubling caused by anomeric forms was also reflected on the H-1, H-2, and H-3 resonances of the adjacent Gal residue. This anomeric splitting was more evident in the spectra recorded at 600 MHz for dp 3–5 HMOs and was consistently highlighted in the assignment tables using a slash (/) notation. This phenomenon was observed less frequently for dp 6–8 HMOs, and the splitting was hardly resolvable, therefore, average chemical shift values were reported to two decimal places.

Similarly, for the Gal residue, located adjacent to the Glc unit at the reducing end, anomeric splitting was evident in nearly all ^{13}C resonances for dp 3–5 HMOs at 600 MHz. However, this effect was less pronounced or unresolved in the larger (dp 6–8) HMOs studied at 800 MHz. In such cases, the average ^{13}C chemical shifts were reported to one decimal place. Where splitting was still observable, the values were separated with a slash notation and provided to two decimal places for higher accuracy.

Another consistent feature was the minor anomeric splitting observed in the H-1 resonance of GlcNAc, the third monosaccharide residue. This phenomenon was observed at 600 MHz in dp 3–5 HMOs but became negligible in the spectra of dp 6–8 HMOs.

One of the most challenging resonances to resolve under the tested conditions was the H-5 resonances of the Gal residues adjacent to the glucose unit at the reducing end for each

HMO with dp 3–5, as well as the H-5 of the other Gal moiety (linked to the GlcNAc unit) in each tetra- and pentasaccharides. For dp 3–5 HMOs, the assignment of this resonance remained uncertain due to insufficient resolution, even with selective TOCSY excitation. However, at 800 MHz, the enhanced resolution enabled the unambiguous assignment of the H-5 resonance in dp 6–8 HMOs.

Among the investigated HMOs, the GlcNAc moiety was fully assignable across the entire range of dp values. Similarly, for HMOs containing a fucose moiety, all resonances associated with this unit could also be completely assigned.

Special consideration was required for HMOs containing both GlcNAc and Neu5Ac moieties, such as for the isomeric pair of LSTa and LSTb. While these HMOs exhibited overlapping *N*-acetyl CH_3 resonances in LSTa, the corresponding signals in LSTb were resolved. The non-overlapping acetyl CH_3 and carbonyl groups of LSTb were unequivocally distinguished and assigned using selective HSQC and HMBC spectra, enabling clear differentiation between the two isomers.

5.2. Comparison of the NMR characteristics of the isomeric tri-, tetra-, and pentasaccharide HMOs

5.2.1. LNT–LNnT

This pair of isomeric tetrasaccharides shares the same monosaccharide composition, differing only in the position of the Gal attachment to the GlcNAc residue. In LNT, Gal elongates GlcNAc at position 3 (type 1 chain), while in LNnT, it attaches at position 4 (type 2 chain). The ^{1}H chemical shifts of the GlcNAc moiety reveal significant differences at positions 2 ($\Delta\delta_{H\text{-}2}$ = 0.10 ppm), 3 ($\Delta\delta_{H\text{-}3}$ = 0.07 ppm), 4 ($\Delta\delta_{H\text{-}4}$ = 0.16 ppm), and 6 ($\Delta\delta_{H\text{-}6b}$ = 0.07 ppm). Similarly, ^{13}C resonances exhibit notable shifts at positions 3 ($\Delta\delta_{C\text{-}3}$ = 9.8 ppm) and 4 ($\Delta\delta_{C\text{-}4}$ = 9.6 ppm) of the GlcNAc unit, reflecting the linkage variations (see Figure 8A).

The amide ^{1}H resonances also differ by $\Delta\delta_{NH}$ = 0.09 ppm, with the ^{15}N chemical shifts being sensitive to the linkage type (βGal1-3βGlcNAc vs. βGal1-4βGlcNAc), showing a $\Delta\delta_{N}$ = 0.50 ppm difference (see Figure 8B). Similar patterns are observed in the core disaccharides containing the Gal-GlcNAc moiety, specifically lacto-*N*-biose (LNB, Gal1-3GlcNAc) and *N*-acetyllactosamine (LacNAc, Gal1-4GlcNAc). These disaccharides exhibit analogous chemical shift variations in their amide (^{1}H and ^{15}N) resonances,

consistent with their respective tetrasaccharides (see Figures A75-A76 and Table A1 in the Appendix).

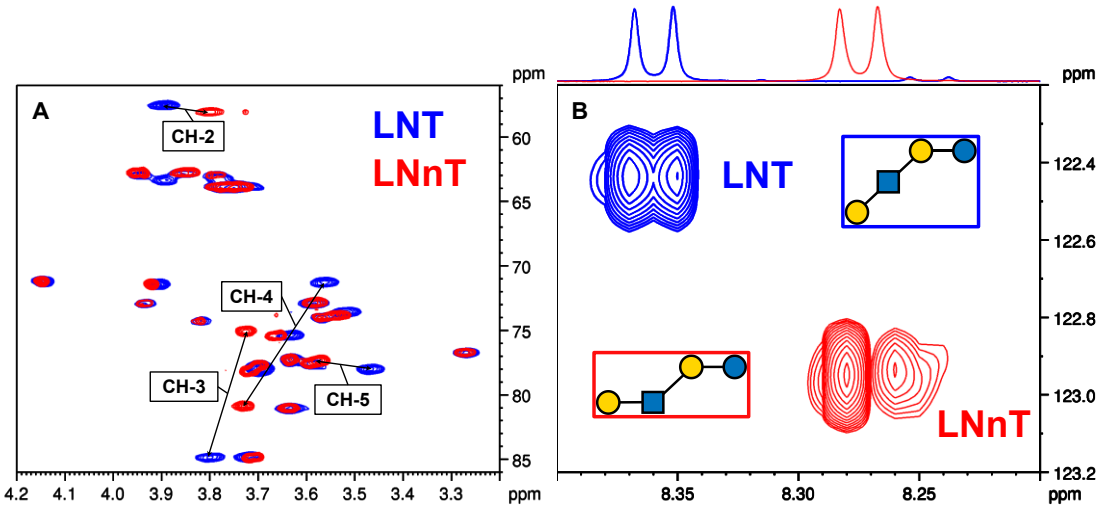

Figure 8. Overlaid 2D NMR spectra of LNT and LNnT. (**A**) Overlaid ^{1}H-^{13}C HSQC spectra of LNT and LNnT, illustrating ^{1}H and ^{13}C NMR chemical shift perturbations of the GlcNAc moiety. (**B**) Overlaid ^{1}H-^{15}N HSQC spectra of LNT and LNnT, highlighting the distinct ^{1}H-^{15}N correlations of the GlcNAc unit in these isomeric tetrasaccharides [13].

5.2.2. LNFP II–LNFP III

These isomeric pentasaccharides differ in the attachment of the Fuc and Gal moieties to the GlcNAc residue. In LNFP II, Fuc attaches at position 4 and Gal at position 3, while in LNFP III, this configuration is reversed (see Figure 9A). The ^{1}H and the ^{13}C NMR chemical shifts of the GlcNAc unit show substantial differences at the elongation sites: at position 3 ($\Delta\delta_{H\text{-}3} = 0.20$ ppm and $\Delta\delta_{C\text{-}3} = 1.1$ ppm) and at position 4 ($\Delta\delta_{H\text{-}4} = 0.19$ ppm and $\Delta\delta_{C\text{-}4} = 0.9$ ppm). The Fuc moiety also displays noticeable variations, with $\Delta\delta_{H\text{-}1} = 0.10$ ppm and $\Delta\delta_{C\text{-}1} = 0.6$ ppm and $\Delta\delta_{H\text{-}2} = 0.11$ ppm. Similar effects are observed in the Gal moiety at the connection site ($\Delta\delta_{C\text{-}1} = 1.09$ ppm).

The amide resonances demonstrate modest differences ($\Delta\delta_{NH}$= 0.03 ppm), with ^{15}N chemical shifts showing a slightly larger variation ($\Delta\delta_{N}$ = 0.12 ppm) (Figure 9A).

5.2.3. LSTa–LSTb

This pair of pentasaccharides contains two different *N*-acetyl groups due to the presence of both GlcNAc and Neu5Ac moieties. LSTa has a linear structure with the Neu5Ac unit

linked to the Gal moiety, while LSTb adopts a branched structure, with GlcNAc connected to both Gal and Neu5Ac (see Figure 9B).

Significant differences are evident in the ^{1}H NMR assignments at position 3 of the Gal unit ($\Delta\delta_{H\text{-}3}$ = 0.45 ppm), indicating the presence or absence of the Neu5Ac unit. Corresponding ^{13}C resonances also show large shifts at positions 2 and 3 of the Gal unit ($\Delta\delta_{C\text{-}2}$ = 1.6 ppm and $\Delta\delta_{C\text{-}3}$ = 3.0 ppm) and at positions 5 and 6 of the GlcNAc moiety ($\Delta\delta_{C\text{-}5}$ = 1.5 ppm and $\Delta\delta_{C\text{-}6}$ = 2.2 ppm, respectively). Additionally, the axial H-3 resonance of Neu5Ac provides a clear and reliable distinction between the isomers, with a characteristic shift of $\Delta\delta_{H\text{-}3ax}$ = 0.10 ppm.

The distinction between the *N*-acetyl groups of GlcNAc and Neu5Ac is confirmed through 2D TOCSY experiments. Although the ^{1}H amide shifts are minor ($\Delta\delta_{NH}$ = 0.01 for GlcNAc and $\Delta\delta_{NH}$ = 0.02 ppm for Neu5Ac), the ^{15}N chemical shifts are more pronounced ($\Delta\delta_{N}$ = 0.20 ppm for GlcNAc and $\Delta\delta_{N}$ = 0.23 ppm for Neu5Ac) aiding in isomeric distinction (Figure 9B).

5.2.4. 3'SL–6'SL

In these trisaccharides, Neu5Ac connects to the lactose core at different positions. Distinct chemical shift differences are observed at positions 3 and 6 of the Gal unit in both ^{1}H ($\Delta\delta_{H\text{-}3}$ = 0.44 ppm; $\Delta\delta_{H\text{-}6}$ = 0.22 ppm) and ^{13}C ($\Delta\delta_{C\text{-}3}$ 3 = 3.0 ppm; $\Delta\delta_{C\text{-}6}$ = 2.5 ppm) spectra. As with the LST isomers, the axial H-3 resonance of Neu5Ac is sensitive to structural variations ($\Delta\delta_{H\text{-}3ax}$ = 0.06 ppm).

The amide ^{1}H ($\Delta\delta_{NH}$ = 0.02 ppm) and ^{15}N ($\Delta\delta_{N}$ = 0.03 ppm) resonances show minimal sensitivity to the differing linkages (Figure 9C).

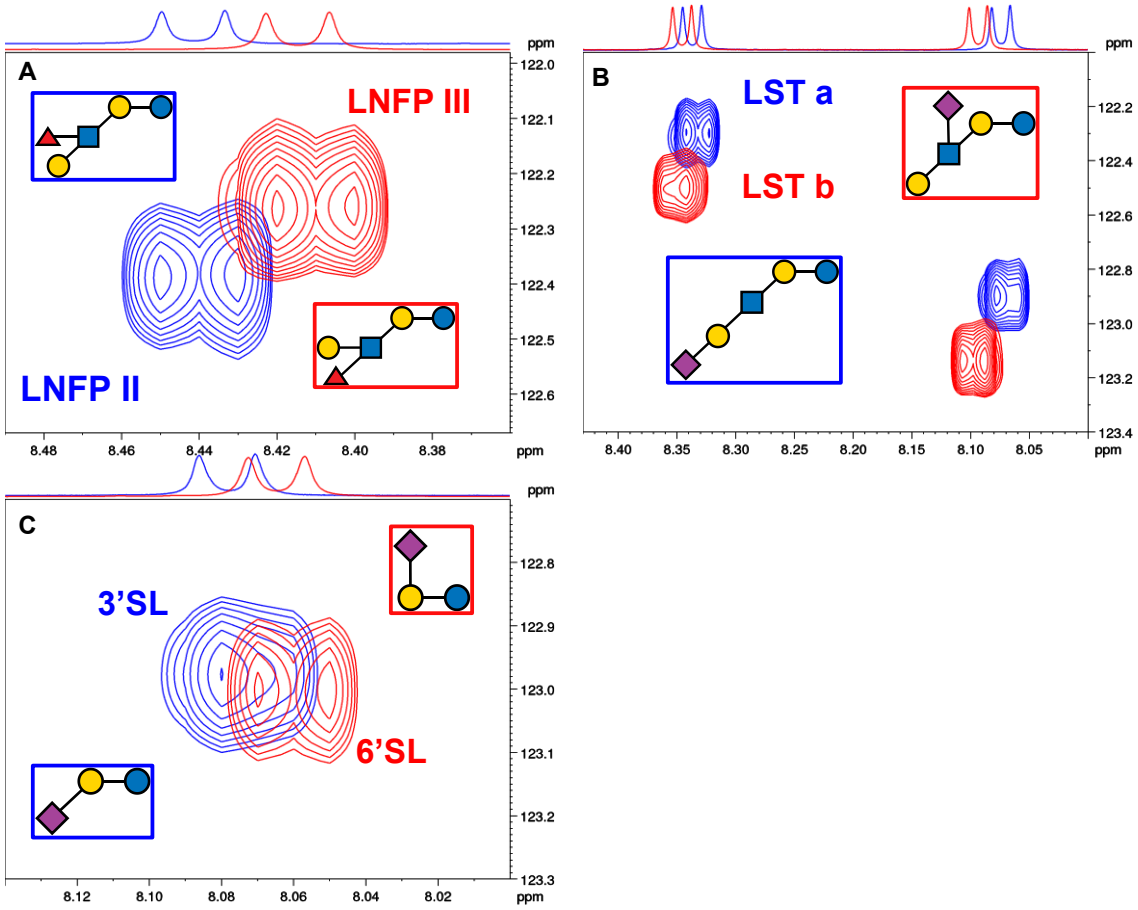

Figure 9. Overlaid ^{1}H-^{15}N HSQC spectra of (**A**) LNFP II and LNFP III, (**B**) LSTa and LSTb, (**C**) 3'SL and 6'SL, highlighting the distinct ^{1}H-^{15}N correlations of the GlcNAc and/or Neu5Ac unit in these isomeric HMO pairs [13].

5.3. Using ^{1}H-^{15}N HSQC-TOCSY to distinguish tri-, tetra-, and pentasaccharide isomers

The complete ^{1}H, ^{13}C, and ^{15}N NMR assignment of each HMO enables a detailed comparison of the GlcNAc moiety, a shared structural component in all oligosaccharides (see Tables 1 and 2). The recorded data reveal significant chemical shift perturbations in both the ^{1}H and ^{15}N resonances of the *N*-acetyl groups, as well as in the ^{1}H signals of the GlcNAc unit. To combine these effects and improve resolution, ^{1}H-^{15}N HSQC-TOCSY experiments were conducted at natural abundance. This method correlates the protons within the GlcNAc spin system to the ^{15}N chemical shifts of the acetamide group, providing a sensitive means of identifying subtle structural differences in isomeric HMOs. Although the ^{1}H-^{15}N HSQC-TOCSY experiment has lower sensitivity than a

regular ^{1}H-^{15}N HSQC, this limitation is negligible for HMOs, which are highly soluble and available in sufficient amounts for analysis.

5.3.1. Application to tetrasaccharide isomers: LNT and LNnT

Figure 10 presents the overlaid ^{1}H-^{15}N HSQC-TOCSY spectra for LNT and LNnT, two common HMO tetrasaccharides with the subtle difference in the position of the Gal attachment to the GlcNAc residue. Their GlcNAc spin systems display therefore distinct patterns and the 0.50 ppm difference in their ^{15}N chemical shifts makes their ^{1}H NMR pattern readily distinguishable. This experiment simplifies the crowded "CH region" and emphasizes the ^{1}H chemical shifts of the entire GlcNAc moiety, providing a clear distinction between the glycosidic linkages connecting Gal and GlcNAc. Combining the ^{1}H and ^{15}N chemical shifts therefore aids in providing a simple distinction between the two isomers.

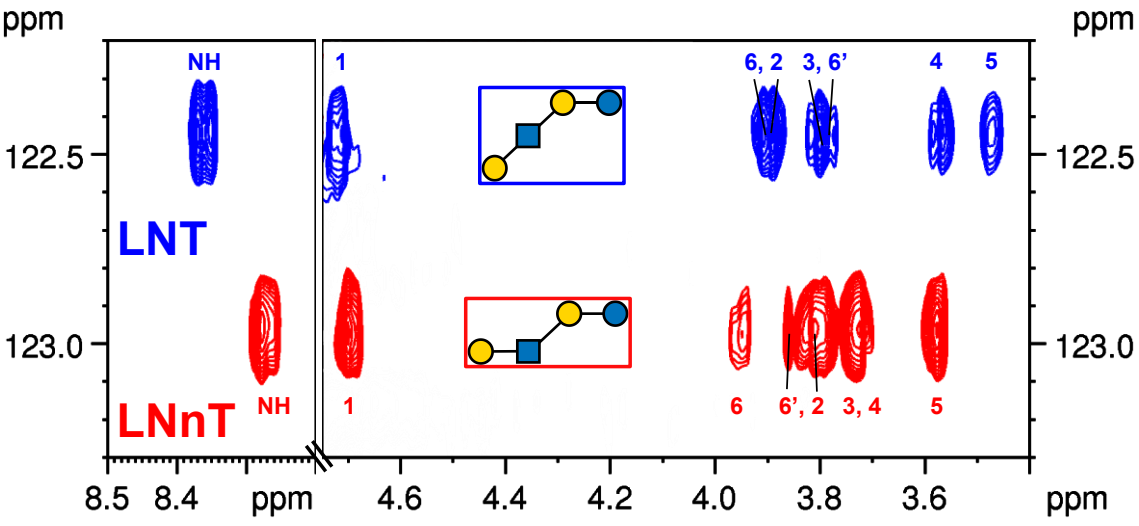

Figure 10. Overlaid ^{1}H-^{15}N HSQC-TOCSY spectra of LNT and LNnT with the ^{1}H NMR assignment of their GlcNAc moiety [13].

5.3.2. Application to tri- and pentasaccharide isomers: LNFP II and LNFP III, 3'SL and 6'-SL

The pentasaccharides LNFP II and LNFP III contain an additional Fuc unit linked to GlcNAc at different positions. Their ^{1}H-^{15}N HSQC-TOCSY spectra (see Figure 11) reveal unique chemical shift patterns, enabling straightforward differentiation.

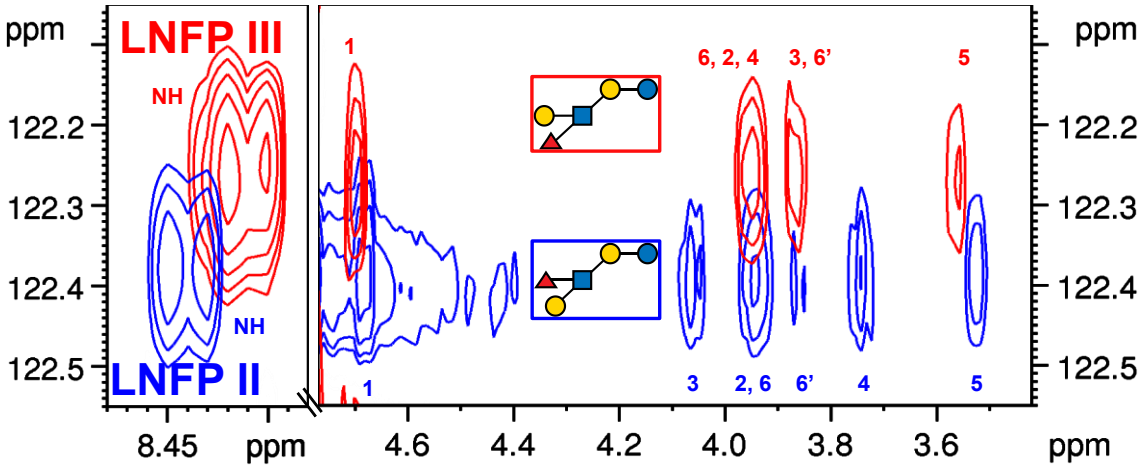

Figure 11. Overlaid ^{1}H-^{15}N HSQC-TOCSY spectra of LNFP II and LNFP III with the ^{1}H NMR assignment of their GlcNAc moiety [13].

This method is similarly effective for sialylated HMOs, where the Neu5Ac acetamide group provides a useful reporter. The sialyllactose isomers 3'SL and 6'SL exhibit distinct ^{1}H NMR patterns correlated with their ^{15}N chemical shifts (see Figure 12).

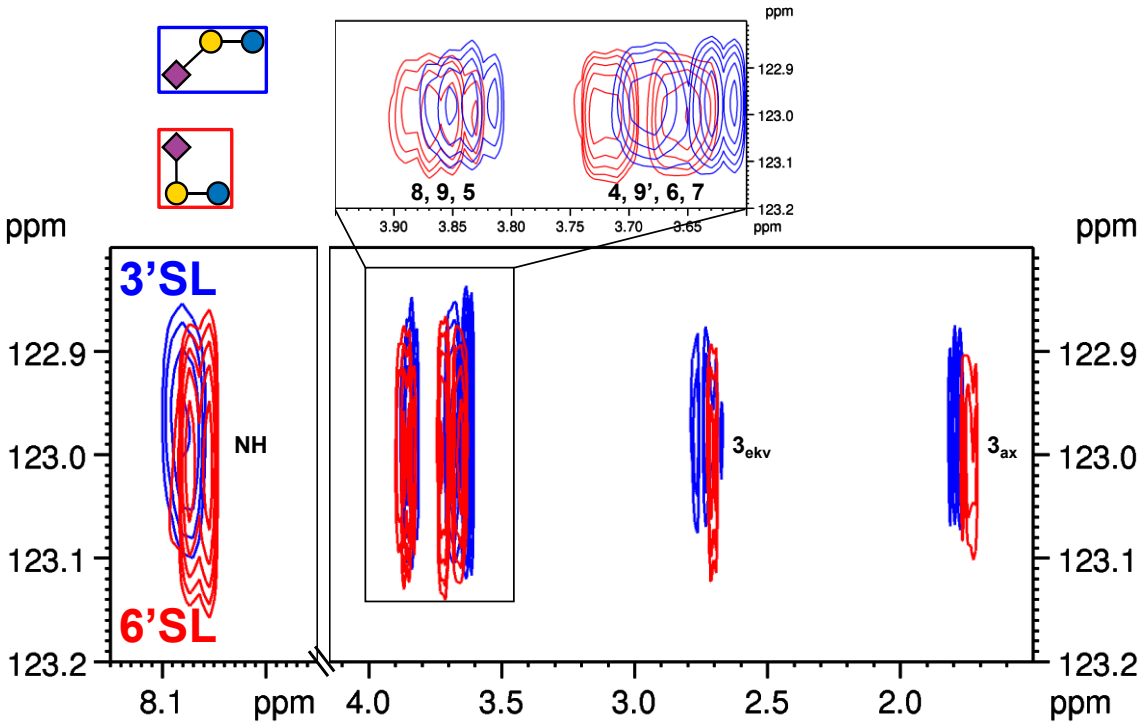

Figure 12. Overlaid ^{1}H-^{15}N HSQC-TOCSY spectra of 3'SL and 6'SL with the ^{1}H NMR assignment of their Neu5Ac moiety [13].

5.3.3. Dual reporter moieties in LSTa and LSTb

The ^{1}H-^{15}N HSQC-TOCSY method is especially valuable for isomers containing two reporter moieties, such as LSTa and LSTb. These isomers feature both GlcNAc and Neu5Ac units, with Neu5Ac linked to either Gal or GlcNAc. As shown in Figure 13, the spectra exhibit two distinct regions corresponding to the GlcNAc and Neu5Ac moieties. Even minor differences in Neu5Ac linkage are observable in the H-3ax chemical shifts. Both LSTa and LSTb share an LNT-type core structure, but the sialylation significantly influences GlcNAc chemical shifts, further aiding isomer identification. The perturbations observed for GlcNAc are highlighted in Figure 13.

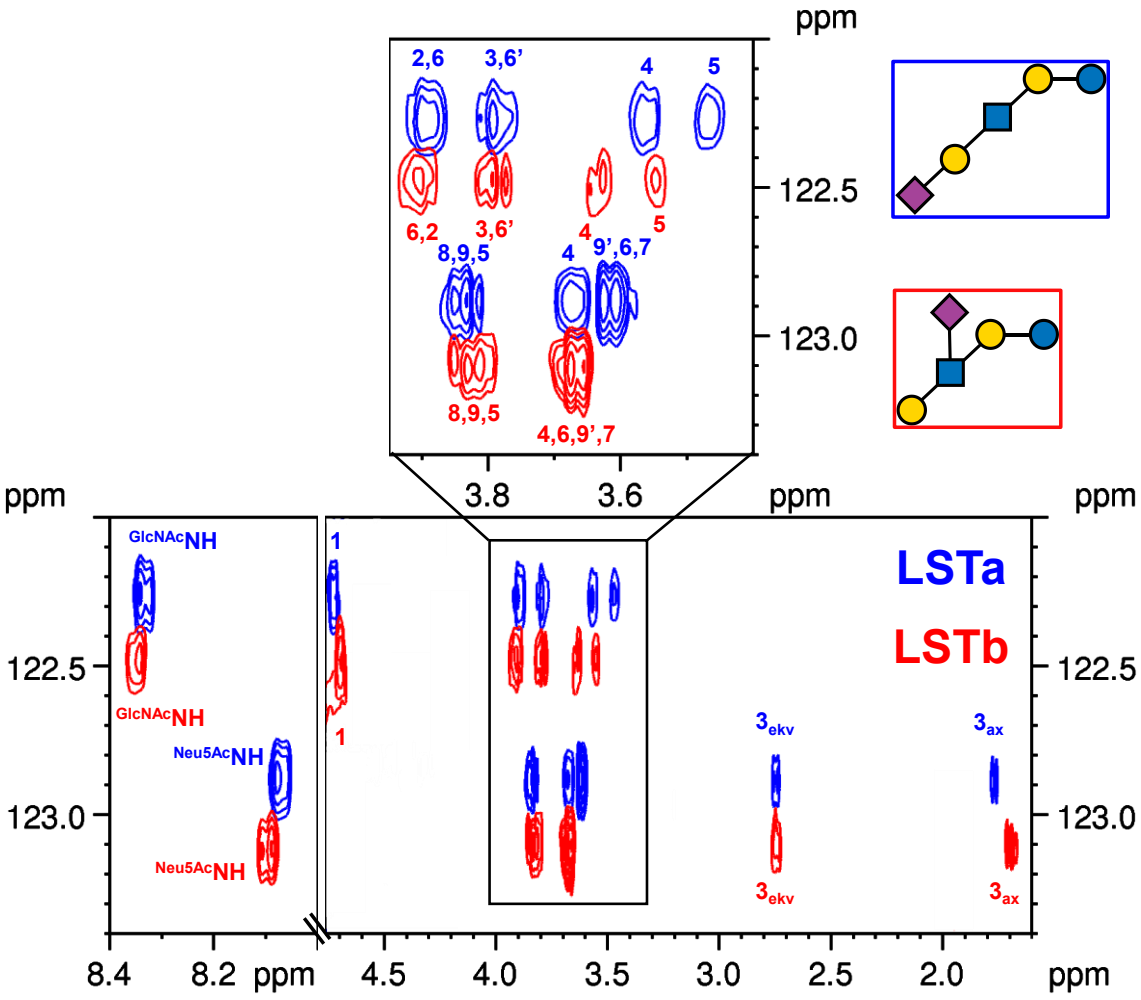

Figure 13. Overlaid ^{1}H-^{15}N HSQC-TOCSY spectra of isomeric LSTa and LSTb with the ^{1}H NMR assignment of their GlcNAc and Neu5Ac moieties [13].

5.3.4. Limitations of the method

The limitations of this approach were assessed using the ^{15}N HSQC spectrum of para-LNnH, a hexasaccharide containing two GlcNAc reporter moieties, under unbuffered conditions. Here, no significant chemical shift differences were observed for the ^{1}H and ^{15}N nuclei of the two acetamide groups. The ^{1}H-^{15}N HSQC cross-peaks completely overlapped, appearing as a single correlation at the same values as LNnT (see Figure A77). Thus, the method could not distinguish the GlcNAc residues in para-LNnH at 600 MHz.

5.3.5. Evaluation with a model compound

A further model compound (a non-HMO tetrasaccharide) possessing repeating GlcNAc units (*N*,*N*′,*N*″,*N*‴-tetraacetylchitotetraose) was also investigated. Although the ^{15}N and ^{1}H resonances of alpha and beta anomers of GlcNAc at the reducing end differed significantly, further GlcNAc residues showed no chemical shift perturbation, and therefore their ^{15}N and ^{1}H resonances could not be resolved (see Figures A78-A79 in the Appendix).

Recent work by Wiesinger and Nestor offers further insight into the properties of similar chitin oligomers. Their study utilized advanced ^{1}H-^{15}N HSQC and ^{1}H-^{15}N HSQC-TOCSY techniques to investigate GlcNAc residues, focusing on distinguishing *cis-trans* isomerism of the *N*-acetyl group and minor conformational states. This method complements our analysis by providing enhanced resolution for unresolved resonances, and their rigorous approach highlights the potential of such techniques for distinguishing more complex structures. Additionally, the evaluation of several HSQC pulse sequences, including BEST-HSQC and CP-HISQC, provided practical strategies for improving spectral resolution and sensitivity [100]. Although identifying of *cis-trans* isomers of the *N*-acetyl moiety in HMOs was beyond the scope of our study, we also observed the presence of the minor (*cis*) isomer in most of the samples. This finding suggests that additional structural variations may exist, warranting further investigation with more specialized NMR techniques. In this context, isotope-edited and isotope-filtered NMR experiments could be particularly valuable for the detailed characterization of HMOs provided that isotope-labelled HMOs are available, as they can help resolve minor conformational states that might otherwise remain undetected.

5.4. Comparison of the NMR characteristics of the hexa-, hepta- and octasaccharide HMOs

5.4.1. Key correlations in hexa-, hepta- and octasaccharides

To elucidate the structural relationships between individual monosaccharide units within the investigated HMOs, characteristic key correlations were identified using NMR techniques. These correlations provide critical insights into the spatial connectivity and linkage specificity of hexa-, hepta-, and octasaccharide HMOs.

An HMBC correlation was observed between the H-1 anomeric proton of the β-Gal^{3,6} monomer unit (lactose at the reducing end) and the C-4 carbon atom of the Glc unit. Additionally, the H-4 proton resonance of the β-Gal^{3,6} unit at the reducing end exhibited a distinctive, non-overlapping chemical shift (~4.14 ppm), allowing selective gradient experiments for targeted analysis.

Beyond standard intrapyranose correlations, selective gradient ROESY experiments revealed spatial proximity between β-Gal^{3,6} H-4 and β-GlcNAc^{3} H-1. Furthermore, an HMBC cross-peak between β-GlcNAc^{3} H-1 and β-Gal^{3,6} C-3 confirmed their direct connectivity.

The β-Gal^{3,6} unit at the reducing end exhibited substitution at position 6, which resulted in a significantly higher shift (~71.4 ppm) for the C-6 carbon compared to other monosaccharide units (~62–64 ppm). Consequently, an HMBC cross-peak was observed between β-Gal^{3,6} C-6 and β-GlcNAc^{6} H-1.

Moreover, the β-GlcNAc^{6} units were consistently substituted with a Gal$^{4(6)}$ unit at position 4 in all investigated HMOs. This was confirmed by an HMBC cross-peak between Gal$^{4(6)}$ H-1 and β-GlcNAc^{6} C-4. Depending on the backbone type (LNH or LNnH), β-GlcNAc^{3} was substituted at position 3 or 4 with either a Gal$^{3(3)}$ or Gal$^{4(3)}$ unit, respectively. These linkages were verified through HMBC cross-peaks between Gal$^{3(3)/4(3)}$ H-1 and β-GlcNAc^{3} C-3/C-4.

For HMOs containing Fuc building blocks at position 3 of the β-GlcNAc^{3} and/or β-GlcNAc^{6} monosaccharide units, distinct HMBC correlations were detected between Fuc H-1 and β-GlcNAc$^{3/6}$ C-3. Furthermore, selective gradient ROESY experiments identified additional correlations between Fuc H-1 and the CH_3 (acetyl) resonances of β-GlcNAc$^{3/6}$,

as well as between the CH_3 resonance(s) of Fuc and the H-2 resonance(s) of the outermost Gal ($Gal^{3(3)}$ / $Gal^{4(3)}$ / $Gal^{4(6)}$) attached to β-$GlcNAc^{3/6}$ at position 3 and/or 4.

These crucial correlations are visually depicted in Figure 14, where arrows illustrate inter-monosaccharide relationships, and atom numbering clarifies their connectivity. Additionally, each monosaccharide unit is abbreviated, with circled portions highlighting the Le^x motif when linked to GlcNAc at position (3) or (6) in DFLNnH.

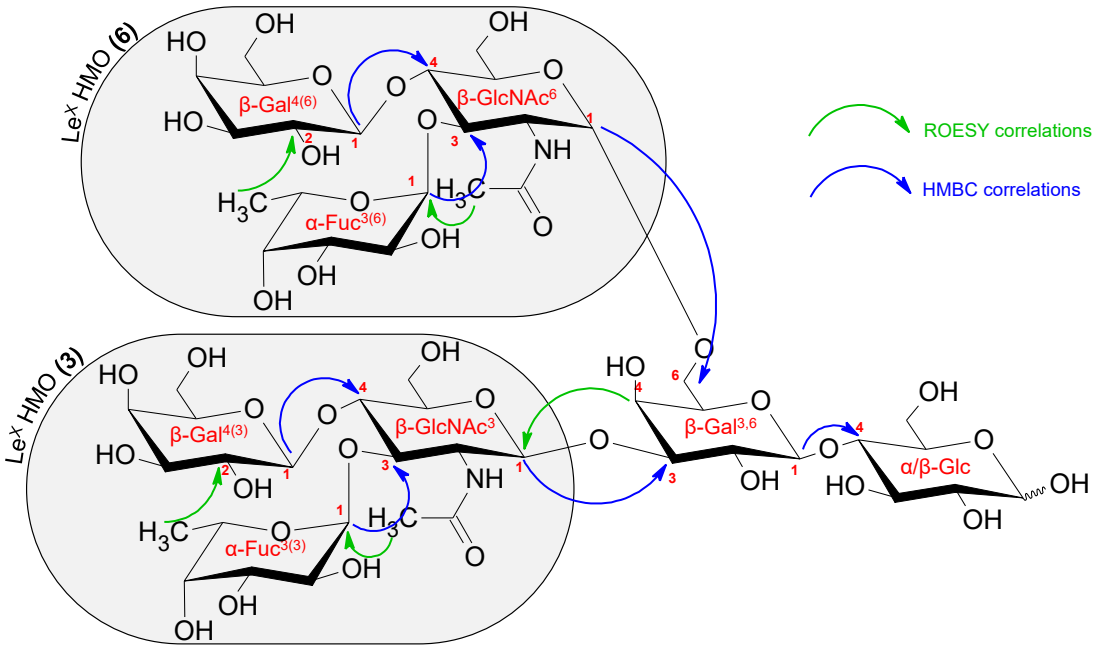

Figure 14. Key correlations in establishing the connectivities between individual monosaccharide units illustrated on the structure of DFLNnH. The grey circles refer to the Le^x motifs [99].

5.4.2. ^1H-^{15}N HSQC spectra reveal the significance of 2D correlations as distinctive structural unit characteristics

Building on our prior results, where we established the unique role of GlcNAc as an NMR-active "reporter" moiety due to its ^1H-^{15}N HSQC correlations, we have extended this approach to hexa-, hepta-, and octasaccharide HMOs (LNH, LNnH, and their α1-3 mono- and difucosylated derivatives), each featuring two GlcNAc monosaccharide units serving as reporter moieties. This methodology enables the identification of structural isomers and fucosylated derivatives based on their distinct ^1H-^{15}N HSQC fingerprints.

5.4.2.1. Resolving NH resonance overlaps using ^{1}H-^{15}N HSQC

In the ^{1}H-^{15}N HSQC spectrum of each HMO, two distinct correlations were identified in the F1 dimension, despite potential NH proton resonance overlap in the F2 dimension (Figure 15). Given the severe NH resonance overlap in the ^{1}H dimension, direct differentiation of GlcNAc units using 1D spectra alone is challenging. However, the ^{1}H-^{15}N HSQC spectrum enables clear resolution of these cross-peaks, facilitating the distinction of the two GlcNAc units.

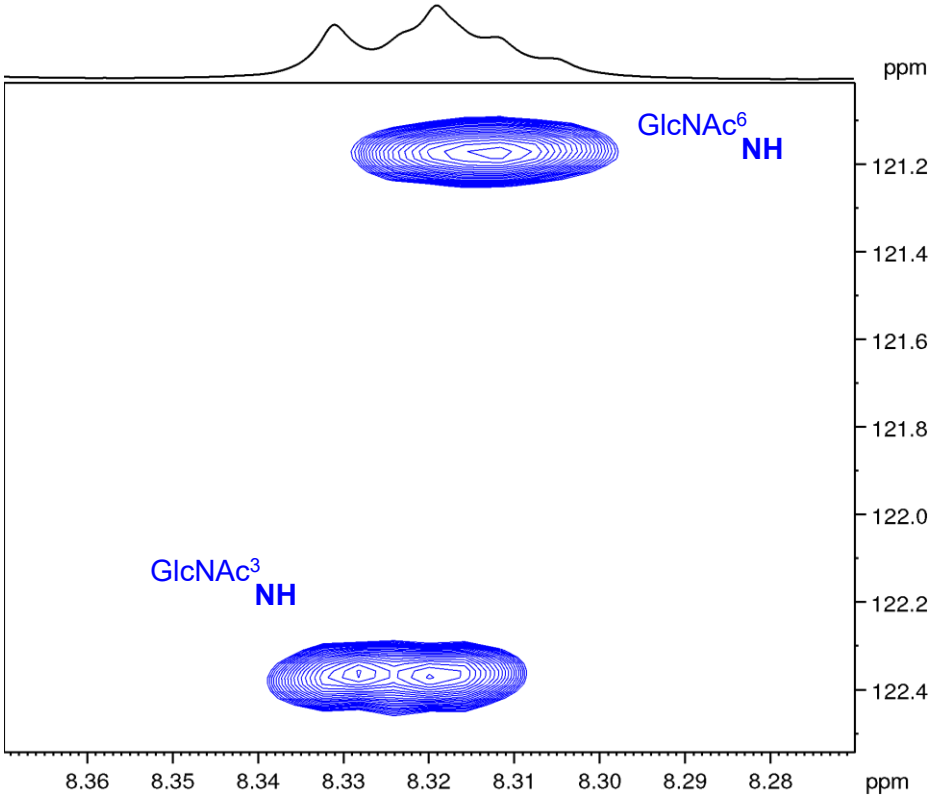

Figure 15. The severe NH resonance overlap in the ^{1}H dimension exhibits well-resolved cross-peaks when using ^{1}H-^{15}N HSQC on the MFLNH III heptasaccharide, thereby allowing the distinction of the two GlcNAc units [99].

5.4.2.2. Comparing ^{1}H-^{15}N HSQC correlations across HMOs

Comparing all twelve ^{1}H-^{15}N HSQC correlations in all six HMOs revealed significant cross-peak overlaps, indicating similar NMR chemical shifts for the *N*-acetyl group of GlcNAc units across different structures. These were condensed into five distinct ^{1}H-^{15}N fingerprint regions (denoted A–E), serving as unique identifiers of GlcNAc substructures through the investigated HMOs (Figure 16).

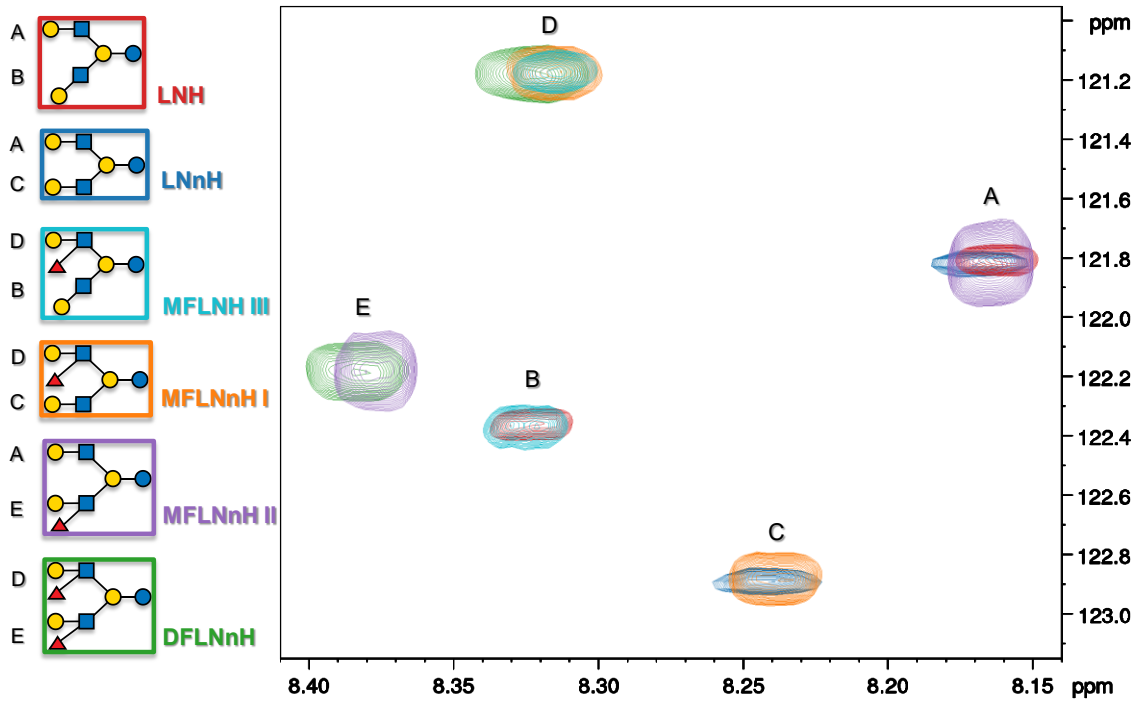

Figure 16. Overlaid ^{1}H-^{15}N HSQC spectra of the investigated HMOs reveal five distinct GlcNAc units (A, B, C, D, E) across the structures, as evidenced by overlapping NMR chemical shifts [99].

By comparing the overlapping NH cross-peaks with the assigned GlcNAc moiety of each HMO, three critical structural insights were derived:

(i) Whether the GlcNAc moiety carries a Fuc substituent with an α1-3 bond.

(ii) Its connection to the lactose subunit at the reducing end (β1-3 or β1-6 bond).

(iii) Its linkage with the outermost Gal (as part of a type-1 or type-2 chain).

To standardize the interpretation of ^{1}H-^{15}N correlations, we assigned distinct alphabetical labels (A–E) to GlcNAc-containing substructures in the investigated HMOs. This classification provides a systematic framework for distinguishing core hexasaccharides (LNH, LNnH) and their fucosylated derivatives, as well as their structural analogues in tetra- and pentasaccharides (Figures 16 and 17).

5.4.2.3. Classification of GlcNAc-containing substructures

This classification was further extended to distinguish structurally related tetra- and pentasaccharides lacking β-Gal6 branching, where corresponding B' and C' notations were introduced. Additionally, fucosylated derivatives (e.g., LNFP III) were assigned the

E' label, ensuring consistency in representing HMOs across different levels of structural complexity.

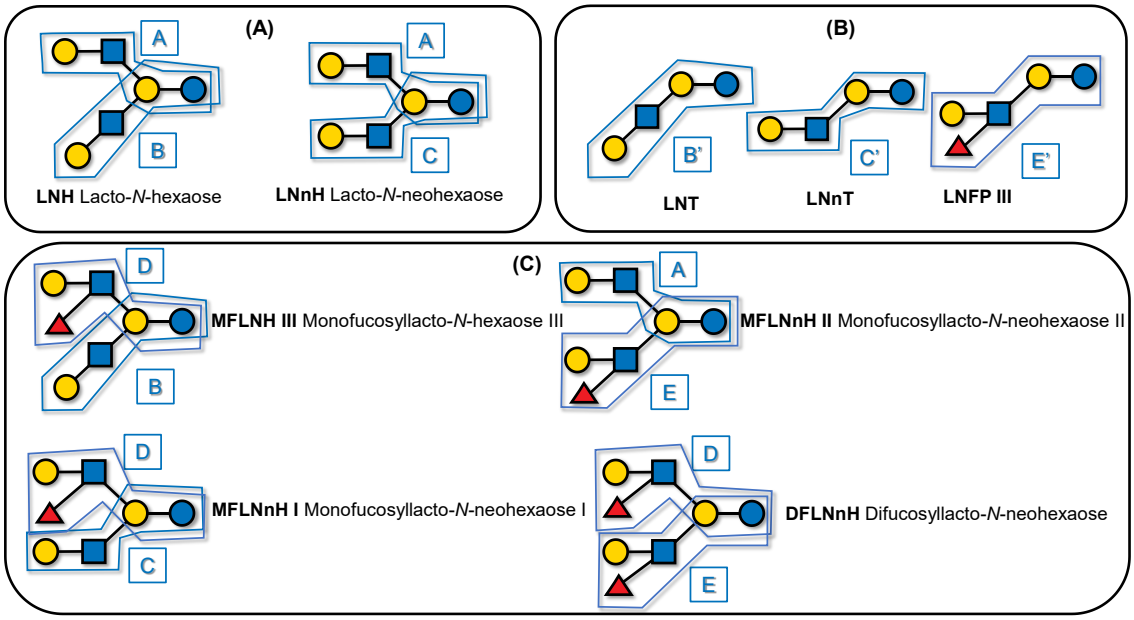

Figure 17. Alphabetical classification of GlcNAc-containing substructures present in the investigated HMOs based on their ^{1}H-^{15}N HSQC correlations. (**A**) Hexasaccharide core structures: LNH (A, B) and LNnH (A, C). (**B**) Tetrasaccharides (LNT, LNnT) and their fucosylated derivative (LNFP III) lack branching at β-Gal6 and are denoted as B', C', and E', respectively. (**C**) Le^{x} motif-containing hepta- and octasaccharides were classified according to their core hexasaccharides and fucosylation pattern [99].

5.4.2.4. The impact of β-Gal6 branching on ^{1}H-^{15}N HSQC correlations

The effect of β-Gal6 branching on ^{1}H-^{15}N HSQC correlations was particularly noteworthy. Our findings reveal that even minor structural variations – such as the presence or absence of β-Gal6 branching – significantly impact ^{1}H-^{15}N HSQC correlations of GlcNAc units attached to the same β-Gal. Specifically, the absence of β-Gal6 branching leads to consistently higher ^{1}H and ^{15}N NMR chemical shifts, demonstrating a uniform perturbation effect across both nuclei (Figure 18).

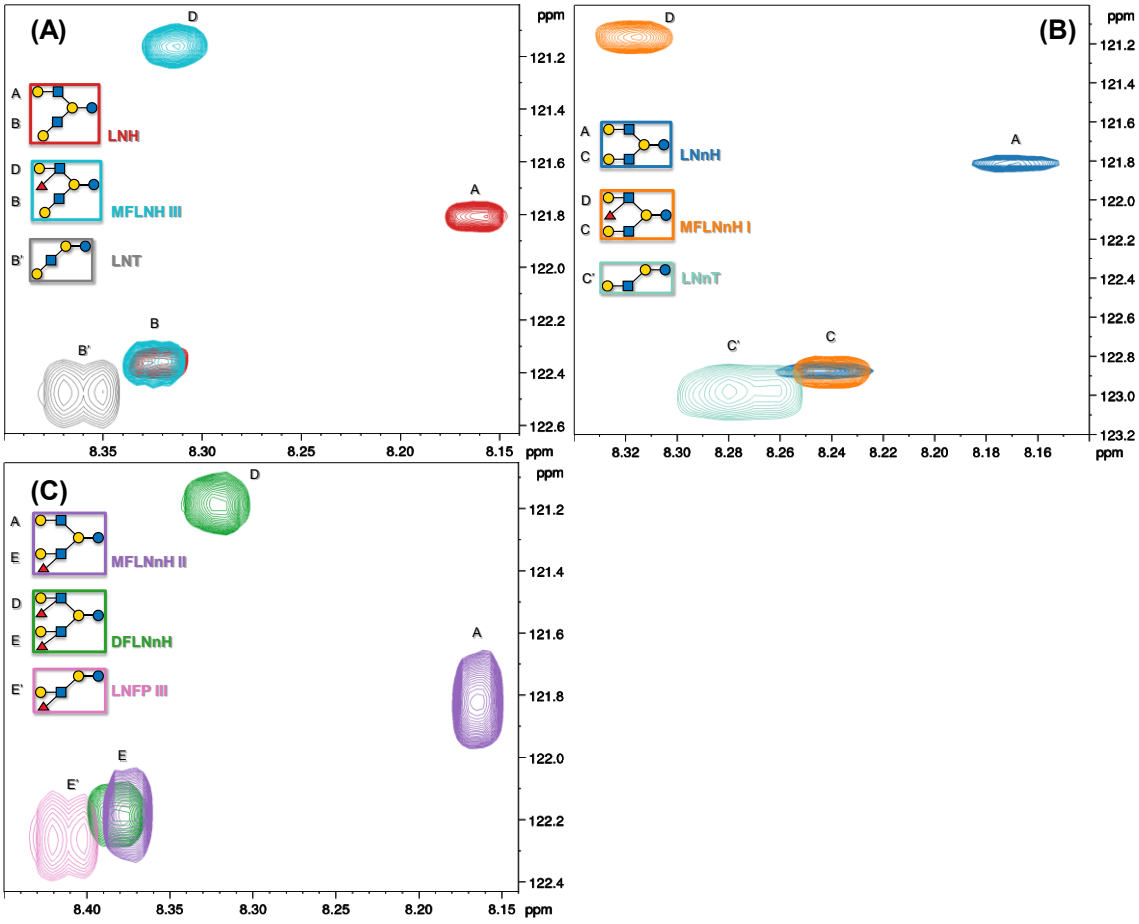

Figure 18. The effect of β-Gal6 branching on ^{1}H-^{15}N HSQC correlations in GlcNAc units attached to the same β-Gal at position 3, leading to increased ^{1}H and ^{15}N chemical shifts. (**A**) LNH, MFLNH III, and LNT (comparison of B' and B). (**B**) LNnH, MFLNnH I, and LNnT (comparison of C' and C). (**C**) MFLNnH II, DFLNnH, and LNFP III (comparison of E' and E) [99].

Our results underscore that the ^{1}H-^{15}N HSQC correlations of "reporter" GlcNAc moieties are highly sensitive to fucosylation patterns and branching in Le^{x} HMOs. This sensitivity provides a powerful tool for distinguishing structural isomers and variations, further highlighting the utility of 2D NMR methods for detailed structural characterization of HMOs.

5.4.3. Application of the ^{1}H-^{15}N HSQC method for HMO mixture analysis

To assess the effectiveness of the developed ^{1}H-^{15}N HSQC method, we applied it to a structurally diverse HMO mixture. The sample, an isolated fraction of neutral oligosaccharides (HMO-dp7), represents a naturally occurring mixture of diverse HMOs.

The experiment was performed under the same solution conditions and NMR parameters as the individual HMO analyses to ensure consistency.

The ^{1}H-^{15}N HSQC correlations of the GlcNAc units in the HMO mixture spectrum were identical to those observed in individual HMO samples, enabling precise identification. This direct correlation enabled the precise identification of HMOs within the mixture, confirming that the established fingerprinting approach is applicable to complex, multi-component systems (Figure 19).

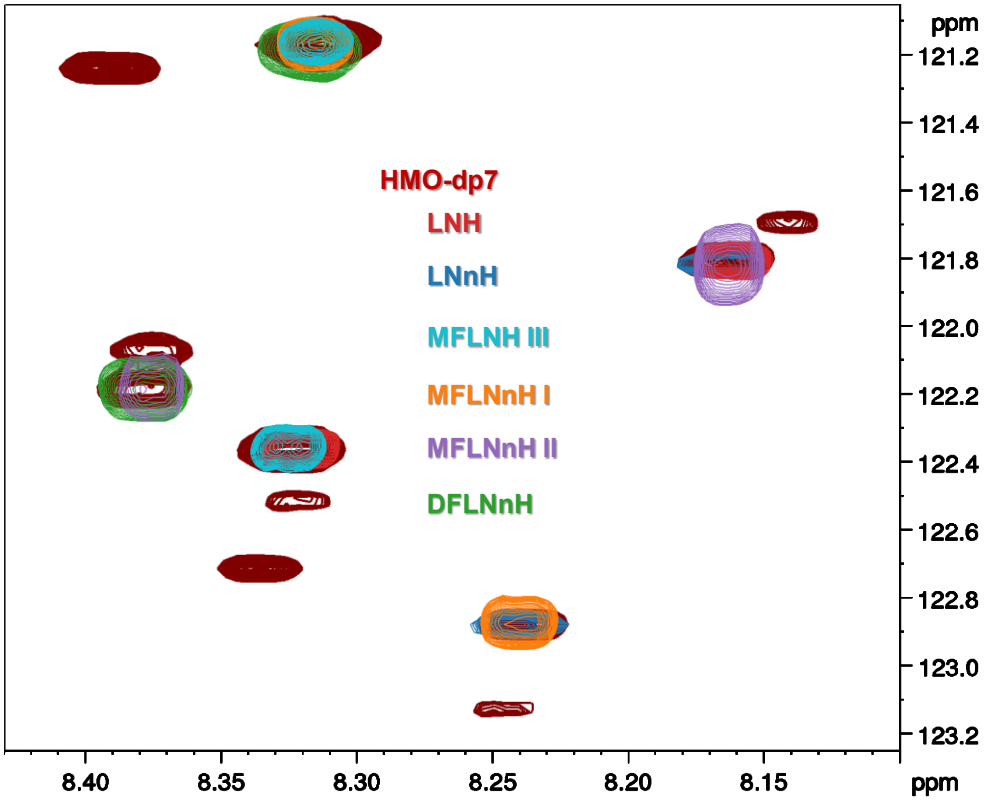

Figure 19. Overlaid ^{1}H-^{15}N HSQC spectra of the HMO-dp7 mixture and individual HMOs, demonstrating consistent GlcNAc correlations for precise structural identification [99].

In non-overlapping spectral regions, additional HMOs featuring alternative fucosylation patterns – notably Le^{a} and Le^{b} motifs – or variations in branching such as linear para-isomers could be inferred. This underscores the method's ability not only to identify known structures but also to detect structural heterogeneity within HMO mixtures.

These results highlight the power of ^{1}H-^{15}N HSQC as a rapid and precise method for characterizing HMO mixtures, establishing a distinctive spectral fingerprint for Le^{x}-bearing HMOs. By enabling structural distinction of key fucosylation patterns, this

method provides critical insights into HMO-biomacromolecule interactions, furthering our understanding of their biological roles. As a non-destructive and highly selective NMR-based approach, it offers new opportunities for advancing HMO glycoscience and exploring their structural complexity.

The ability to resolve and classify Le^x-bearing HMOs is particularly valuable considering the broader biological relevance of structurally similar motifs. For instance, sialyl Lewis X (sLe^x), which shares the same core structure with additional sialylation, is known to mediate key processes in immune recognition and cell adhesion. The biological significance of sLe^x in leukocyte trafficking and cancer metastasis underscores the importance of precise structural investigations of related glycan motifs, supporting future studies on their functional implications [101].

6. CONCLUSIONS

In this thesis, we have conducted a comprehensive structural and isomeric characterization of HMOs using ^{1}H-^{15}N NMR methods. By integrating HSQC and HSQC-TOCSY methodologies, we have demonstrated their effectiveness in distinguishing HMO isomers with high specificity. Our findings contribute to glycoscience by refining analytical techniques that enhance the structural elucidation of complex oligosaccharides.

For the first time, we have applied 2D heteronuclear ^{15}N NMR experiments for the characterization of isomeric HMOs. We systematically characterized the ^{15}N NMR resonances of GlcNAc- and Neu5Ac-containing HMOs, presenting a detailed investigation of nitrogen chemical shifts in these bioactive carbohydrates. By establishing ^{1}H-^{15}N chemical shift correlations, we introduced a novel approach for differentiating structural isomers, particularly in distinguishing trisaccharide, tetrasaccharide, and pentasaccharide HMOs (3'SL, 6'SL, LNFP II, LNFP III, LSTa, LSTb). Our results demonstrate that GlcNAc and Neu5Ac moieties serve as sensitive reporter units, reflecting the chemical environment within different HMOs. Notably, LNT and LNnT exhibited the largest ^{15}N chemical shift perturbations, whereas the Neu5Ac moiety in 3'SL and 6'SL was less responsive to structural variation. These results demonstrate that ^{1}H-^{15}N NMR methods provide a powerful complement to existing MS-based methods, offering a non-destructive and highly selective technique for structural determination.

Furthermore, we extended the application of ^{1}H-^{15}N HSQC spectroscopy to larger HMOs isolated from human milk, including hexa-, hepta-, and octasaccharides (LNH, LNnH, MFLNH III, MFLNnH I, MFLNnH II, DFLNnH), revealing critical insights into fucosylation patterns, glycosidic linkage effects, and β-Gal6 branching. Special emphasis was placed on the Lewis X motif, where we demonstrated that GlcNAc units could effectively report on branching and fucosylation patterns, aiding in the structural characterization of Le^{x}-containing HMOs. Our identification of characteristic ^{1}H-^{15}N HSQC spectral regions enables the classification of GlcNAc-containing substructures, facilitating the rapid assignment of HMO compositions in biological samples.

As part of our study, we also explored the potential of ^{1}H-^{15}N HSQC techniques for analysing HMO mixtures. While applied to a specific mixture, our findings indicate that

this approach could serve as a valuable complementary tool for future investigations into complex oligosaccharide compositions.

Overall, we have established ^{1}H-^{15}N HSQC NMR as a powerful tool for HMO structural characterization, offering enhanced resolution and specificity for isomeric differentiation. Our findings provide a robust analytical foundation for future research in glycoscience, with applications ranging from infant nutrition optimization to the development of bioactive oligosaccharide-based therapeutics. Furthermore, our approach has the potential to be expanded for studying glycan interactions and broader glycan structural diversity, paving the way for novel applications in both academic research and industrial analysis.

7. SUMMARY

Our work presents the structural and isomeric characterization of human milk oligosaccharides (HMOs) using advanced ^{1}H-^{15}N NMR spectroscopy. HMOs, a diverse class of bioactive carbohydrates found in human milk, play essential roles in infant nutrition, immune modulation, and microbial interactions. Despite their significance, structural elucidation remains challenging due to their complexity and isomeric diversity. Our study aimed to refine non-destructive, high-resolution NMR techniques to enhance HMO differentiation, particularly through the application of ^{1}H-^{15}N HSQC and HSQC-TOCSY experiments.

Our research focused on the complete resonance assignments of various HMOs, ranging from trisaccharides to octasaccharides, including fucosylated and sialylated structures. A key outcome was the establishment of ^{1}H-^{15}N NMR as a powerful tool for distinguishing isomeric HMOs based on nitrogen chemical shifts of GlcNAc and Neu5Ac moieties, which serve as structural "reporters." Our study demonstrated that ^{1}H-^{15}N HSQC spectra reveal subtle structural differences, aiding in isomer identification beyond conventional ^{1}H-^{13}C NMR methods.

Additionally, our research explored the impact of Lewis X motifs and glycosidic linkages on HMO structural variation. The developed NMR approach was successfully applied to an HMO mixture, demonstrating its applicability for rapid and precise structural characterization.

In conclusion, this study advances glycan analysis by integrating heteronuclear 2D NMR techniques for isomeric resolution, providing a robust analytical framework for future studies on HMOs in nutritional, biomedical, and industrial applications.

8. REFERENCES

[1] Bode L. Human milk oligosaccharides: Every baby needs a sugar mama. Glycobiology 2012;22:1147–62. https://doi.org/10.1093/glycob/cws074.

[2] Varki A, Cummings RD, Esko JD, Stanley P, Hart GW, Aebi M, Mohnen D, Kinoshita T, Packer NH, Prestegard JH, Schnaar RL, Seeberger PH. Essentials of Glycobiology. Cold Spring Harbor (NY) 2022:823. https://doi.org/10.1101/9781621824213.

[3] Zhang B, Li LQ, Liu F, Wu JY. Human milk oligosaccharides and infant gut microbiota: Molecular structures, utilization strategies and immune function. Carbohydr Polym 2022;276:118738. https://doi.org/10.1016/J.CARBPOL.2021.118738.

[4] Yao Q, Gao Y, Zheng N, Delcenserie V, Wang J. Unlocking the mysteries of milk oligosaccharides: Structure, metabolism, and function. Carbohydr Polym 2024:121911. https://doi.org/10.1016/J.CARBPOL.2024.121911.

[5] Jacobs JP, Lee ML, Rechtman DJ, Sun AK, Autran C, Niklas V. Human milk oligosaccharides modulate the intestinal microbiome of healthy adults. Sci Rep 2023;13:1–15. https://doi.org/10.1038/s41598-023-41040-5.

[6] Zhang S, Li T, Xie J, Zhang D, Pi C, Zhou L, Yang W. Gold standard for nutrition: a review of human milk oligosaccharide and its effects on infant gut microbiota. Microb Cell Fact 2021;20:1–16. https://doi.org/10.1186/S12934-021-01599-Y.

[7] Zhu Y, Zhang W, Mu W. Human Milk Oligosaccharides: The New Gold Standard for Premium Infant Formula. J Agric Food Chem 2022;70:2061–3. https://doi.org/10.1021/acs.jafc.2c00475.

[8] Bych K, Mikš MH, Johanson T, Hederos MJ, Vigsnæs LK, Becker P. Production of HMOs using microbial hosts — from cell engineering to large scale production. Curr Opin Biotechnol 2019;56:130–7. https://doi.org/10.1016/J.COPBIO.2018.11.003.

[9] Finke B, Stahl B, Pfenninger A, Karas M, Daniel H, Sawatzki G. Analysis of high-molecular-weight oligosaccharides from human milk by liquid chromatography and MALDI-MS. Anal Chem 1999;71:3755–62. https://doi.org/10.1021/AC990094Z.

[10] Ruhaak LR, Lebrilla CB. Advances in Analysis of Human Milk Oligosaccharides. Advances in Nutrition 2012;3:406S-414S. https://doi.org/10.3945/AN.112.001883.

[11] Varki A, Cummings RD, Aebi M, Packer NH, Seeberger PH, Esko JD, Stanley P, Hart G, Darvill A, Kinoshita T, Prestegard JJ, Schnaar RL, Freeze HH, Marth JD, Bertozzi CR, Etzler ME, Frank M, Vliegenthart JFG, Lütteke T, Perez S, Bolton E, Rudd P, Paulson J, Kanehisa M, Toukach P, Aoki-Kinoshita KF, Dell A, Narimatsu H, York W, Taniguchi N, Kornfeld S. Symbol Nomenclature for

Graphical Representations of Glycans. Glycobiology 2015;25:1323–4. https://doi.org/10.1093/GLYCOB/CWV091.

[12] Urashima T, Hirabayashi J, Sato S, Kobata A. Human Milk Oligosaccharides as Essential Tools for Basic and Application Studies on Galectins. Trends in Glycoscience and Glycotechnology 2018;30:SE51–65. https://doi.org/10.4052/TIGG.1734.1SE.

[13] Garádi Z, Tóth A, Gáti T, Dancsó A, Béni S. Utilizing the 1H-15N NMR Methods for the Characterization of Isomeric Human Milk Oligosaccharides. Int J Mol Sci 2023;24:2180. https://doi.org/10.3390/IJMS24032180.

[14] Walsh C, Lane JA, van Sinderen D, Hickey RM. From lab bench to formulated ingredient: Characterization, production, and commercialization of human milk oligosaccharides. J Funct Foods 2020;72. https://doi.org/10.1016/J.JFF.2020.104052.

[15] Hegar B, Wibowo Y, Basrowi RW, Ranuh RG, Sudarmo SM, Munasir Z, Atthiyah AF, Widodo AD, Supriatmo, Kadim M, Suryawan A, Diana NR, Manoppo C, Vandenplas Y. The Role of Two Human Milk Oligosaccharides, 2′-Fucosyllactose and Lacto-N-Neotetraose, in Infant Nutrition. Pediatr Gastroenterol Hepatol Nutr 2019;22:330–40. https://doi.org/10.5223/PGHN.2019.22.4.330.

[16] Soyyilmaz B, Mikš MH, Röhrig CH, Matwiejuk M, Meszaros-matwiejuk A, Vigsnæs LK. The mean of milk: A review of human milk oligosaccharide concentrations throughout lactation. Nutrients 2021;13:2737. https://doi.org/10.3390/NU13082737/S1.

[17] Thurl S, Munzert M, Boehm G, Matthews C, Stahl B. Systematic review of the concentrations of oligosaccharides in human milk. Nutr Rev 2017;75:920–33. https://doi.org/10.1093/NUTRIT/NUX044.

[18] Barnum CR, Paviani B, Couture G, Masarweh C, Chen Y, Huang YP, Markel K, Mills DA, Lebrilla CB, Barile D, Yang M, Shih PM. Engineered plants provide a photosynthetic platform for the production of diverse human milk oligosaccharides. Nat Food 2024;5:480–90. https://doi.org/10.1038/s43016-024-00996-x.

[19] McGuire MK, Meehan CL, McGuire MA, Williams JE, Foster J, Sellen DW, Kamau-Mbuthia EW, Kamundia EW, Mbugua S, Moore SE, Prentice AM, Kvist LJ, Otoo GE, Brooker SL, Price WJ, Shafii B, Placek C, Lackey KA, Robertson B, Manzano S, Ruíz L, Rodríguez JM, Pareja RG, Bode L. What's normal? Oligosaccharide concentrations and profiles in milk produced by healthy women vary geographically. Am J Clin Nutr 2017;105:1086–100. https://doi.org/10.3945/AJCN.116.139980.

[20] Bode L. The functional biology of human milk oligosaccharides. Early Hum Dev 2015;91:619–22. https://doi.org/10.1016/J.EARLHUMDEV.2015.09.001.

[21] Wacklin P, Mäkivuokko H, Alakulppi N, Nikkilä J, Tenkanen H, Räbinä J, Partanen J, Aranko K, Mättö J. Secretor Genotype (FUT2 gene) Is Strongly Associated with the Composition of Bifidobacteria in the Human Intestine. PLoS One 2011;6:e20113. https://doi.org/10.1371/JOURNAL.PONE.0020113.

[22] Hundshammer C, Minge O. In Love with Shaping You—Influential Factors on the Breast Milk Content of Human Milk Oligosaccharides and Their Decisive Roles for Neonatal Development. Nutrients 2020;12:3568. https://doi.org/10.3390/NU12113568.

[23] Jantscher-Krenn E, Lauwaet T, Bliss LA, Reed SL, Gillin FD, Bode L. Human milk oligosaccharides reduce Entamoeba histolytica attachment and cytotoxicity in vitro. British Journal of Nutrition 2012;108:1839–46. https://doi.org/10.1017/S0007114511007392.

[24] Ruiz-Palacios GM, Cervantes LE, Ramos P, Chavez-Munguia B, Newburg DS. Campylobacter jejuni Binds Intestinal H(O) Antigen (Fucα1, 2Galβ1, 4GlcNAc), and Fucosyloligosaccharides of Human Milk Inhibit Its Binding and Infection. Journal of Biological Chemistry 2003;278:14112–20. https://doi.org/10.1074/JBC.M207744200.

[25] Lin AE, Autran CA, Szyszka A, Escajadillo T, Huang M, Godula K, Prudden AR, Boons GJ, Lewis AL, Doran KS, Nizet V, Bode L. Human milk oligosaccharides inhibit growth of group B Streptococcus. Journal of Biological Chemistry 2017;292:11243–9. https://doi.org/10.1074/JBC.M117.789974.

[26] Cheng L, Akkerman R, Kong C, Walvoort MTC, de Vos P. More than sugar in the milk: human milk oligosaccharides as essential bioactive molecules in breast milk and current insight in beneficial effects. Crit Rev Food Sci Nutr 2021;61:1184–200. https://doi.org/10.1080/10408398.2020.1754756.

[27] Ackerman DL, Doster RS, Weitkamp JH, Aronoff DM, Gaddy JA, Townsend SD. Human Milk Oligosaccharides Exhibit Antimicrobial and Antibiofilm Properties against Group B Streptococcus. ACS Infect Dis 2017;3:595–605. https://doi.org/10.1021/acsinfecdis.7b00064.

[28] Wang C, Zhang M, Guo H, Yan J, Liu F, Chen J, Li Y, Ren F. Human Milk Oligosaccharides Protect against Necrotizing Enterocolitis by Inhibiting Intestinal Damage via Increasing the Proliferation of Crypt Cells. Mol Nutr Food Res 2019;63:1900262. https://doi.org/10.1002/MNFR.201900262.

[29] Kong C, Elderman M, Cheng L, de Haan BJ, Nauta A, de Vos P. Modulation of Intestinal Epithelial Glycocalyx Development by Human Milk Oligosaccharides and Non-Digestible Carbohydrates. Mol Nutr Food Res 2019;63:1900303. https://doi.org/10.1002/MNFR.201900303.

[30] Eiwegger T, Stahl B, Schmitt J, Boehm G, Gerstmayr M, Pichler J, Dehlink E, Loibichler C, Urbanek R, Szépfalusi Z. Human Milk–Derived Oligosaccharides and Plant-Derived Oligosaccharides Stimulate Cytokine Production of Cord Blood

T-Cells In Vitro. Pediatr Res 2004;56:536–40. https://doi.org/10.1203/01.pdr.0000139411.35619.b4.

[31] Fukuda S, Toh H, Hase K, Oshima K, Nakanishi Y, Yoshimura K, Tobe T, Clarke JM, Topping DL, Suzuki T, Taylor TD, Itoh K, Kikuchi J, Morita H, Hattori M, Ohno H. Bifidobacteria can protect from enteropathogenic infection through production of acetate. Nature 2011;469:543–7. https://doi.org/10.1038/nature09646.

[32] Guo S, Gillingham T, Guo Y, Meng D, Zhu W, Allen Walker W, Ganguli K. Secretions of Bifidobacterium infantis and Lactobacillus acidophilus Protect Intestinal Epithelial Barrier Function. J Pediatr Gastroenterol Nutr 2017;64:404–12. https://doi.org/10.1097/MPG.0000000000001310.

[33] Lewis ED, Richard C, Larsen BM, Field CJ. The Importance of Human Milk for Immunity in Preterm Infants. Clin Perinatol 2017;44:23–47. https://doi.org/10.1016/J.CLP.2016.11.008.

[34] Wang B, Brand-Miller J, McVeagh P, Petocz P. Concentration and distribution of sialic acid in human milk and infant formulas. Am J Clin Nutr 2001;74:510–5. https://doi.org/10.1093/AJCN/74.4.510.

[35] Wang B, McVeagh P, Petocz P, Brand-Miller J. Brain ganglioside and glycoprotein sialic acid in breastfed compared with formula-fed infants. Am J Clin Nutr 2003;78:1024–9. https://doi.org/10.1093/AJCN/78.5.1024.

[36] Wang B. Sialic acid is an essential nutrient for brain development and cognition. Annu Rev Nutr 2009;29:177–222. https://doi.org/10.1146/ANNUREV.NUTR.28.061807.155515.

[37] Wang B, Yu B, Karim M, Hu H, Sun Y, McGreevy P, Petocz P, Held S, Brand-Miller J. Dietary sialic acid supplementation improves learning and memory in piglets. Am J Clin Nutr 2007;85:561–9. https://doi.org/10.1093/AJCN/85.2.561.

[38] Han L, Costello CE. Electron transfer dissociation of milk oligosaccharides. J Am Soc Mass Spectrom 2011;22:997–1013. https://doi.org/10.1007/S13361-011-0117-9.

[39] Grabarics M, Lettow M, Kirschbaum C, Greis K, Manz C, Pagel K. Mass Spectrometry-Based Techniques to Elucidate the Sugar Code. Chem Rev 2022;122:7840–908. https://doi.org/10.1021/acs.chemrev.1c00380.

[40] Mank M, Welsch P, Heck AJR, Stahl B. Label-free targeted LC-ESI-MS2 analysis of human milk oligosaccharides (HMOS) and related human milk groups with enhanced structural selectivity. Anal Bioanal Chem 2019;411:231–50. https://doi.org/10.1007/S00216-018-1434-7.

[41] Mank M, Hauner H, Heck AJR, Stahl B. Targeted LC-ESI-MS2 characterization of human milk oligosaccharide diversity at 6 to 16 weeks post-partum reveals clear

staging effects and distinctive milk groups. Anal Bioanal Chem 2020;412:6887–907. https://doi.org/10.1007/S00216-020-02819-X.

[42] Cao C, Cheng Y, Zheng Y, Huang B, Guo Z, Yu L, Mulloy B, Tajadura-Ortega V, Chai W, Yan J, Liang X. Isolation of Human Milk Difucosyl Nona- and Decasaccharides by Ultrahigh-Temperature Preparative PGC-HPLC and Identification of Novel Difucosylated Heptaose and Octaose Backbones by Negative-Ion ESI-MSn. Anal Chem 2024;96:6170–9. https://doi.org/10.1021/ACS.ANALCHEM.3C05008.

[43] Rathahao-Paris E, Delvaux A, Li M, Guillon B, Venot E, Fenaille F, Adel-Patient K, Alves S. Rapid structural characterization of human milk oligosaccharides and distinction of their isomers using trapped ion mobility spectrometry time-of-flight mass spectrometry. Journal of Mass Spectrometry 2022;57:e4885. https://doi.org/10.1002/JMS.4885.

[44] Delvaux A, Rathahao-Paris E, Guillon B, Cholet S, Adel-Patient K, Fenaille F, Junot C, Alves S. Trapped ion mobility spectrometry time-of-flight mass spectrometry for high throughput and high resolution characterization of human milk oligosaccharide isomers. Anal Chim Acta 2021;1180:338878. https://doi.org/10.1016/J.ACA.2021.338878.

[45] Huang Y, Dodds ED. Ion mobility studies of carbohydrates as group i adducts: Isomer specific collisional cross section dependence on metal ion radius. Anal Chem 2013;85:9728–35. https://doi.org/10.1021/ac402133f.

[46] Huang Y, Dodds ED. Ion-neutral collisional cross sections of carbohydrate isomers as divalent cation adducts and their electron transfer products. Analyst 2015;140:6912–21. https://doi.org/10.1039/C5AN01093D.

[47] Tang Y, Pu Y, Gao J, Hong P, Costello CE, Lin C. De Novo Glycan Sequencing by Electronic Excitation Dissociation and Fixed-Charge Derivatization. Anal Chem 2018;90:3793–801. https://doi.org/10.1021/acs.analchem.7b04077.

[48] Porfirio S, Archer-Hartmann S, Brett Moreau G, Ramakrishnan G, Haque R, Kirkpatrick BD, Petri WA, Azadi P. New strategies for profiling and characterization of human milk oligosaccharides. Glycobiology 2020;30:774–86. https://doi.org/10.1093/GLYCOB/CWAA028.

[49] Hermansson K, Jansson PE, Kenne L, Widmalm G, Lindh F. A 1H and 13C NMR study of oligosaccharides from human milk. Application of the computer program CASPER. Carbohydr Res 1992;235:69–81. https://doi.org/10.1016/0008-6215(92)80079-G.

[50] Rundlöf T, Widmalm G. NMR analysis of the trisaccharide 2′-fucosyllactose by heteronuclear trans-glycosidic coupling constants and molecular simulations. Magnetic Resonance in Chemistry 2001;39:381–5. https://doi.org/10.1002/MRC.866.

[51] Chai W, Piskarev VE, Zhang Y, Lawson AM, Kogelberg H. Structural determination of novel lacto-N-decaose and its monofucosylated analogue from human milk by electrospray tandem mass spectrometry and 1H NMR spectroscopy. Arch Biochem Biophys 2005;434:116–27. https://doi.org/10.1016/J.ABB.2004.09.035.

[52] Kogelberg H, Piskarev VE, Zhang Y, Lawson AM, Chai W. Determination by electrospray mass spectrometry and 1H-NMR spectroscopy of primary structures of variously fucosylated neutral oligosaccharides based on the iso-lacto-N-octaose core. Eur J Biochem 2004;271:1172–86. https://doi.org/10.1111/J.1432-1033.2004.04021.X.

[53] Van Leeuwen SS, Schoemaker RJW, Gerwig GJ, Van Leusen-Van Kan EJM, Dijkhuizen L, Kamerling JP. Rapid milk group classification by 1H NMR analysis of Le and H epitopes in human milk oligosaccharide donor samples. Glycobiology 2014;24:728–39. https://doi.org/10.1093/GLYCOB/CWU036.

[54] van Leeuwen SS, Stoutjesdijk E, ten Kate GA, Schaafsma A, Dijck-Brouwer J, Muskiet FAJ, Dijkhuizen L. Regional variations in human milk oligosaccharides in Vietnam suggest FucTx activity besides FucT2 and FucT3. Sci Rep 2018;8:1–11. https://doi.org/10.1038/s41598-018-34882-x.

[55] van Leeuwen SS. Challenges and Pitfalls in Human Milk Oligosaccharide Analysis. Nutrients 2019;11:2684. https://doi.org/10.3390/NU11112684.

[56] Xiao Z, Guo Y, Liu Y, Li L, Zhang Q, Wen L, Wang X, Kondengaden SM, Wu Z, Zhou J, Cao X, Li X, Ma C, Wang PG. Chemoenzymatic Synthesis of a Library of Human Milk Oligosaccharides. Journal of Organic Chemistry 2016;81:5851–65. https://doi.org/10.1021/ACS.JOC.6B00478.

[57] Praticò G, Capuani G, Tomassini A, Baldassarre ME, Delfini M, Miccheli A. Exploring human breast milk composition by NMR-based metabolomics. Nat Prod Res 2014;28:95–101. https://doi.org/10.1080/14786419.2013.843180.

[58] Smilowitz JT, O'Sullivan A, Barile D, German JB, Lönnerdal B, Slupsky CM. The Human Milk Metabolome Reveals Diverse Oligosaccharide Profiles. J Nutr 2013;143:1709–18. https://doi.org/10.3945/JN.113.178772.

[59] Spevacek AR, Smilowitz JT, Chin EL, Underwood MA, German JB, Slupsky CM. Infant Maturity at Birth Reveals Minor Differences in the Maternal Milk Metabolome in the First Month of Lactation. J Nutr 2015;145:1698–708. https://doi.org/10.3945/JN.115.210252.

[60] Wang A, Koleva P, du Toit E, Geddes DT, Munblit D, Prescott SL, Eggesbø M, Johnson CC, Wegienka G, Shimojo N, Campbell D, Kozyrskyj AL, Slupsky CM. The Milk Metabolome of Non-secretor and Lewis Negative Mothers. Front Nutr 2021;7:576966. https://doi.org/10.3389/FNUT.2020.576966.

[61] Neu V, Hoffmann W, Weiß TD, Puhl M, Abikhodr A, Warnke S, Ben Faleh A, Klinck S, Pommer M, Kellner S, Maier W. Validated Multimethod Approach for Full Characterization of 2′-Fucosyl-d-lactose as an Industrially Produced Human Milk Oligosaccharide. Anal Chem 2024;96:18615–24. https://doi.org/10.1021/ACS.ANALCHEM.4C01926.

[62] Grabarics M, Csernák O, Balogh R, Béni S. Analytical characterization of human milk oligosaccharides – potential applications in pharmaceutical analysis. J Pharm Biomed Anal 2017;146:168–78. https://doi.org/10.1016/J.JPBA.2017.08.039.

[63] Auer F, Jarvas G, Guttman A. Recent advances in the analysis of human milk oligosaccharides by liquid phase separation methods. Journal of Chromatography B 2021;1162:122497. https://doi.org/10.1016/J.JCHROMB.2020.122497.

[64] Mantovani V, Galeotti F, Maccari F, Volpi N. Recent advances on separationand characterization of human milkoligosaccharides. Electrophoresis 2016;37:1514–24. https://doi.org/10.1002/elps.201500477.

[65] Csernák O, Rácz B, Alberti Á, Béni S. Quantitative analysis of 3'- and 6'-sialyllactose in human milk samples by HPLC-MS/MS: A validated method for the comparison of two consecutive lactation periods in the same woman. J Pharm Biomed Anal 2020;184:113184. https://doi.org/10.1016/J.JPBA.2020.113184.

[66] Sarkozy D, Borza B, Domokos A, Varadi E, Szigeti M, Meszaros-Matwiejuk A, Molnar-Gabor D, Guttman A. Ultrafast high-resolution analysis of human milk oligosaccharides by multicapillary gel electrophoresis. Food Chem 2021;341:128200. https://doi.org/10.1016/J.FOODCHEM.2020.128200.

[67] Rusin M, Woźniakiewicz A, Gołąb M, Dobrowolska-Iwanek J, Huras H, Staśkiewicz M, Lauterbach R, Woźniakiewicz M. Development of a capillary electrophoresis method with laser-induced fluorescence detection for the characterization of oligosaccharides in human milk. Monatsh Chem 2024;155:825–34. https://doi.org/10.1007/S00706-024-03239-8.

[68] Balogh R, Szarka S, Béni S. Determination and quantification of 2'-O-fucosyllactose and 3-O-fucosyllactose in human milk by GC–MS as O-trimethylsilyl-oxime derivatives. J Pharm Biomed Anal 2015;115:450–6. https://doi.org/10.1016/J.JPBA.2015.07.043.

[69] Christensen AS, Skov SH, Lendal SE, Hornshøj BH. Quantifying the human milk oligosaccharides 2'-fucosyllactose and 3-fucosyllactose in different food applications by high-performance liquid chromatography with refractive index detection. J Food Sci 2020;85:332–9. https://doi.org/10.1111/1750-3841.15005.

[70] Ellingson DJ, Ruosch AJ, Foster KL, Duchniak KM, Laessig IM. Analysis of Six Human Milk Oligosaccharides (HMO) in Infant Formula and Adult Nutritionals by 2AB Labeling and Quantification with HILIC-FLD: First Action 2022.02. J AOAC Int 2022;106:112–26. https://doi.org/10.1093/JAOACINT/QSAC112.

[71] Tonon KM, Miranda A, Abrão ACFV, de Morais MB, Morais TB. Validation and application of a method for the simultaneous absolute quantification of 16 neutral and acidic human milk oligosaccharides by graphitized carbon liquid chromatography – electrospray ionization – mass spectrometry. Food Chem 2019;274:691–7. https://doi.org/10.1016/J.FOODCHEM.2018.09.036.

[72] Prieto PA, Miklus MB, Barber CM, Tennyson SM. A Validated Method for Detection and Quantitation of 2'Fucosyllactose in Infant Formula Matrices. Journal of Food Chemistry and Nutrition 2019;7. https://doi.org/10.33687/JFCN.007.01.2843.

[73] Gu F, Kate GAT, Arts ICW, Penders J, Thijs C, Lindner C, Nauta A, Van Leusen E, Van Leeuwen SS, Schols HA. Combining HPAEC-PAD, PGC-LC-MS, and 1D 1H NMR to Investigate Metabolic Fates of Human Milk Oligosaccharides in 1-Month-Old Infants: A Pilot Study. J Agric Food Chem 2021;69:6495–509. https://doi.org/10.1021/ACS.JAFC.0C07446.

[74] An P, Lan D, Zhang Y, Feng D, An H, Zheng L, Wu Z, Wang D, Zhong Q. Quantitative nuclear magnetic analysis of human milk oligosaccharides 2'-fucosyllactose and 3-fucosyllactose in complicated food matrices. Food Chem 2025:142821. https://doi.org/10.1016/J.FOODCHEM.2025.142821.

[75] Strum JS, Kim J, Wu S, De Leoz MLA, Peacock K, Grimm R, German JB, Mills DA, Lebrilla CB. Identification and accurate quantitation of biological oligosaccharide mixtures. Anal Chem 2012;84:7793–801. https://doi.org/10.1021/AC301128S.

[76] Molnár-Gábor D, Lengyel M, Krongaard T. Rapid Method for Quantitation of Seven Human Milk Oligosaccharides in Infant Formula and Premix. Carbohydr Res 2024:109149. https://doi.org/10.1016/J.CARRES.2024.109149.

[77] Pomin VH. Advances in glycosaminoglycanomics by 15N-NMR spectroscopy. Anal Bioanal Chem 2013;405:3035–48. https://doi.org/10.1007/S00216-013-6803-7.

[78] Limtiaco JFK, Langeslay DJ, Beni S, Larive CK. Getting to know the nitrogen next door: HNMBC measurements of amino sugars. Journal of Magnetic Resonance 2011;209:323–31. https://doi.org/10.1016/J.JMR.2011.01.029.

[79] Langeslay DJ, Beni S, Larive CK. A closer look at the nitrogen next door: 1H- 15N NMR methods for glycosaminoglycan structural characterization. Journal of Magnetic Resonance 2012;216:169–74. https://doi.org/10.1016/J.JMR.2012.01.018.

[80] Langeslay DJ, Beni S, Larive CK. Detection of the 1H and 15N NMR resonances of sulfamate groups in aqueous solution: A new tool for heparin and heparan sulfate characterization. Anal Chem 2011;83:8006–10. https://doi.org/10.1021/AC202144M.

[81] Langeslay DJ, Beecher CN, Naggi A, Guerrini M, Torri G, Larive CK. Characterizing the microstructure of heparin and heparan sulfate using N -sulfoglucosamine 1H and 15N NMR chemical shift analysis. Anal Chem 2013;85:1247–55. https://doi.org/10.1021/AC3032788.

[82] Beecher CN, Larive CK. 1H and 15N NMR Characterization of the Amine Groups of Heparan Sulfate Related Glucosamine Monosaccharides in Aqueous Solution. Anal Chem 2015;87:6842–8. https://doi.org/10.1021/ACS.ANALCHEM.5B01181.

[83] Langeslay DJ, Young RP, Beni S, Beecher CN, Mueller LJ, Larive CK. Sulfamate proton solvent exchange in heparin oligosaccharides: Evidence for a persistent hydrogen bond in the antithrombin-binding pentasaccharide Arixtra. Glycobiology 2012;22:1173–82. https://doi.org/10.1093/GLYCOB/CWS085.

[84] Blundell CD, DeAngelis PL, Day AJ, Almond A. Use of 15N-NMR to resolve molecular details in isotopically-enriched carbohydrates: sequence-specific observations in hyaluronan oligomers up to decasaccharides. Glycobiology 2004;14:999–1009. https://doi.org/10.1093/GLYCOB/CWH117.

[85] Blundell CD, Reed MAC, Almond A. Complete assignment of hyaluronan oligosaccharides up to hexasaccharides. Carbohydr Res 2006;341:2803–15. https://doi.org/10.1016/J.CARRES.2006.09.023.

[86] Pomin VH, Sharp JS, Li X, Wang L, Prestegard JH. Characterization of glycosaminoglycans by 15N NMR spectroscopy and in vivo isotopic labeling. Anal Chem 2010;82:4078–88. https://doi.org/10.1021/AC1001383.

[87] Pomin VH, Pinto MMM, Emília De Sousa M, Correia Da Silva M. 1H and 15N NMR Analyses on Heparin, Heparan Sulfates and Related Monosaccharides Concerning the Chemical Exchange Regime of the N-Sulfo-Glucosamine Sulfamate Proton. Pharmaceuticals 2016, Vol 9, Page 58 2016;9:58. https://doi.org/10.3390/PH9030058.

[88] Green AR, Li K, Lockard B, Young RP, Mueller LJ, Larive CK. Investigation of the Amide Proton Solvent Exchange Properties of Glycosaminoglycan Oligosaccharides. Journal of Physical Chemistry B 2019;123:4653–62. https://doi.org/10.1021/ACS.JPCB.9B01794.

[89] Hwang TL, Shaka AJ. Water Suppression That Works. Excitation Sculpting Using Arbitrary Wave-Forms and Pulsed-Field Gradients. J Magn Reson A 1995;112:275–9. https://doi.org/10.1006/JMRA.1995.1047.

[90] Dua VK, Goso K, Dube VE, Allen Bush C. Characterization of lacto-N-hexaose and two fucosylated derivatives from human milk by high-performance liquid chromatography and proton NMR spectroscopy. J Chromatogr A 1985;328:259–69. https://doi.org/10.1016/S0021-9673(01)87396-9.

[91] Bandara MD, Stine KJ, Demchenko A V. Chemical synthesis of human milk oligosaccharides: lacto-N-neohexaose (Galβ1 → 4GlcNAcβ1→)2 3,6Galβ1 → 4Glc. Org Biomol Chem 2020;18:1747–53. https://doi.org/10.1039/D0OB00172D.

[92] Bandara MD, Stine KJ, Demchenko A V. Chemical Synthesis of Human Milk Oligosaccharides: Lacto- N-hexaose Galβ1→3GlcNAcβ1→3 [Galβ1→4GlcNAcβ1→6] Galβ1→4Glc. Journal of Organic Chemistry 2019;84:16192–8. https://doi.org/10.1021/ACS.JOC.9B02701.

[93] Lezyk M, Jers C, Kjaerulff L, Gotfredsen CH, Mikkelsen MD, Mikkelsen JD. Novel α-L-Fucosidases from a Soil Metagenome for Production of Fucosylated Human Milk Oligosaccharides. PLoS One 2016;11:e0147438. https://doi.org/10.1371/JOURNAL.PONE.0147438.

[94] Michalak M, Larsen DM, Jers C, Almeida JRM, Willer M, Li H, Kirpekar F, Kjærulff L, Gotfredsen CH, Nordvang RT, Meyer AS, Mikkelsen JD. Biocatalytic production of 3′-sialyllactose by use of a modified sialidase with superior trans-sialidase activity. Process Biochemistry 2014;49:265–70. https://doi.org/10.1016/J.PROCBIO.2013.10.023.

[95] Holck J, Larsen DM, Michalak M, Li H, Kjærulff L, Kirpekar F, Gotfredsen CH, Forssten S, Ouwehand AC, Mikkelsen JD, Meyer AS. Enzyme catalysed production of sialylated human milk oligosaccharides and galactooligosaccharides by Trypanosoma cruzi trans-sialidase. N Biotechnol 2014;31:156–65. https://doi.org/10.1016/J.NBT.2013.11.006.

[96] Chen X. Human Milk Oligosaccharides (HMOS): Structure, Function, and Enzyme-Catalyzed Synthesis. Adv Carbohydr Chem Biochem 2015;72:113–90. https://doi.org/10.1016/BS.ACCB.2015.08.002.

[97] De Leoz MLA, Wu S, Strum JS, Niñonuevo MR, Gaerlan SC, Mirmiran M, German JB, Mills DA, Lebrilla CB, Underwood MA. A quantitative and comprehensive method to analyze human milk oligosaccharide structures in the urine and feces of infants. Anal Bioanal Chem 2013;405:4089–105. https://doi.org/10.1007/S00216-013-6817-1.

[98] Wu S, Tao N, Bruce German J, Grimm R, B. Lebrilla C. Development of an Annotated Library of Neutral Human Milk Oligosaccharides. J Proteome Res 2010;9:4138–51. https://doi.org/10.1021/pr100362f.

[99] Garádi Z, Dancsó A, Piskarev V, Béni S. From mother's milk to structural insights: 1H–15N NMR analysis of Lewis X antigen-bearing oligosaccharides isolated from human milk. Carbohydr Polym 2025;347:122534. https://doi.org/10.1016/J.CARBPOL.2024.122534.

[100] Wiesinger P, Nestor G. NMR spectroscopic studies of chitin oligomers – Resolution of individual residues and characterization of minor amide cis

conformations. Carbohydr Polym 2024:123122. https://doi.org/10.1016/J.CARBPOL.2024.123122.

[101] Tang L, Zhang J, Oumata N, Mignet N, Sollogoub M, Zhang Y. Sialyl Lewis X (sLex):Biological Functions, Synthetic Methods and Therapeutic Implications. Eur J Med Chem 2025:117315. https://doi.org/10.1016/J.EJMECH.2025.117315.

9. BIBLIOGRAPHY of the candidate's publications

Regarding the topic of the thesis:

Garádi Z, Tóth A, Gáti T, Dancsó A, Béni S. Utilizing the ^{1}H-^{15}N NMR Methods for the Characterization of Isomeric Human Milk Oligosaccharides. Int J Mol Sci 2023;24:2180. https://doi.org/10.3390/IJMS24032180.

Garádi Z, Dancsó A, Piskarev V, Béni S. From mother's milk to structural insights: ^{1}H–^{15}N NMR analysis of Lewis X antigen-bearing oligosaccharides isolated from human milk. Carbohydr Polym 2025;347:122534. https://doi.org/10.1016/J.CARBPOL.2024.122534.

Other publications:

Garádi Z, Dékány M, Móricz ÁM, Gaál A, Papp V, Béni S, Ványolós A. Antimicrobial, Antioxidant and Antiproliferative Secondary Metabolites from Inonotus nidus-pici. Molecules 2021, Vol 26, Page 5453 2021;26:5453. https://doi.org/10.3390/MOLECULES26185453.

Gyűjtő I, Porcs-Makkay M, Lukács G, Pusztai G, **Garádi Z**, Tóth G, Nyulasi B, Simig G, Volk B. Synthesis of 4-methyl-2H-1,2,3-benzothiadiazine 1,1-dioxides and their further transformation via alkylation and reduction steps. Synth Commun 2019;49:3475–85. https://doi.org/10.1080/00397911.2019.1673777.

Nagy S, Fehér Z, Dargó G, Barabás J, **Garádi Z**, Mátravölgyi B, Kisszékelyi P, Dargó G, Huszthy P, Höltzl T, Balogh GT, Kupai J. Comparison of Cinchona Catalysts Containing Ethyl or Vinyl or Ethynyl Group at Their Quinuclidine Ring. Materials 2019, Vol 12, Page 3034 2019;12:3034. https://doi.org/10.3390/MA12183034.

Porcs-Makkay M, Gyűjtő I, Lukács G, Komáromi A, Tóth G, **Garádi Z**, Simig G, Volk B. Synthesis, Alkylation and Reduction of 4-Aryl-2H-1,2,3-benzothiadiazine 1,1-dioxides. ChemistrySelect 2019;4:8295–300. https://doi.org/10.1002/SLCT.201901212.

Ayanlowo AG, **Garádi Z**, Boldizsár I, Darcsi A, Nedves AN, Varjas B, Simon A, Alberti Á, Riethmüller E. UHPLC-DPPH method reveals antioxidant tyramine and octopamine derivatives in Celtis occidentalis. J Pharm Biomed Anal 2020;191:113612. https://doi.org/10.1016/J.JPBA.2020.113612.

Nemes A, Csóka T, Béni S, **Garádi Z**, Szabó D, Rábai J. Chiral α-Amino Acid-Based NMR Solvating Agents. Helv Chim Acta 2020;103:e2000081. https://doi.org/10.1002/HLCA.202000081.

Móricz ÁM, Krüzselyi D, Ott PG, **Garádi Z**, Béni S, Morlock GE, Bakonyi J. Bioactive clerodane diterpenes of giant goldenrod (Solidago gigantea Ait.) root extract. J Chromatogr A 2021;1635:461727. https://doi.org/10.1016/J.CHROMA.2020.461727.

Kisszékelyi P, Fehér Z, Nagy S, Bagi P, Kozma P, **Garádi Z**, Dékány M, Huszthy P, Mátravölgyi B, Kupai J. Synthesis of C3-Symmetric Cinchona-Based Organocatalysts and Their Applications in Asymmetric Michael and Friedel–Crafts Reactions. Symmetry 2021, Vol 13, Page 521 2021;13:521. https://doi.org/10.3390/SYM13030521.

Felegyi-Tóth CA, **Garádi Z**, Darcsi A, Csernák O, Boldizsár I, Béni S, Alberti Á. Isolation and quantification of diarylheptanoids from European hornbeam (Carpinus betulus L.) and HPLC-ESI-MS/MS characterization of its antioxidative phenolics. J Pharm Biomed Anal 2022;210:114554. https://doi.org/10.1016/J.JPBA.2021.114554.

Baglyas M, Ott PG, **Garádi Z**, Glavnik V, Béni S, Vovk I, Móricz ÁM. High-performance thin-layer chromatography – antibacterial assay first reveals bioactive clerodane diterpenes in giant goldenrod (Solidago gigantea Ait.). J Chromatogr A 2022;1677:463308. https://doi.org/10.1016/J.CHROMA.2022.463308.

Pósa SP, Dargó G, Nagy S, Kisszékelyi P, **Garádi Z**, Hámori L, Szakács G, Kupai J, Tóth S. Cytotoxicity of cinchona alkaloid organocatalysts against MES-SA and MES-SA/Dx5 multidrug-resistant uterine sarcoma cell lines. Bioorg Med Chem 2022;67:116855. https://doi.org/10.1016/J.BMC.2022.116855.

Várnai B, Zsila F, Szakács Z, **Garádi Z**, Malanga M, Béni S. Sulfobutylation of Beta-Cyclodextrin Enhances the Complex Formation with Mitragynine: An NMR and Chiroptical Study. Int J Mol Sci 2022;23:3844. https://doi.org/10.3390/IJMS23073844/S1.

Felegyi-Tóth CA, Tóth Z, **Garádi Z**, Boldizsár I, Nedves AN, Simon A, Felegyi K, Alberti Á, Riethmüller E. Membrane Permeability and Aqueous Stability Study of Linear and Cyclic Diarylheptanoids from Corylus maxima. Pharmaceutics 2022;14:1250. https://doi.org/10.3390/PHARMACEUTICS14061250/S1.

Koványi-Lax G, Hargitai C, Ábrányi-Balogh P, Nagy T, Tóth G, **Garádi Z**, Németh G, Pandur A, Horváth S, Dancsó A, Simig G, Volk B. Experimental and computational study of BF3-catalyzed transformations of ortho-(pivaloylaminomethyl)benzaldehydes: an unexpected difference from TFA catalysis. Org Biomol Chem 2022;20:1933–44. https://doi.org/10.1039/D1OB02308J.

Felegyi K, **Garádi Z**, Rácz B, Tóth G, Papp V, Boldizsár I, Dancsó A, Spengler G, Béni S, Ványolós A. Polyporenic Acids from the Mushroom Buglossoporus quercinus Possess Chemosensitizing and Efflux Pump Inhibitory Activities on Colo 320 Adenocarcinoma Cells. Journal of Fungi 2023;9:923. https://doi.org/10.3390/JOF9090923/S1.

Felegyi K, **Garádi Z**, Studzińska-Sroka E, Papp V, Boldizsár I, Dancsó A, Béni S, Zalewski P, Ványolós A. Anticholinesterase and Antityrosinase Secondary Metabolites from the Fungus Xylobolus subpileatus. Molecules 2024;29:213. https://doi.org/10.3390/MOLECULES29010213/S1.

Dargó G, Erdélyi D, Molnár B, Kisszékelyi P, **Garádi Z**, Kupai J. A novel recyclable organocatalyst for the gram-scale enantioselective synthesis of (S)-baclofen. Beilstein Journal of Organic Chemistry 19:133 2023;19:1811–24. https://doi.org/10.3762/BJOC.19.133.

Pollák P, **Garádi Z**, Volk B, Dancsó A, Simig G, Milen M. Studies on the total syntheses of β-carboline alkaloids orthoscuticellines A and B. Nat Prod Res 2024. https://doi.org/10.1080/14786419.2024.2306600.

Nagy S, Richter D, Dargó G, Orbán B, Gémes G, Höltzl T, **Garádi Z**, Fehér Z, Kupai J. Cinchona-Based Hydrogen-Bond Donor Organocatalyst Metal Complexes: Asymmetric Catalysis and Structure Determination. ChemistryOpen 2024;13:e202300180. https://doi.org/10.1002/OPEN.202300180.

10. ACKNOWLEDGEMENTS

I am deeply indebted to my supervisor, Szabolcs Béni, from whom I have learned immensely both professionally and personally over the years. His work ethic and perspective will continue to inspire me throughout my career. I am grateful to him for his endless help and support.

I am infinitely thankful to my superiors, Balázs Volk and Imre Kapui at Egis Pharmaceuticals Plc., whose support made it possible for me to complete my doctoral work. I owe gratitude to my colleagues: András Dancsó, from whom I have learned the most, and to Péter Kővágó and Mónika Mezővári, who supported my progress in our daily work. I also extend my thanks to Gábor Tóth, Györgyi Koványiné Lax and Éva Szabó for their valuable advice and contributions to my professional development.

I greatly appreciate Zoltán Szakács (from Gedeon Richter Plc.) for his readiness to provide professional guidance whenever I needed it, and for his attentive responses to my questions.

I am thankful to all my colleagues at the Department of Pharmacognosy at Semmelweis University, for their support during my doctoral studies. Special thanks to Bianka Várnai and Eszter Kalydi for their support and friendship.

Lastly, I am grateful to my family for their unwavering encouragement and support throughout this journey.

APPENDIX

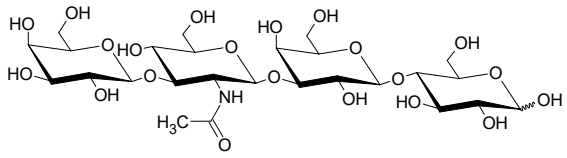

LNT

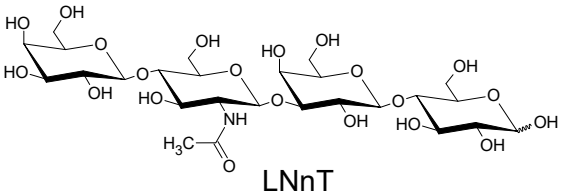

LNnT

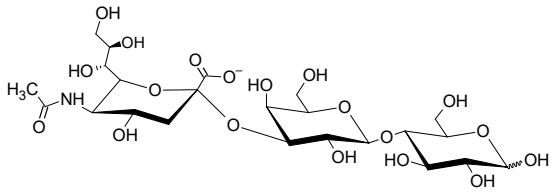

3'SL

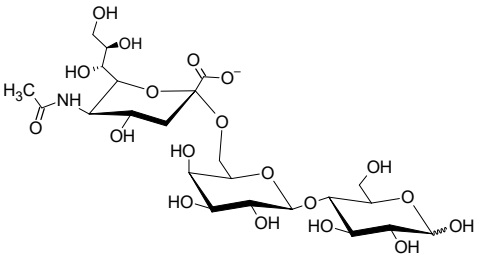

6'SL

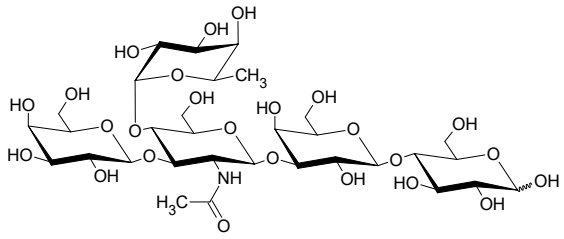

LNFP II

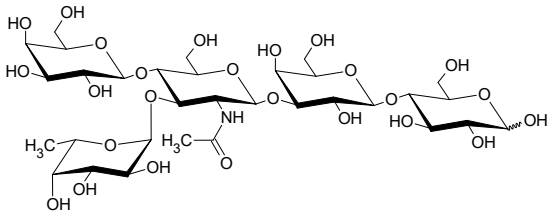

LNFP III

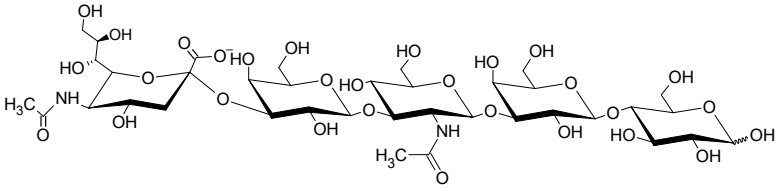

LSTa

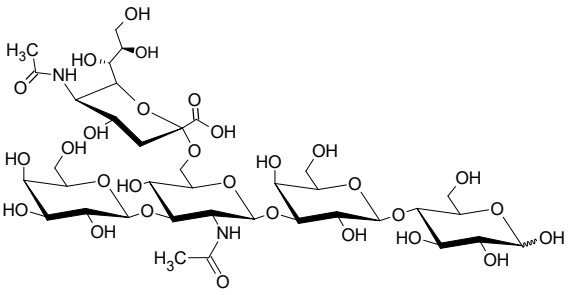

LSTb

Figure A1. Chemical structures of the investigated tri-, tetra-, and pentasaccharide HMOs

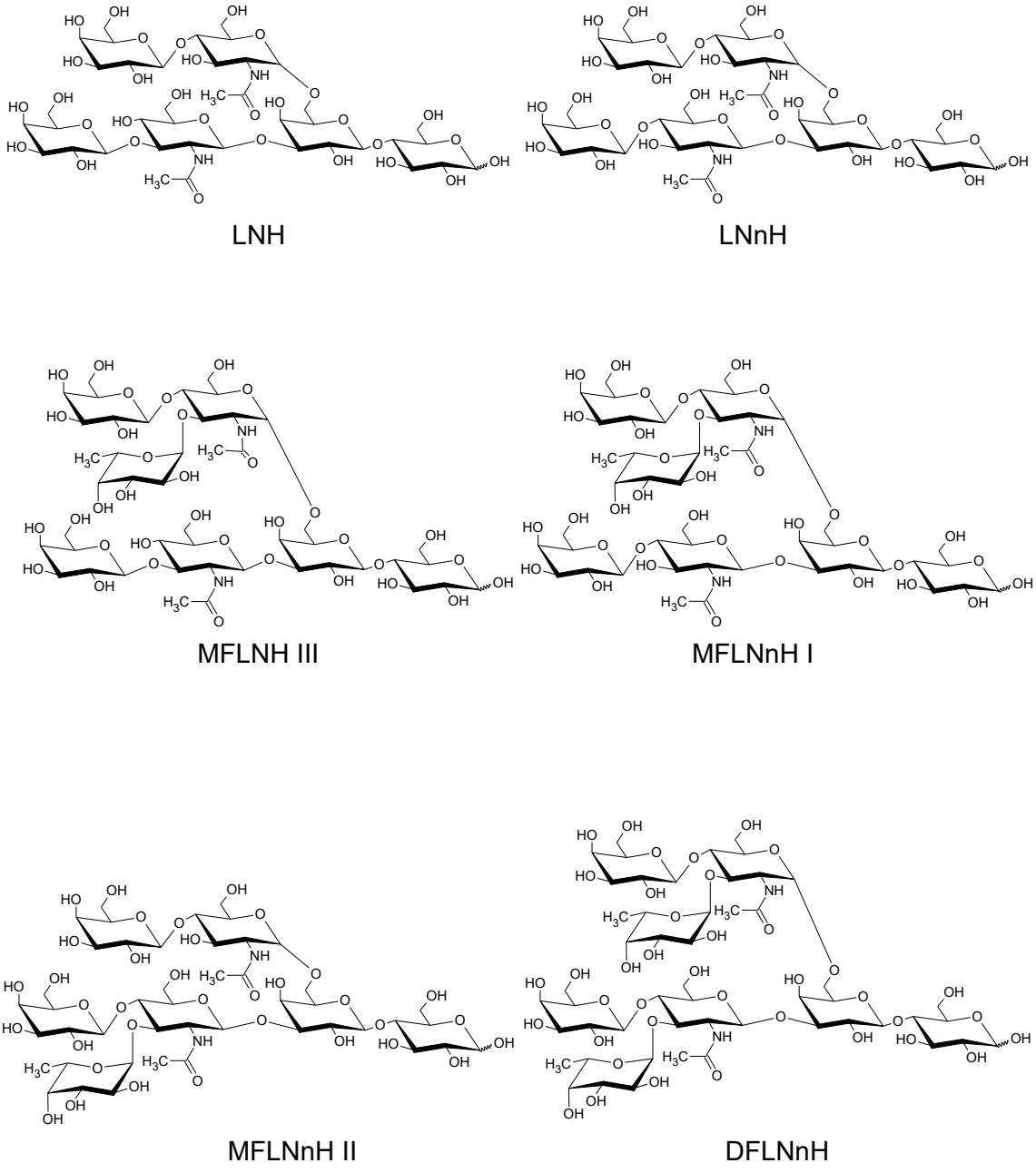

Figure A2. Chemical structures of the investigated hexa-, hepta-, and octasaccharide HMOs

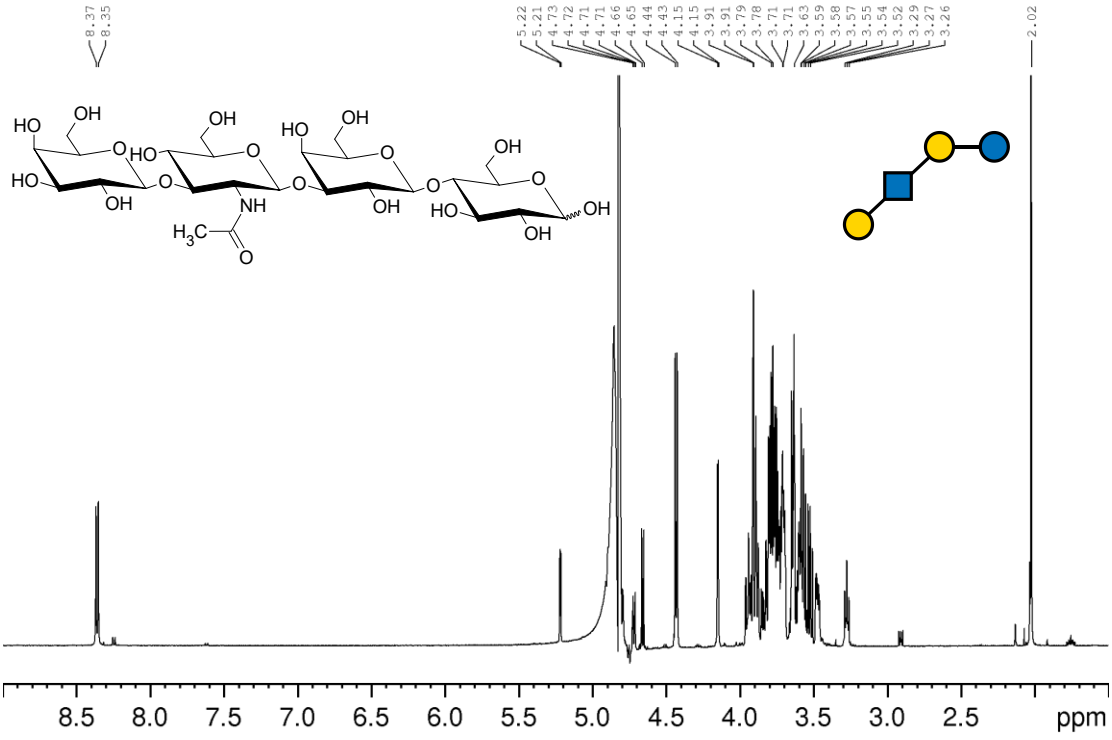

Figure A3. ^{1}H NMR spectrum of LNT (H_2O:D_2O 9:1 *v/v* solvent at pH 3.0)

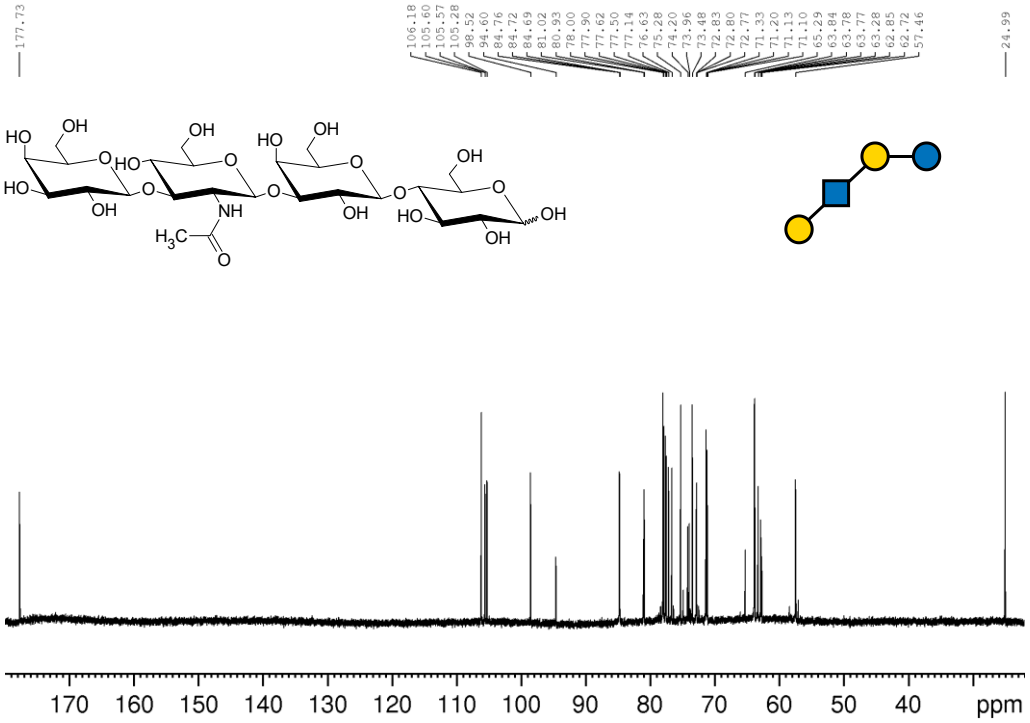

Figure A4. ^{13}C NMR spectrum of LNT (H_2O:D_2O 9:1 *v/v* solvent at pH 3.0)

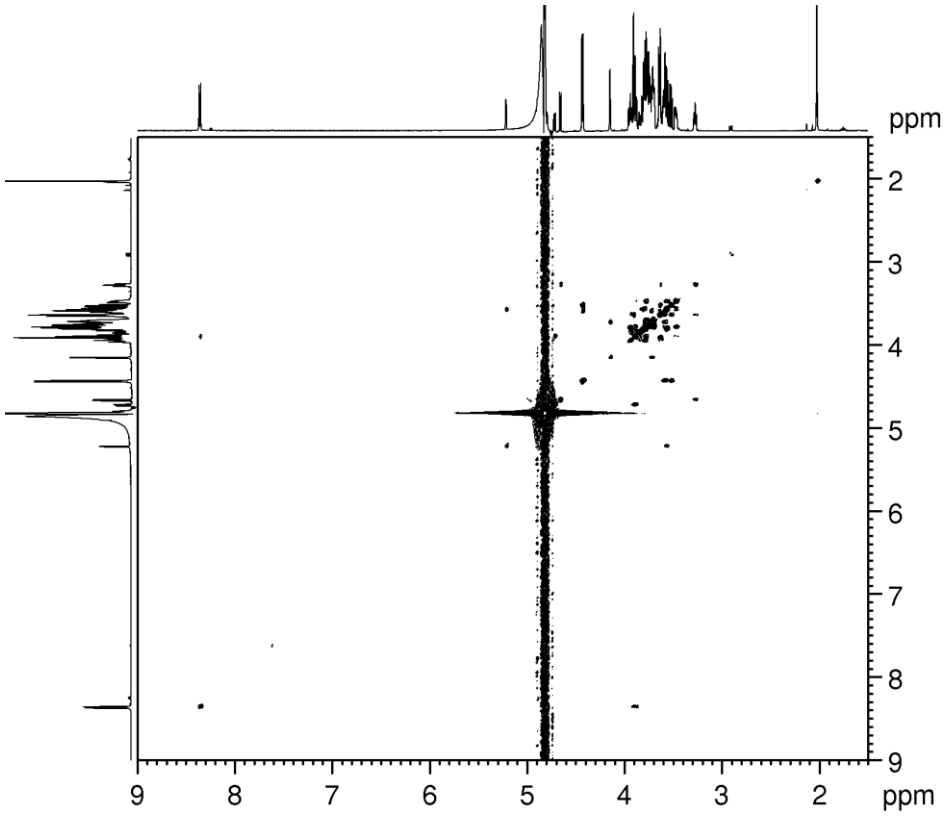

Figure A5. ^{1}H -^{1}H COSY spectrum of LNT (H_2O:D_2O 9:1 *v/v* solvent at pH 3.0)

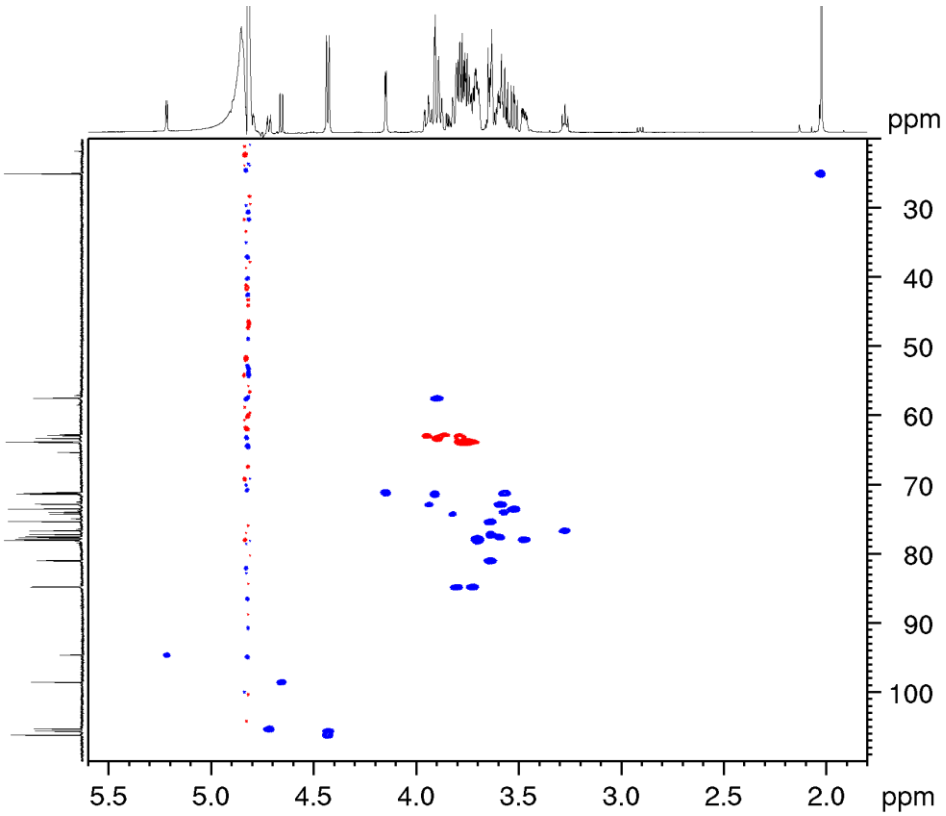

Figure A6. ^{1}H -^{13}C HSQC spectrum of LNT (H_2O:D_2O 9:1 *v/v* solvent at pH 3.0)

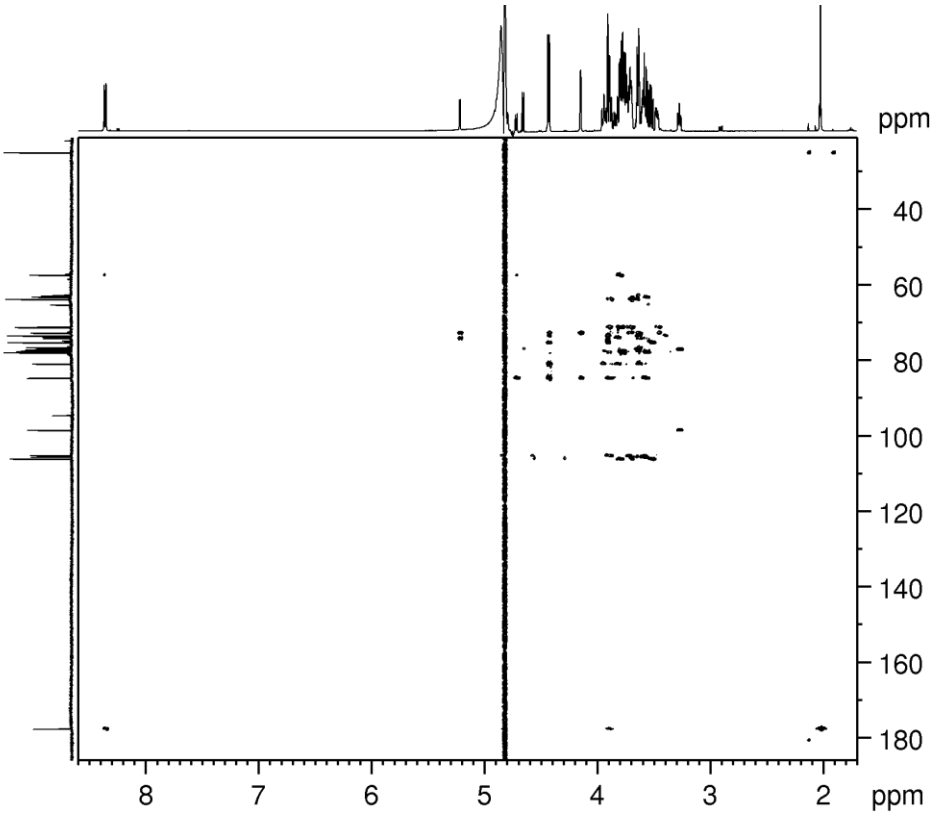

Figure A7. ^{1}H -^{13}C HMBC spectrum of LNT (H_2O:D_2O 9:1 *v/v* solvent at pH 3.0)

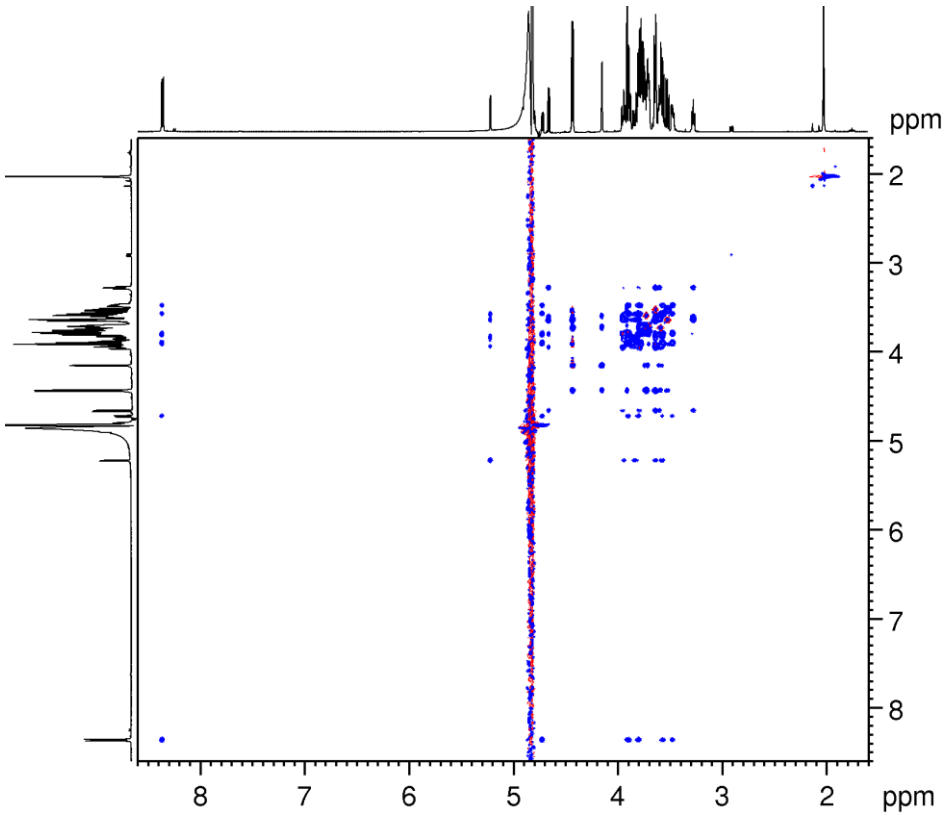

Figure A8. ^{1}H -^{1}H TOCSY spectrum of LNT (H_2O:D_2O 9:1 *v/v* solvent at pH 3.0)

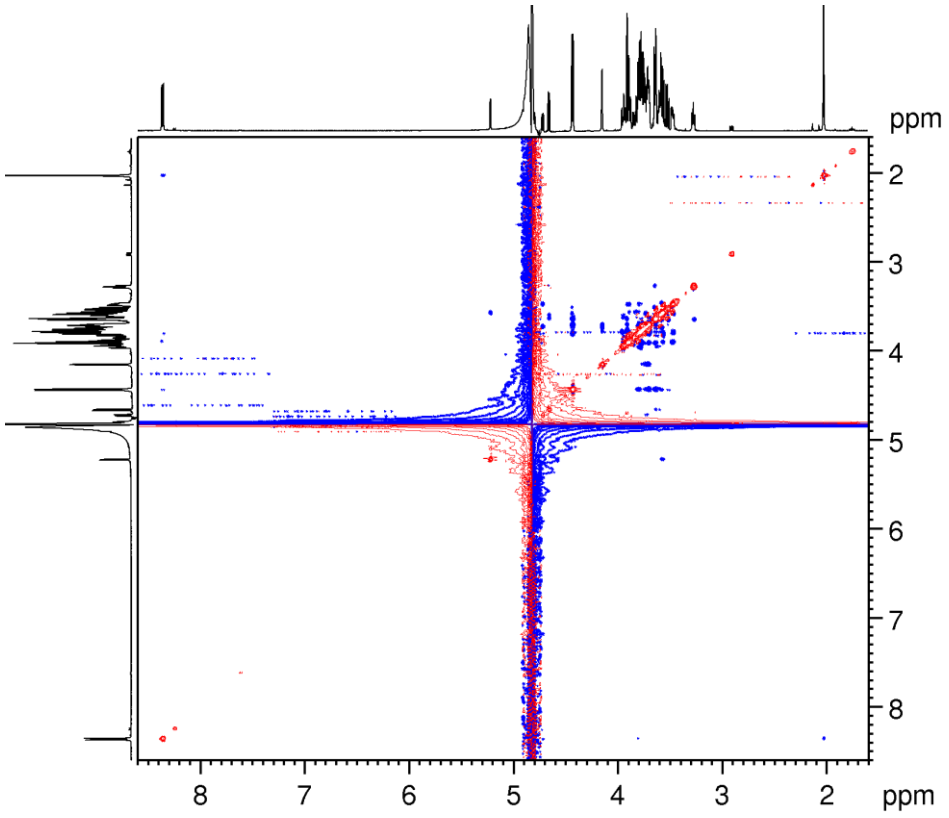

Figure A9. ^{1}H -^{1}H ROESY spectrum of LNT (H_2O:D_2O 9:1 *v/v* solvent at pH 3.0)

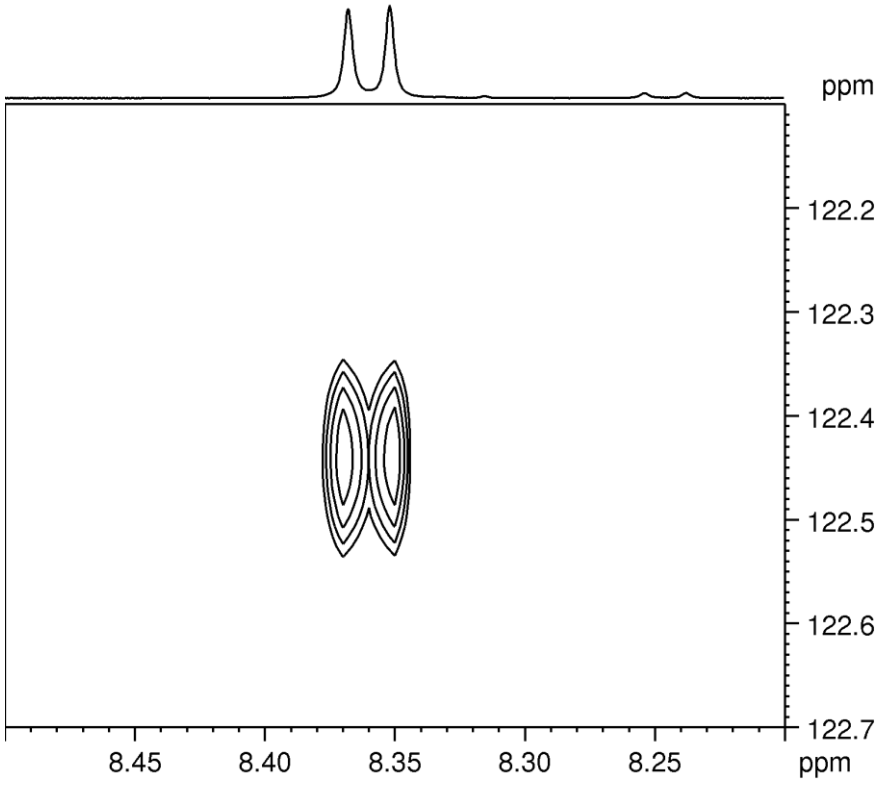

Figure A10. ^{1}H -^{15}N HSQC spectrum of LNT (H_2O:D_2O 9:1 *v/v* solvent at pH 3.0)

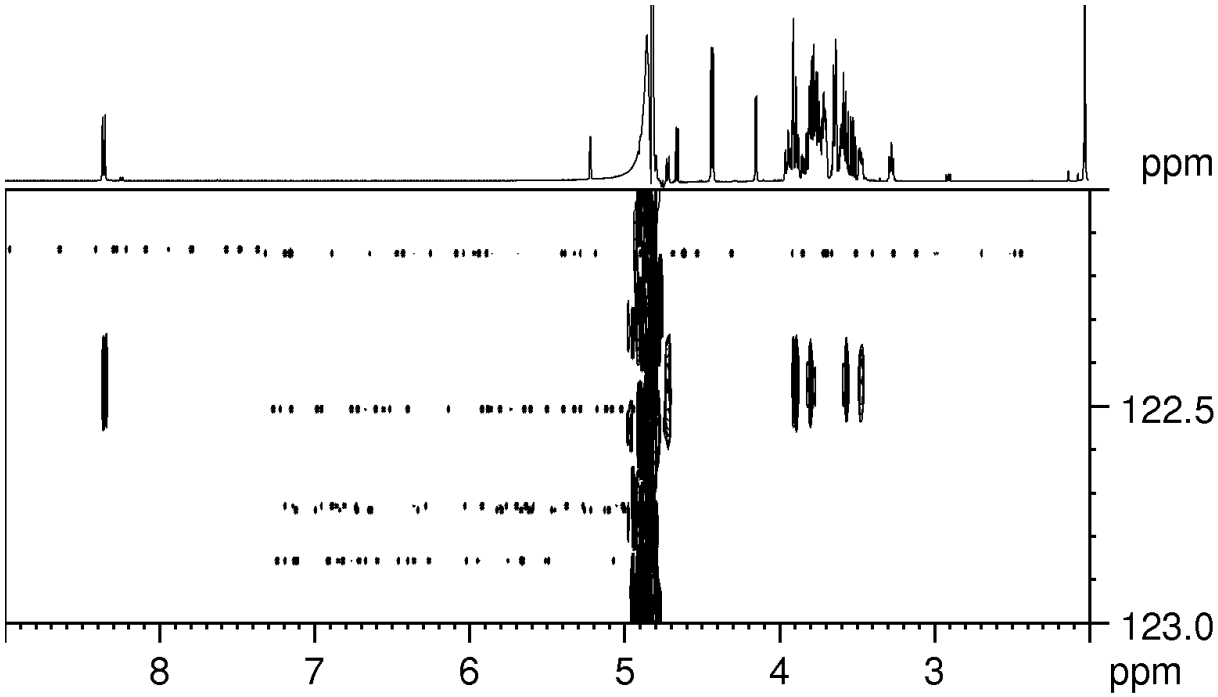

Figure A11. ^{1}H -^{15}N HSQC-TOCSY spectrum of LNT (H_2O:D_2O 9:1 *v/v* solvent at pH 3.0)

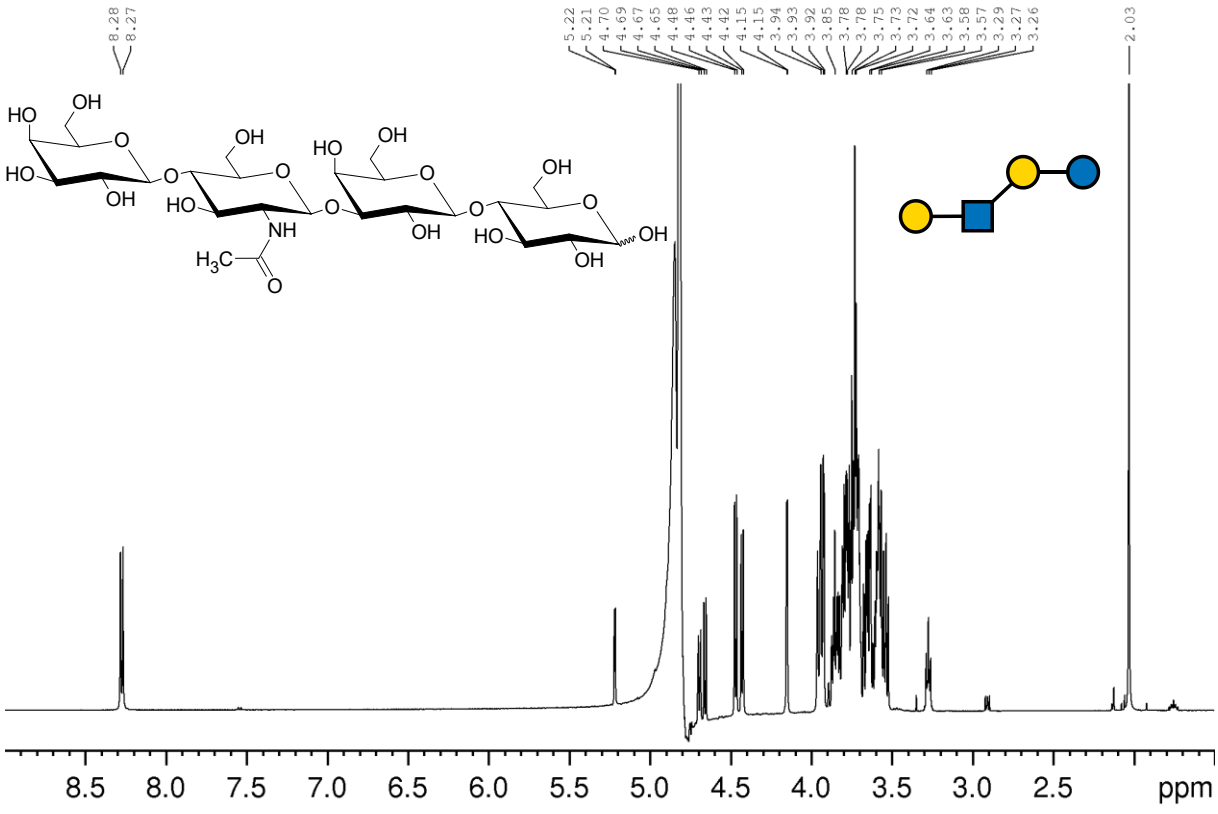

Figure A12. ^{1}H NMR spectrum of LNnT (H_2O:D_2O 9:1 *v/v* solvent at pH 3.0)

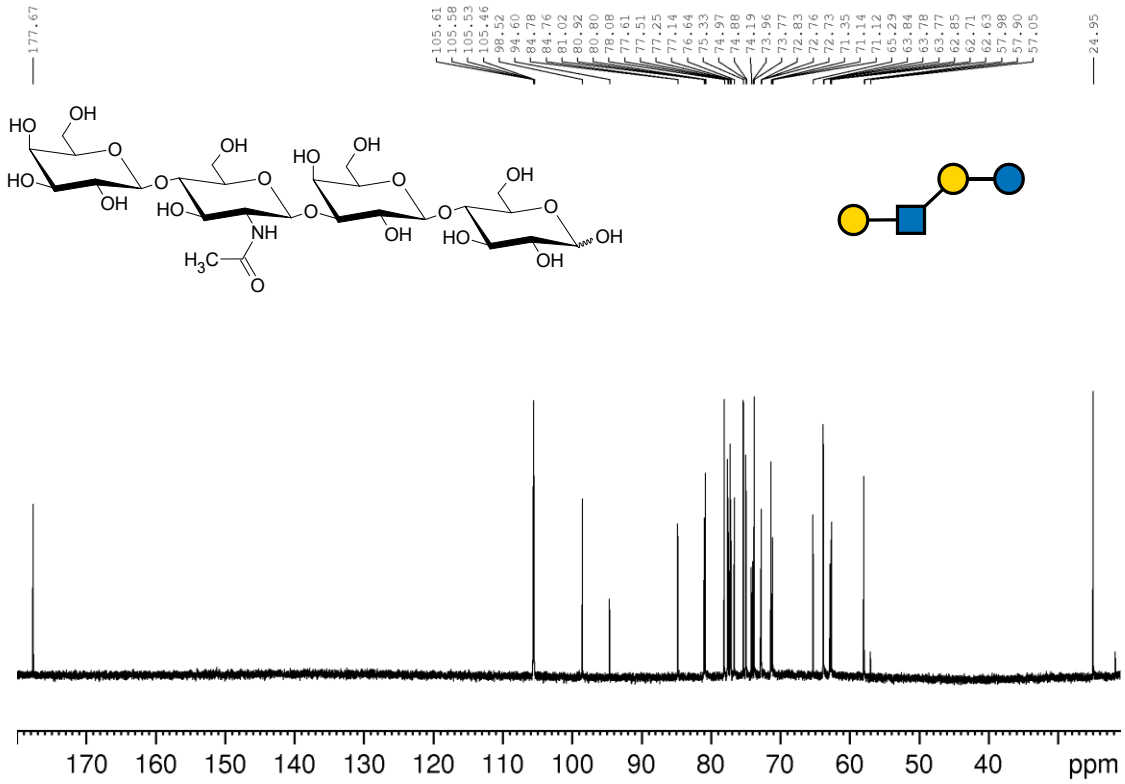

Figure A13. ^{13}C NMR spectrum of LNnT (H_2O:D_2O 9:1 *v/v* solvent at pH 3.0)

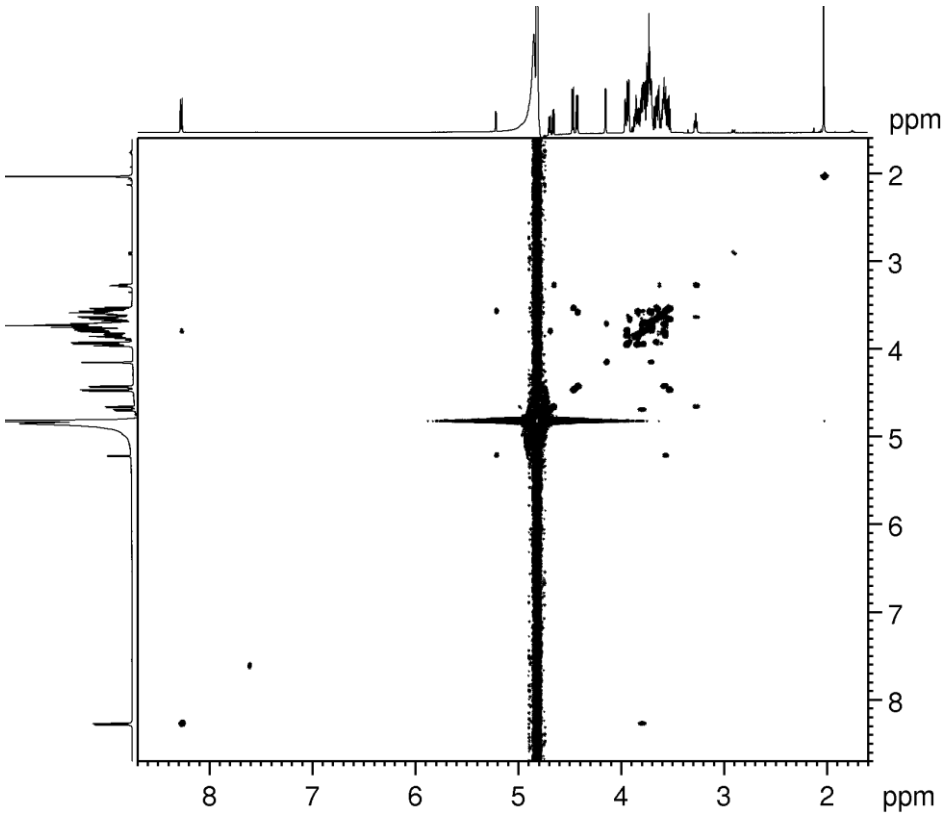

Figure A14. ^{1}H -^{1}H COSY spectrum of LNnT (H_2O:D_2O 9:1 *v/v* solvent at pH 3.0)

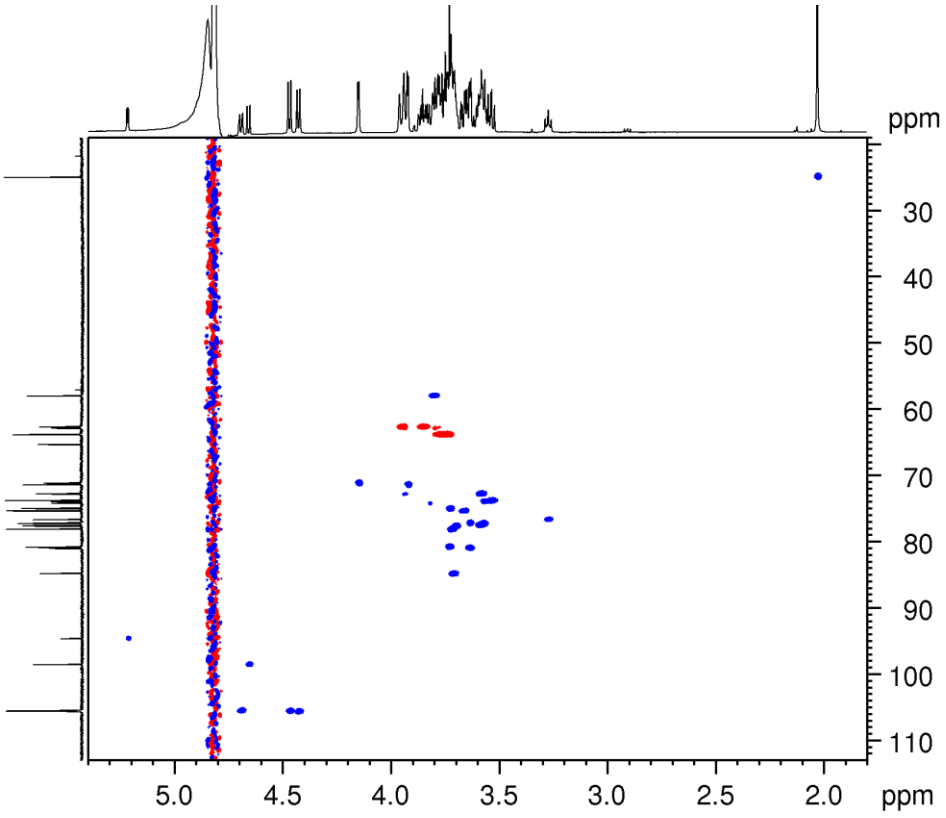

Figure A15. ^{1}H -^{13}C HSQC spectrum of LNnT (H_2O:D_2O 9:1 *v/v* solvent at pH 3.0)

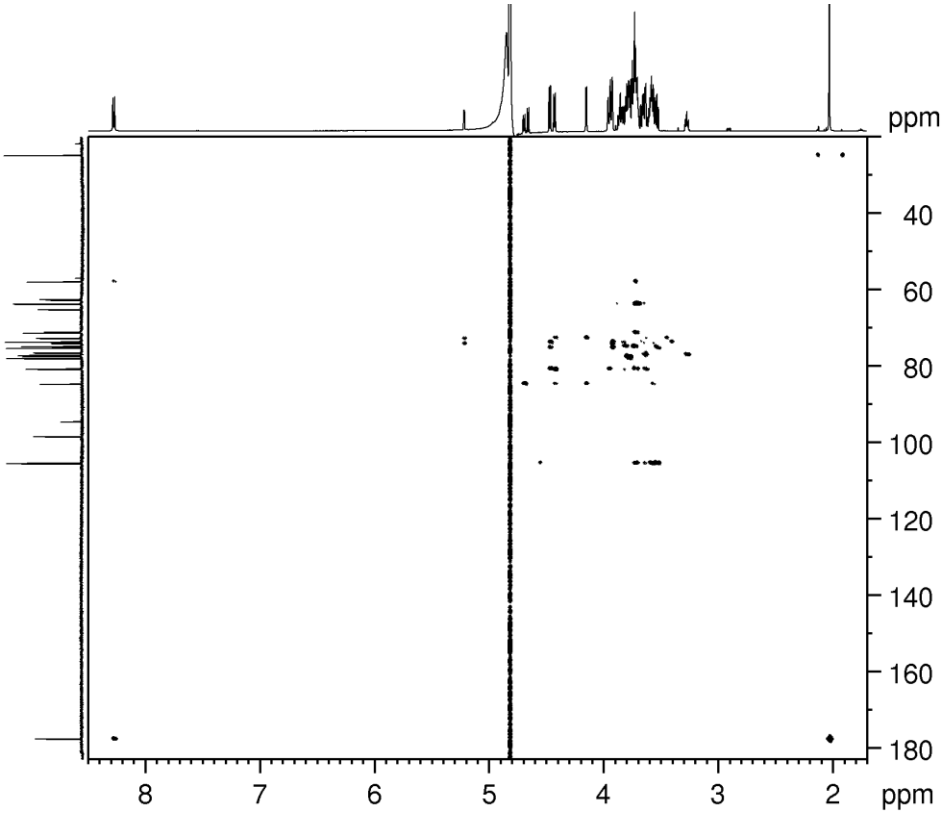

Figure A16. ^{1}H -^{13}C HMBC spectrum of LNnT (H_2O:D_2O 9:1 *v/v* solvent at pH 3.0)

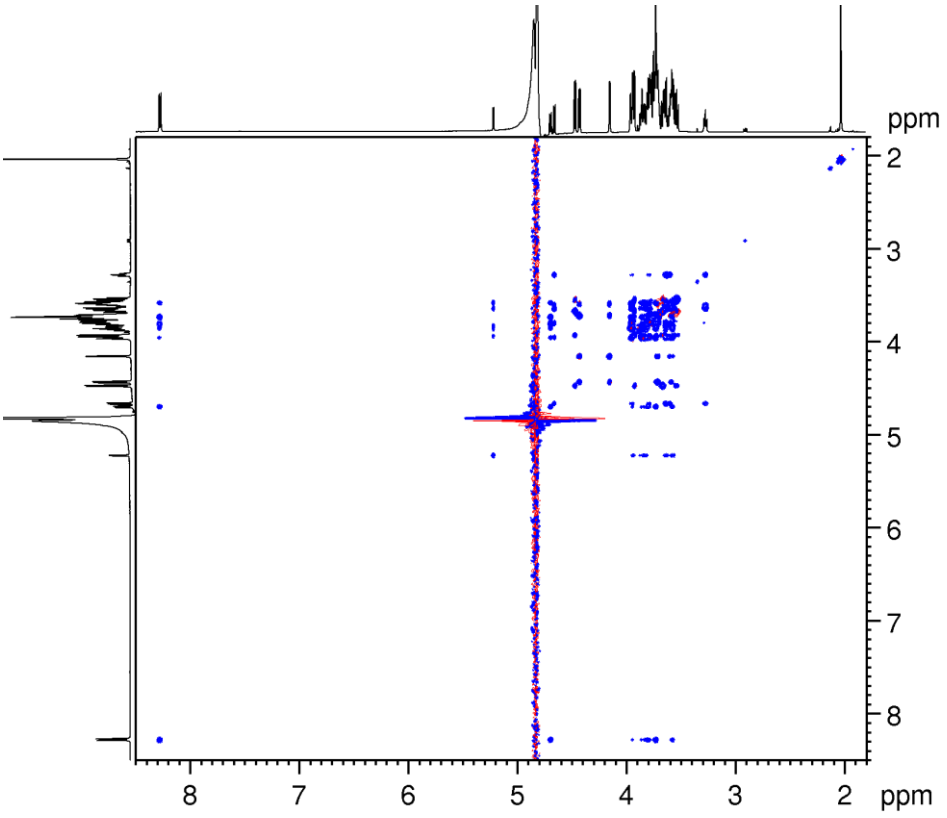

Figure A17. ^{1}H -^{1}H TOCSY spectrum of LNnT (H_2O:D_2O 9:1 *v/v* solvent at pH 3.0)

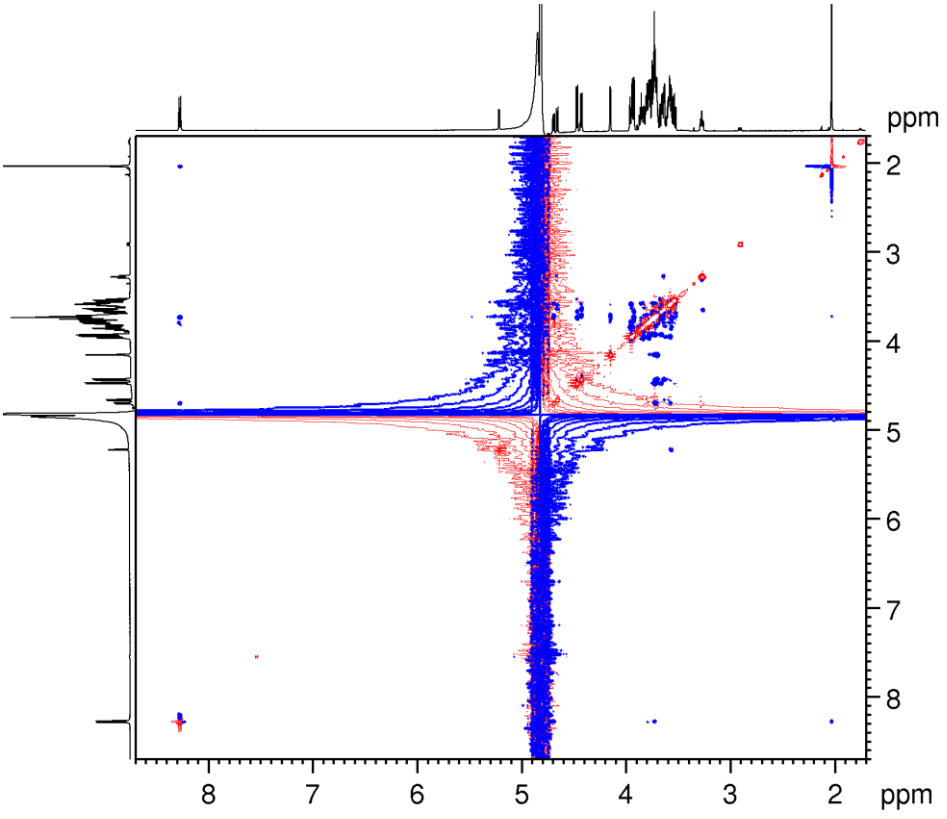

Figure A18. ^{1}H -^{1}H ROESY spectrum of LNnT (H_2O:D_2O 9:1 *v/v* solvent at pH 3.0)

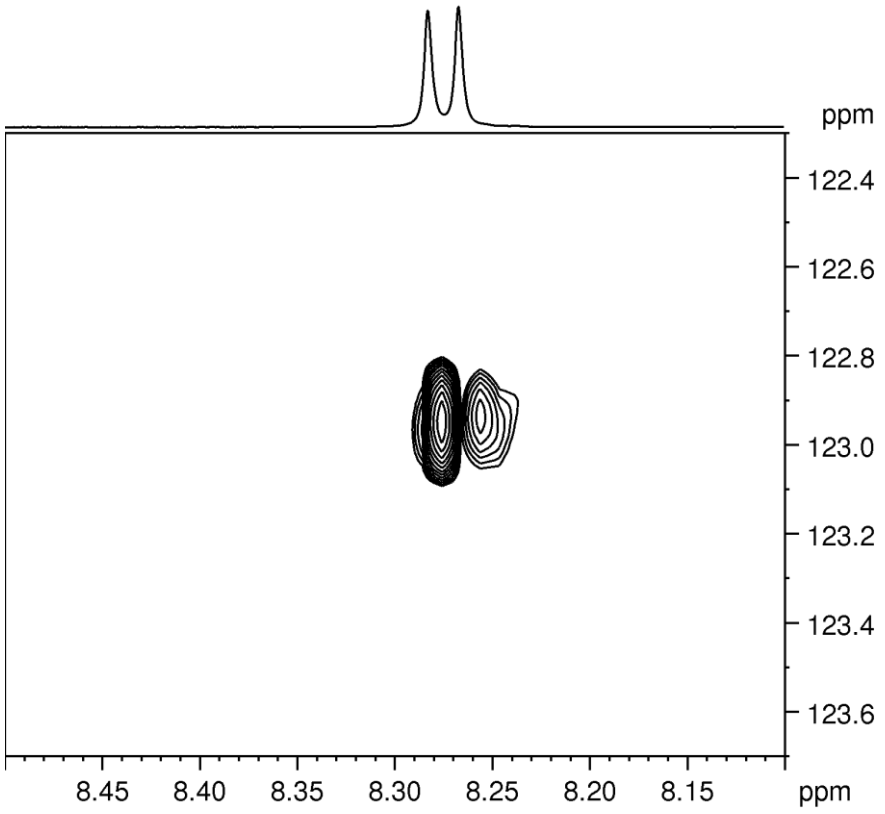

Figure A19. ^{1}H -^{15}N HSQC spectrum of LNnT (H_2O:D_2O 9:1 *v/v* solvent at pH 3.0)

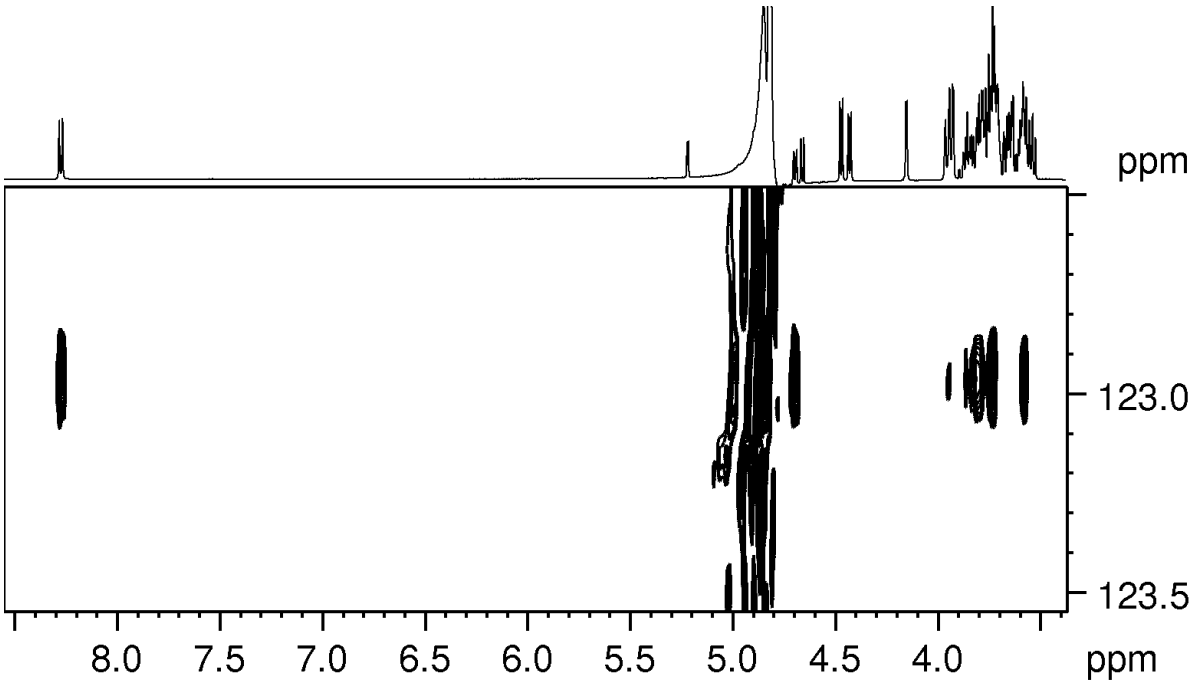

Figure A20. ^{1}H -^{15}N HSQC-TOCSY spectrum of LNnT (H_2O:D_2O 9:1 *v/v* solvent at pH 3.0)

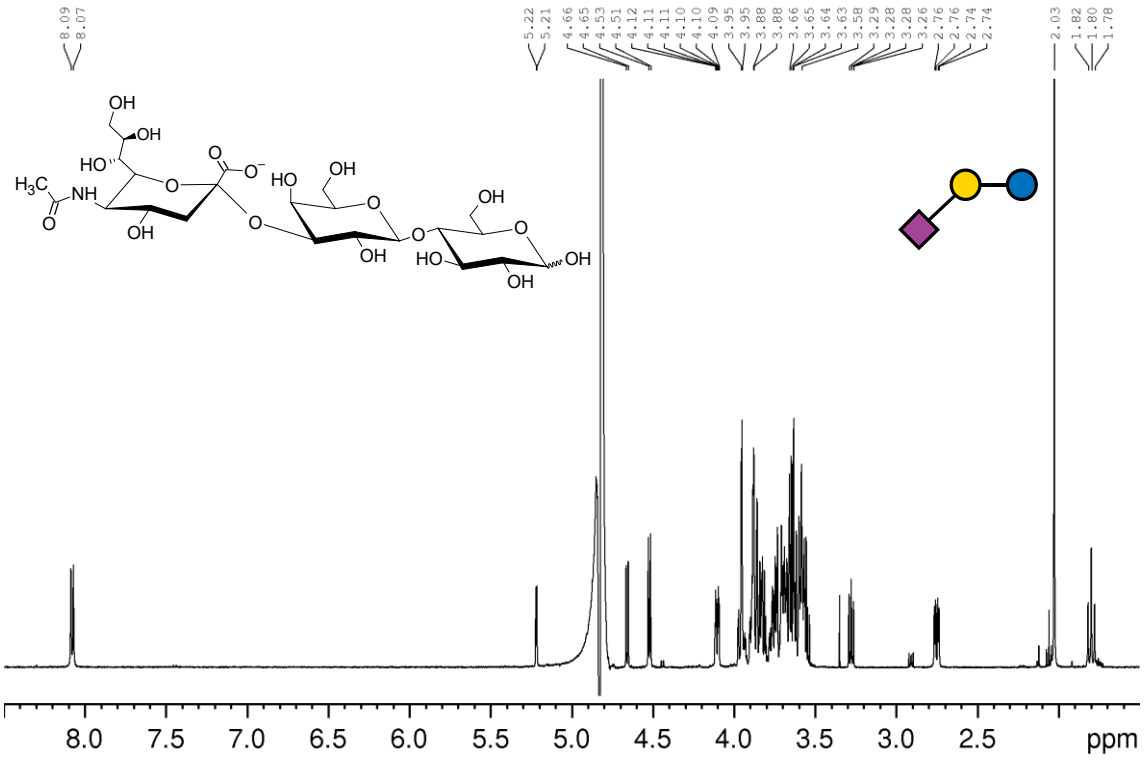

Figure A21. ^{1}H NMR spectrum of 3'SL sodium salt (H_2O:D_2O 9:1 *v/v* solvent at pH 3.0)

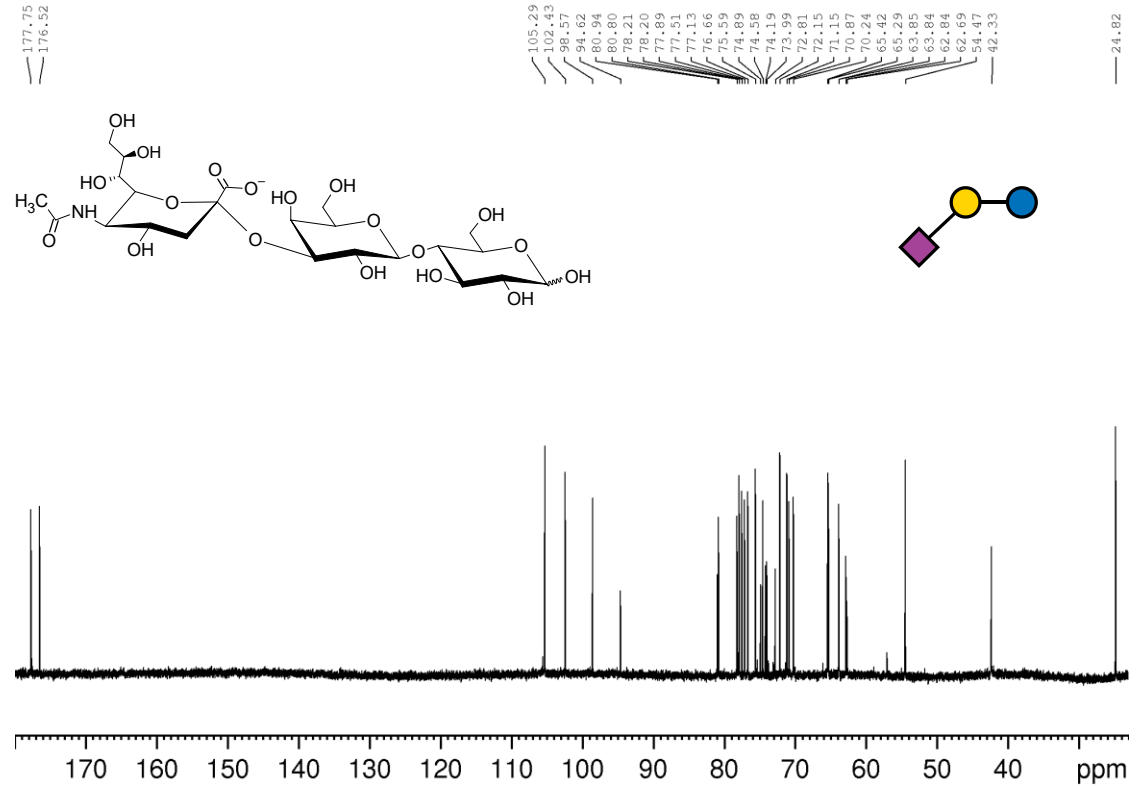

Figure A22. ^{13}C NMR spectrum of 3'SL sodium salt (H_2O:D_2O 9:1 *v/v* solvent at pH 3.0)

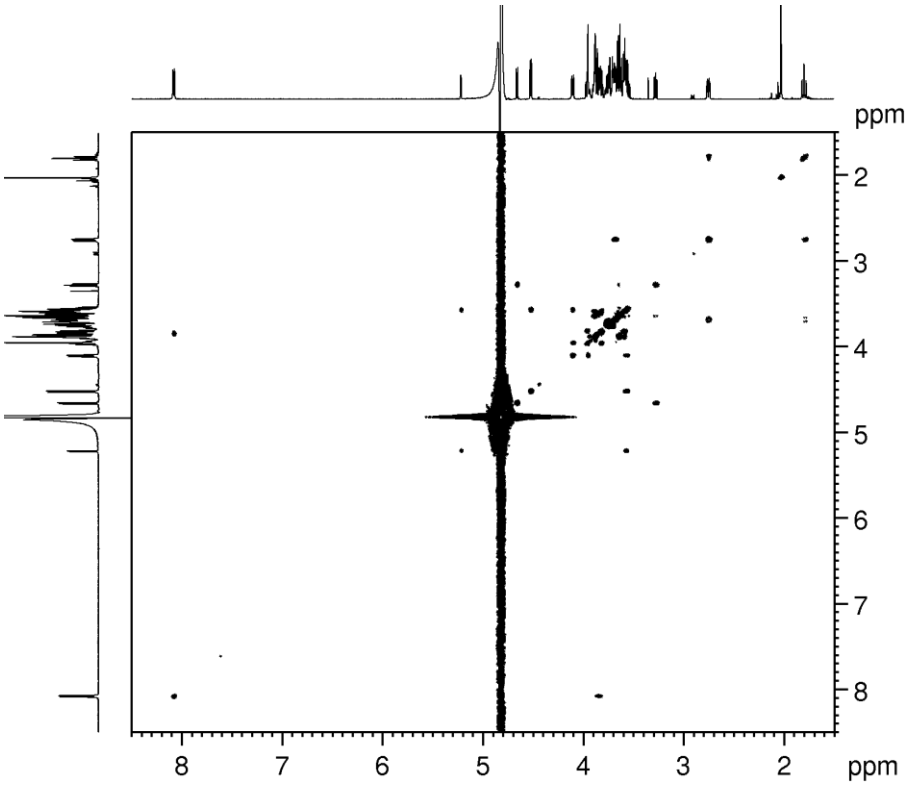

Figure A23. ^{1}H -^{1}H COSY spectrum of 3'SL sodium salt (H_2O:D_2O 9:1 *v/v* solvent at pH 3.0)

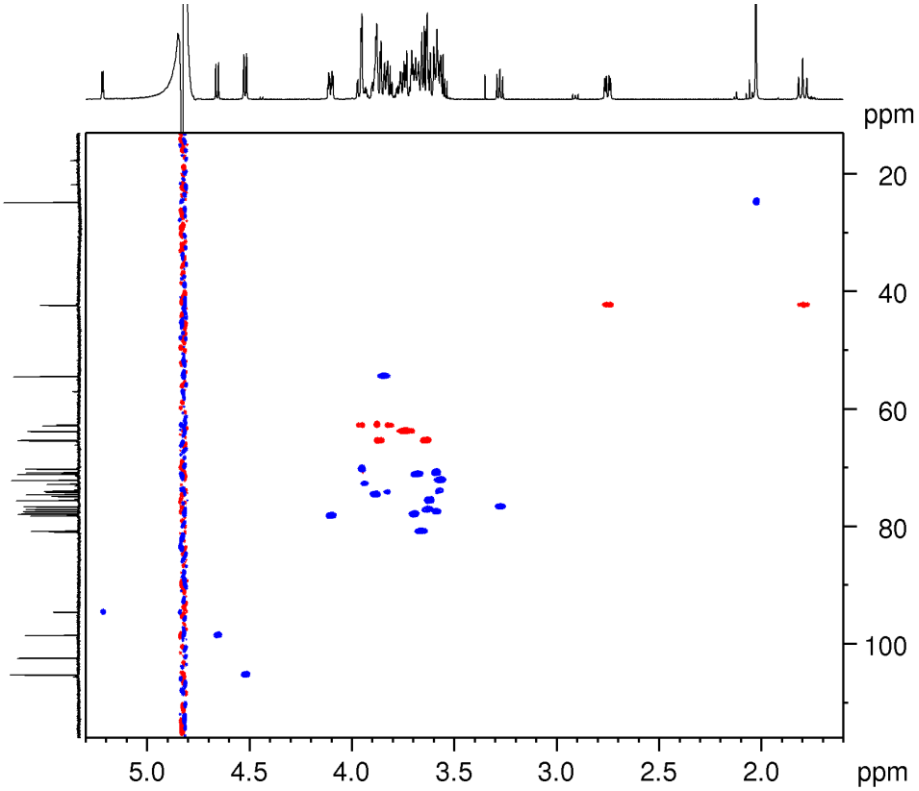

Figure A24. ^{1}H -^{13}C HSQC spectrum of 3'SL sodium salt (H_2O:D_2O 9:1 *v/v* solvent at pH 3.0)

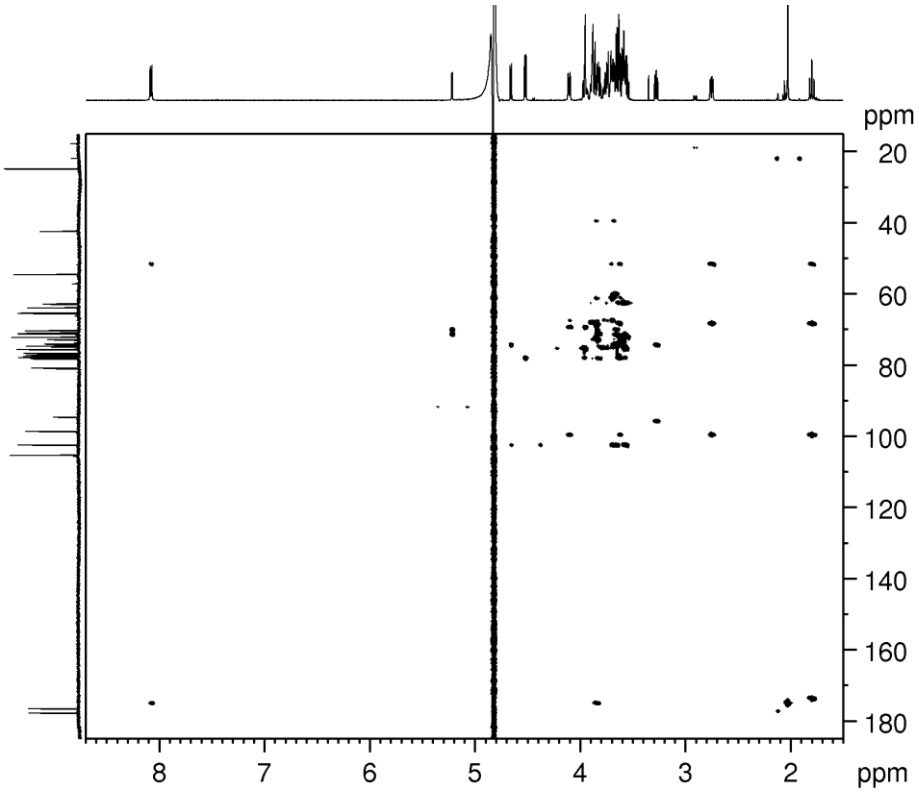

Figure A25. ^{1}H -^{13}C HMBC spectrum of 3'SL sodium salt (H_2O:D_2O 9:1 *v/v* solvent at pH 3.0)

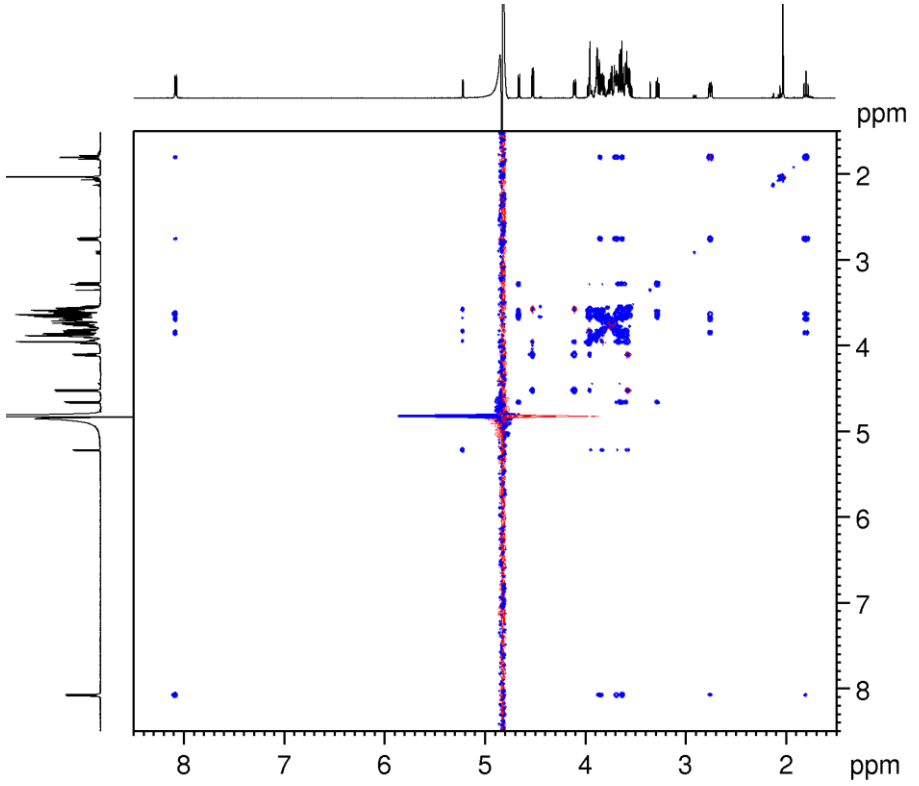

Figure A26. ^{1}H -^{1}H TOCSY spectrum of 3'SL sodium salt (H_2O:D_2O 9:1 *v/v* solvent at pH 3.0)

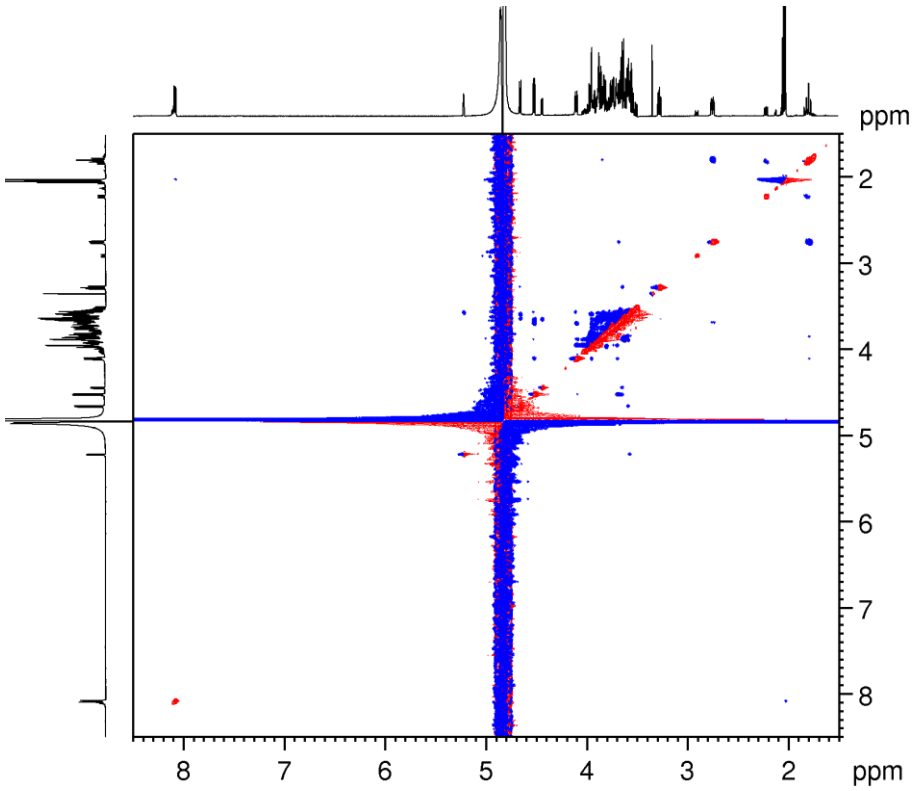

Figure A27. ^{1}H -^{1}H ROESY spectrum of 3'SL sodium salt (H_2O:D_2O 9:1 *v/v* solvent at pH 3.0)

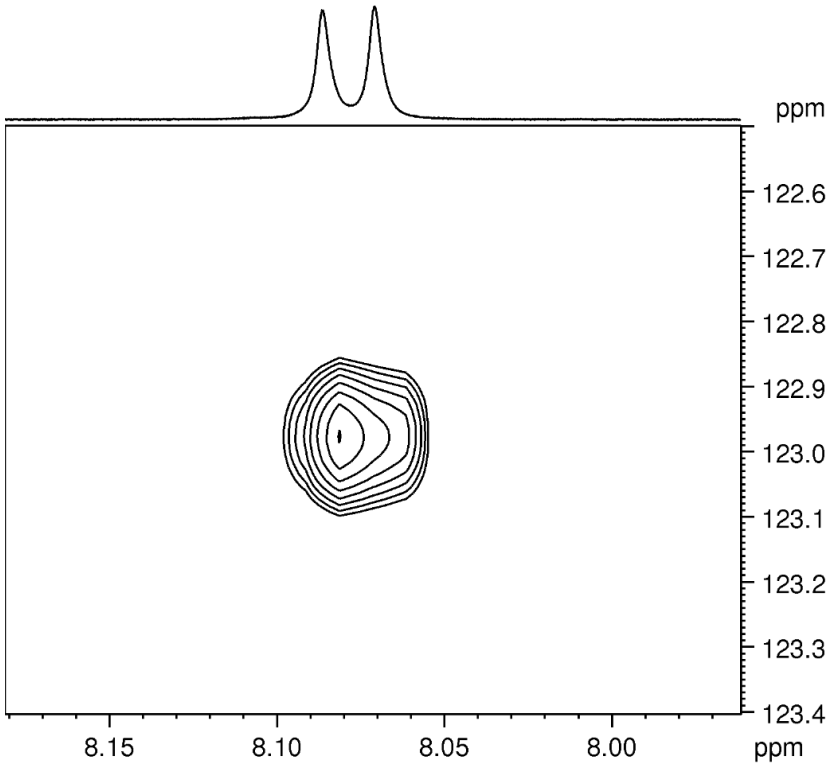

Figure A28. ^{1}H -^{15}N HSQC spectrum of 3'SL sodium salt (H_2O:D_2O 9:1 *v/v* solvent at pH 3.0)

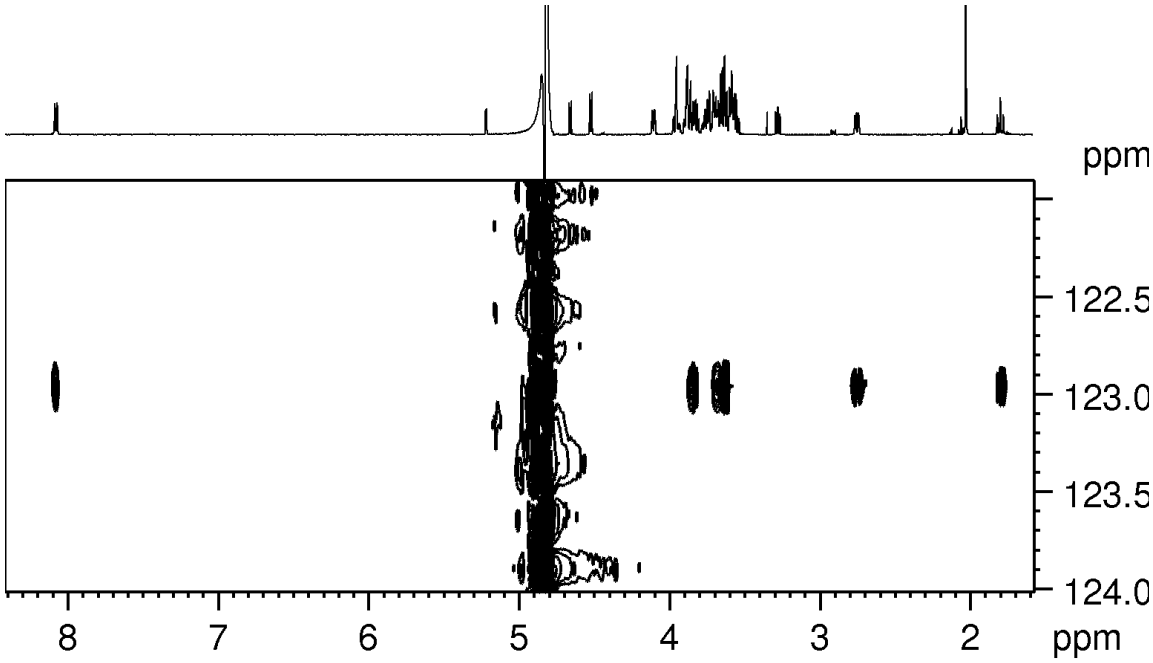

Figure A29. ^{1}H -^{15}N HSQC-TOCSY spectrum of 3'SL sodium salt (H_2O:D_2O 9:1 *v/v* solvent at pH 3.0)

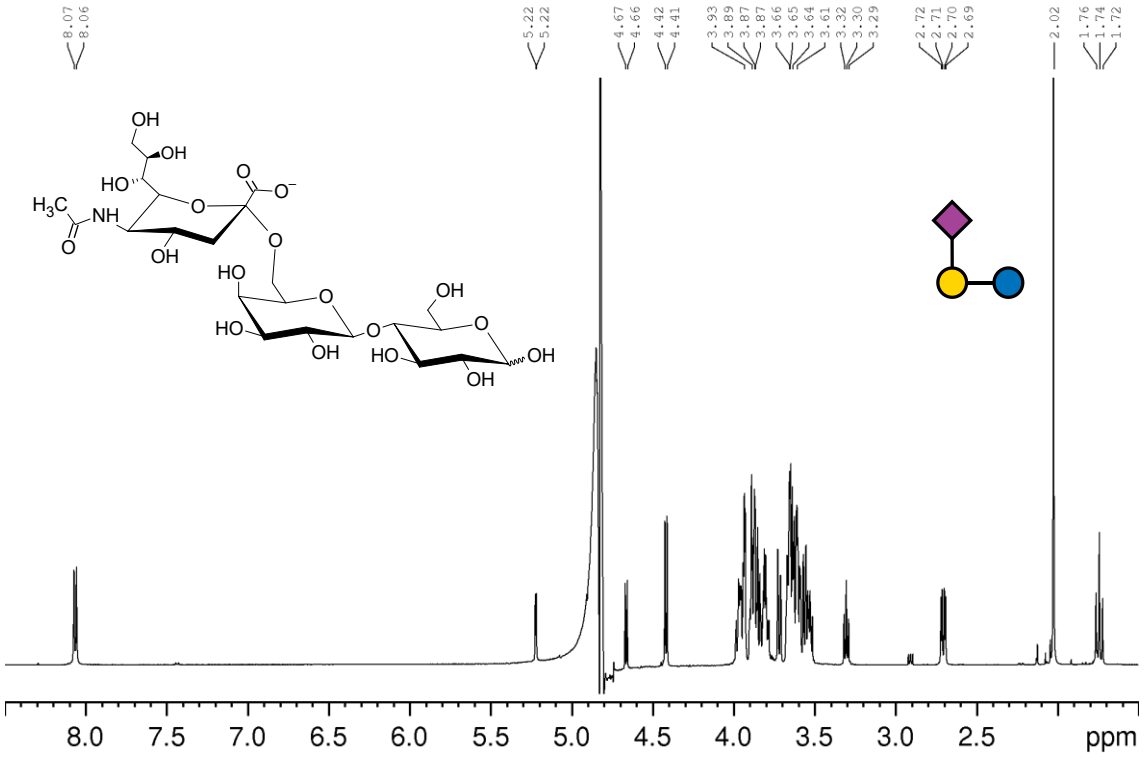

Figure A30. ^{1}H NMR spectrum of 6'SL sodium salt (H_2O:D_2O 9:1 *v/v* solvent at pH 3.0)

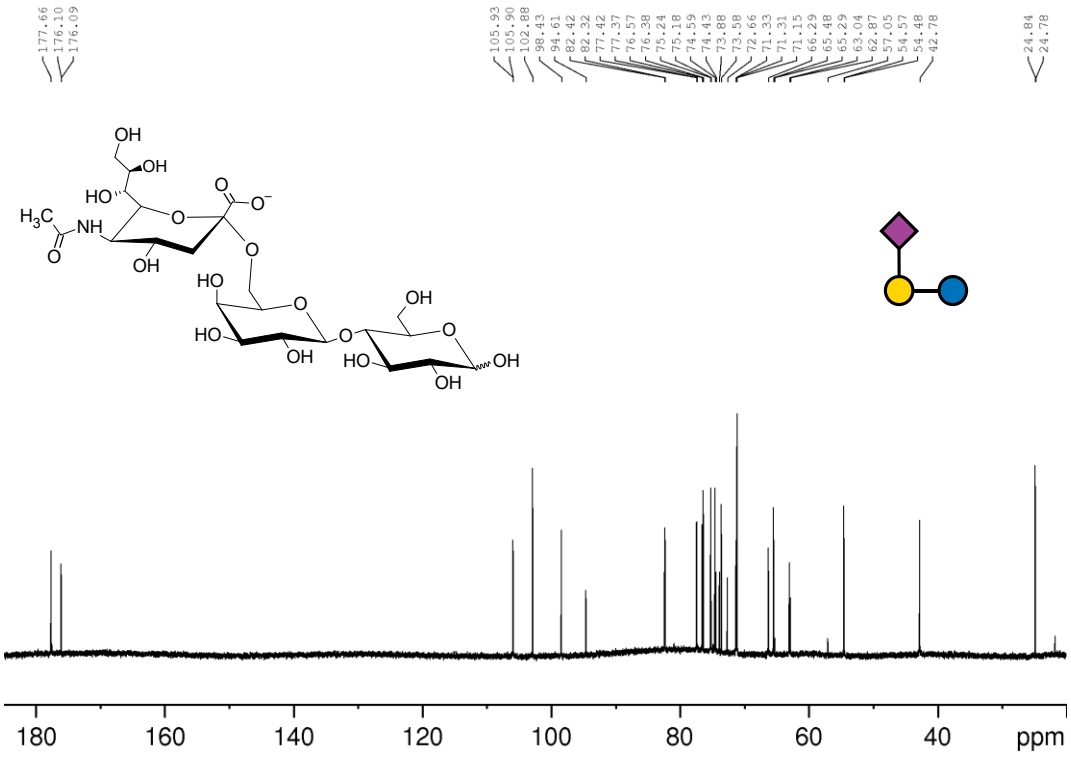

Figure A31. ^{13}C NMR spectrum of 6'SL sodium salt (H_2O:D_2O 9:1 *v/v* solvent at pH 3.0)

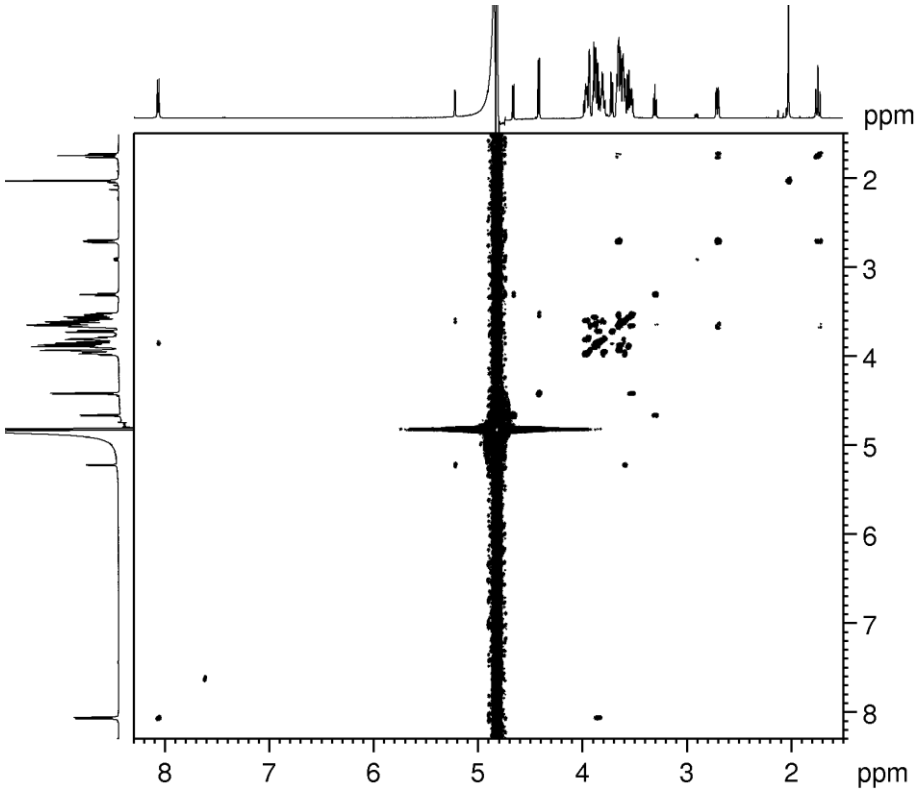

Figure A32. ^{1}H -^{1}H COSY spectrum of 6'SL sodium salt (H_2O:D_2O 9:1 *v/v* solvent at pH 3.0)

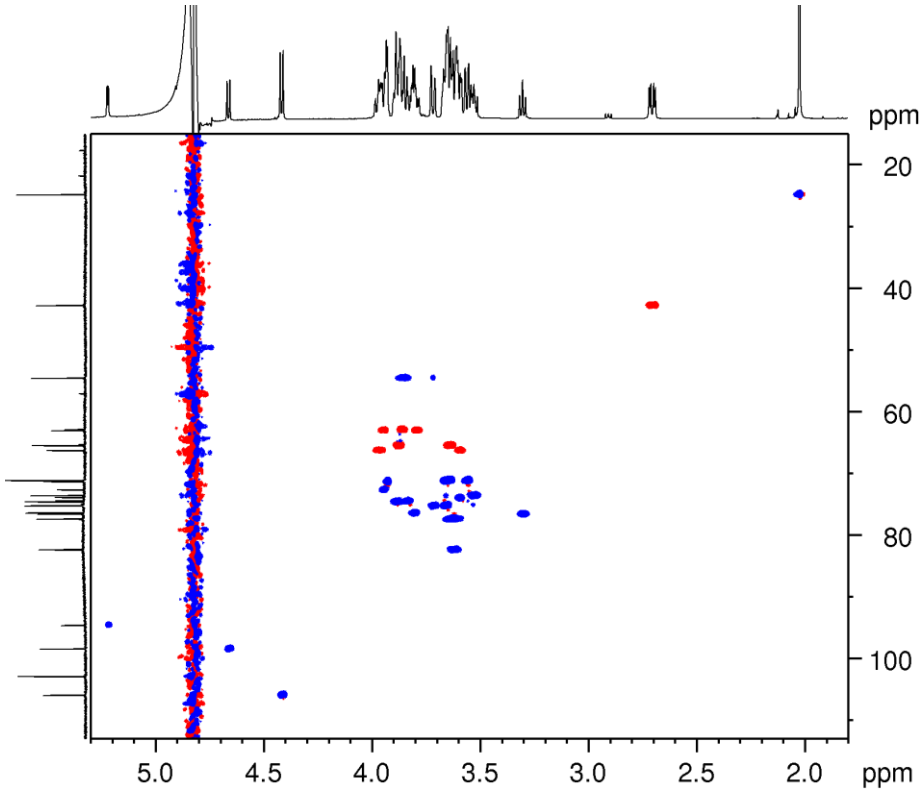

Figure A33. ^{1}H -^{13}C HSQC spectrum of 6'SL sodium salt (H_2O:D_2O 9:1 *v/v* solvent at pH 3.0)

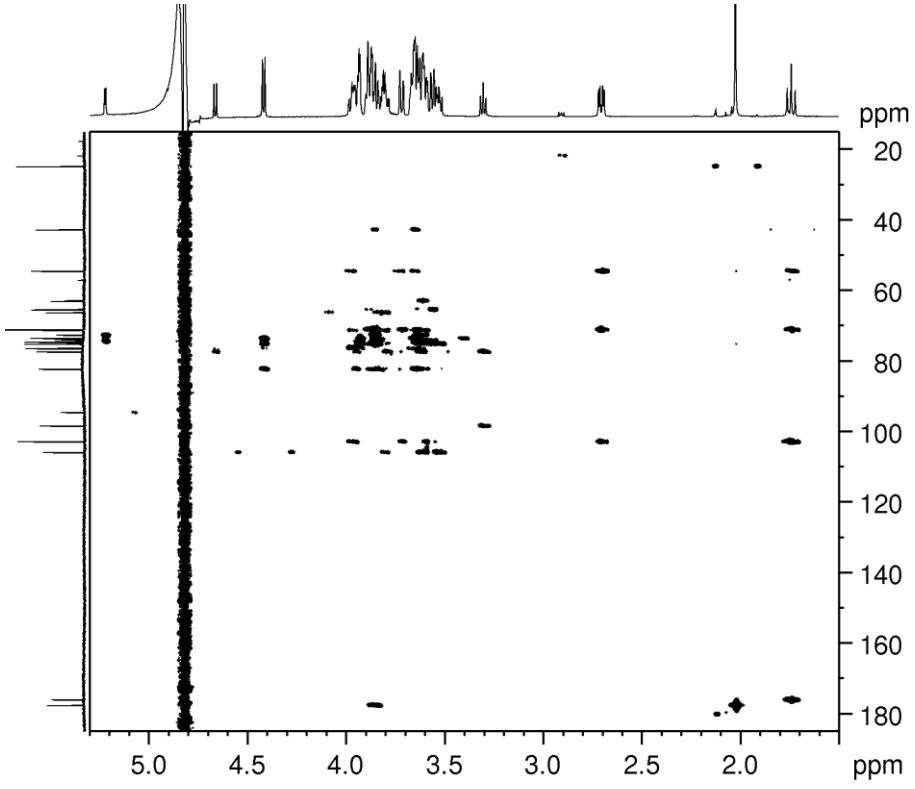

Figure A34. ^{1}H -^{13}C HMBC spectrum of 6'SL sodium salt (H_2O:D_2O 9:1 *v/v* solvent at pH 3.0)

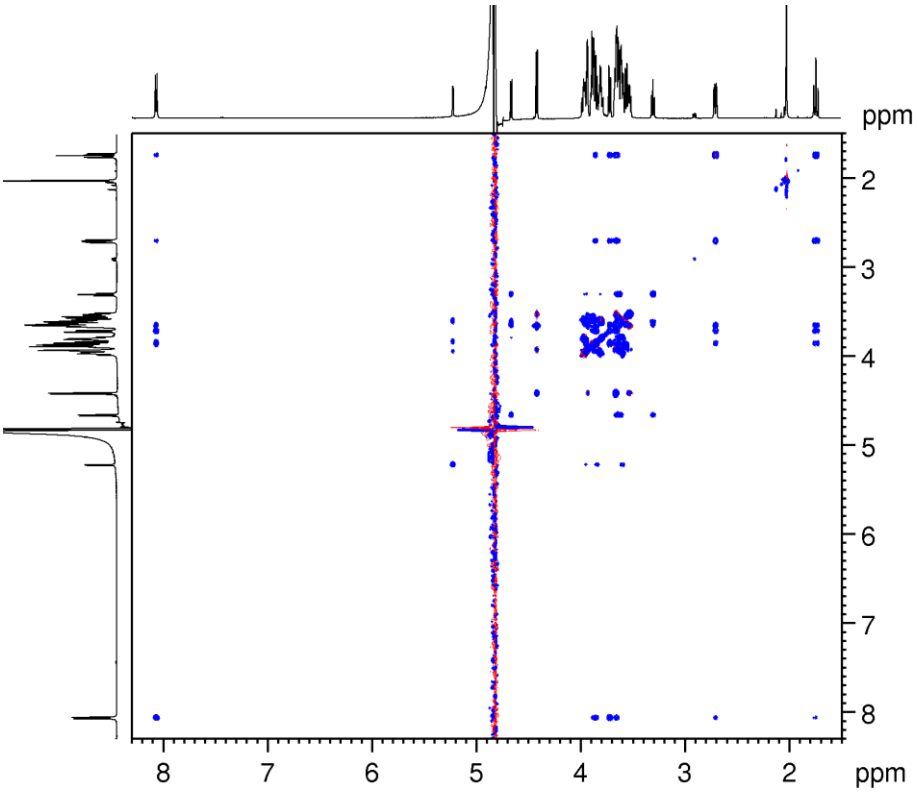

Figure A35. ^{1}H -^{1}H TOCSY spectrum of 6'SL sodium salt (H_2O:D_2O 9:1 *v/v* solvent at pH 3.0)

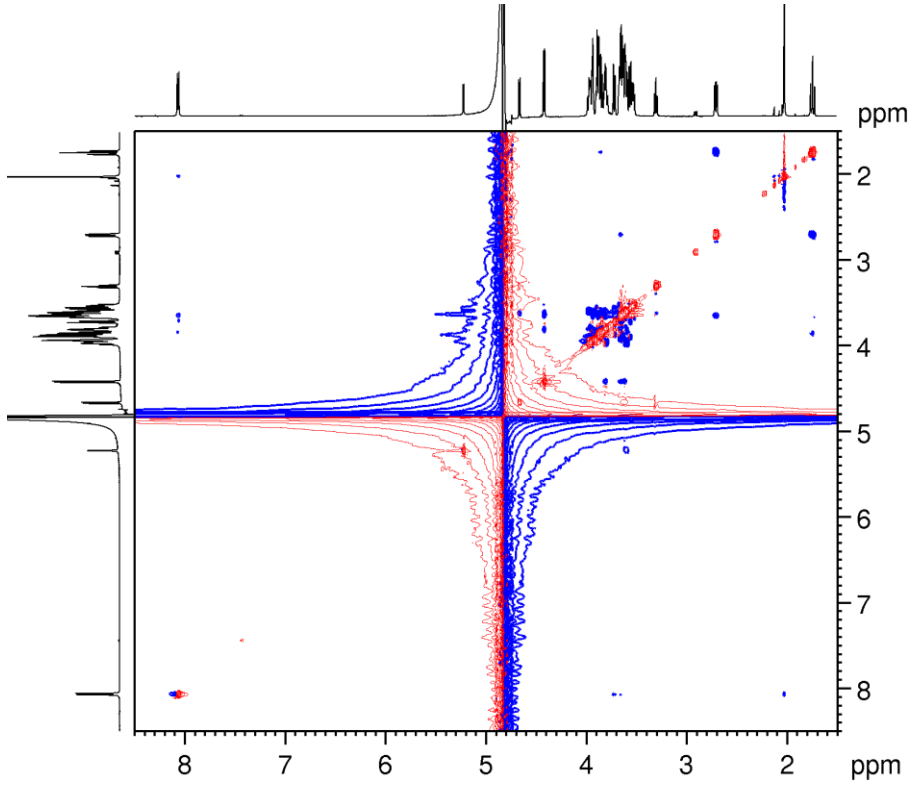

Figure A36. ^{1}H -^{1}H ROESY spectrum of 6'SL sodium salt (H_2O:D_2O 9:1 *v/v* solvent at pH 3.0)

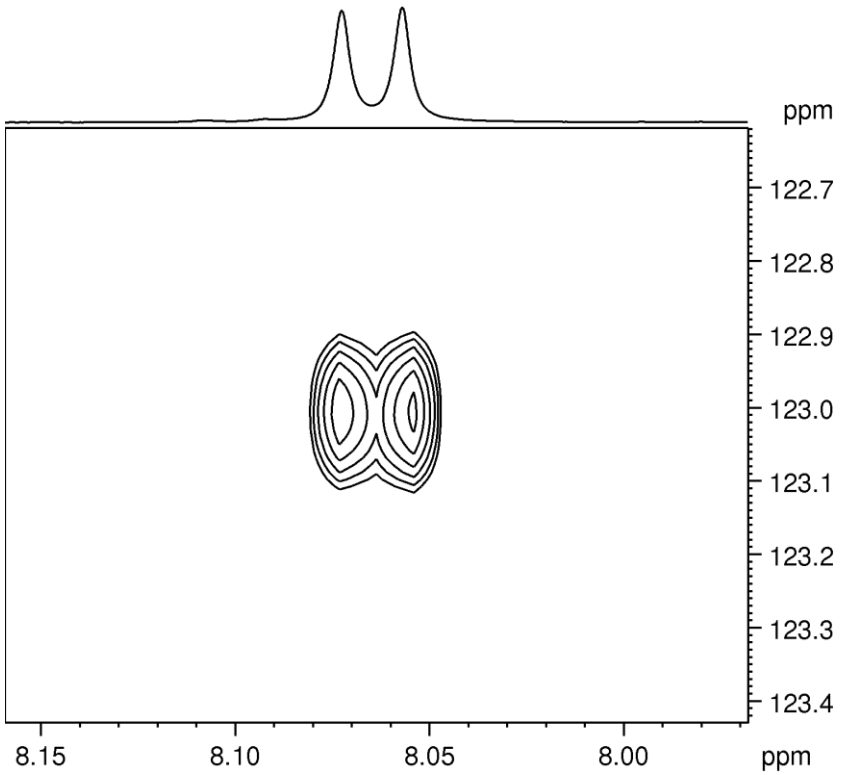

Figure A37. ^{1}H -^{15}N HSQC spectrum of 6'SL sodium salt (H_2O:D_2O 9:1 *v/v* solvent at pH 3.0)

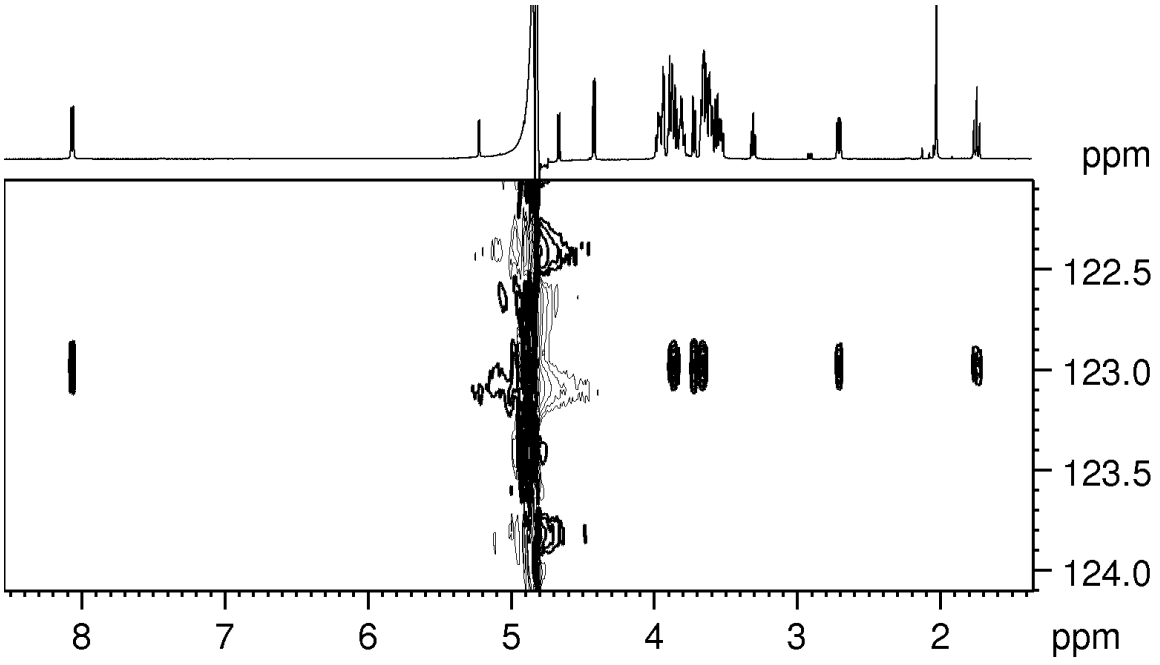

Figure A38. ^{1}H -^{15}N HSQC-TOCSY spectrum of 6'SL sodium salt (H_2O:D_2O 9:1 *v/v* solvent at pH 3.0)

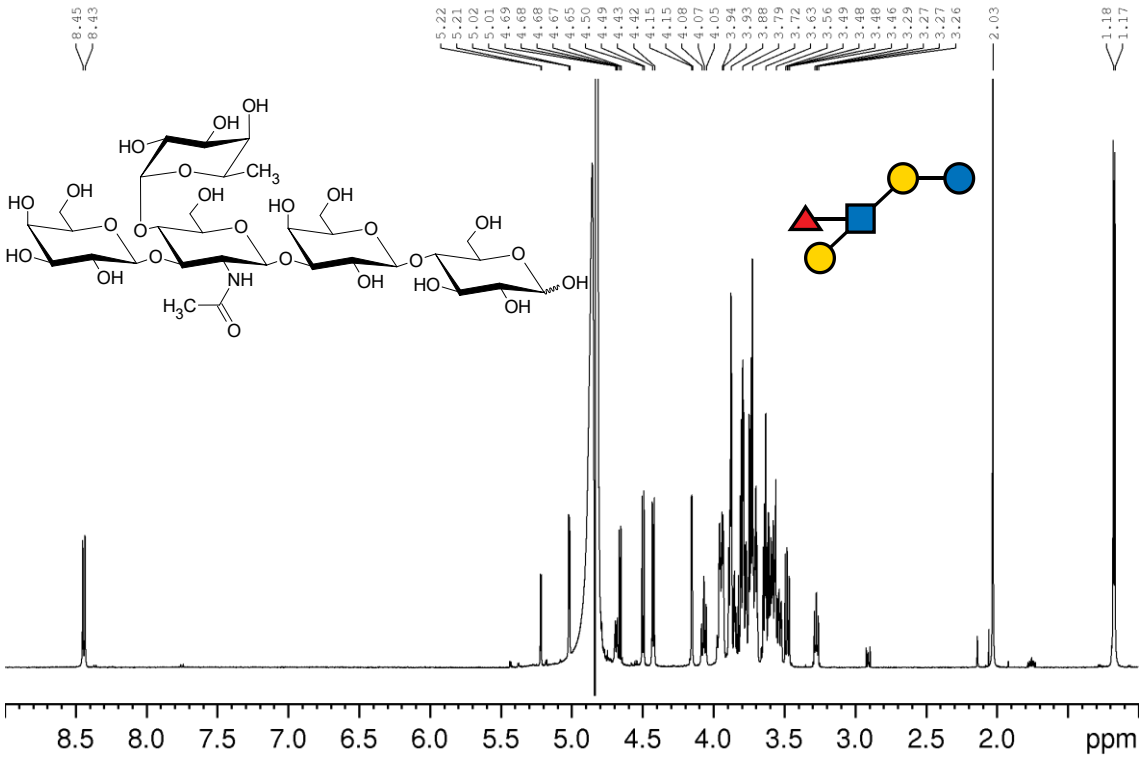

Figure A39. ^{1}H NMR spectrum of LNFP II (H_2O:D_2O 9:1 *v/v* solvent at pH 3.0)

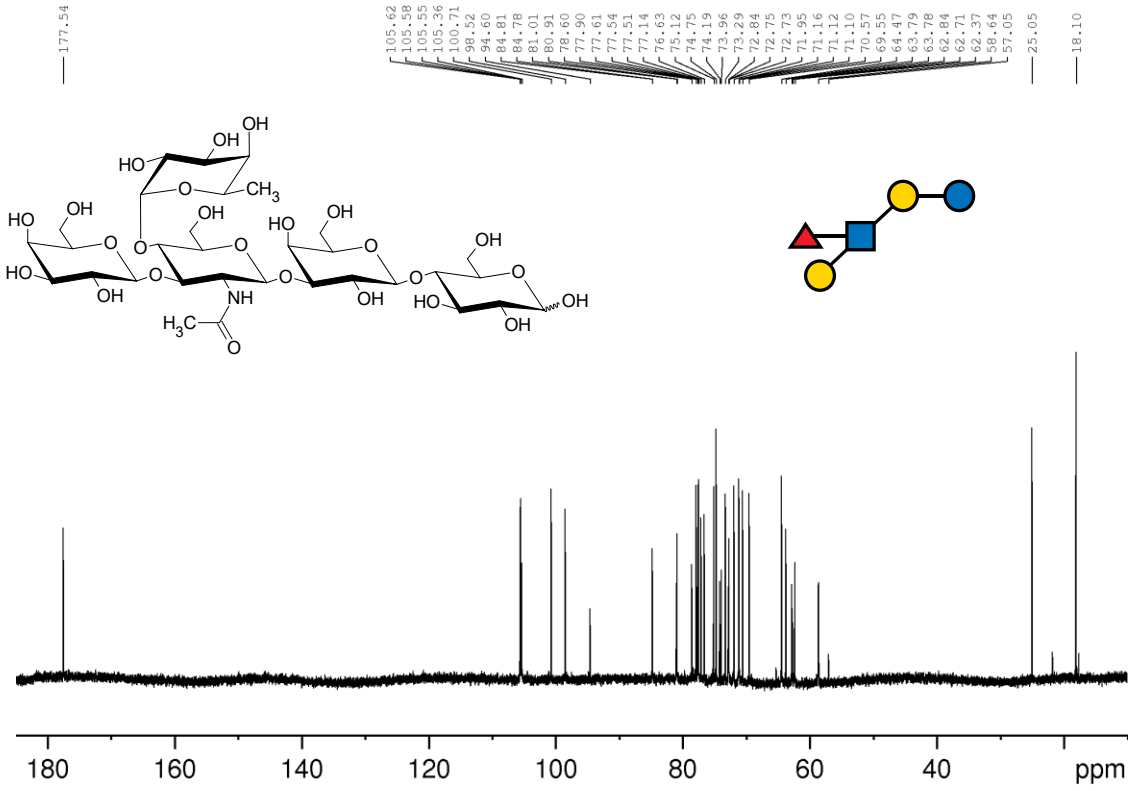

Figure A40. ^{13}C NMR spectrum of LNFP II (H_2O:D_2O 9:1 *v/v* solvent at pH 3.0)

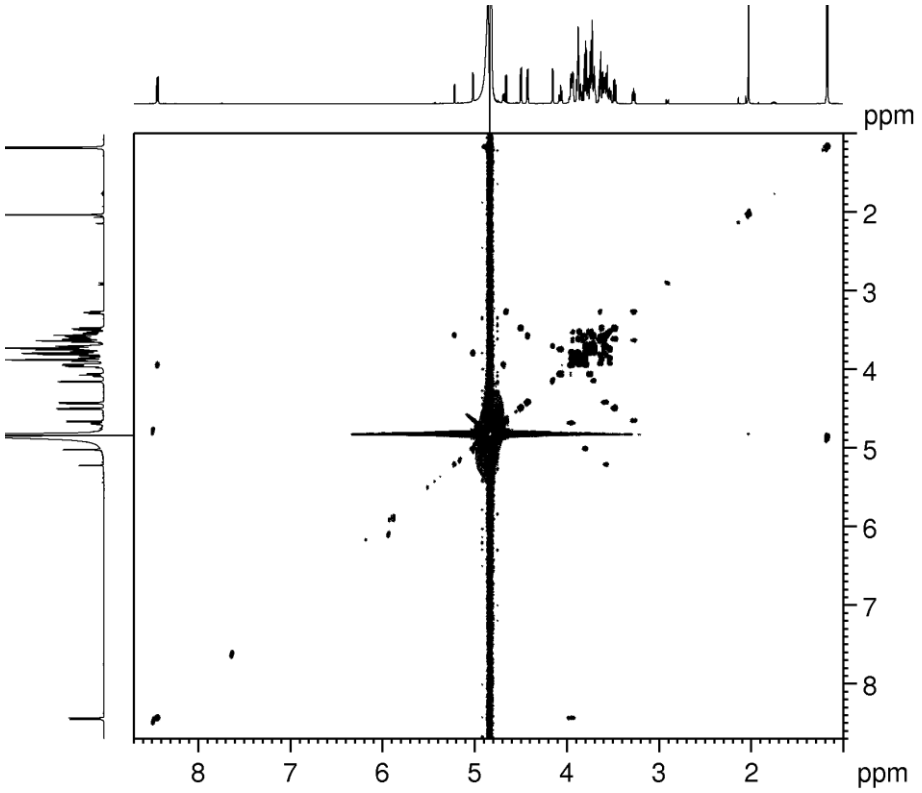

Figure A41. ^{1}H -^{1}H COSY spectrum of LNFP II (H_2O:D_2O 9:1 *v/v* solvent at pH 3.0)

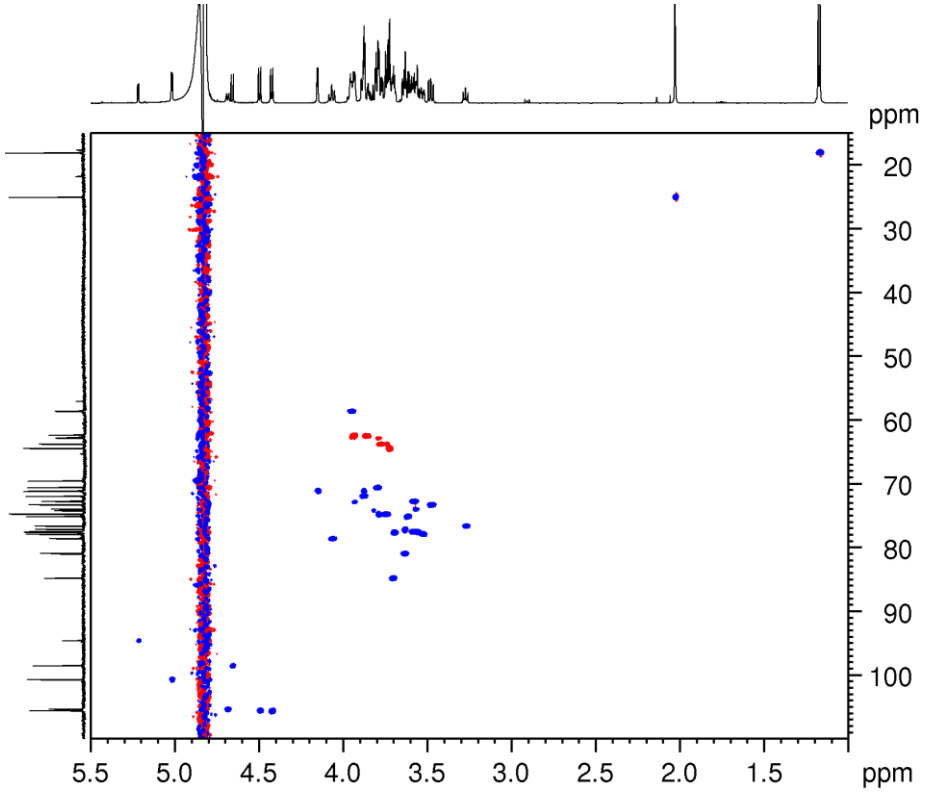

Figure A42. ^{1}H -^{13}C HSQC spectrum of LNFP II (H_2O:D_2O 9:1 *v/v* solvent at pH 3.0)

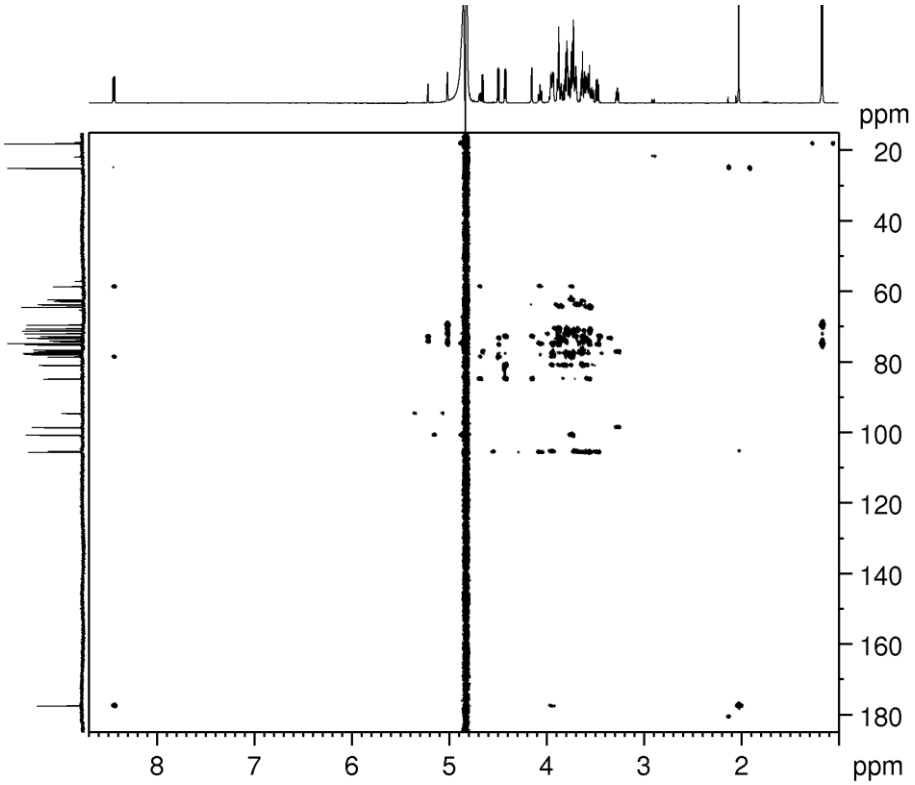

Figure A43. ^{1}H -^{13}C HMBC spectrum of LNFP II (H_2O:D_2O 9:1 *v/v* solvent at pH 3.0)

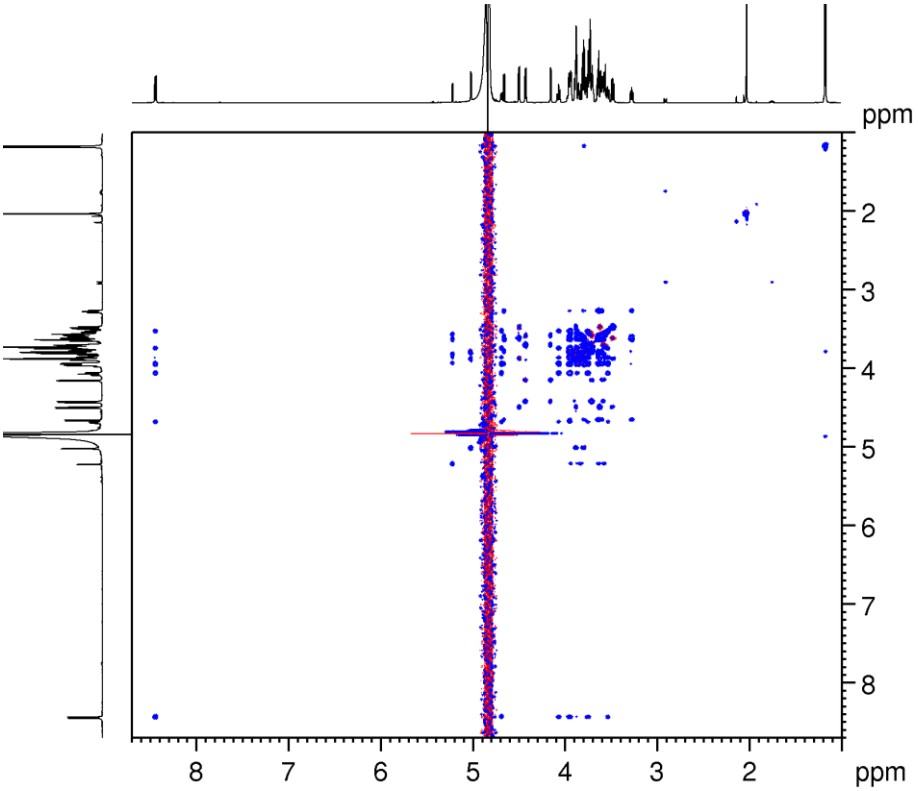

Figure A44. ^{1}H -^{1}H TOCSY spectrum of LNFP II (H_2O:D_2O 9:1 *v/v* solvent at pH 3.0)

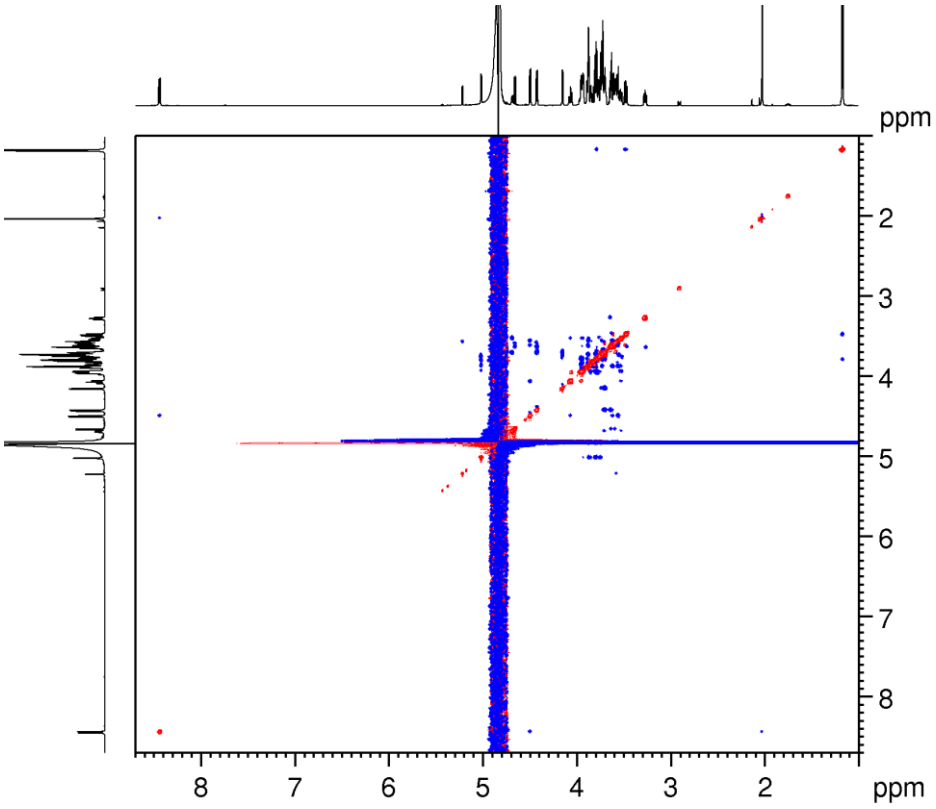

Figure A45. ^{1}H -^{1}H ROESY spectrum of LNFP II (H_2O:D_2O 9:1 *v/v* solvent at pH 3.0)

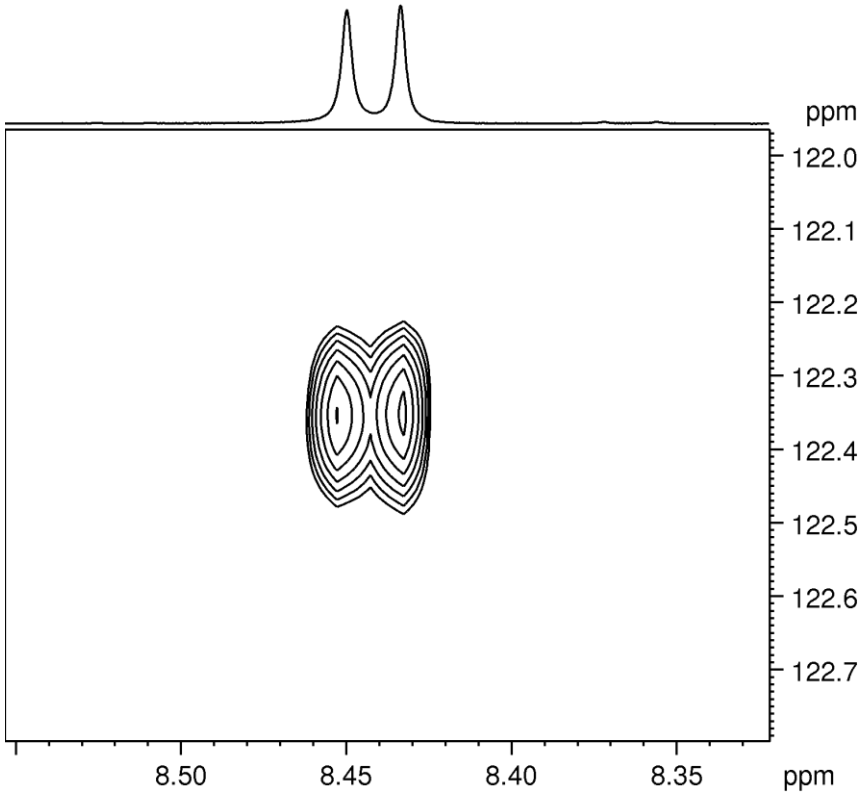

Figure A46. ^{1}H -^{15}N HSQC spectrum of LNFP II (H_2O:D_2O 9:1 *v/v* solvent at pH 3.0)

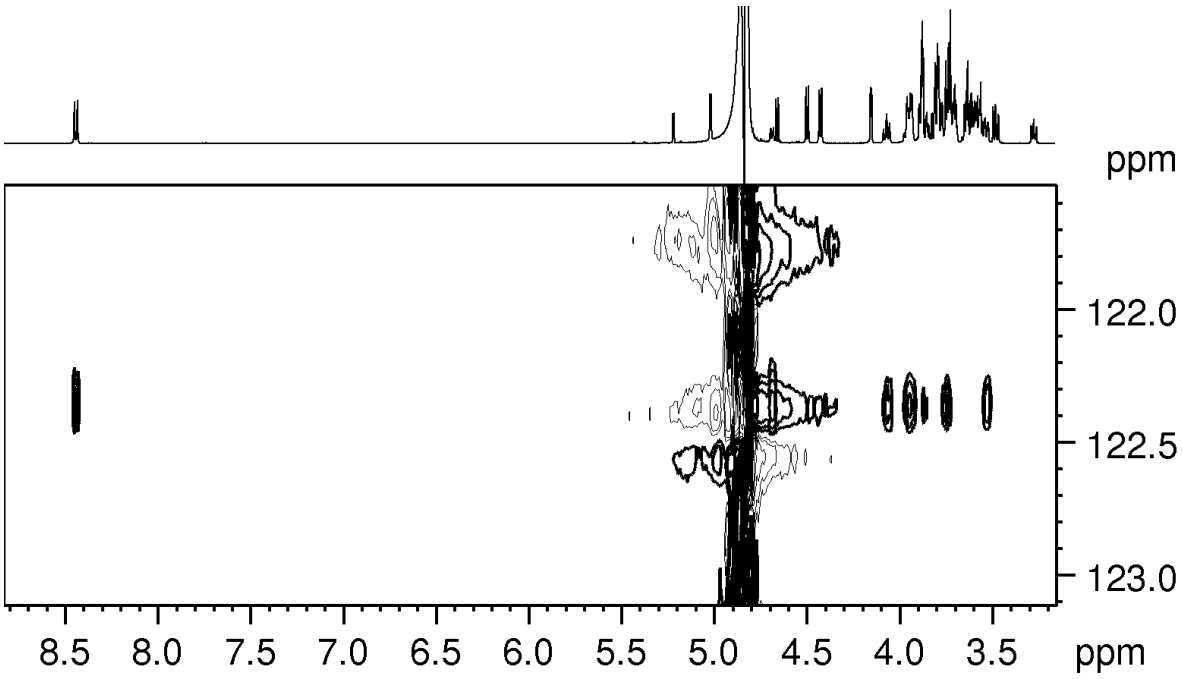

Figure A47. ^{1}H -^{15}N HSQC-TOCSY spectrum of LNFP II (H_2O:D_2O 9:1 *v/v* solvent at pH 3.0)

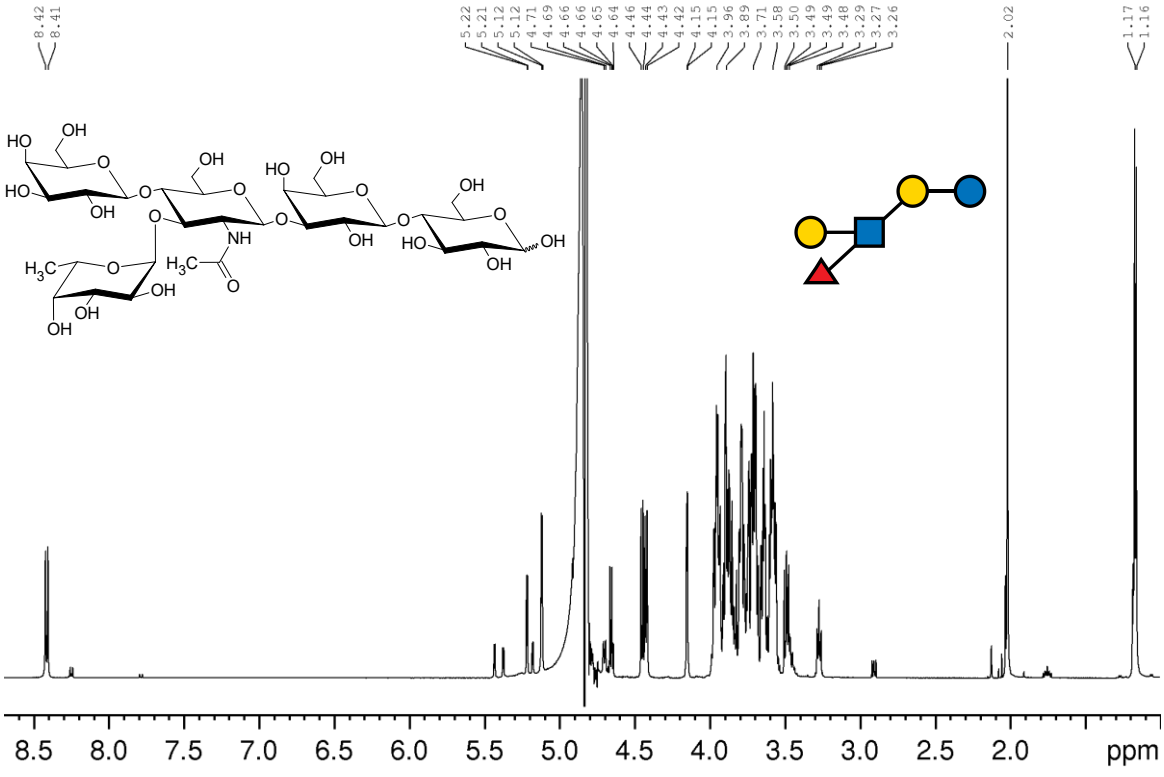

Figure A48. ^{1}H NMR spectrum of LNFP III (H_2O:D_2O 9:1 *v/v* solvent at pH 3.0)

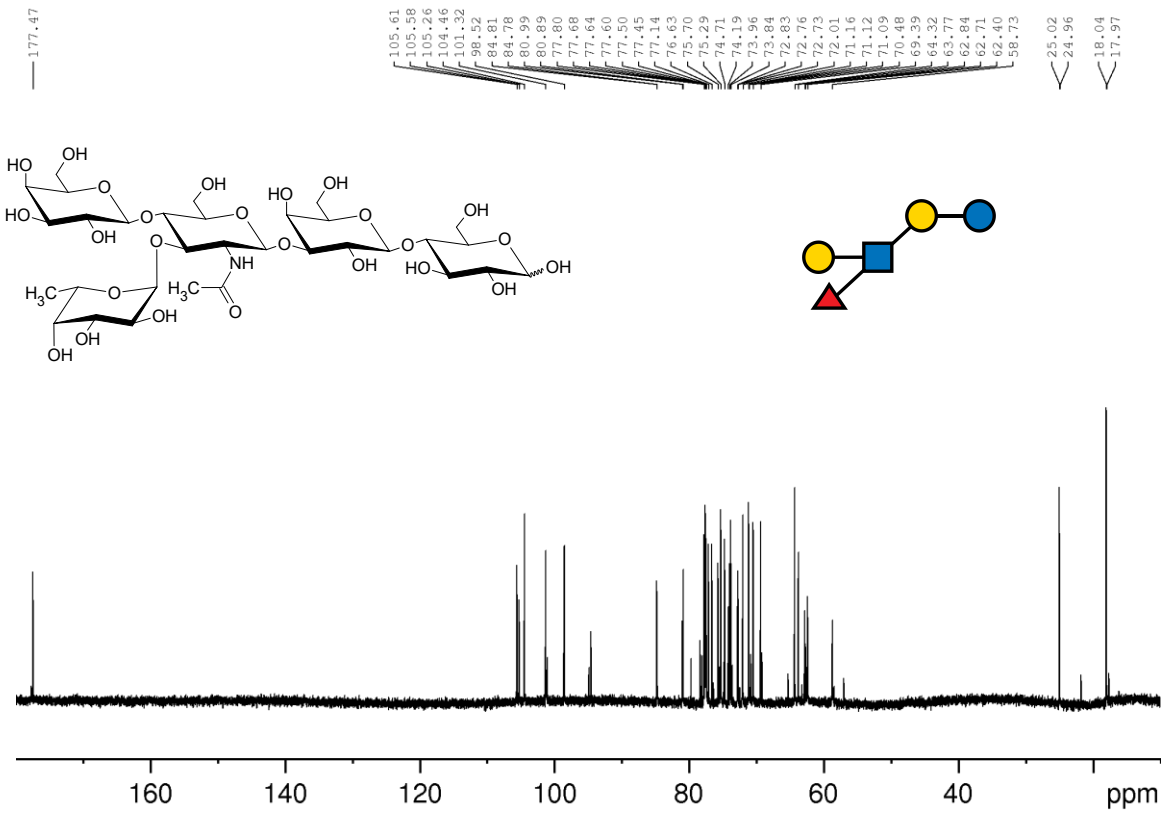

Figure A49. ^{13}C NMR spectrum of LNFP III (H_2O:D_2O 9:1 *v/v* solvent at pH 3.0)

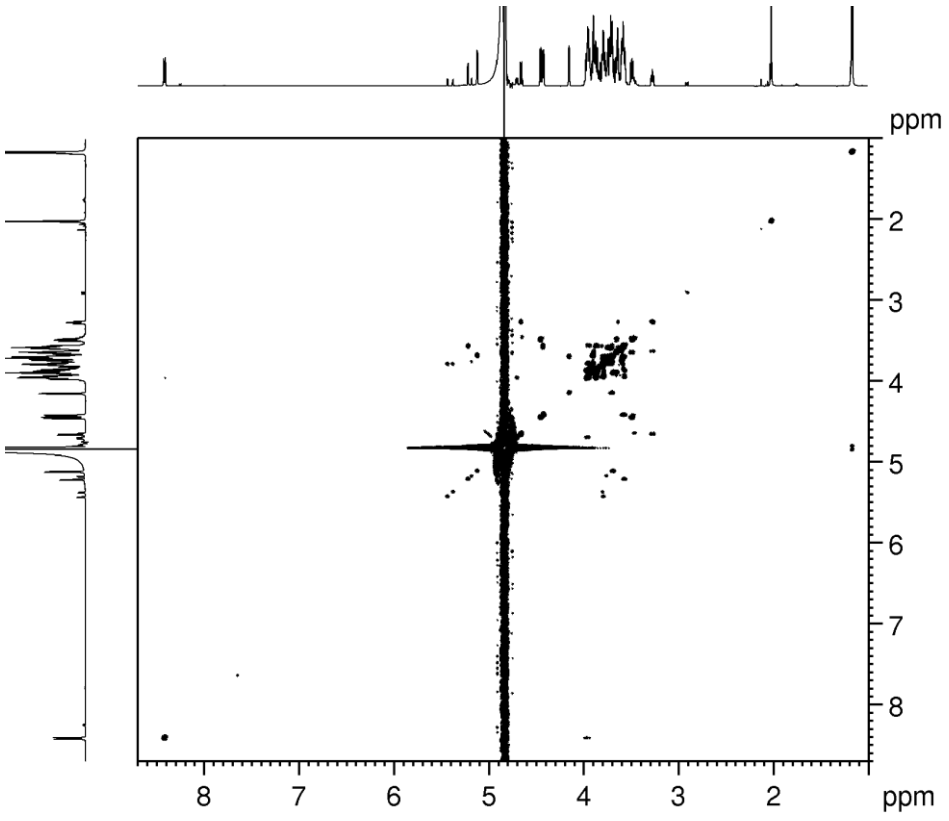

Figure A50. ^{1}H -^{1}H COSY spectrum of LNFP III (H_2O:D_2O 9:1 *v/v* solvent at pH 3.0)

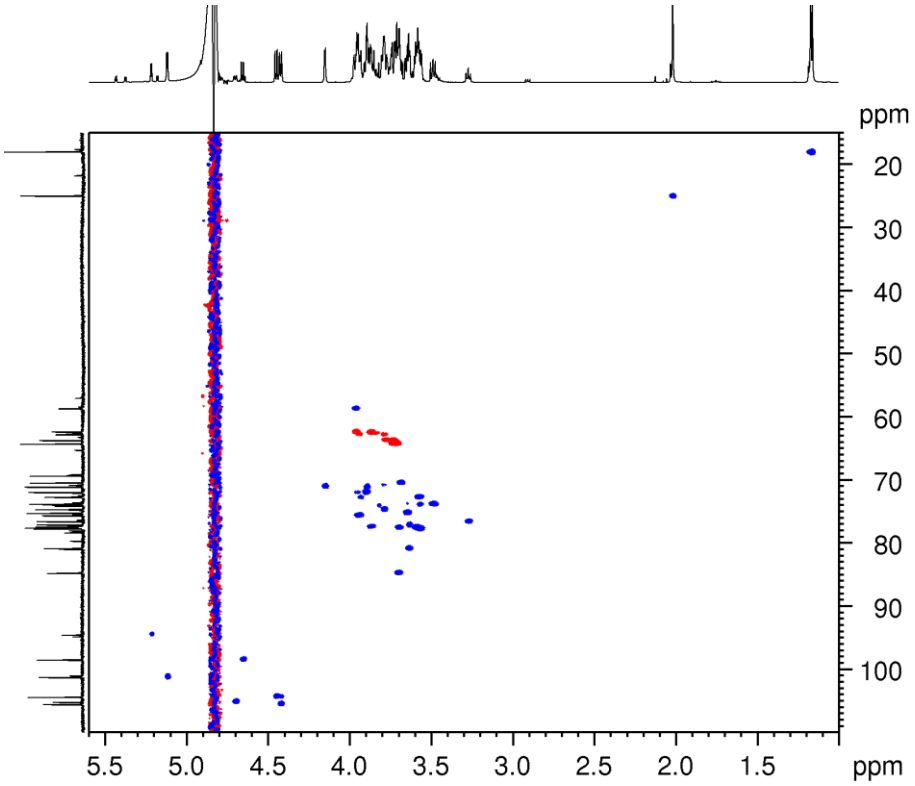

Figure A51. ^{1}H -^{13}C HSQC spectrum of LNFP III (H_2O:D_2O 9:1 *v/v* solvent at pH 3.0)

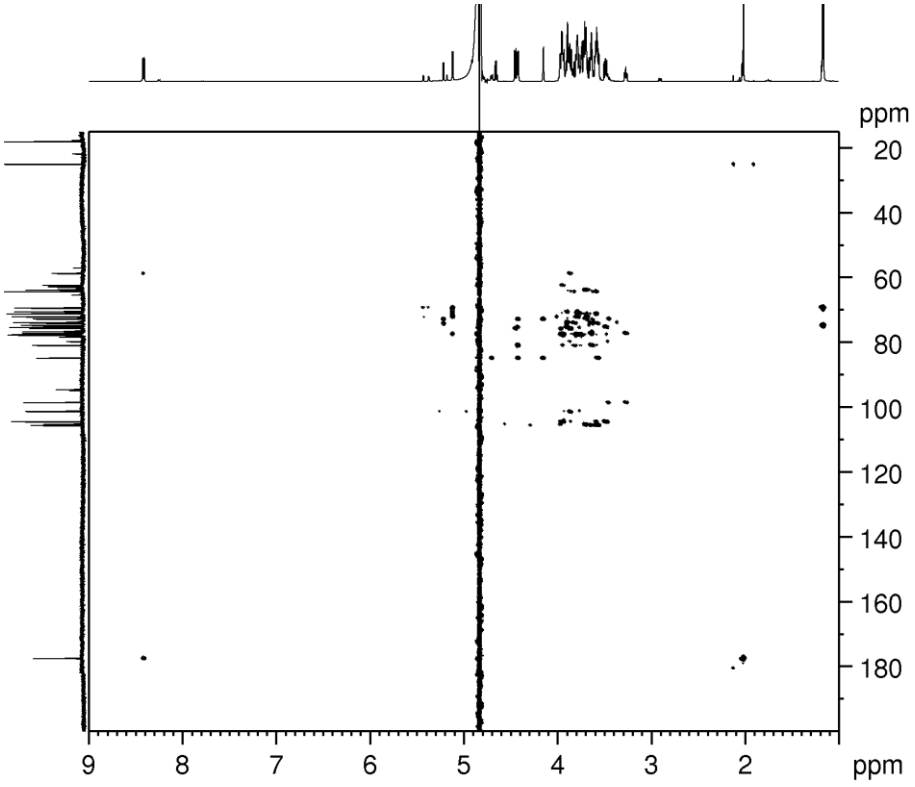

Figure A52. ^{1}H -^{13}C HMBC spectrum of LNFP III (H_2O:D_2O 9:1 *v/v* solvent at pH 3.0)

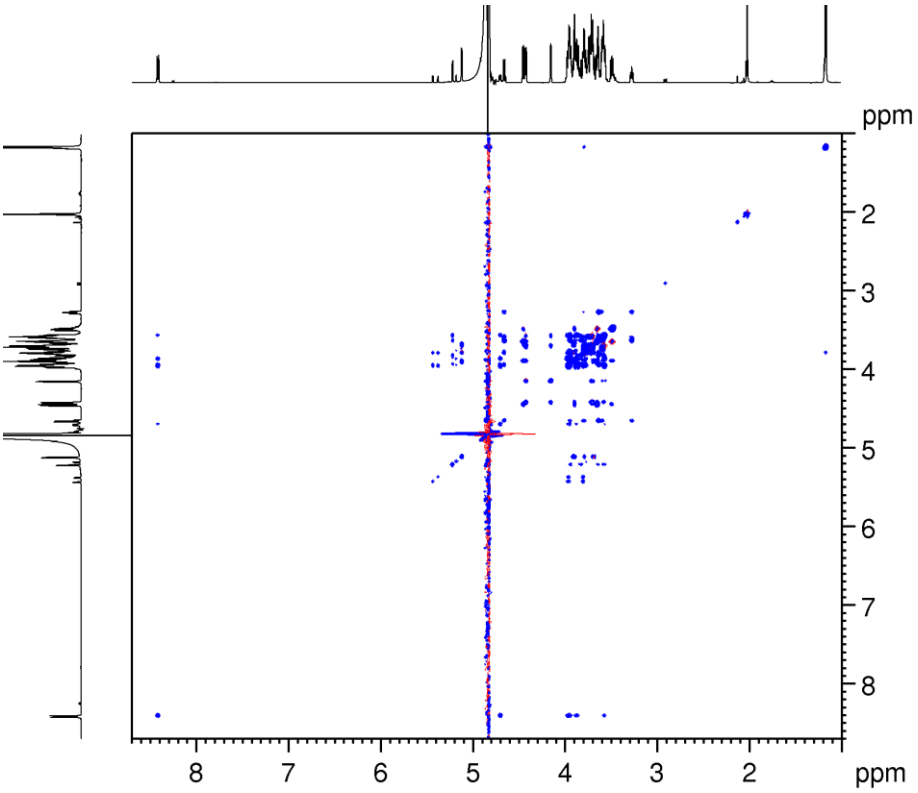

Figure A53. ^{1}H -^{1}H TOCSY spectrum of LNFP III (H_2O:D_2O 9:1 *v/v* solvent at pH 3.0)

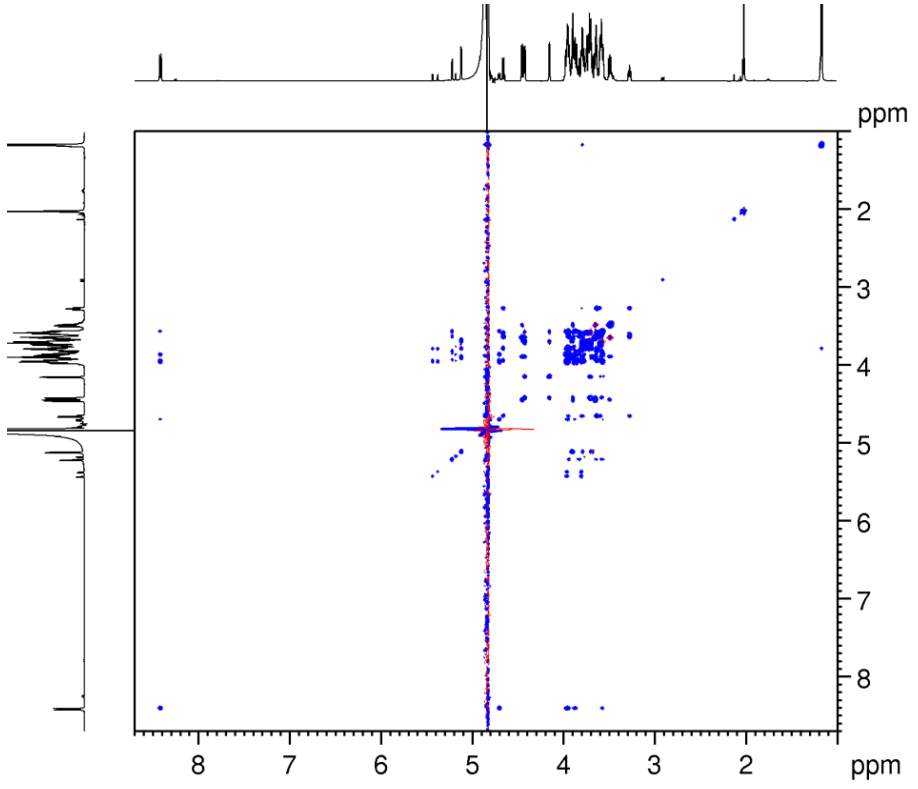

Figure A54. ^{1}H -^{1}H ROESY spectrum of LNFP III (H_2O:D_2O 9:1 *v/v* solvent at pH 3.0)

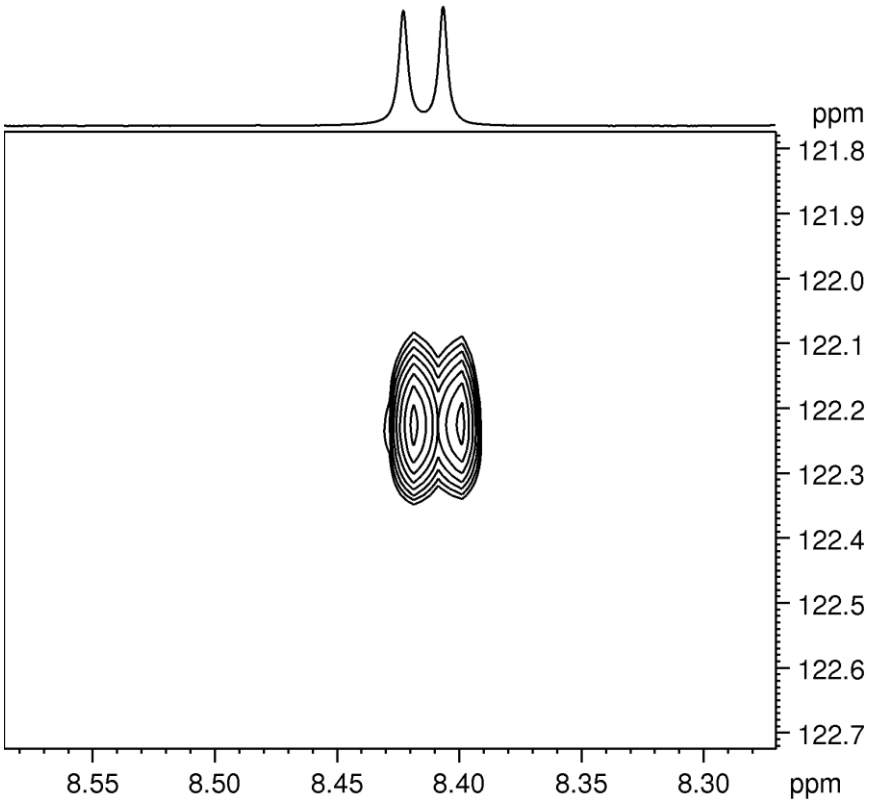

Figure A55. ^{1}H -^{15}N HSQC spectrum of LNFP III (H_2O:D_2O 9:1 *v/v* solvent at pH 3.0)

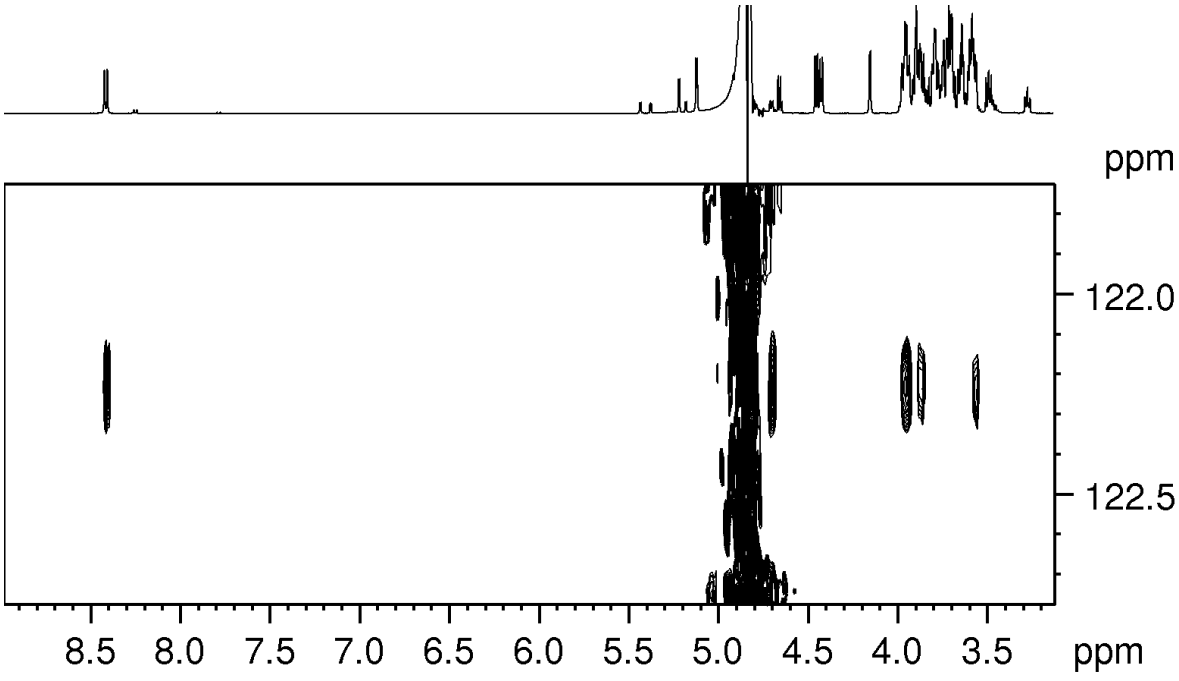

Figure A56. ^{1}H -^{15}N HSQC-TOCSY spectrum of LNFP III (H_2O:D_2O 9:1 *v/v* solvent at pH 3.0)

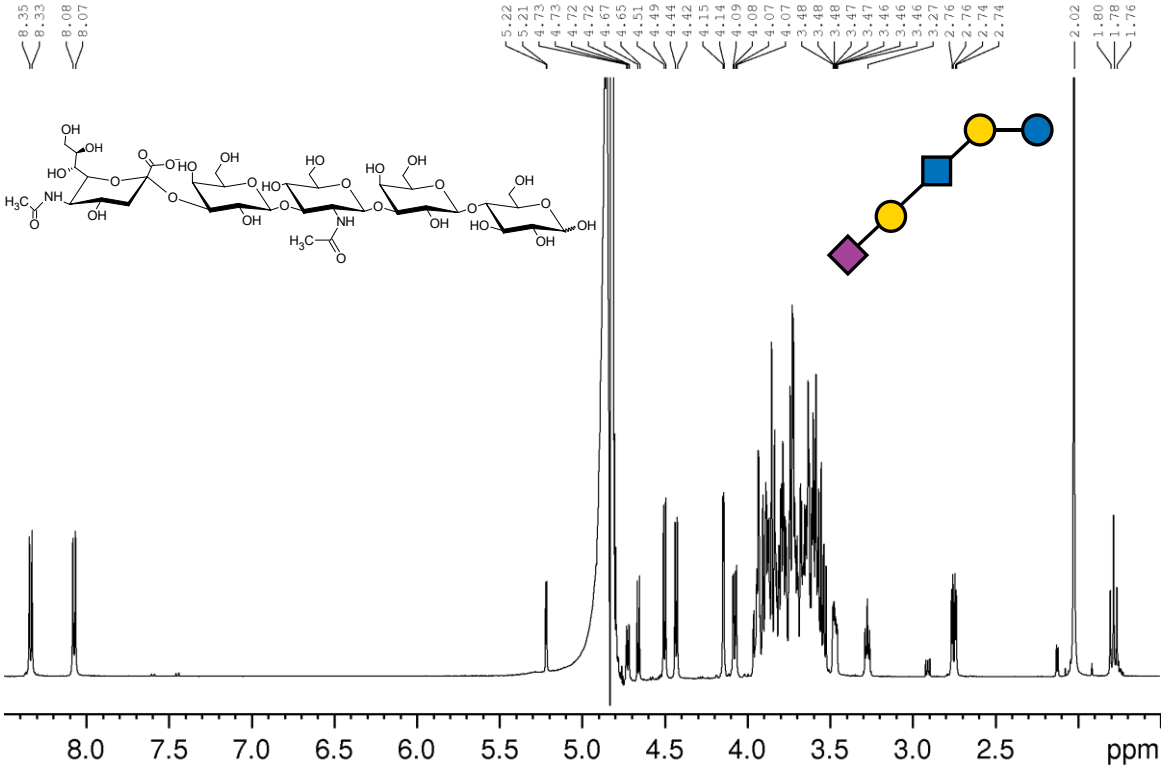

Figure A57. ^{1}H NMR spectrum of LSTa (H_2O:D_2O 9:1 *v/v* solvent at pH 3.0)

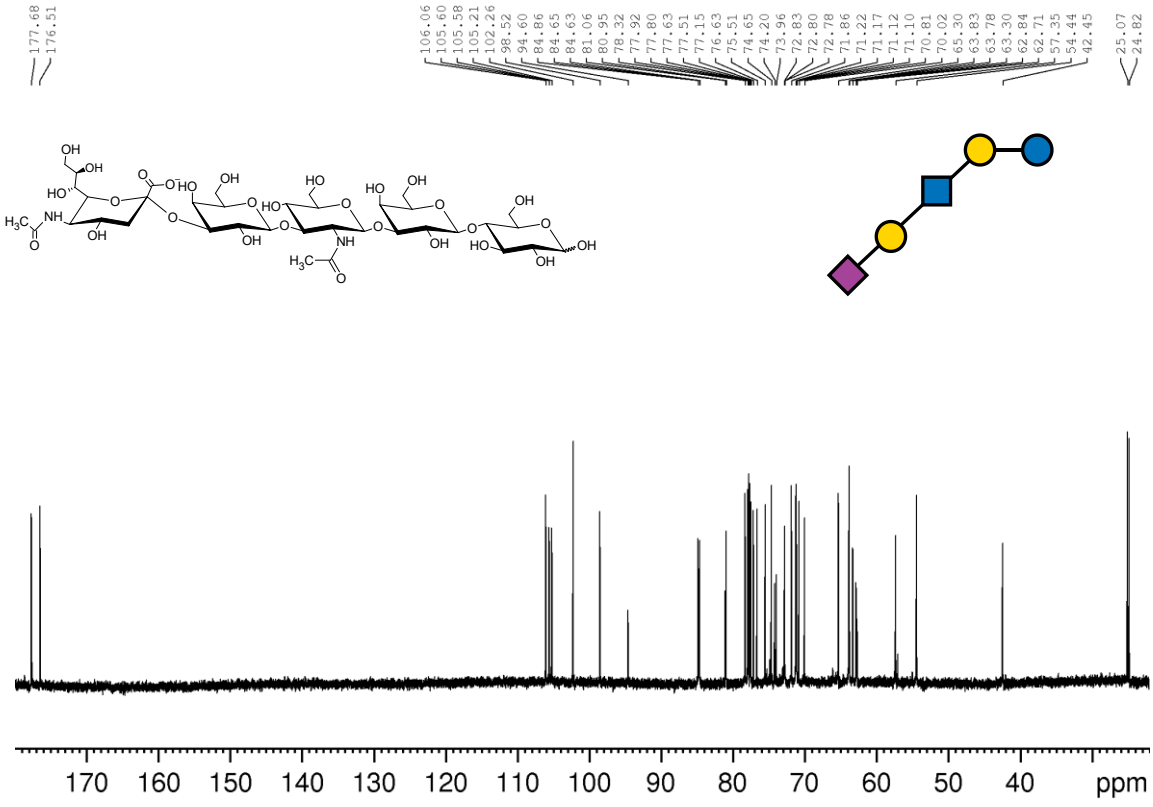

Figure A58. ^{13}C NMR spectrum of LSTa (H_2O:D_2O 9:1 *v/v* solvent at pH 3.0)

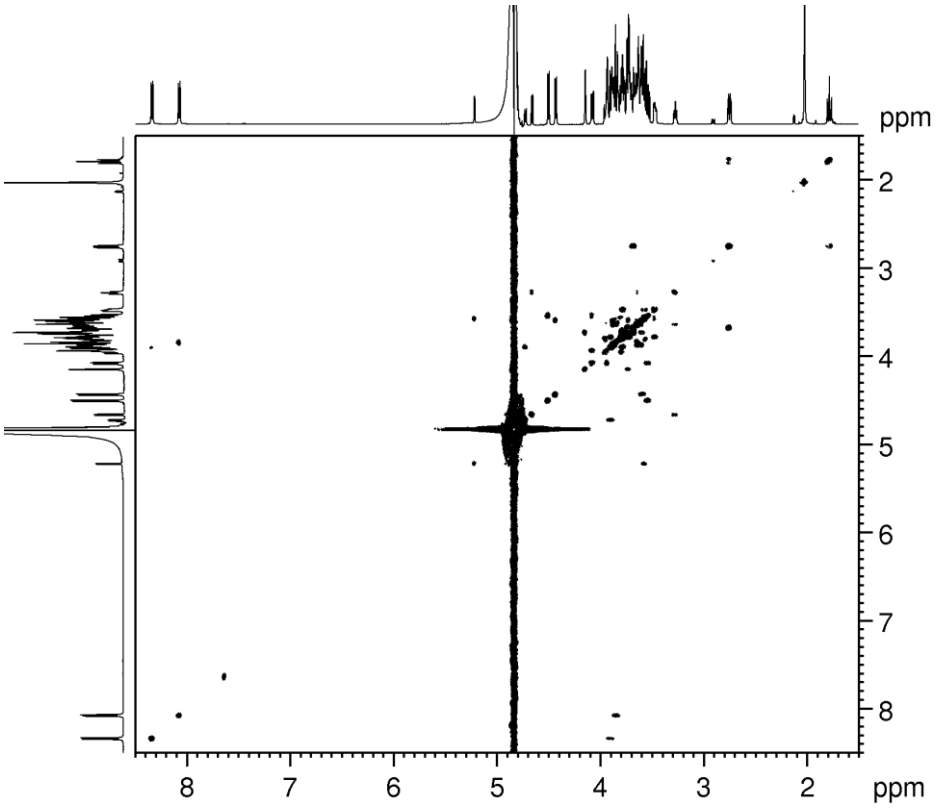

Figure A59. ^{1}H -^{1}H COSY spectrum of LSTa (H_2O:D_2O 9:1 *v/v* solvent at pH 3.0)

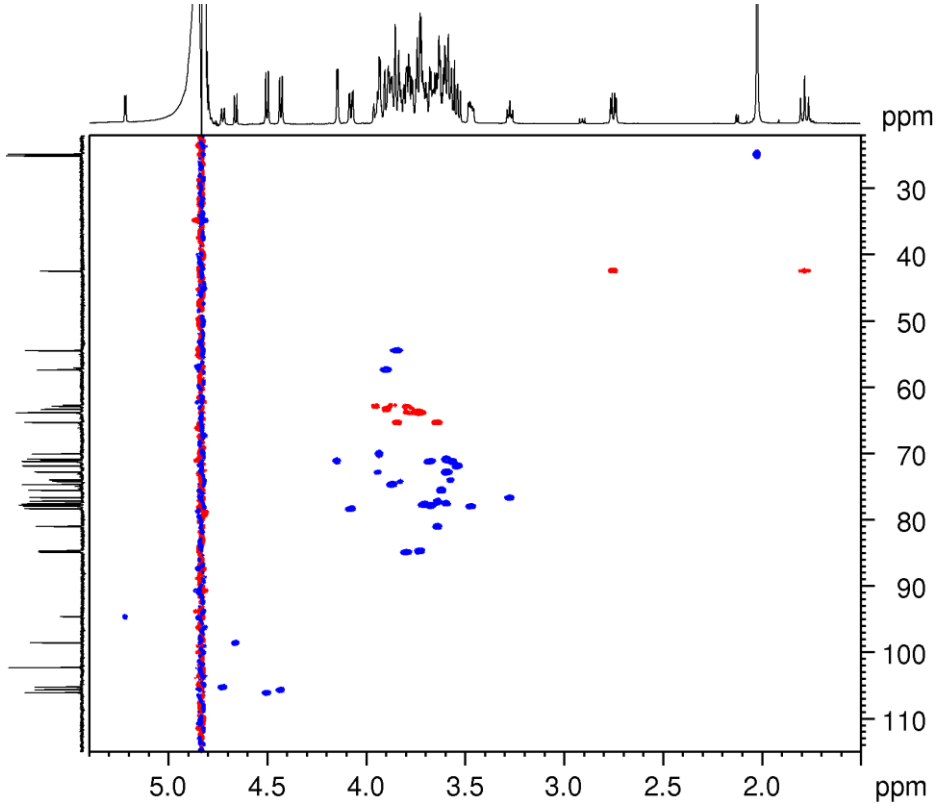

Figure A60. ^{1}H -^{13}C HSQC spectrum of LSTa (H_2O:D_2O 9:1 *v/v* solvent at pH 3.0)

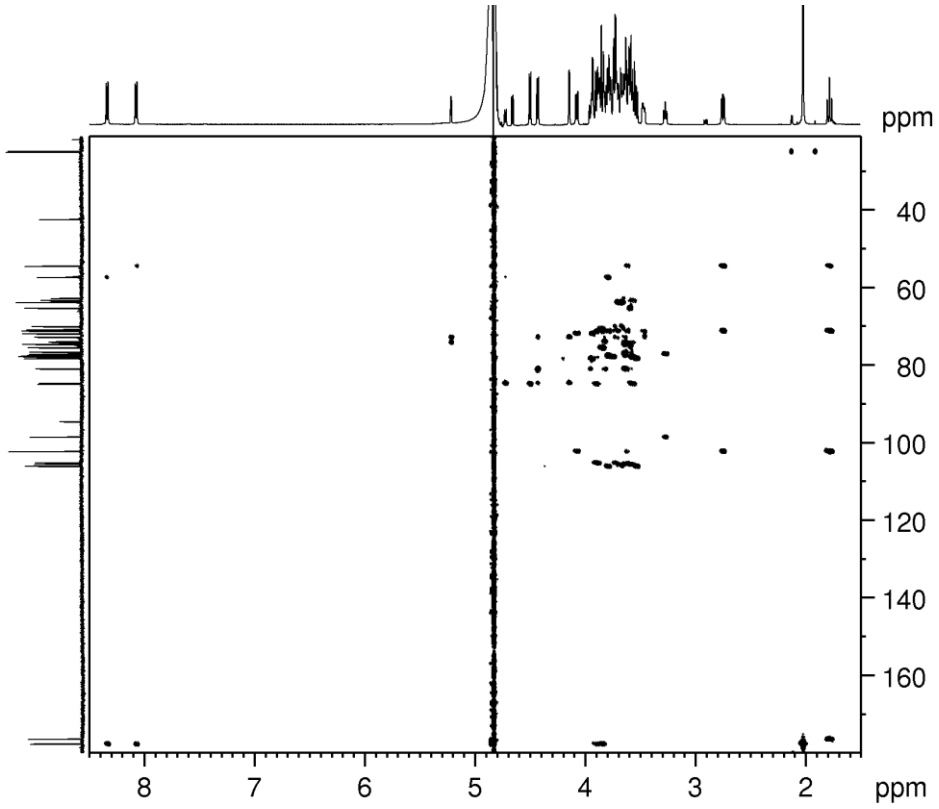

Figure A61. ^{1}H -^{13}C HMBC spectrum of LSTa (H_2O:D_2O 9:1 *v/v* solvent at pH 3.0)

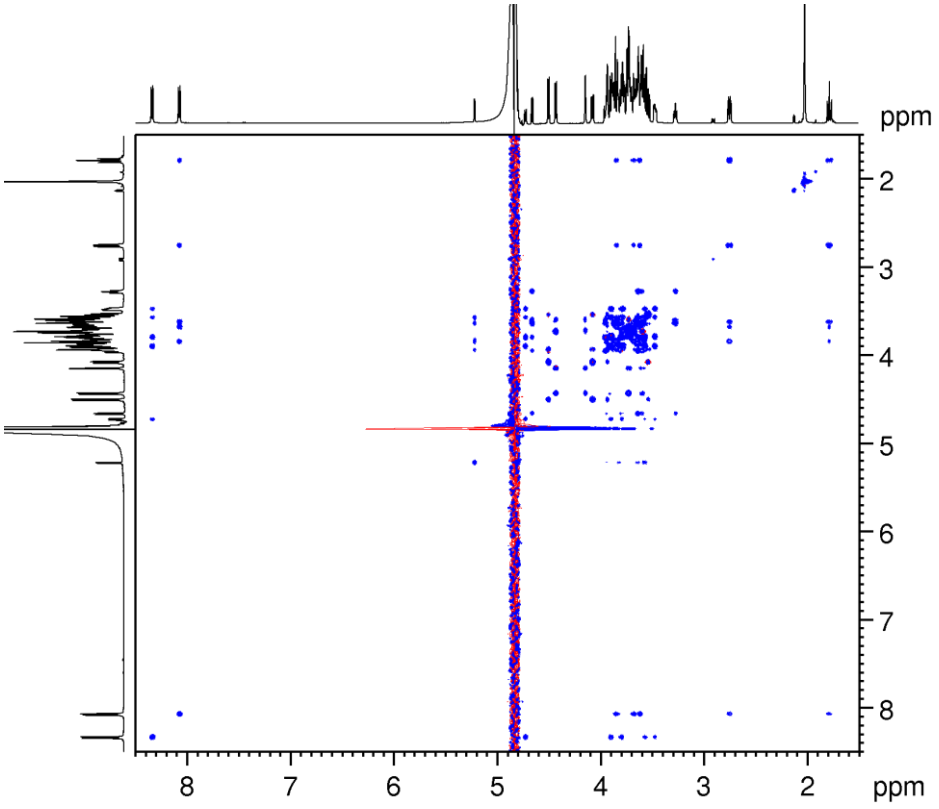

Figure A62. ^{1}H -^{1}H TOCSY spectrum of LSTa (H_2O:D_2O 9:1 *v/v* solvent at pH 3.0)

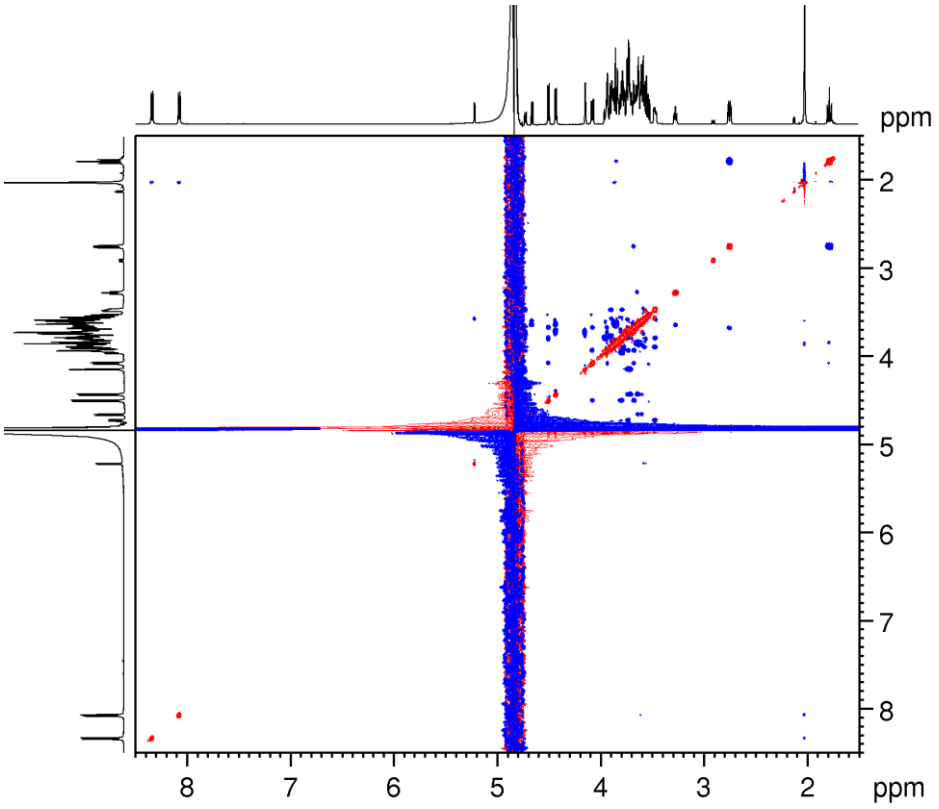

Figure A63. ^{1}H -^{1}H ROESY spectrum of LSTa (H_2O:D_2O 9:1 *v/v* solvent at pH 3.0)

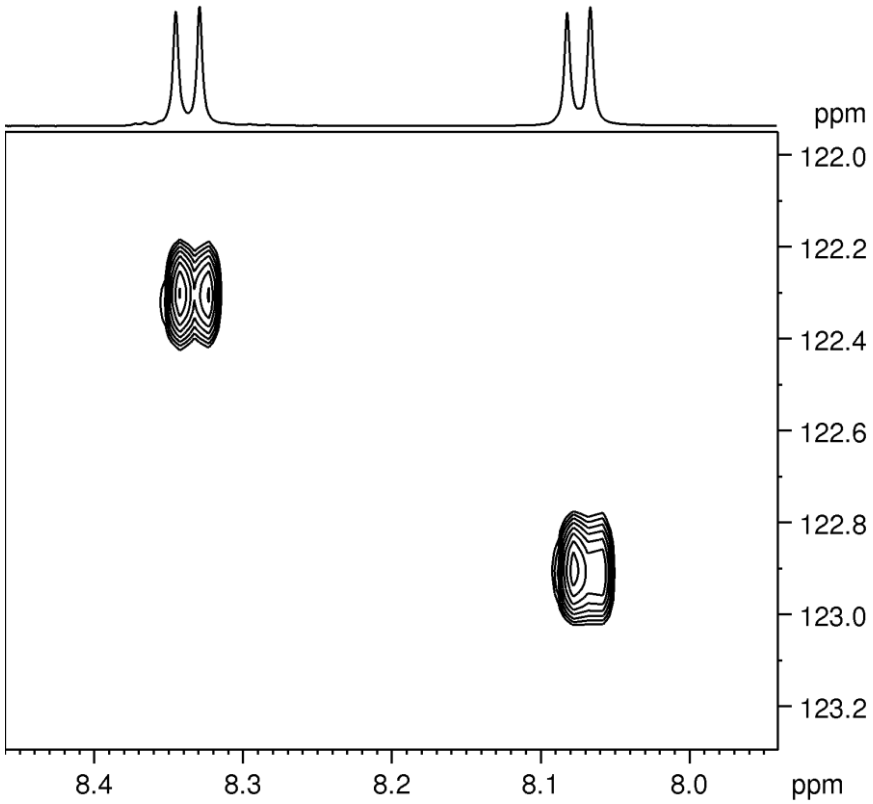

Figure A64. ^{1}H -^{15}N HSQC spectrum of LSTa (H_2O:D_2O 9:1 *v/v* solvent at pH 3.0)

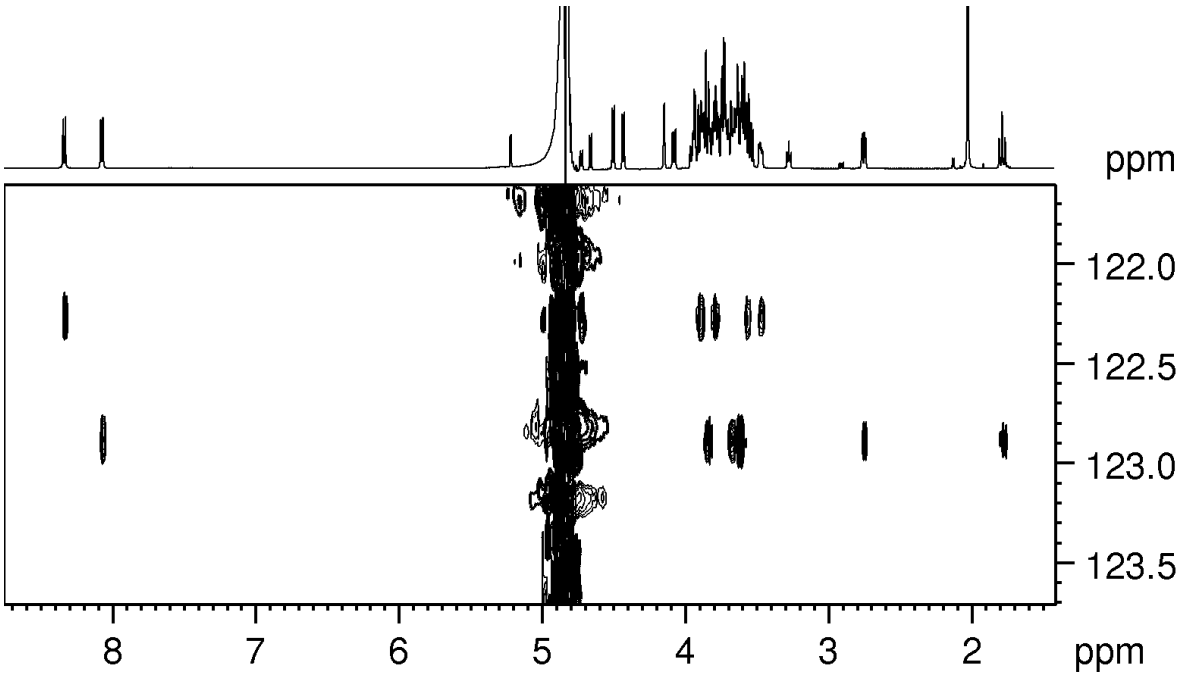

Figure A65. ^{1}H -^{15}N HSQC-TOCSY spectrum of LSTa (H_2O:D_2O 9:1 *v/v* solvent at pH 3.0)

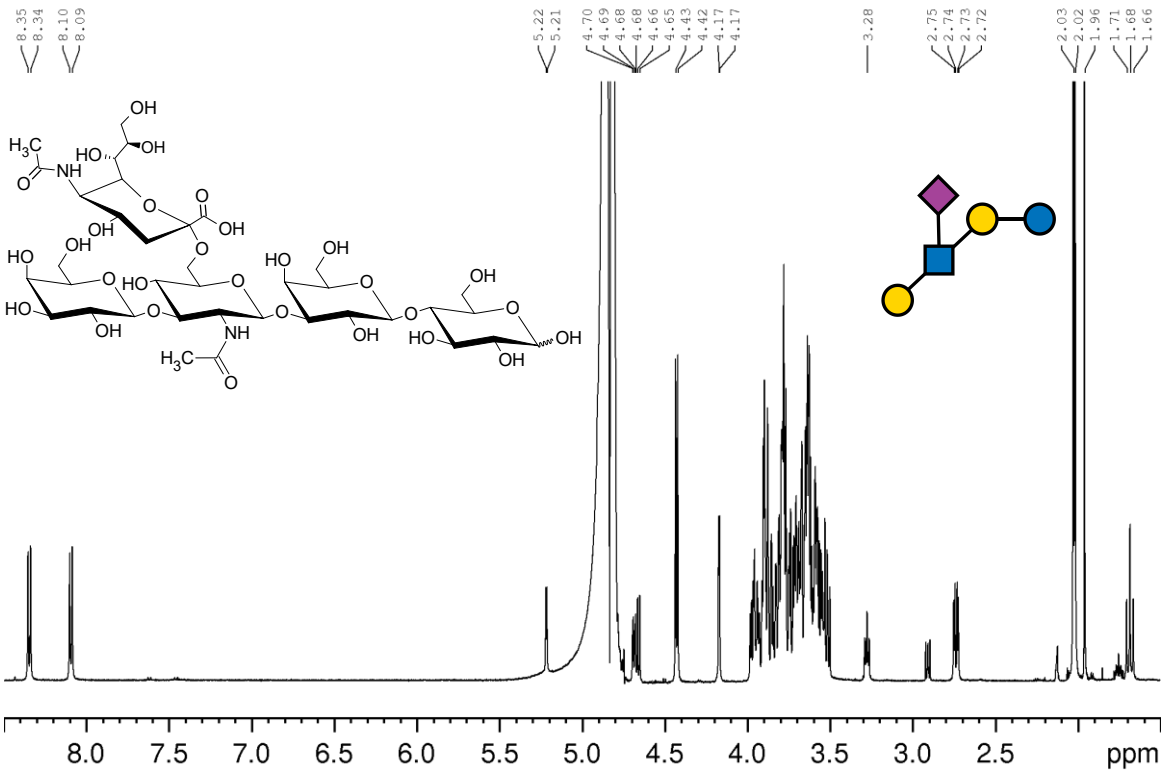

Figure A66. ^{1}H NMR spectrum of LSTb (H_2O:D_2O 9:1 *v/v* solvent at pH 3.0)

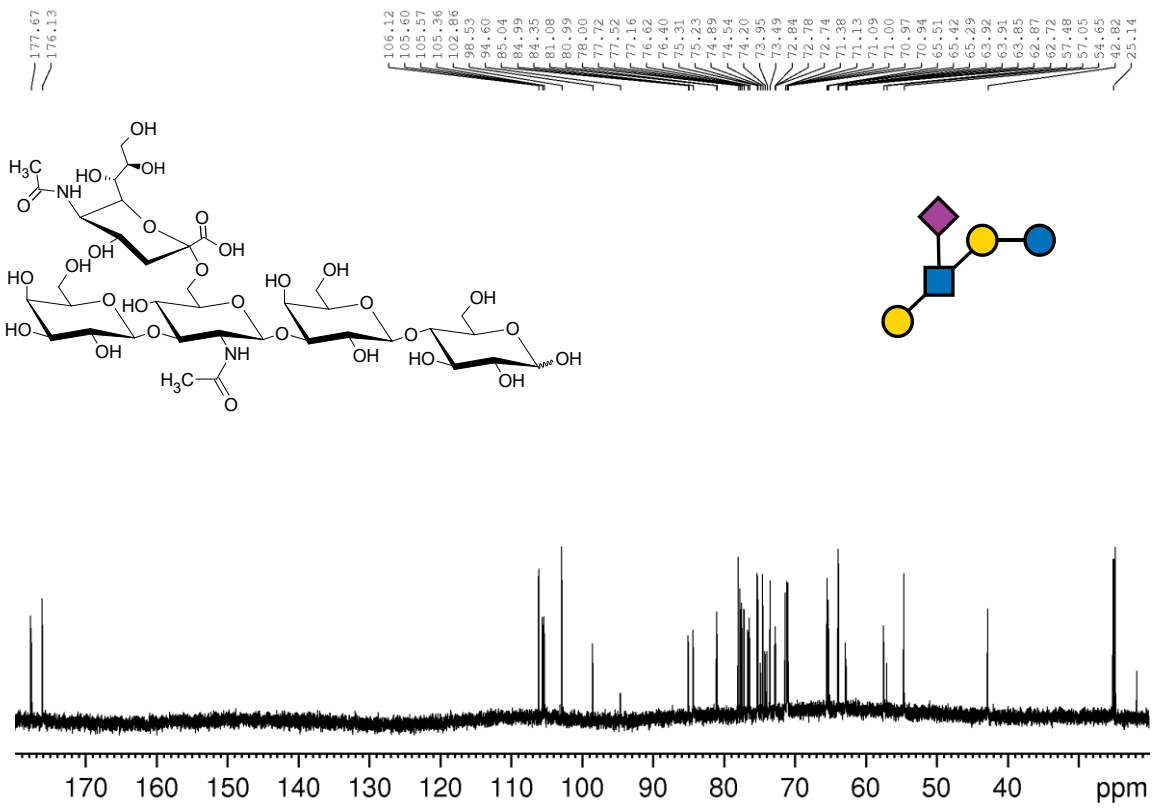

Figure A67. ^{13}C NMR spectrum of LSTb (H_2O:D_2O 9:1 *v/v* solvent at pH 3.0)

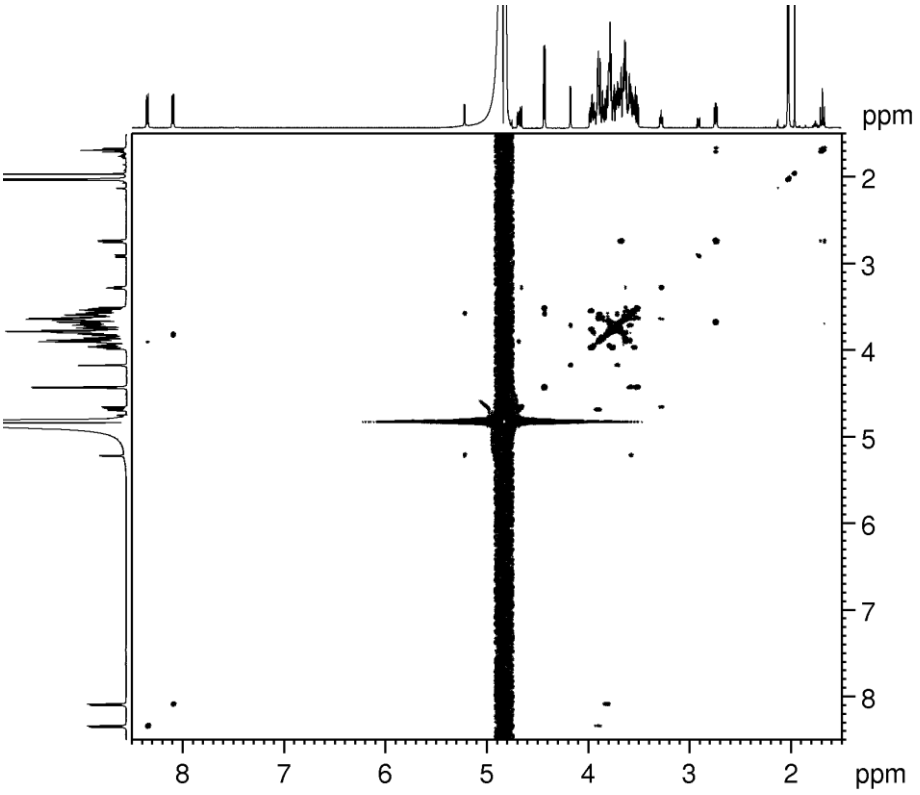

Figure A68. ^{1}H -^{1}H COSY spectrum of LSTb (H_2O:D_2O 9:1 *v/v* solvent at pH 3.0)

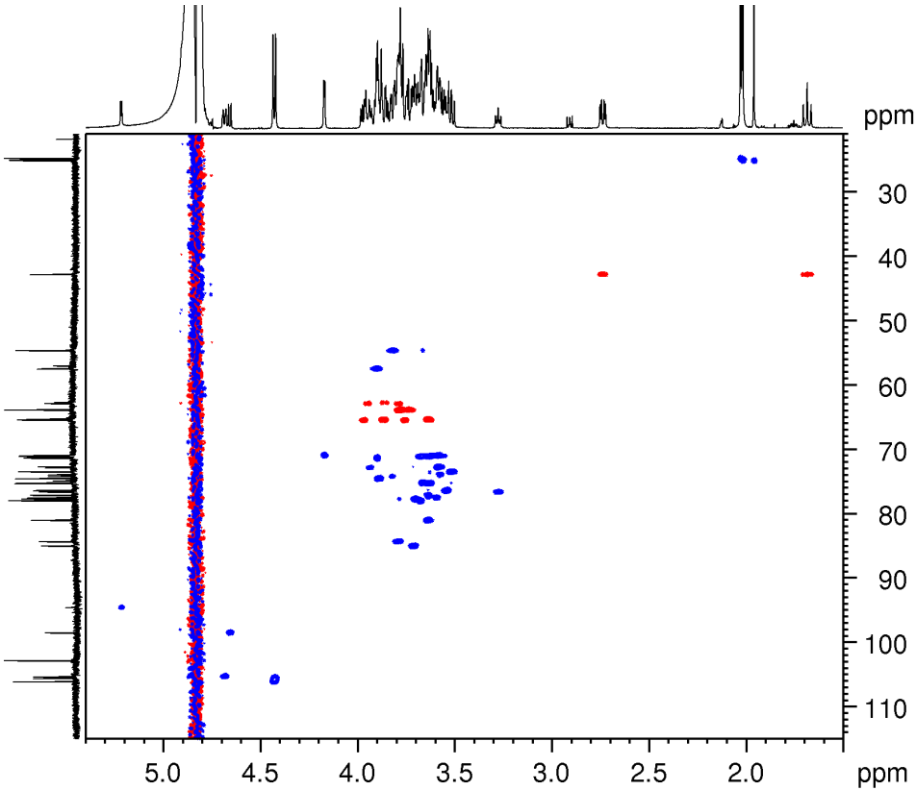

Figure A69. ^{1}H -^{13}C HSQC spectrum of LSTb (H_2O:D_2O 9:1 *v/v* solvent at pH 3.0)

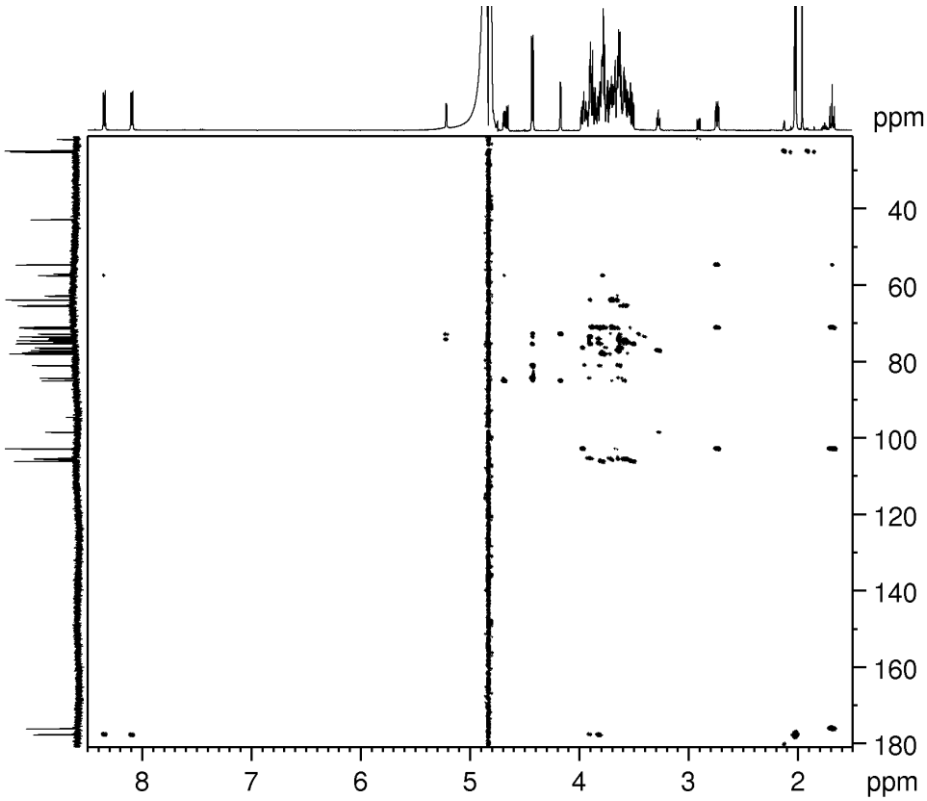

Figure A70. ^{1}H -^{13}C HMBC spectrum of LSTb (H_2O:D_2O 9:1 *v/v* solvent at pH 3.0)

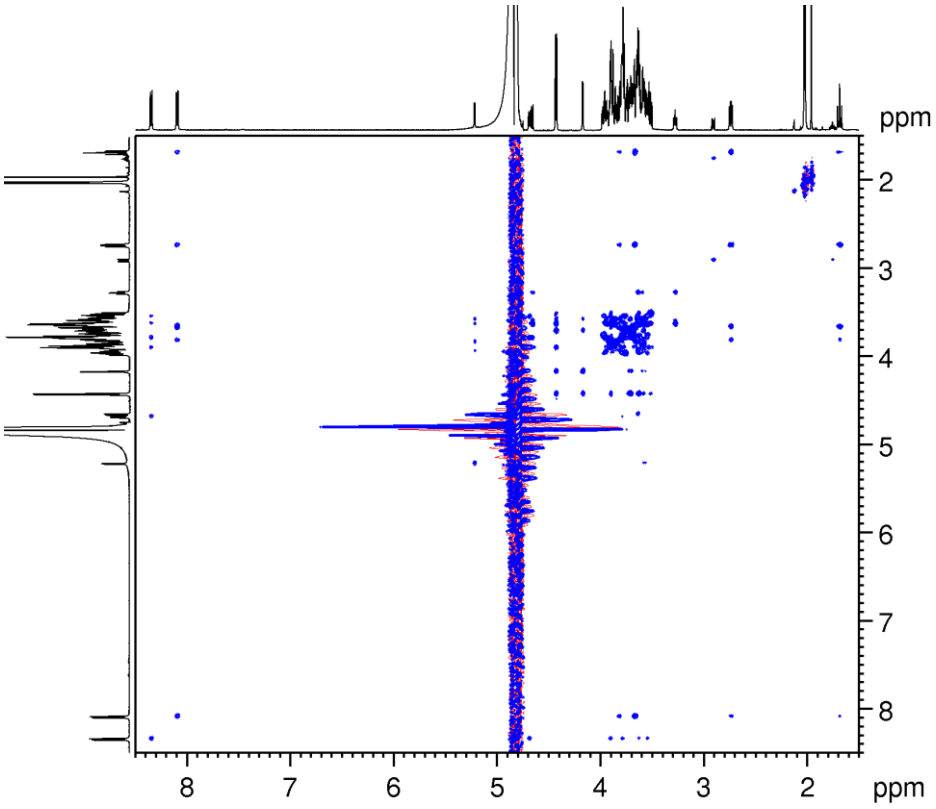

Figure A71. ^{1}H -^{1}H TOCSY spectrum of LSTb (H_2O:D_2O 9:1 *v/v* solvent at pH 3.0)

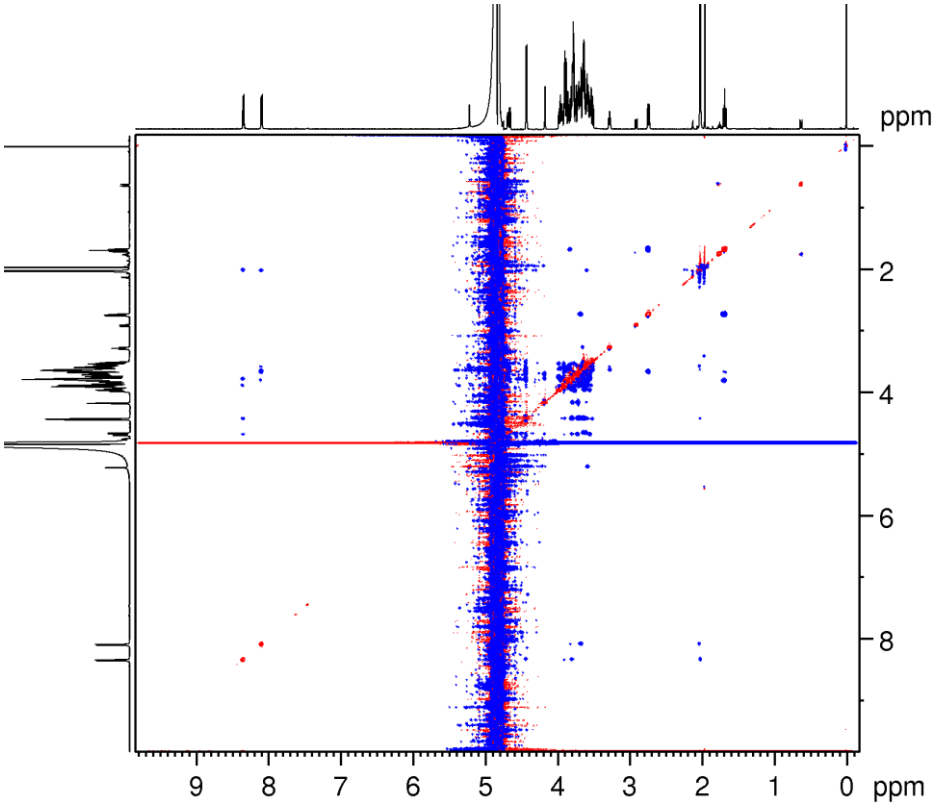

Figure A72. ^{1}H -^{1}H ROESY spectrum of LSTb (H_2O:D_2O 9:1 *v/v* solvent at pH 3.0)

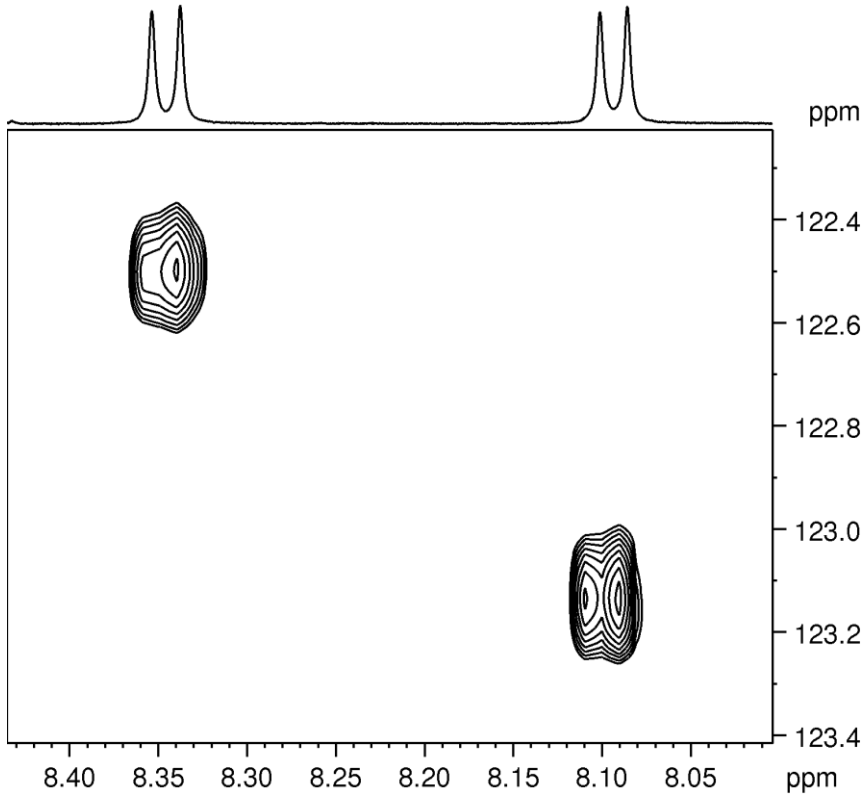

Figure A73. ^{1}H -^{15}N HSQC spectrum of LSTb (H_2O:D_2O 9:1 *v/v* solvent at pH 3.0)

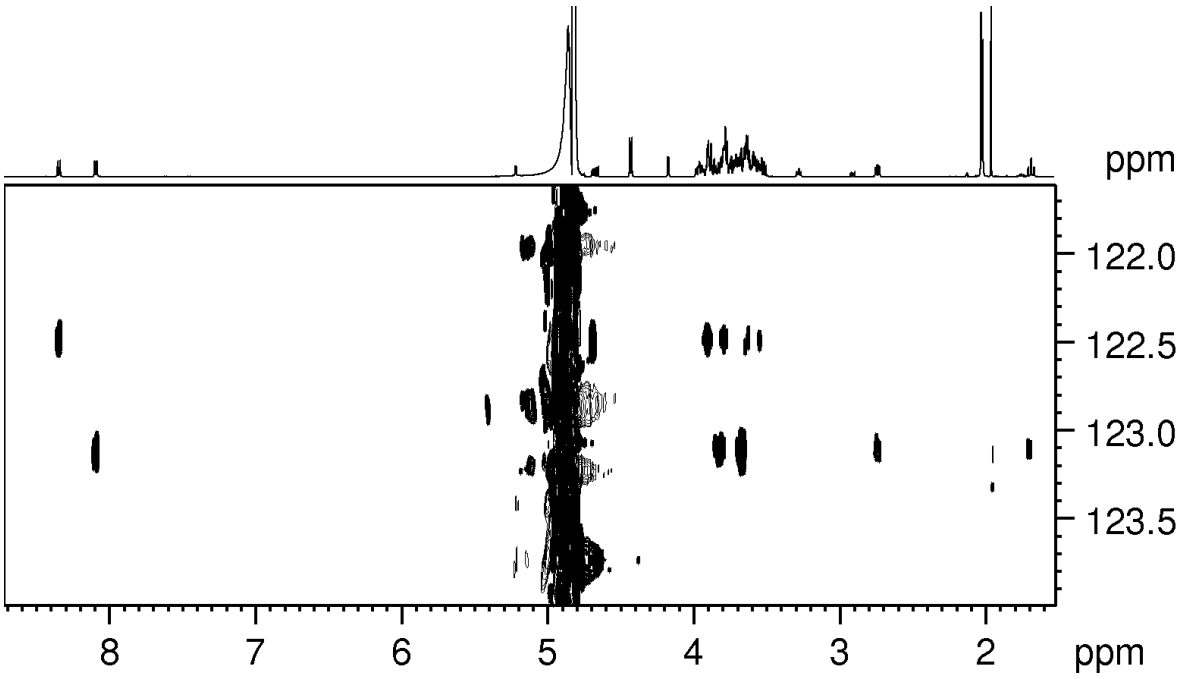

Figure A74. ^{1}H -^{15}N HSQC-TOCSY spectrum of LSTb (H_2O:D_2O 9:1 *v/v* solvent at pH 3.0)

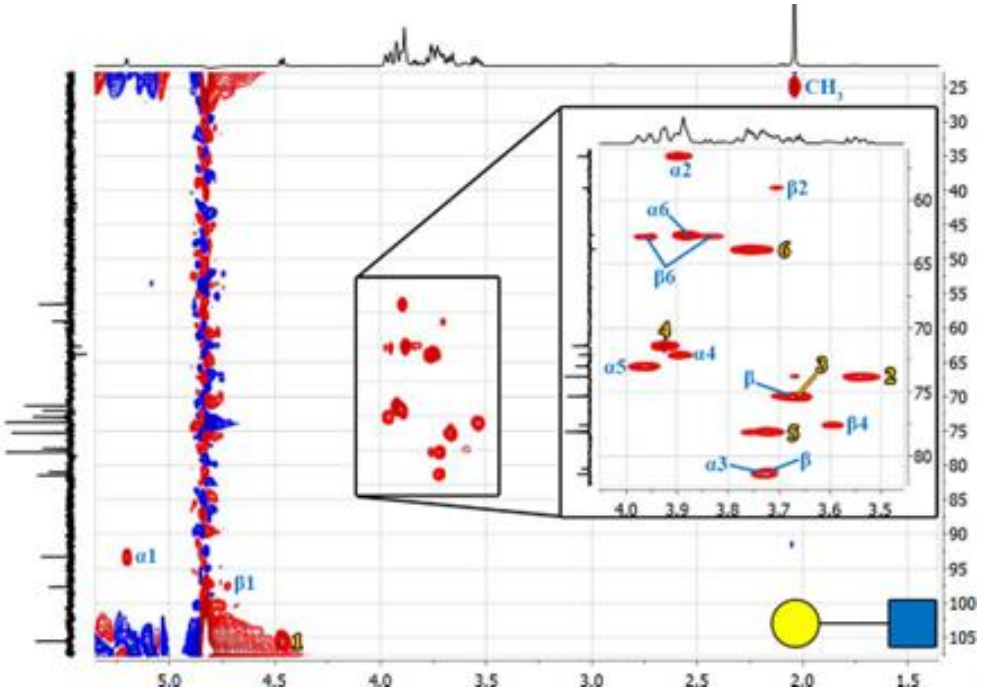

Figure A75. ^{1}H-^{13}C HSQC spectrum of LAcNAc

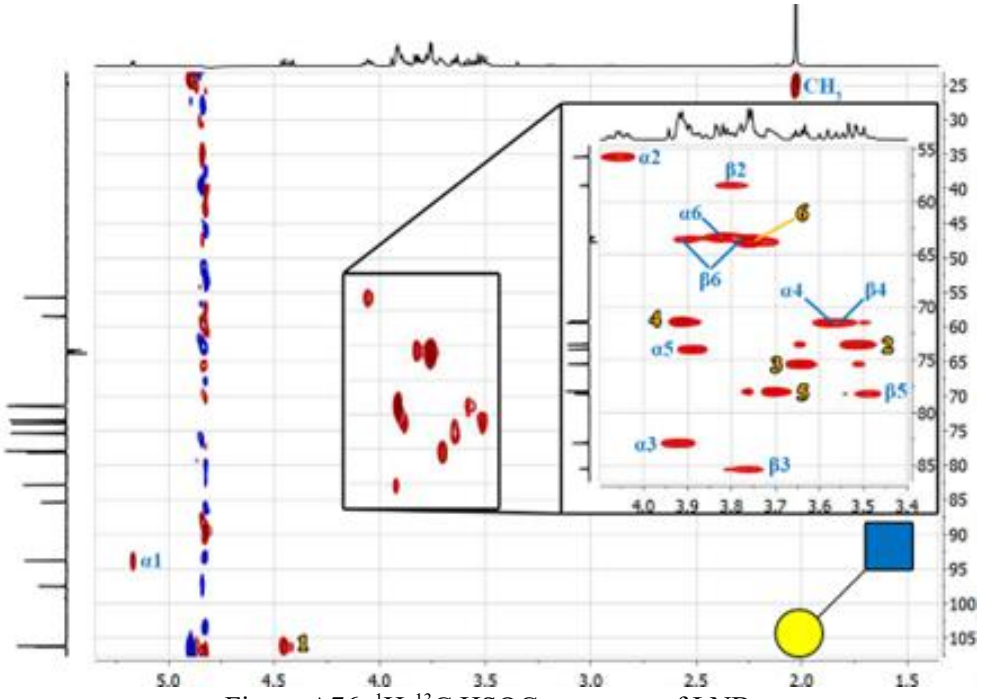

Figure A76. ^{1}H-^{13}C HSQC spectrum of LNB

Table A1. Complete resonance assignment of the disaccharides LacNAc and LNB

	LacNAc								LNB							
	GlcNAc						Gal		GlcNAc						Gal	
	α			β					α			β				
	^{1}H	^{13}C	^{15}N	^{1}H	^{13}C	^{15}N	^{1}H	^{13}C	^{1}H	^{13}C	^{15}N	^{1}H	^{13}C	^{15}N	^{1}H	^{13}C
1	5.20	93.3		4.73	97.7		4.46 / 4.47	105.6	5.17	93.8		o.l.	97.5		4.46/4.42	106.2/106.3
2	3.89	56.6		3.70	59.1		3.54	73.8	4.06	55.7		3.80	58.4		3.52	73.5/73.6
3	3.73	81.4		n.a.	n.a.		3.67	75.4	3.93	82.9		3.76	85.3		3.65	75.4
4	3.89	72.1		3.60	77.6		3.92	71.4	3.58	71.5		3.55	71.4		3.92	71.4
5	3.97	73.0		n.a.	n.a.		3.72	78.1	3.89	74.0		3.49	78.2		3.71	78.0
6	3.88	62.8		3.83 3.96	62.9		3.76	63.9	3.83	63.4		3.76 3.90	63.5		3.76	63.8
NH	**8.20**		**123.65**	**8.25**		**122.88**			**8.23**		**123.19**	**8.33**		**122.28**		

n.a.: not assigned, o.l.: overlapped

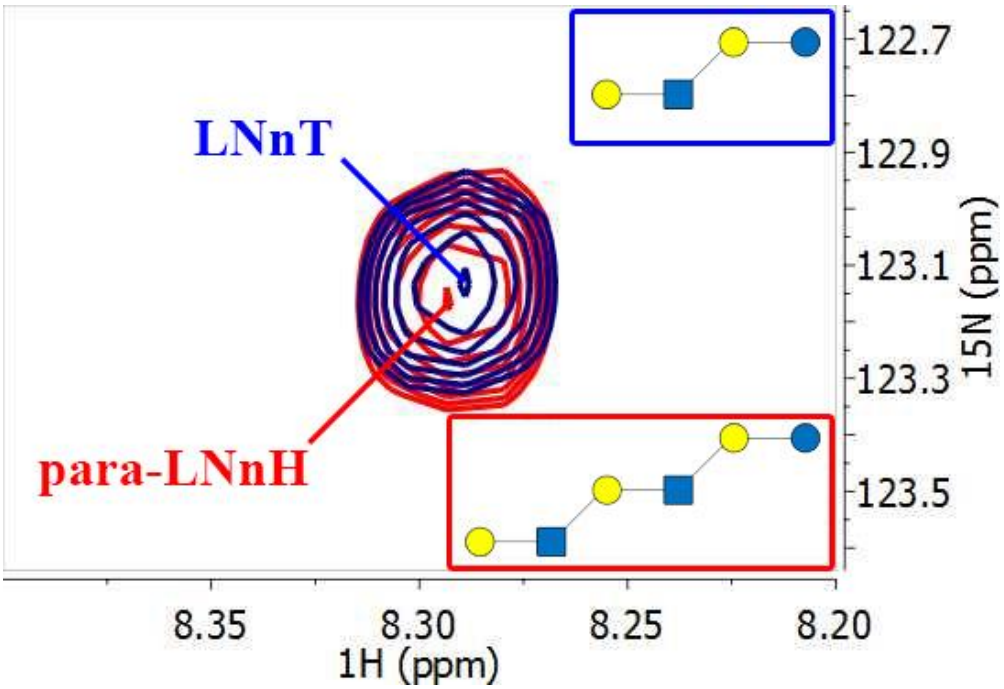

Figure A77. Overlaid ^{1}H-^{15}N HSQC spectra of LNnT and para-LNnH

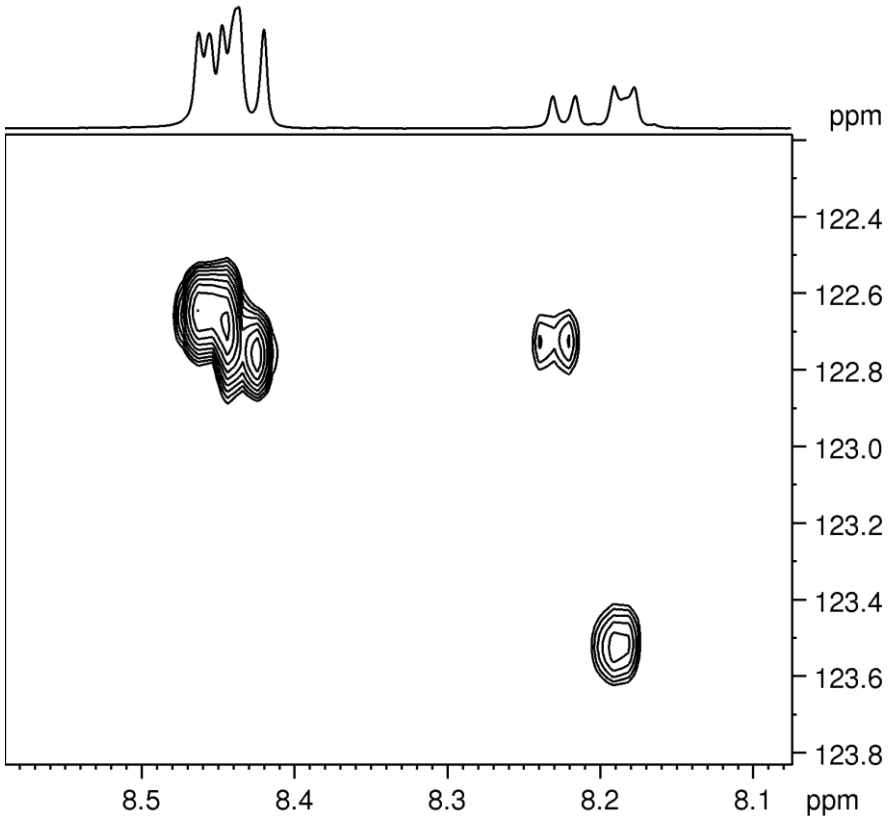

Figure A78. ^{1}H -^{15}N HSQC spectrum of *N*,*N*',*N*'',*N*'''-Tetraacetylchitotetraose (H_2O:D_2O 9:1 *v/v* solvent at pH 3.0)

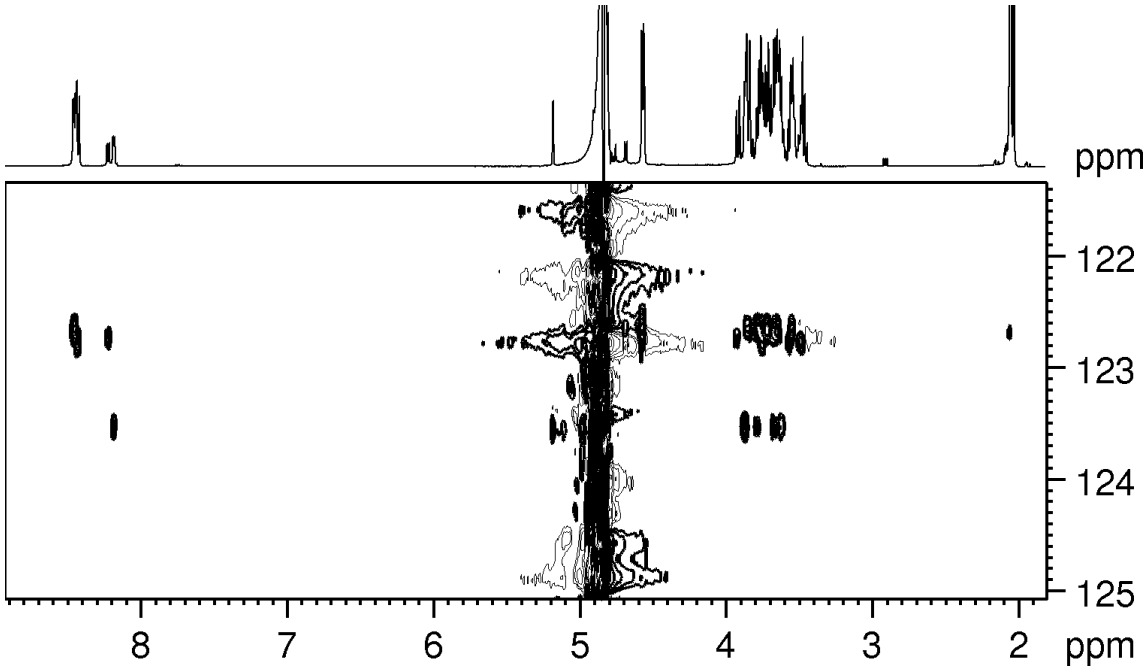

Figure A79. ^{1}H -^{15}N HSQC-TOCSY spectrum of *N*,*N*',*N*'',*N*'''-Tetraacetylchitotetraose (H_2O:D_2O 9:1 *v/v* solvent at pH 3.0)

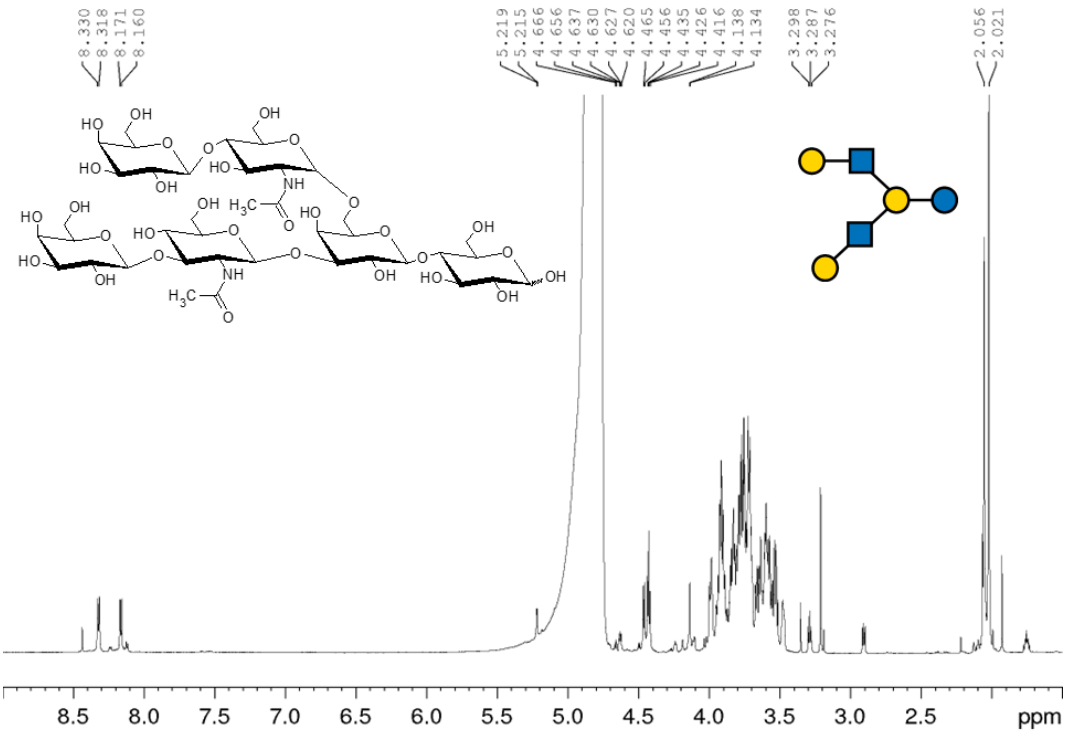

Figure A80. ^{1}H NMR spectrum of LNH (H_2O:D_2O 9:1 *v/v* solvent at pH 3.0)

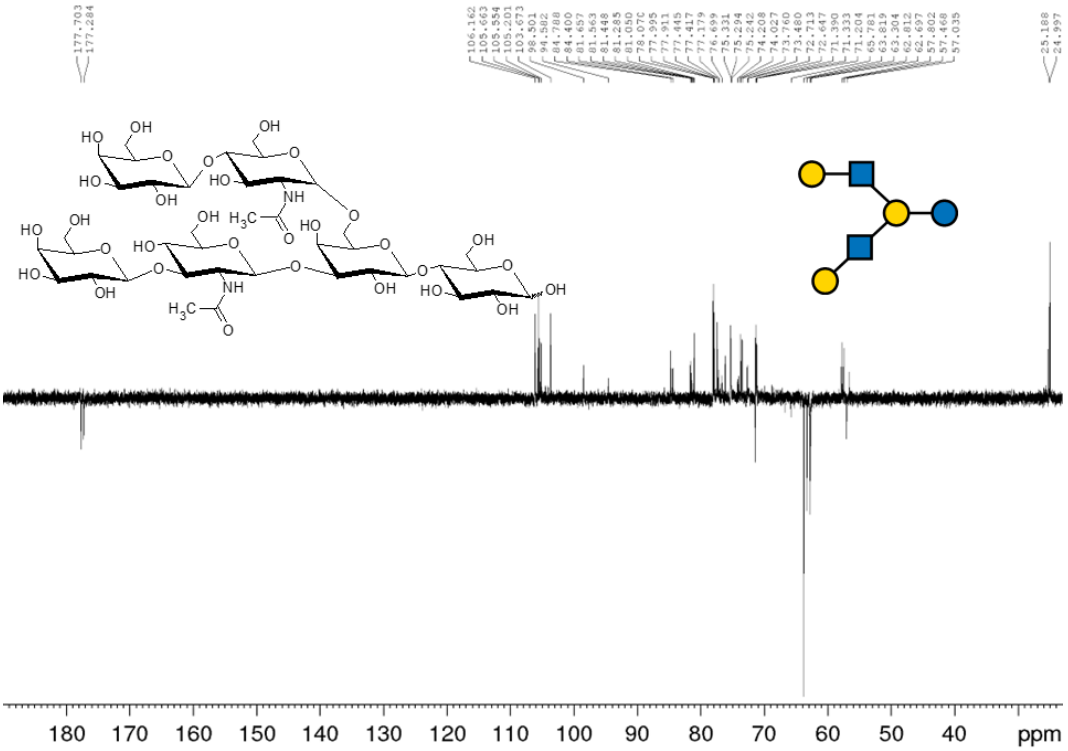

Figure A81. DEPTQ spectrum of LNH (H_2O:D_2O 9:1 *v/v* solvent at pH 3.0)

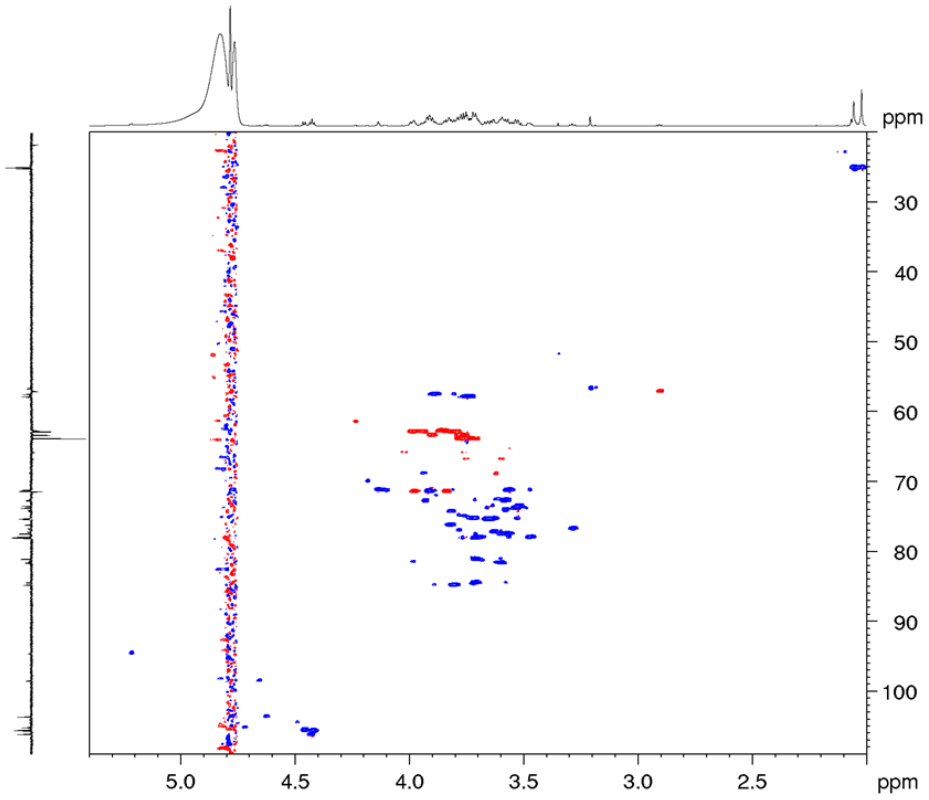

Figure A82. ^{1}H-^{13}C HSQC spectrum of LNH (H_2O:D_2O 9:1 *v/v* solvent at pH 3.0)

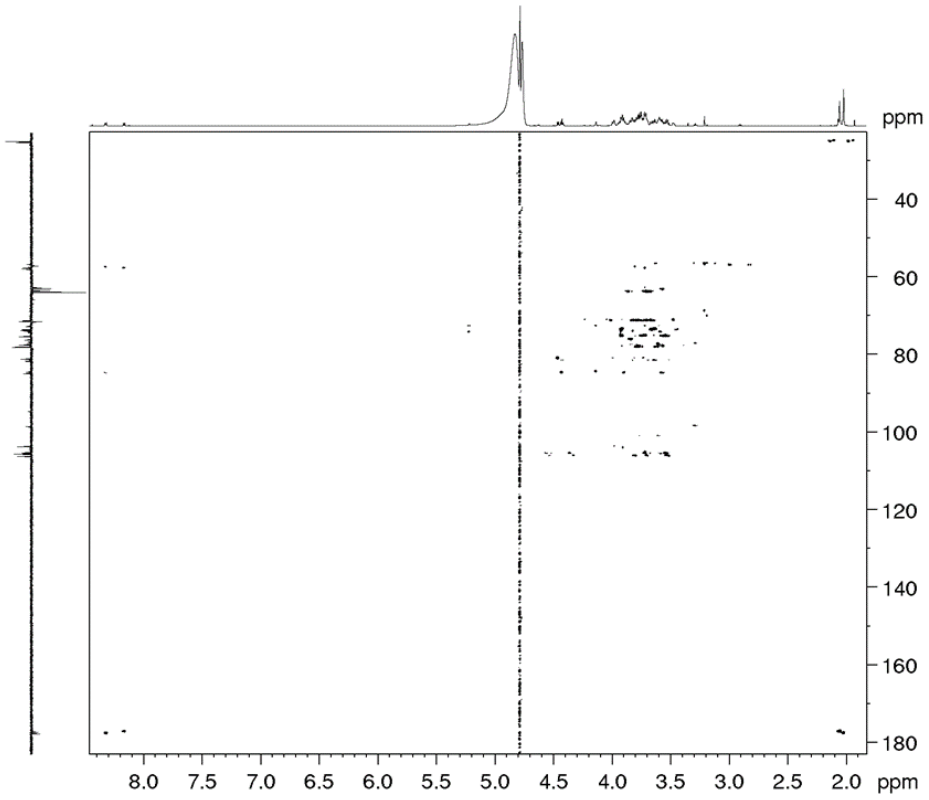

Figure A83. ^{1}H-^{13}C HMBC spectrum of LNH (H_2O:D_2O 9:1 *v/v* solvent at pH 3.0)

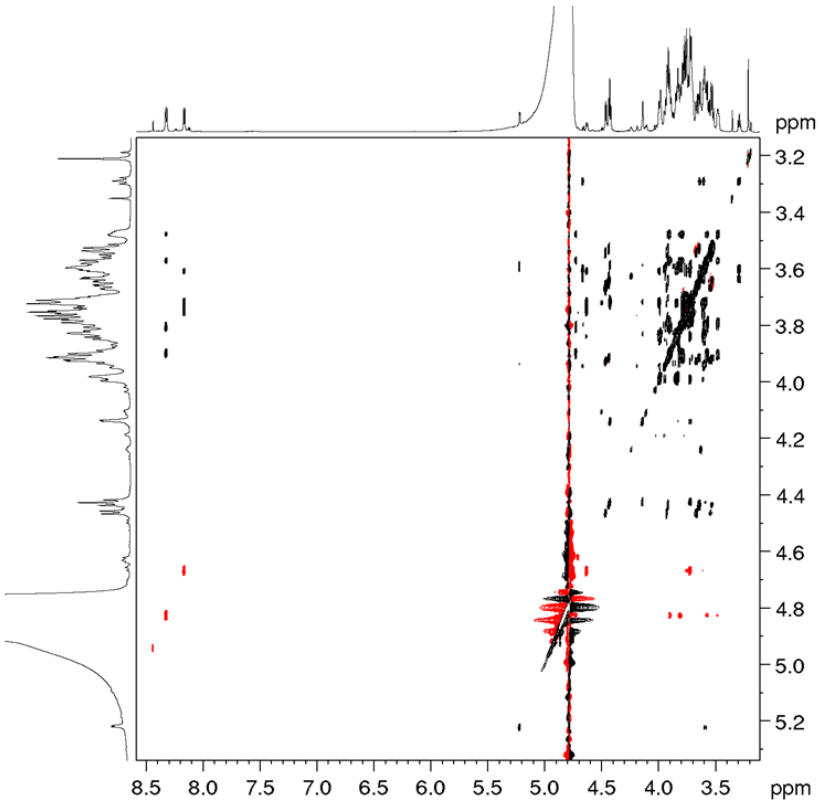

Figure A84. ^{1}H-^{1}H TOCSY spectrum of LNH (H_2O:D_2O 9:1 *v/v* solvent at pH 3.0)

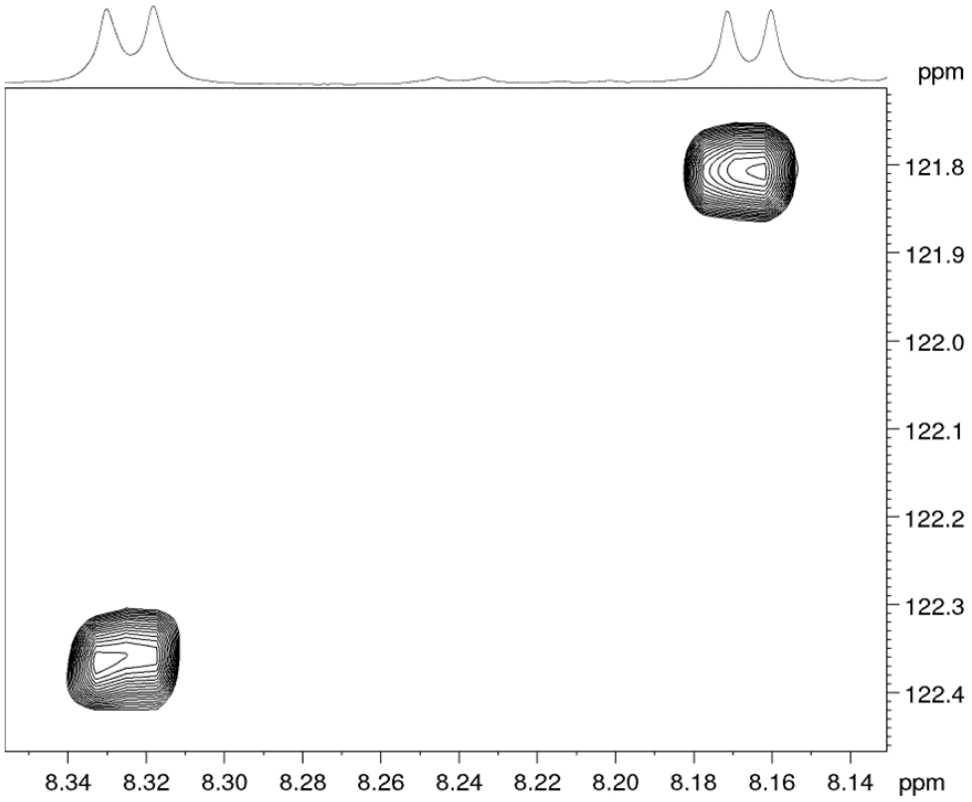

Figure A85. ^{1}H-^{15}N HSQC spectrum of LNH (H_2O:D_2O 9:1 *v/v* solvent at pH 3.0)

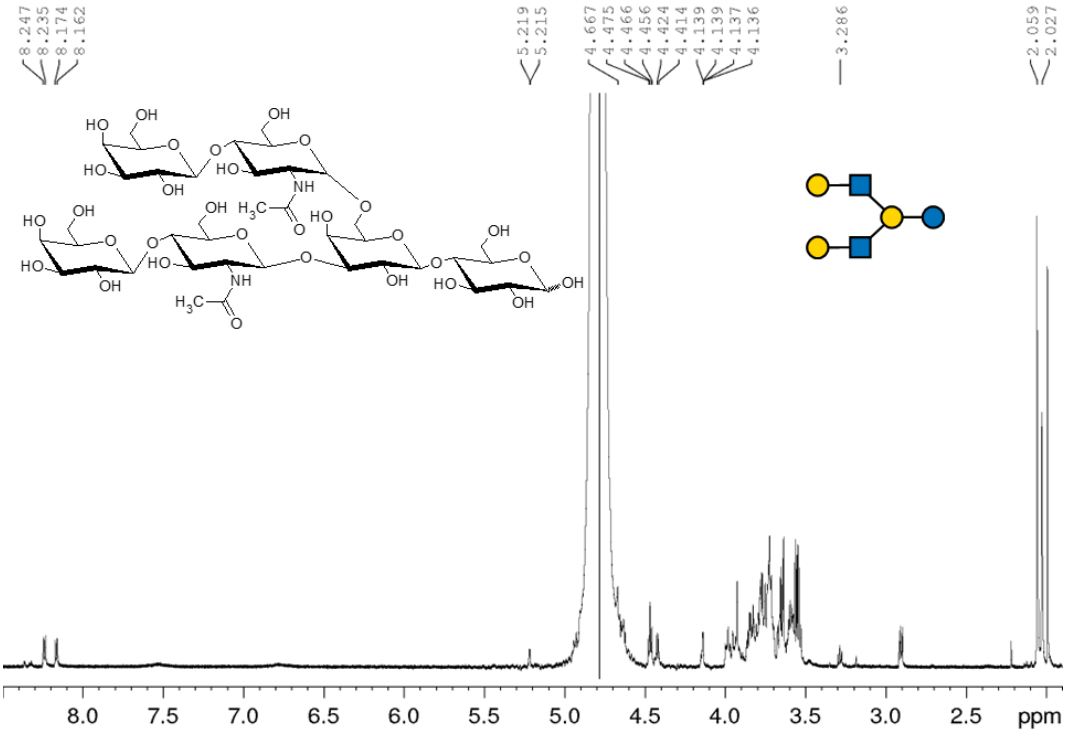

Figure A86. ^{1}H NMR spectrum of LNnH (H_2O:D_2O 9:1 *v/v* solvent at pH 3.0)

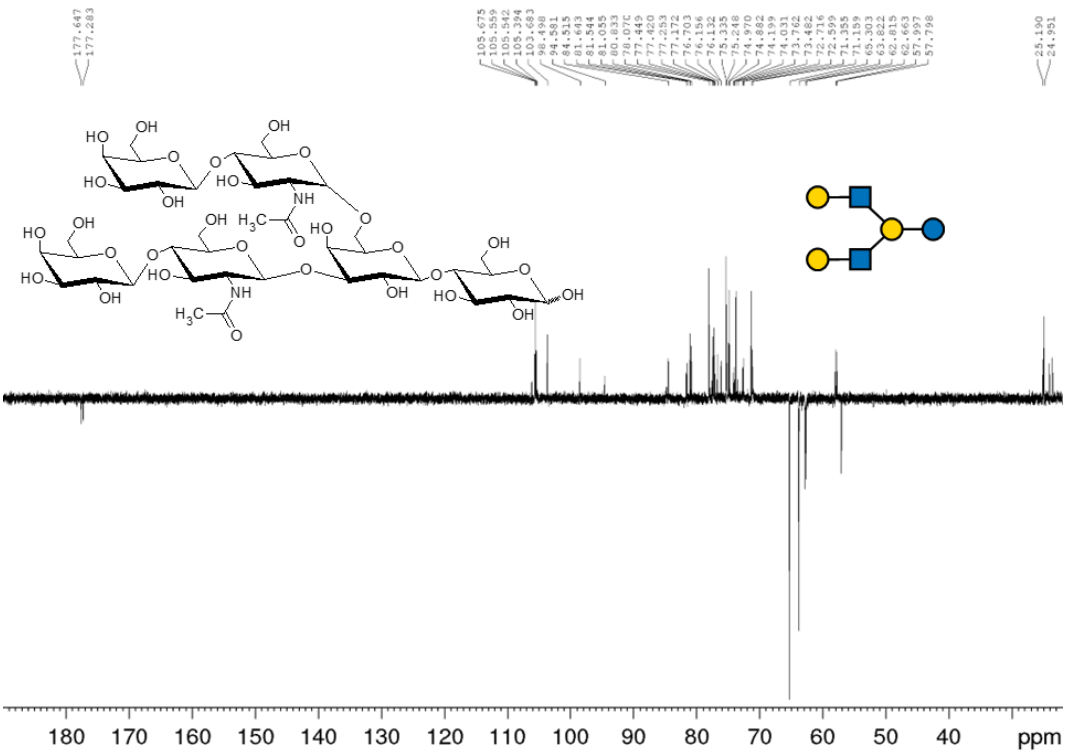

Figure A87. DEPTQ spectrum of LNnH (H_2O:D_2O 9:1 *v/v* solvent at pH 3.0)

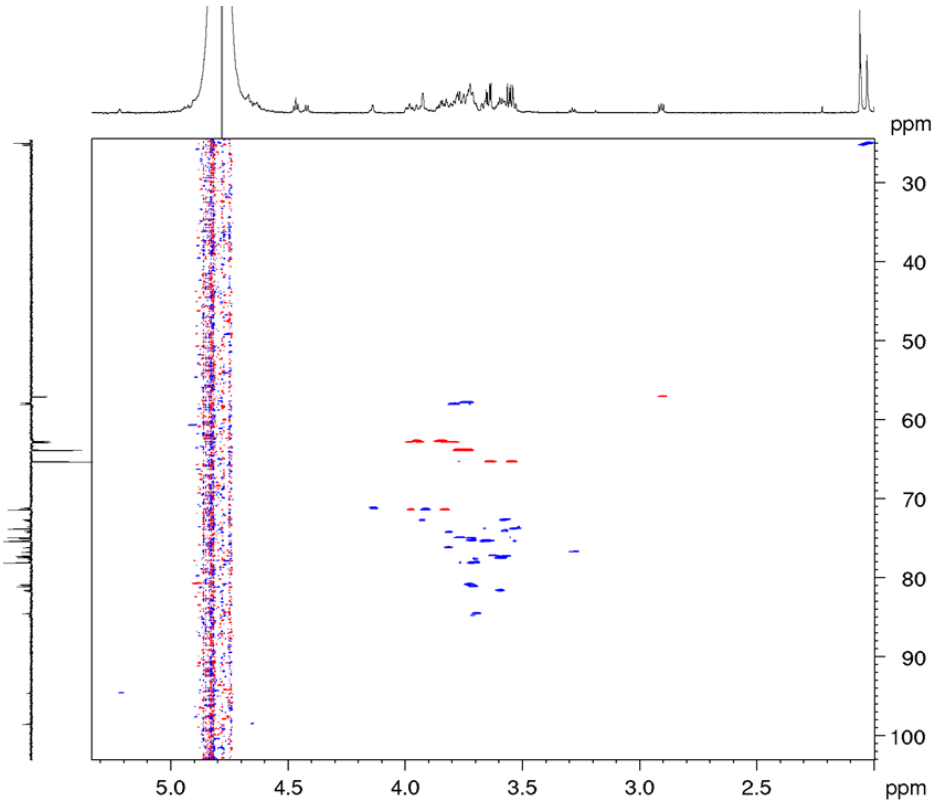

Figure A88.1H-13C HSQC spectrum of LNnH (H_2O:D_2O 9:1 *v/v* solvent at pH 3.0)

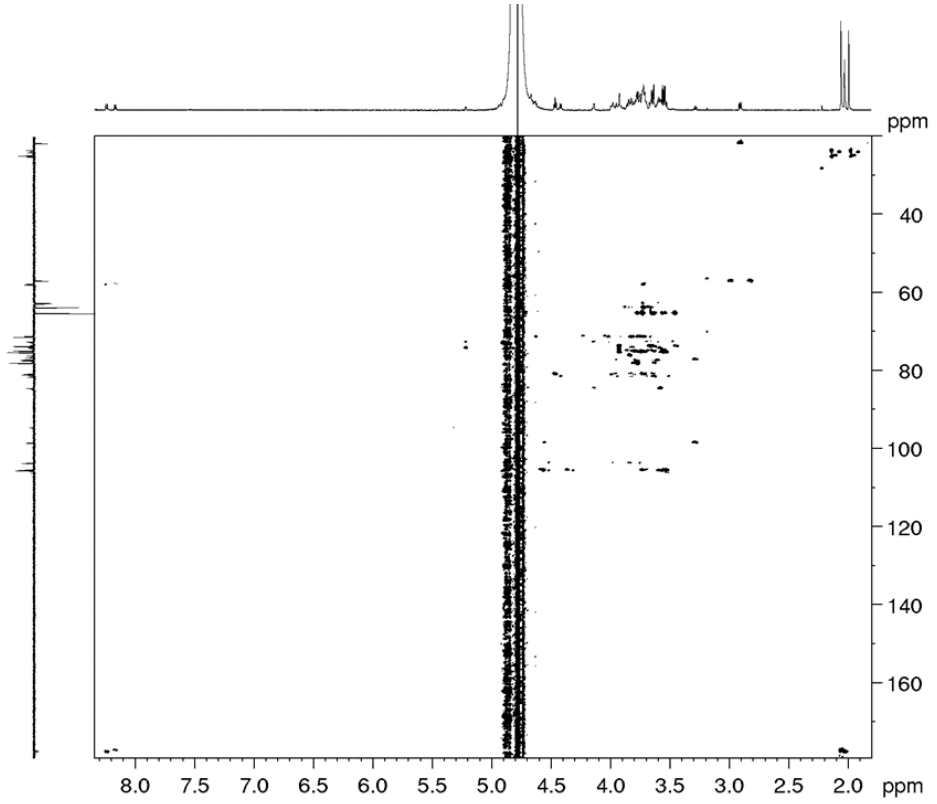

Figure A89. ^{1}H-^{13}C HMBC spectrum of LNnH (H_2O:D_2O 9:1 *v/v* solvent at pH 3.0)

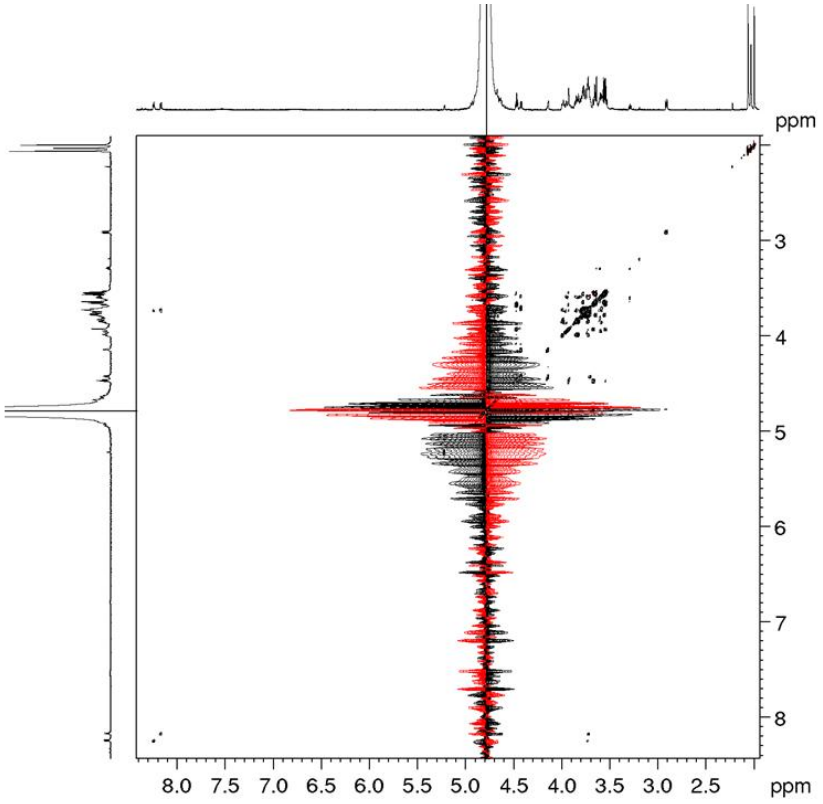

Figure A90. ^{1}H-^{1}H TOCSY spectrum of LNnH (H_2O:D_2O 9:1 *v/v* solvent at pH 3.0)

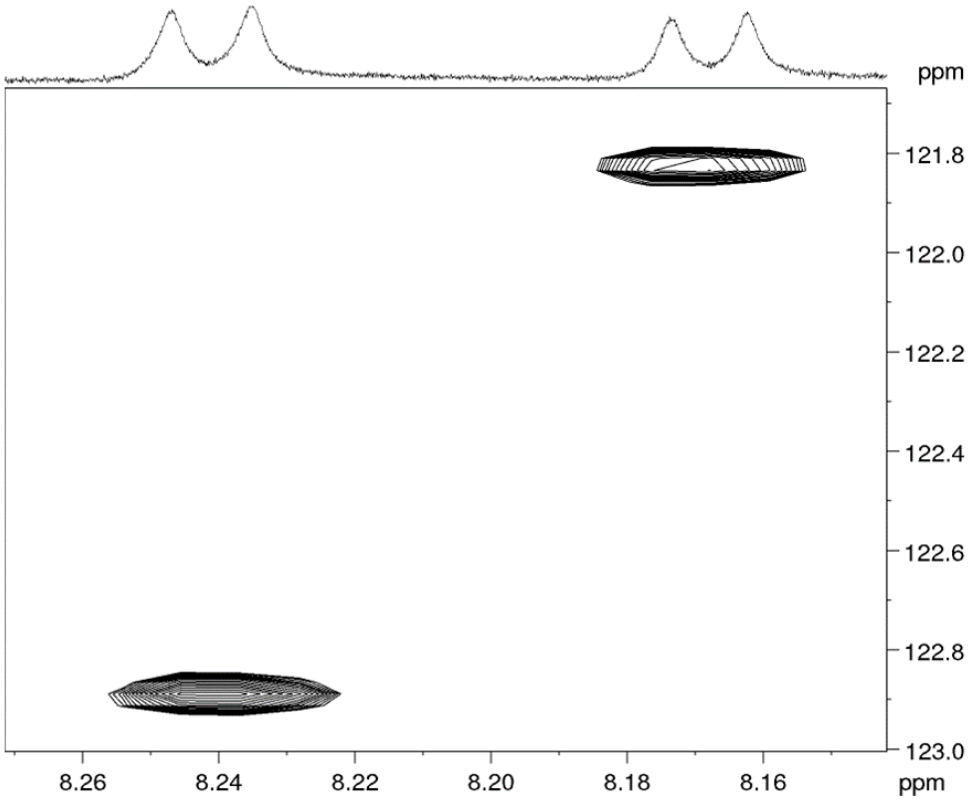

Figure A91.^{1}H-^{15}N HSQC spectrum of LNnH (H_2O:D_2O 9:1 *v/v* solvent at pH 3.0)

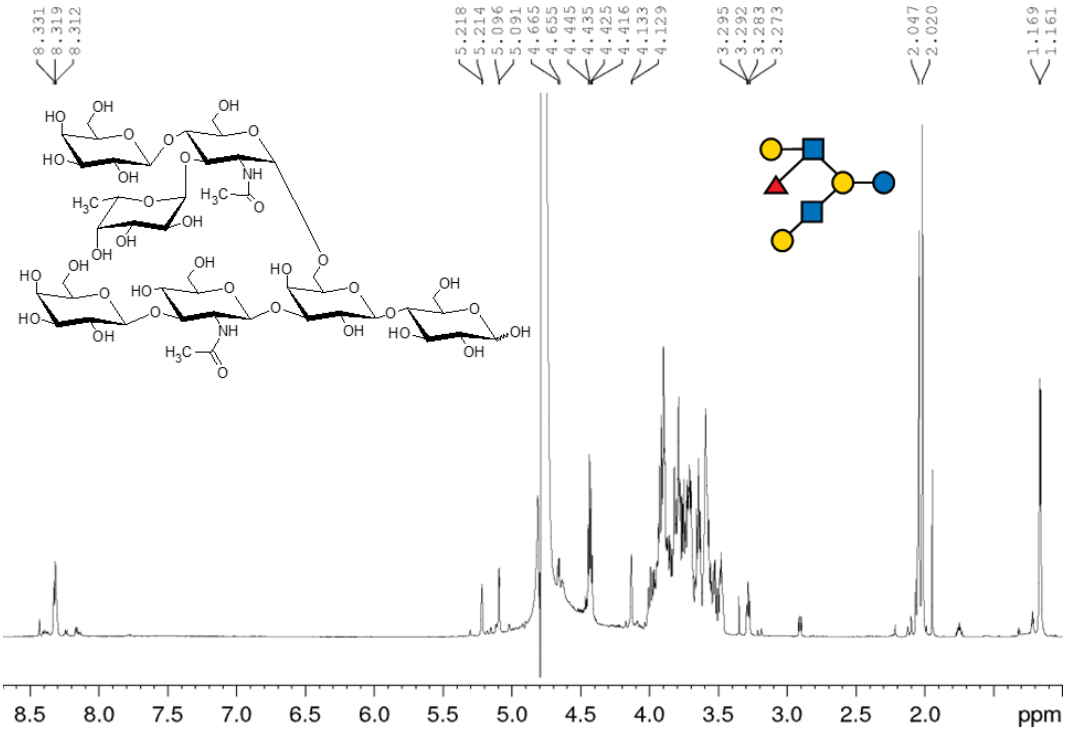

Figure A92. ^{1}H NMR spectrum of MFLNH III (H_2O:D_2O 9:1 *v/v* solvent at pH 3.0)

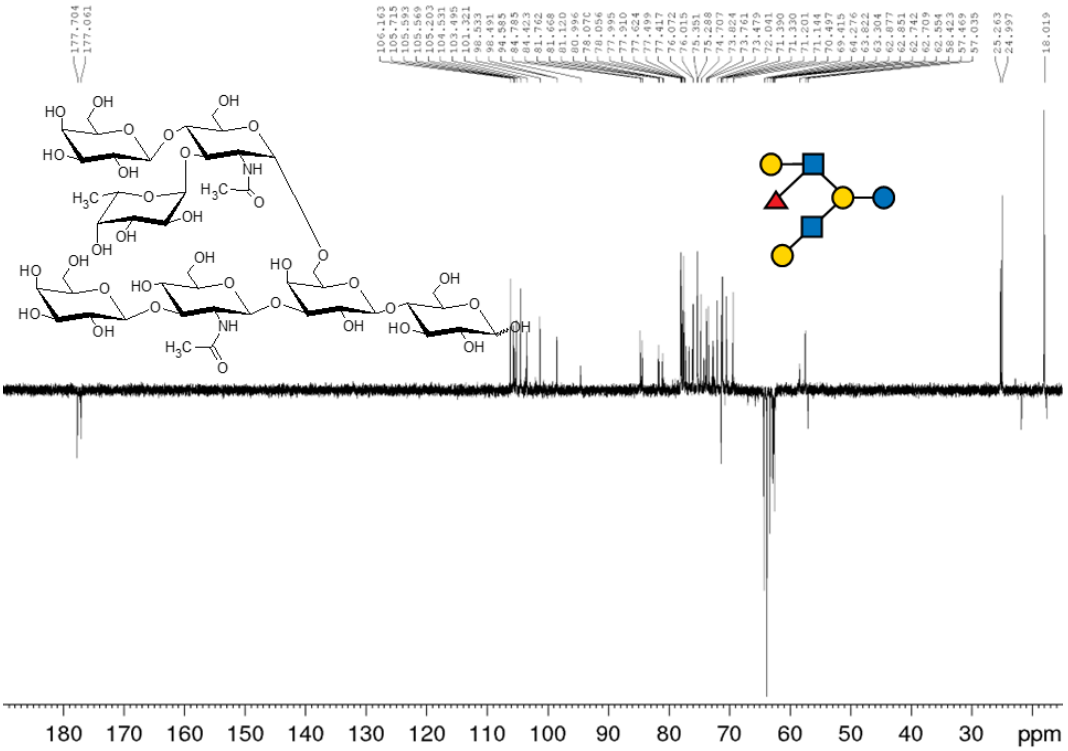

Figure A93. DEPTQ spectrum of MFLNH III (H_2O:D_2O 9:1 *v/v* solvent at pH 3.0)

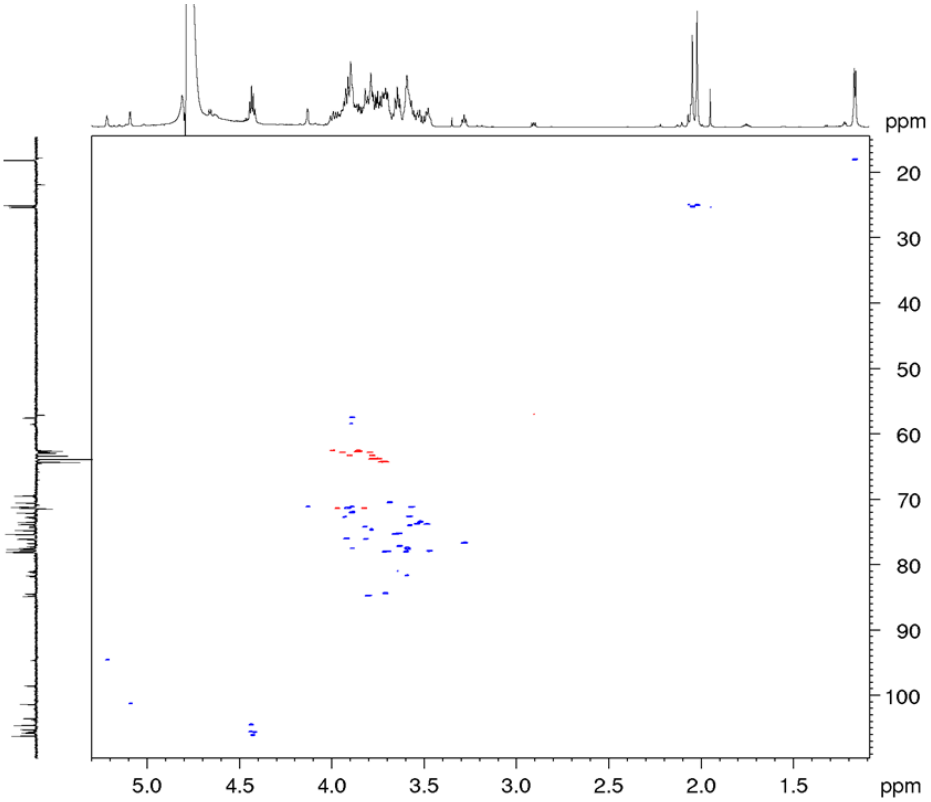

Figure A94.^{1}H-^{13}C HSQC spectrum of MFLNH III (H_2O:D_2O 9:1 *v/v* solvent at pH 3.0)

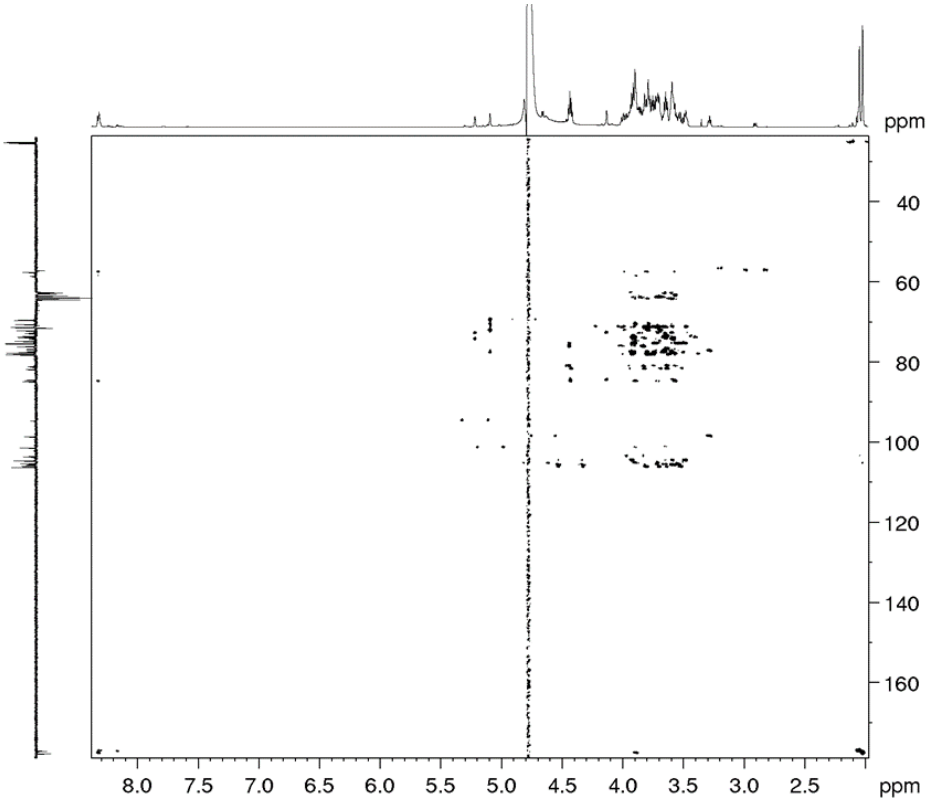

Figure A95.^{1}H-^{13}C HMBC spectrum of MFLNH III (H_2O:D_2O 9:1 *v/v* solvent at pH 3.0)

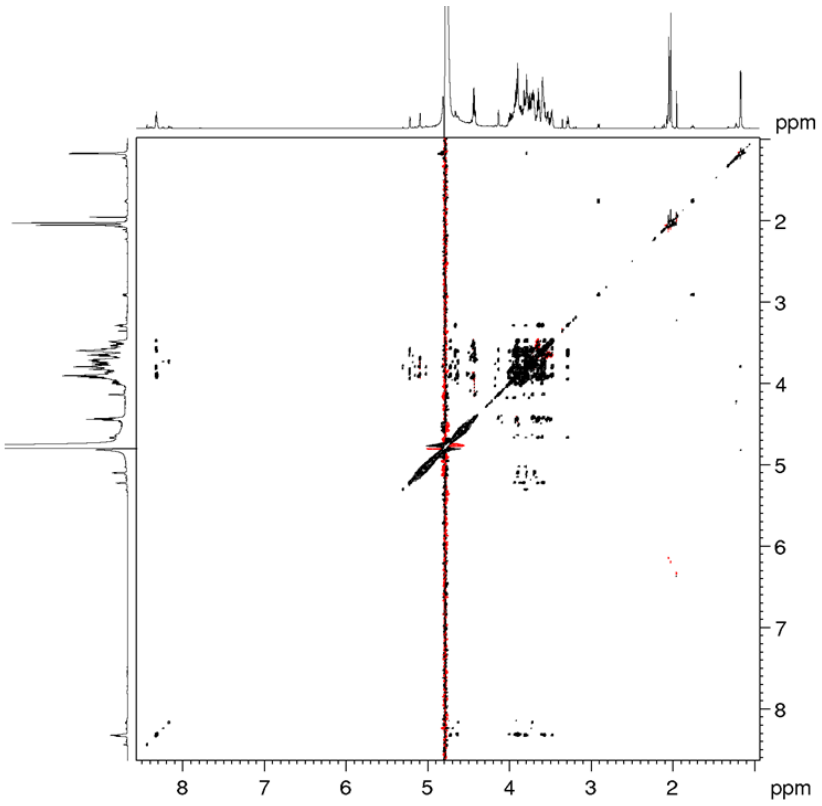

Figure A96. ^{1}H-^{1}H TOCSY spectrum of MFLNH III (H_2O:D_2O 9:1 *v/v* solvent at pH 3.0)

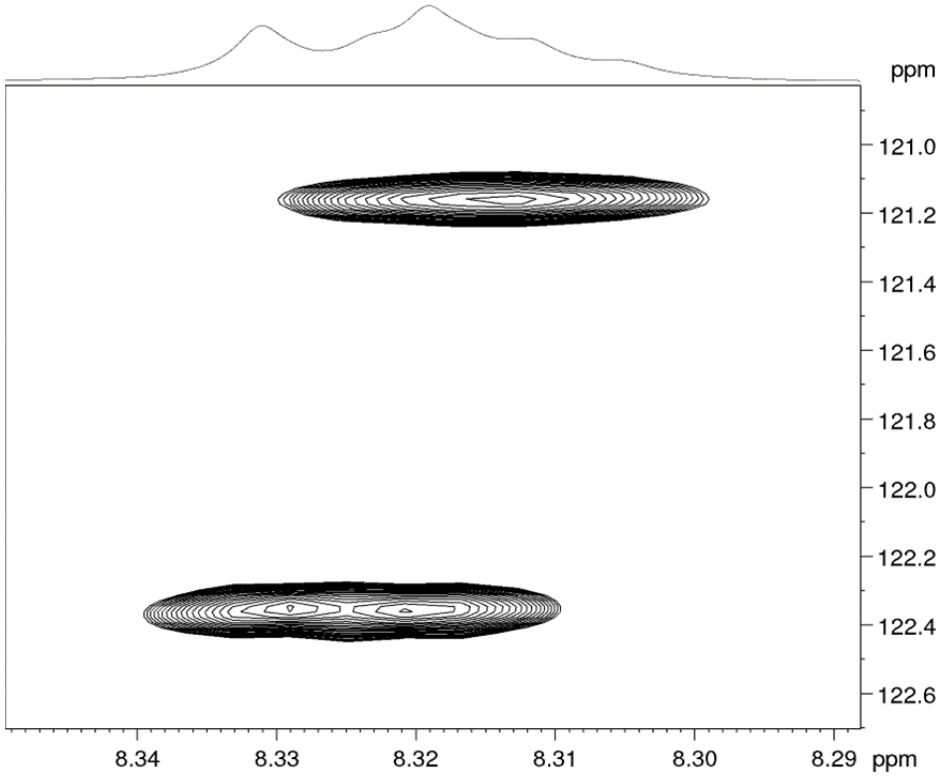

Figure A97. ^{1}H-^{15}N HSQC spectrum of MFLNH III (H_2O:D_2O 9:1 *v/v* solvent at pH 3.0)

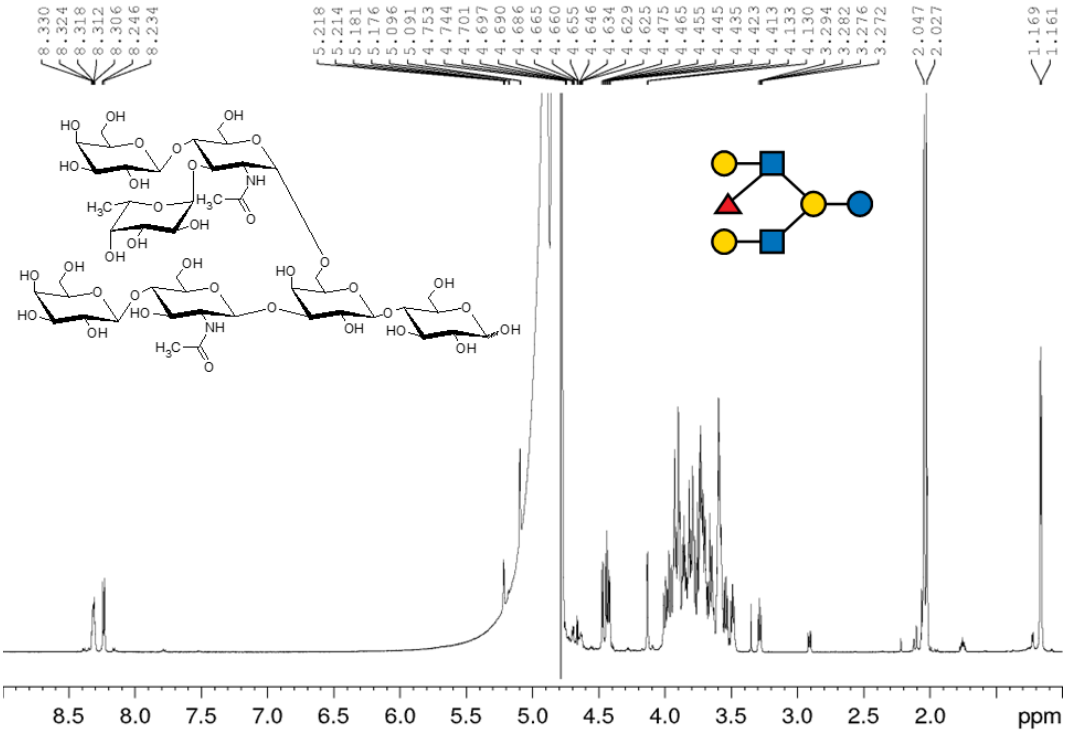

Figure A98. ^{1}H NMR spectrum of MFLNnH I (H_2O:D_2O 9:1 *v/v* solvent at pH 3.0)

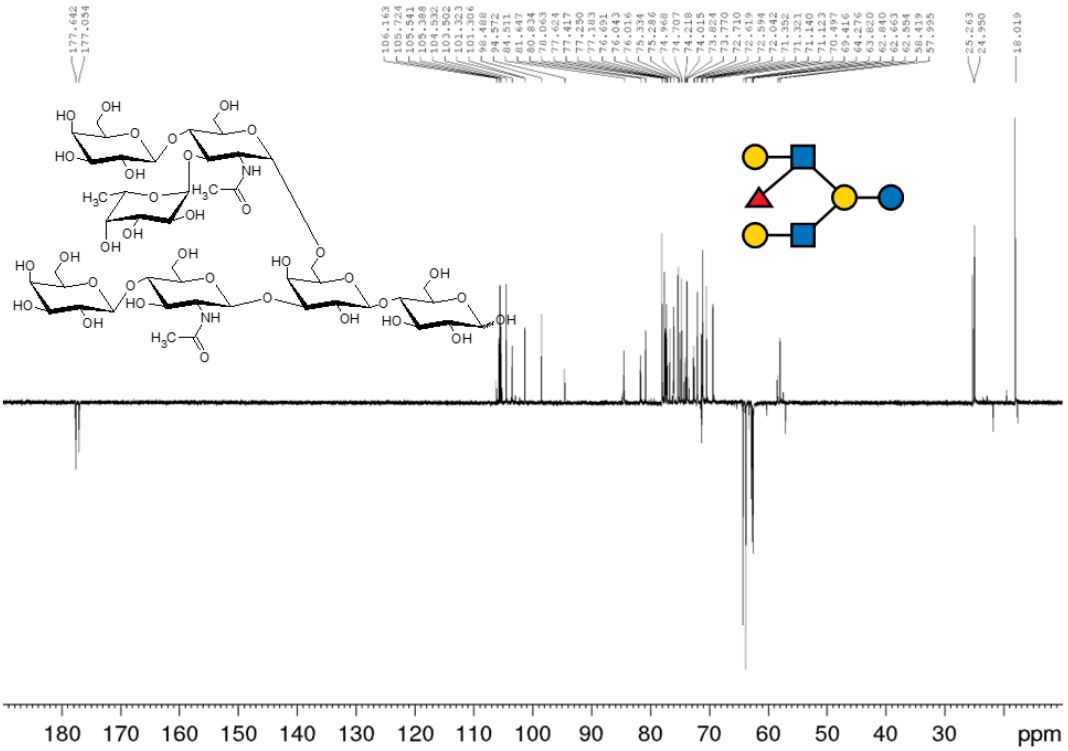

Figure A99. DEPTQ spectrum of MFLNnH I (H_2O:D_2O 9:1 *v/v* solvent at pH 3.0)

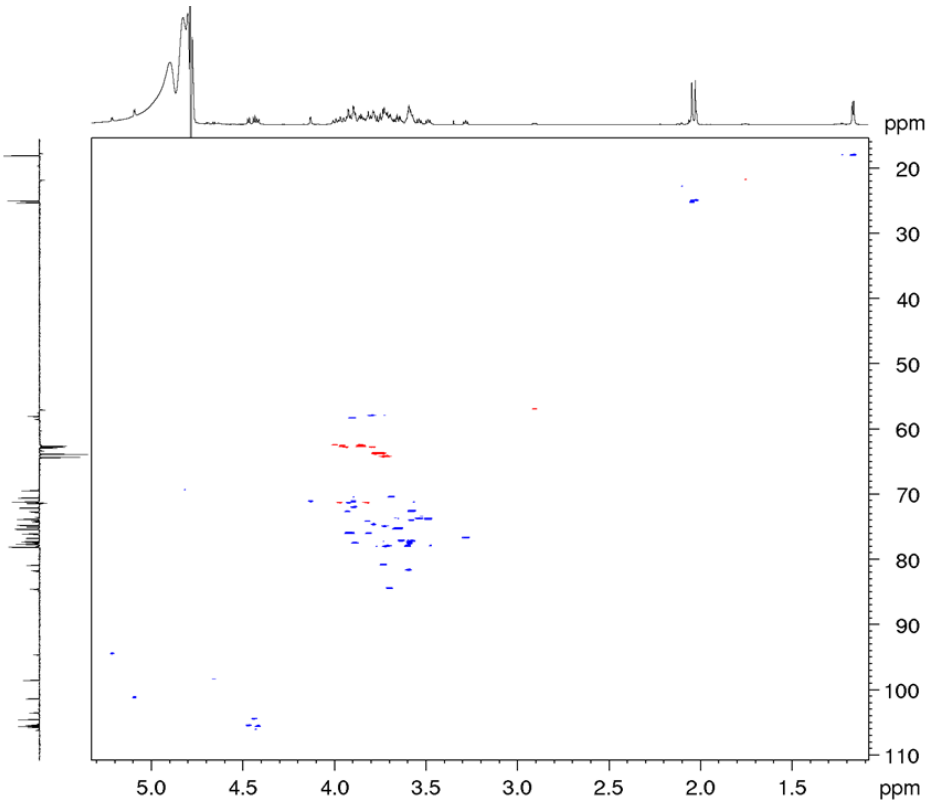

Figure A100. ^{1}H-^{13}C HSQC spectrum of MFLNnH I (H_2O:D_2O 9:1 *v/v* solvent at pH 3.0)

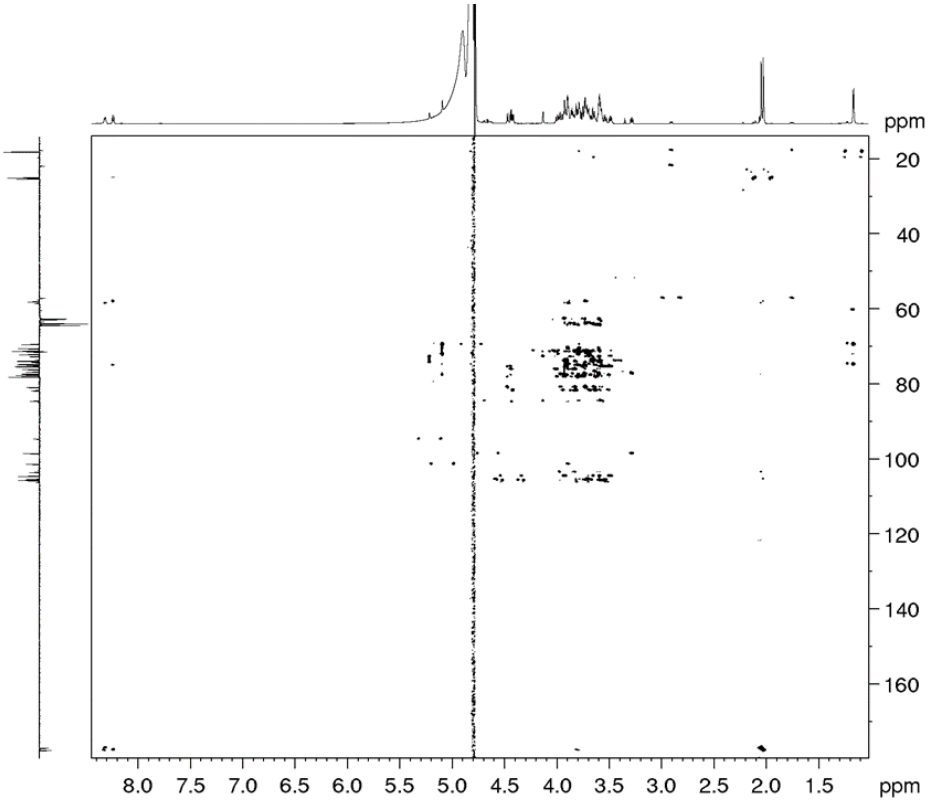

igure A101. ^{1}H-^{13}C HMBC spectrum of MFLNnH I (H_2O:D_2O 9:1 *v/v* solvent at pH 3.0)

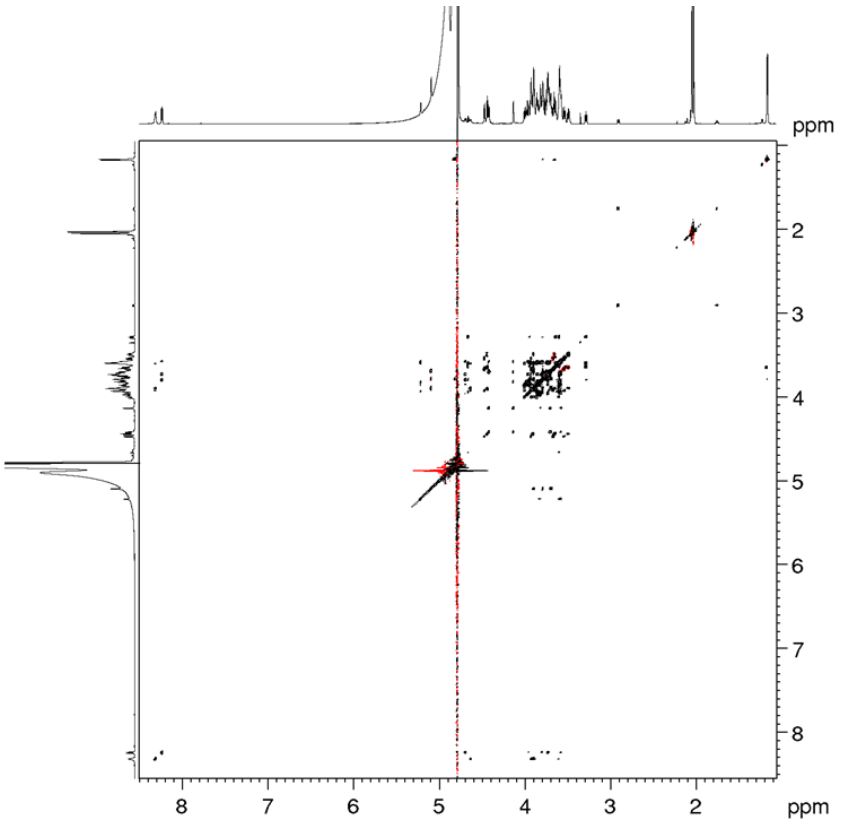

Figure A102. ^{1}H-^{1}H TOCSY spectrum of MFLNnH I (H_2O:D_2O 9:1 *v/v* solvent at pH 3.0)

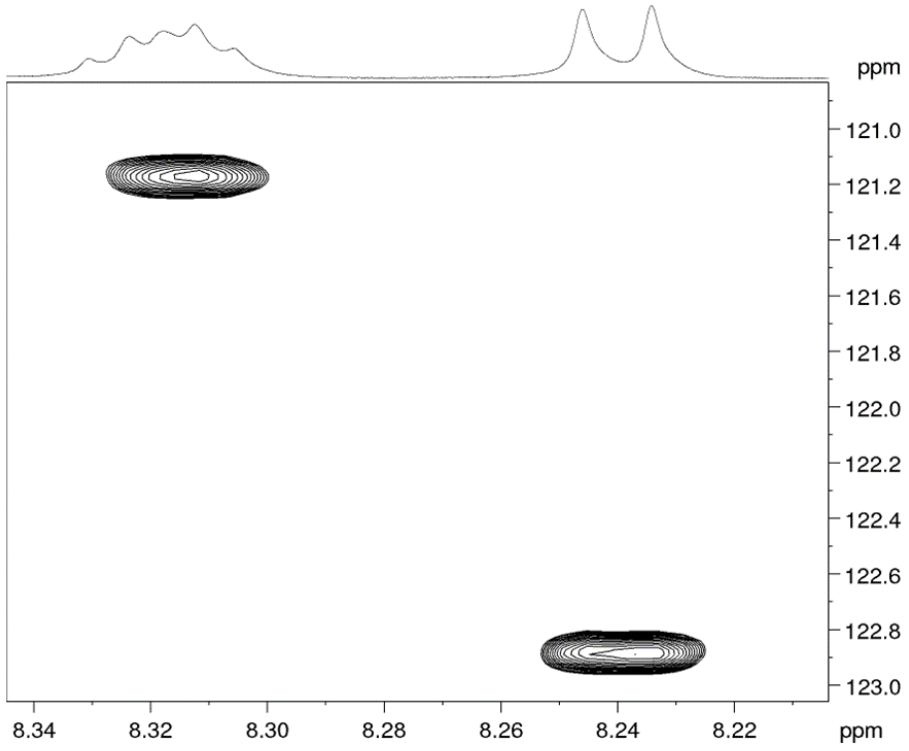

Figure A103. ^{1}H-^{15}N HSQC spectrum of MFLNnH I (H_2O:D_2O 9:1 *v/v* solvent at pH 3.0)

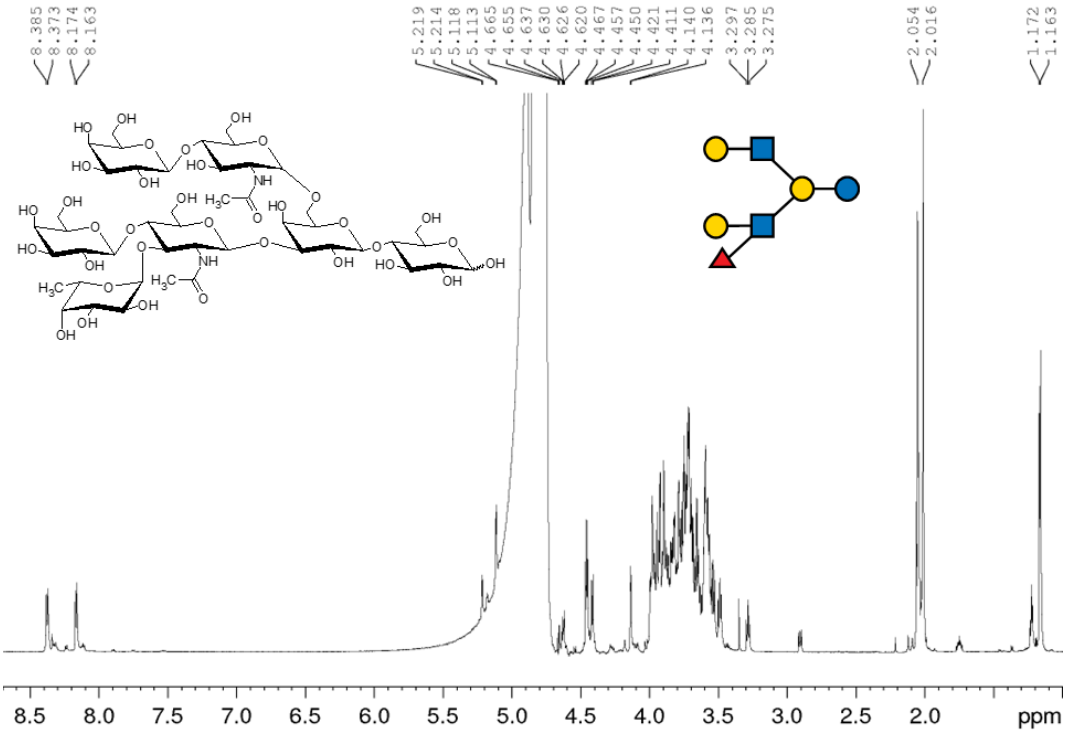

Figure A104. ^{1}H NMR spectrum of MFLNnH II (H_2O:D_2O 9:1 *v/v* solvent at pH 3.0)

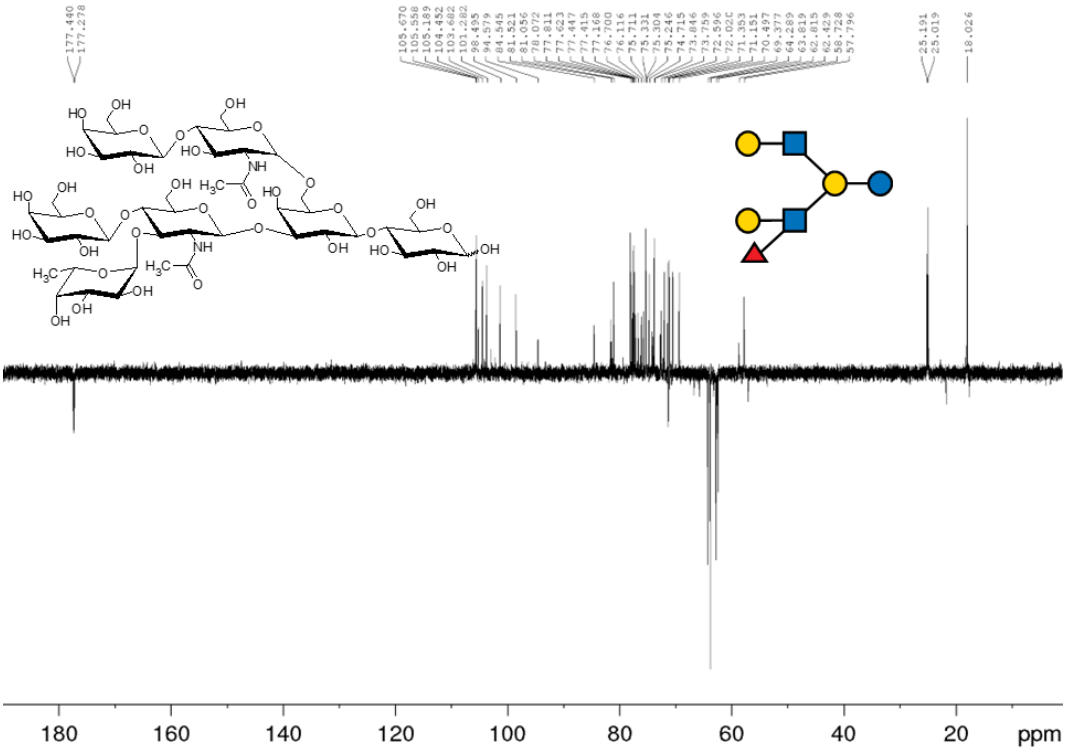

Figure A105. DEPTQ spectrum of MFLNnH II (H_2O:D_2O 9:1 *v/v* solvent at pH 3.0)

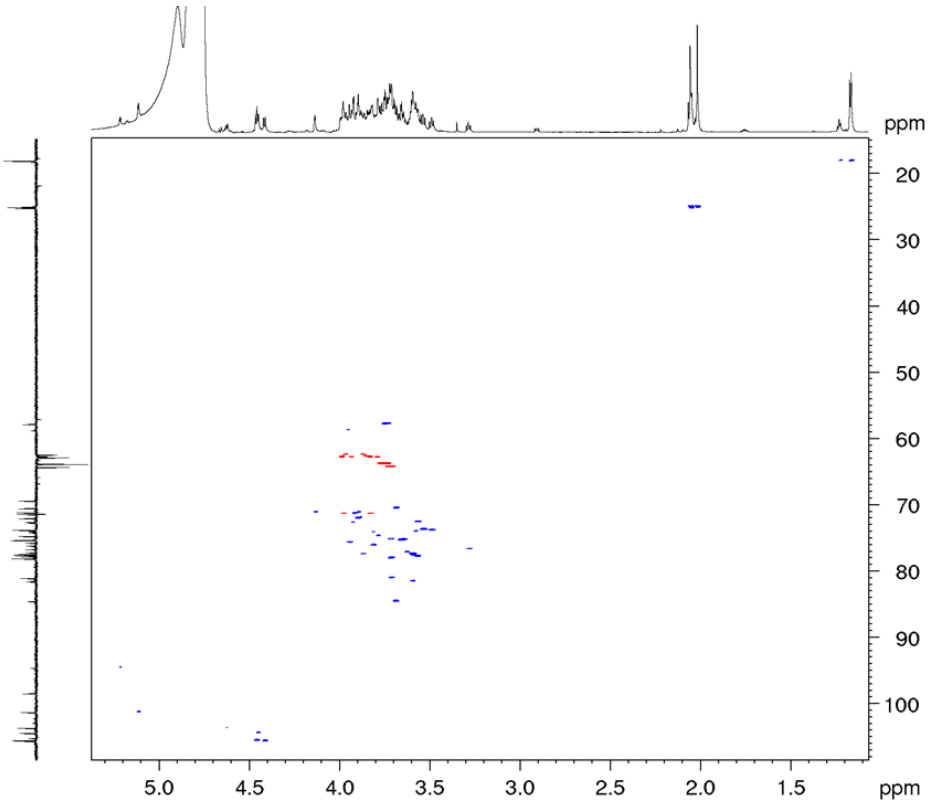

Figure A106. ^{1}H-^{13}C HSQC spectrum of MFLNnH II (H_2O:D_2O 9:1 *v/v* solvent at pH 3.0)

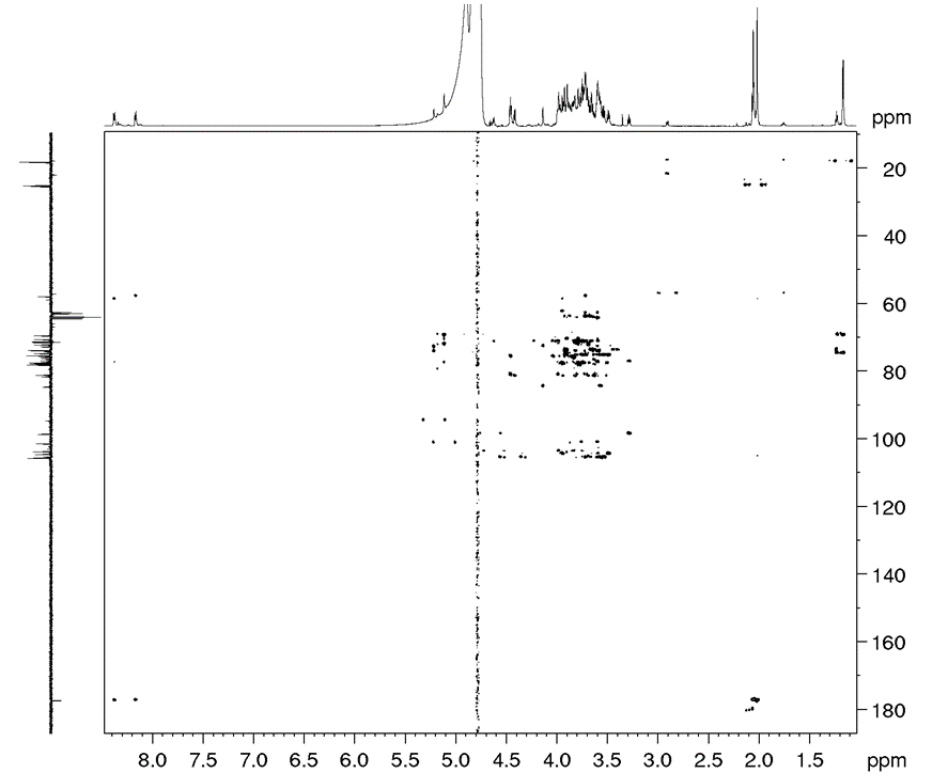

Figure A107. ^{1}H-^{13}C HMBC spectrum of MFLNnH II (H_2O:D_2O 9:1 *v/v* solvent at pH 3.0)

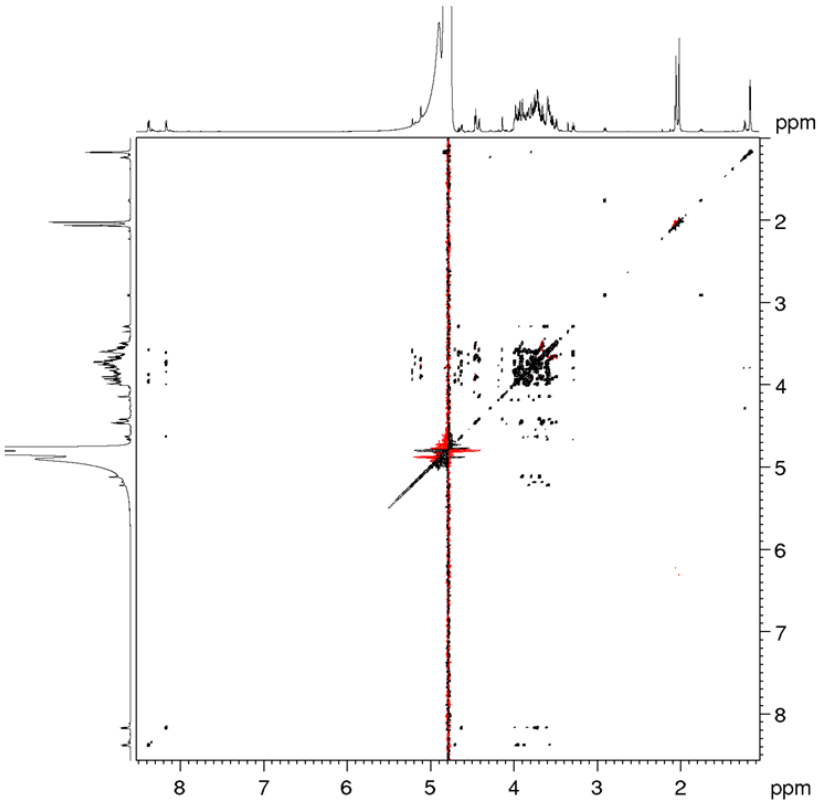

Figure A108. ^{1}H-^{1}H TOCSY spectrum of MFLNnH II (H_2O:D_2O 9:1 *v/v* solvent at pH 3.0)

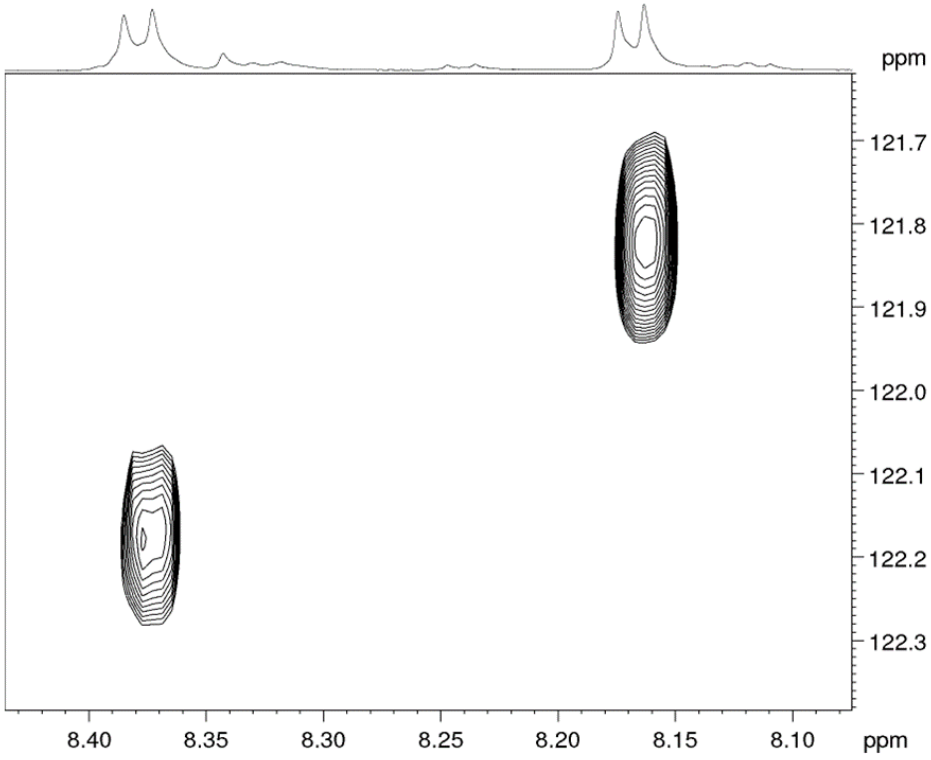

Figure A109. ^{1}H-^{15}N HSQC spectrum of MFLNnH II (H_2O:D_2O 9:1 *v/v* solvent at pH 3.0)

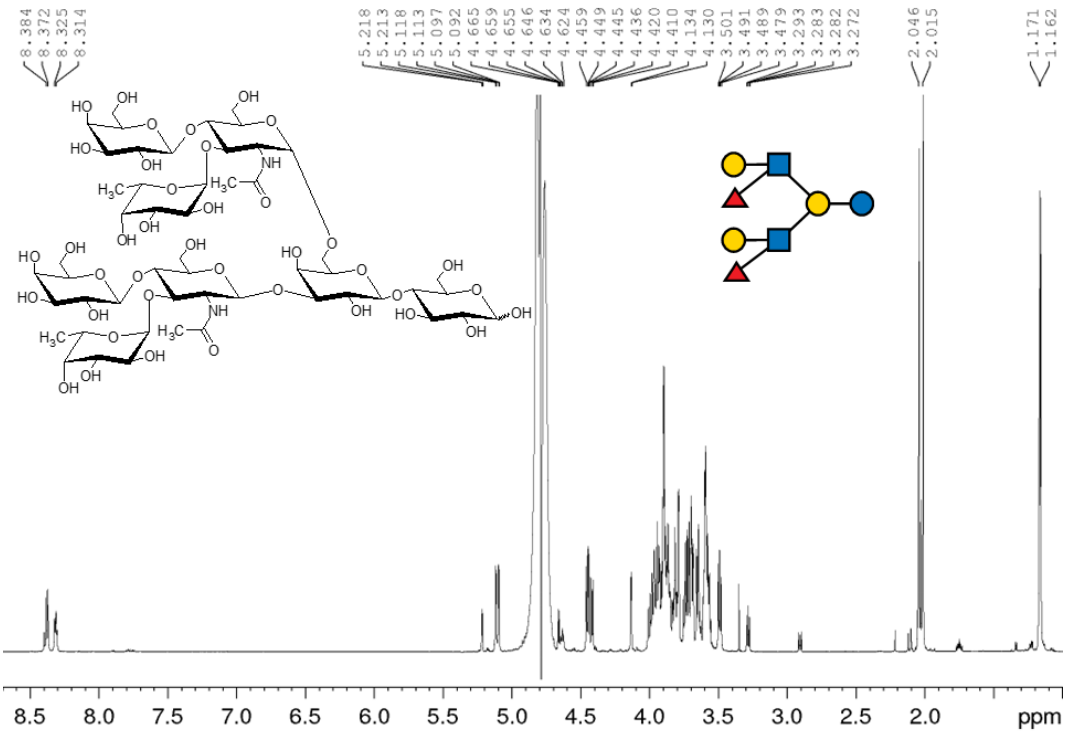

Figure A110. ^{1}H NMR spectrum of DFLNnH (H_2O:D_2O 9:1 *v/v* solvent at pH 3.0)

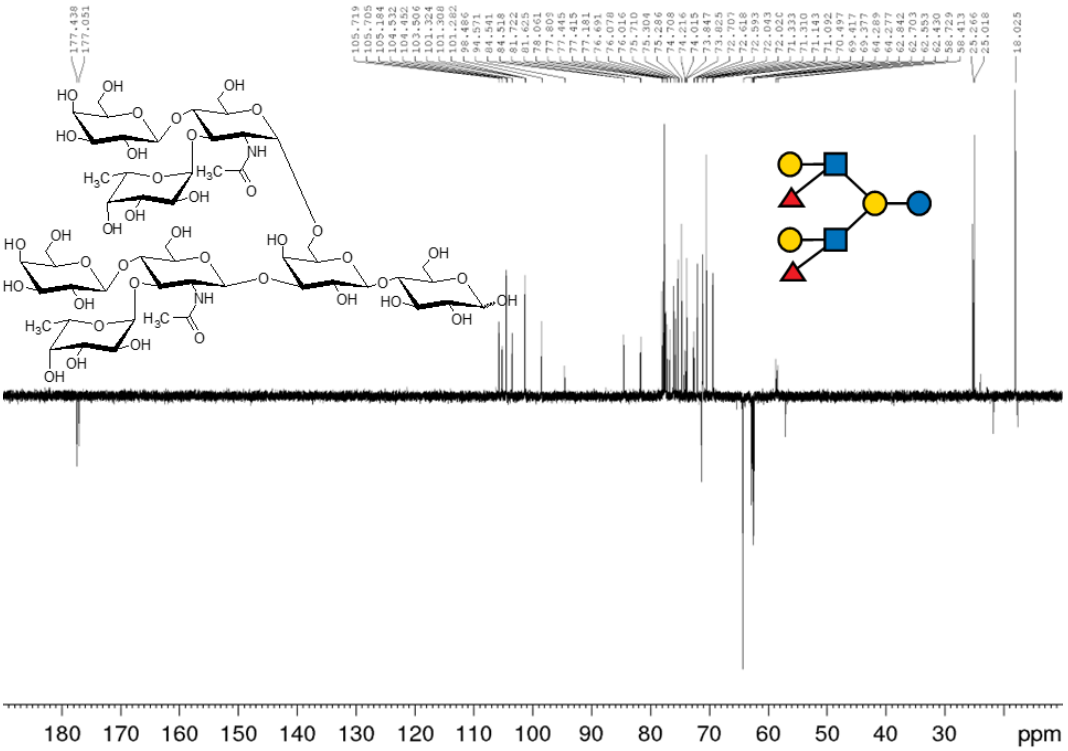

Figure A111. DEPTQ spectrum of DFLNnH (H_2O:D_2O 9:1 *v/v* solvent at pH 3.0)

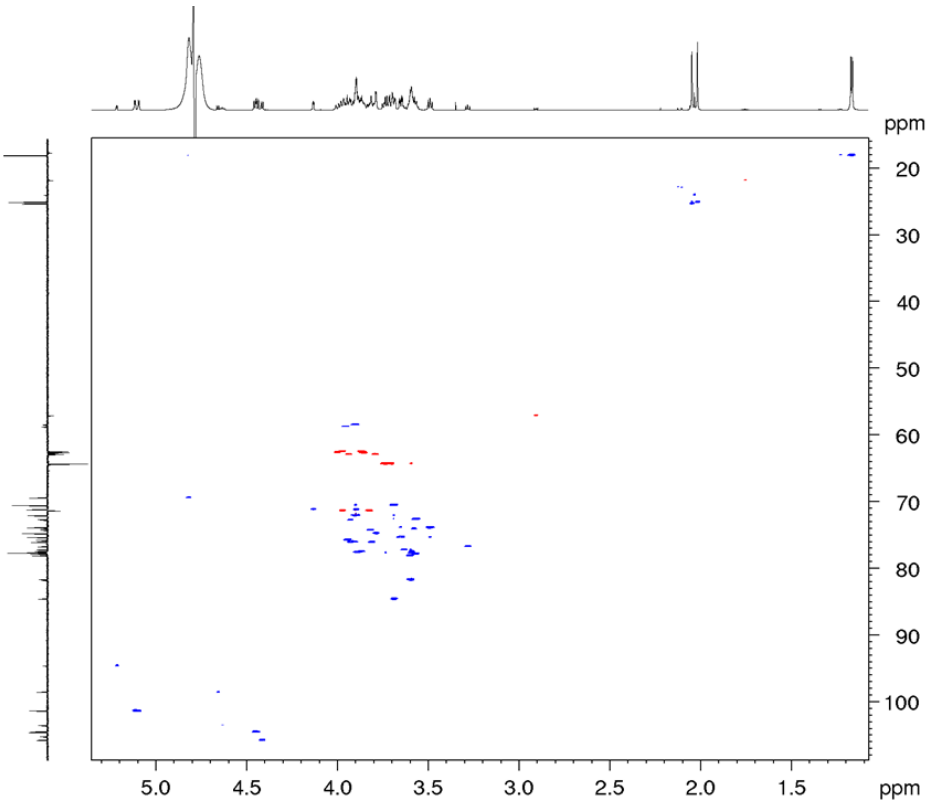

Figure A112. ^{1}H-^{13}C HSQC spectrum of DFLNnH (H_2O:D_2O 9:1 *v/v* solvent at pH 3.0)

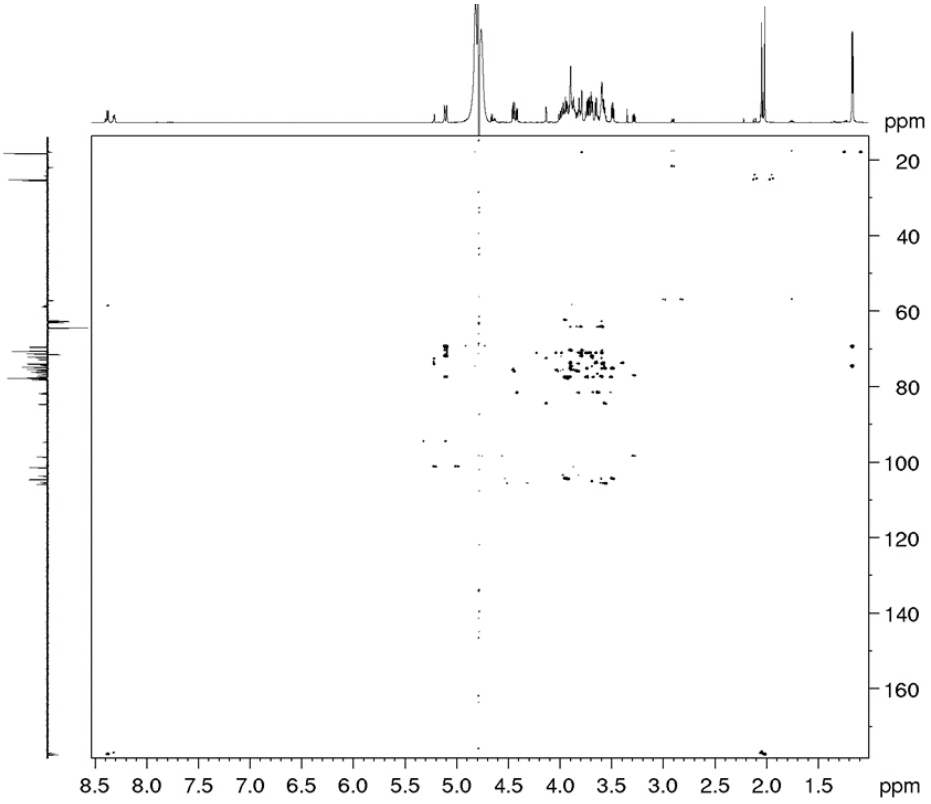

Figure A113. ^{1}H-^{13}C HMBC spectrum of DFLNnH (H_2O:D_2O 9:1 *v/v* solvent at pH 3.0)

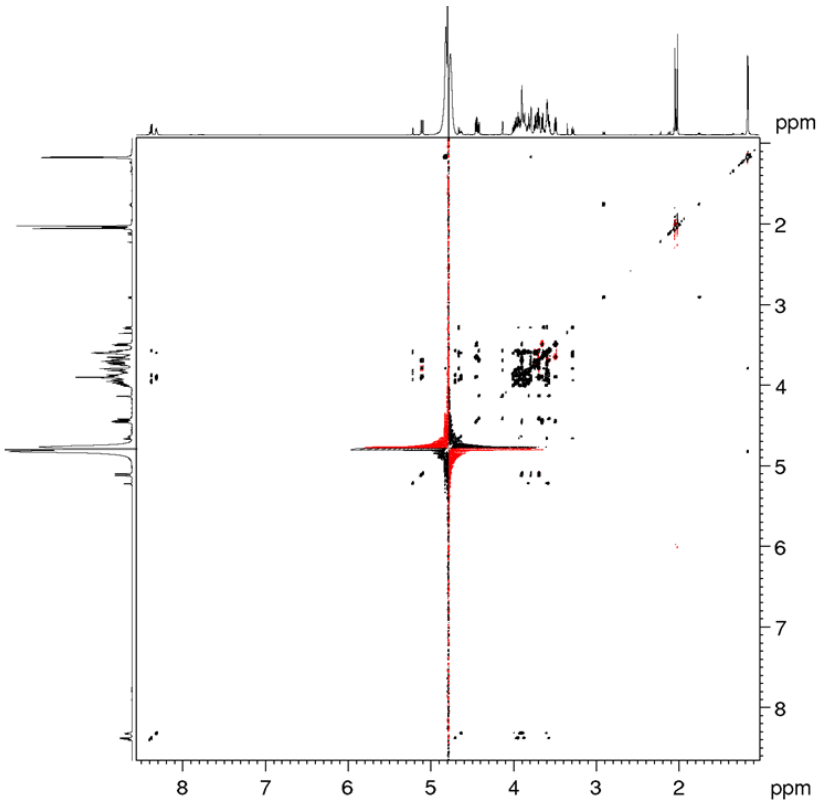

Figure A114. ^{1}H-^{1}H TOCSY spectrum of DFLNnH (H_2O:D_2O 9:1 *v/v* solvent at pH 3.0)

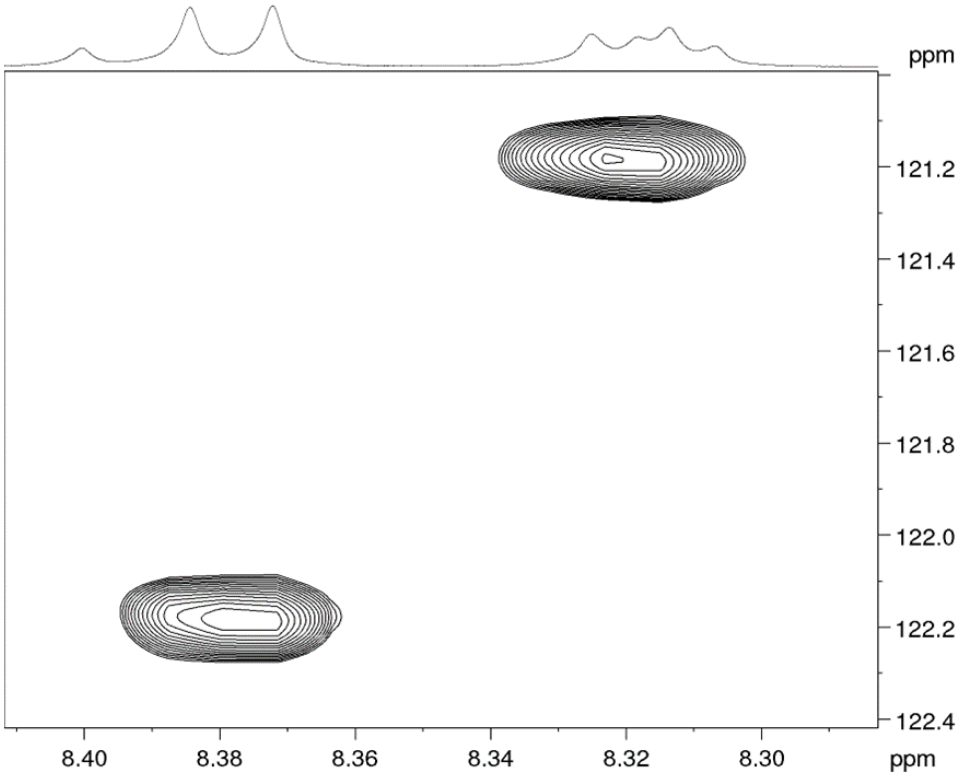

Figure A115. ^{1}H-^{15}N HSQC spectrum of DFLNnH (H_2O:D_2O 9:1 *v/v* solvent at pH 3.0)